Doctoral   Science

Novel Therapeutic Approaches to Treat Brain Cancer Combining Cold Atmospheric Plasma, Therapeutic Prodrugs and Gold Nanoparticles

Zhonglei He
Technological University Dublin

Novel Therapeutic Approaches to Treat Brain Cancer Combining Cold Atmospheric Plasma, Therapeutic Prodrugs and Gold Nanoparticles

Submitted by

Zhonglei He, B.Sc.

PhD

School of Food Science and Environmental Health

Technological University Dublin

Supervisors:

Prof. James F. Curtin, Dr. Furong Tian, Prof. Patrick J. Cullen

May 2020

Abstract

Glioblastoma Multiforme (GBM) makes up approximately 45% of all primary brain tumours. State of the art treatment at present involves concurrent and adjuvant temozolomide (TMZ) with radical radiotherapy which extends median survival from 12.1 months (radical radiotherapy alone) to 14.6 months according to the study of the European Organization for Research and Treatment of Cancer (EORTC) Brain Tumour and Radiotherapy Groups and the National Cancer Institute of Canada (NCIC) Clinical Trials Group. Meanwhile, National Cancer Registry Ireland presented that GBM represents over 40% of all malignant brain tumours and had the worst five-year net survival (4%) compared to overall malignant brain cancer (five-year net survival, 19%) in Ireland. Long term survival of patients with GBM has not been significantly improved in the last 20 years. GBM tumours also have presented high level of resistance to normal treatments. Therefore, novel therapies to treat GBM are urgently needed. This study aimed to investigate efficient therapeutic methods by combining novel interventions, including cold atmospheric plasma (CAP), gold nanoparticles (AuNPs) and specific chemotherapeutic compounds to overcome the barriers of GBM treatment. Over the past decade CAP has emerged as a novel approach in health care area, especially cancer therapy. CAP generates chemically active species such as reactive oxygen species (ROS) and reactive nitrogen species (RNS) and has been demonstrated to act in synergy with a selection of traditional chemotherapeutic compounds which could reduce the effective concentrations of drugs needed at the tumour and may allow for targeted toxicity at sites exposed to the plasma field. AuNPs, well known as biocompatible drug delivery and diagnosis agents for cancer therapy, have been demonstrated to have synergistic anti-cancer effects in combination with CAP treatment.

In this project, for the first time, we investigated and described the detailed mechanism

behind the synergistic anti-cancer effects between AuNPs and CAP treatment. Chapter 2 and Chapter 3 demonstrated that low dose treatment of CAP treatment was capable of promoting the uptake of AuNPs into glioblastoma U373MG cells via stimulated membrane repair clathrin-dependent endocytosis. The intracellular accumulation of AuNPs was tracked using atomic absorbance spectrometry (AAS) and simulated with numerical modelling to identify the enhanced uptake routine. AuNPs were tracked into early endosomes, late endosomes and finally lysosomes using specific fluorescent probes and confocal microscope. The lipid oxidation of cancer cells induced by CAP treatment was confirmed by various methods, including confocal microscopy, Thiobarbituric Acid Reactive Substances (TBARS) assay and flow cytometry. Meanwhile, the related endocytosis pathway was determined to be clathrin dependent using multiple clathrin and caveola specific inhibitors and clathrin siRNA.

In Chapter 4, we performed the screening of 47 prodrug candidates for their cytotoxicity against U373MG cells in combination with CAP treatment. The selection of chemotherapeutic compounds provided by collaborators have been tested to determine dose response curves with or without CAP treatment using Alamar Blue assay, thus, to characterise their synergistic potential in combination with CAP. Two leading candidates which showed significant cytotoxicity with CAP, have been identified from 47 compounds. Furthermore, the mechanism behind the synergistic cytotoxicity between one of the leading candidates, JW-04-061, and CAP treatment has been investigated. It has been demonstrated that reactive species, especially short-lived species, generated in culture medium may play a main role in the oxidation and activation of the prodrug during CAP treatment.

Declaration

I certify that this thesis which I now submit for examination for the award of PhD, is entirely my own work and has not been taken from the work of others, save and to the extent that such work has been cited and acknowledged within the text of my work.

This thesis was prepared according to the regulations for graduate study by research of the Technological University Dublin and has not been submitted in whole or in part for another award in any other third level institution.

The work reported on in this thesis conforms to the principles and requirements of the TU Dublin's guidelines for ethics in research.

TU Dublin has permission to keep, lend or copy this thesis in whole or in part, on condition that any such use of the material of the thesis be duly acknowledged.

Signature _____*Zhonglei He*_____ Date _____05/28/2020_____
Candidate

Abbreviations

AAS	Atomic Absorbance Spectrometry
AgNP	Silver Nanoparticle
AIC	5-aminoimidazole-4-carboxamide
AKT	v-akt murine thymoma viral oncogene homolog
ASK1	Apoptosis signalling regulating kinase 1
ATP	Adenosine Triphosphate
AuNPs	Gold Nanoparticles
BBB	Blood Brain Barrier
BCD	Barrier Coronal Discharges
Bcl2	B-cell lymphoma 2
CaMKII	Calcium/calmodulin-dependent protein kinase II
CAP	Cold Atmospheric Plasma
CBR1	Carbonyl reductase 1
CDs	Cyclodextrins
CI	Combination Index
CLTC	Human Clathrin heavy chain 1
CME	Clathrin-mediated endocytosis
CNS	Central nervous system
CSCs	Cancer stem cells
CT	Computed tomography
DBD	Dielectric Barrier Discharge
DOPE	Phosphatidylethanolamine
EEDF	The electron energy distribution function
EGF	Epidermal Growth Factor

EGFR	Epidermal Growth Factor Receptor
EMT	Epithelial-mesenchymal transition
EORTC	European Organization for Research and Treatment of Cancer
EPR	Enhanced permeation and retention
esiRNA	Endoribonuclease-prepared siRNA
FAK	Anti-phospho-focal adhesion kinase
FDA	The US Food and Drug Administration
GBM	Glioblastoma multiforme
GSCs	Glioma stem-like cells
GSH	Glutathione
GSK-3	Glycogen synthase kinase -3
GSTP1	Glutathione S-transferase pi 1
GzmB	Cytotoxic protein Granzyme B
HA–EGCG	Hyaluronic acid-epigallocatechin gallate conjugates
HIF-1	Hypoxia-inducible factor
IR	Ionizing radiation
JNK	c-Jun N-terminal kinase
LDH	Lactate dehydrogenase
MAPK	Mitogen-activated protein kinase
MCM-41	Mobil Composition of Matter No. 41
MCT	Monocarboxylate transporters
MDA	Malondialdehyde
MGMT	Methylguanine methyltransferase
mPEG	Monomethoxy poly- ethylene glycol
MPS	Mononuclear phagocytic system

MRI	Magnetic resonance imaging
MRS	Magnetic resonance spectroscopy
MTIC	Monomethyl triazene 5- 3-methyltriazen-1-yl - imidazole-4-carboxamide
NAC	N-Acetyl Cysteine
NADPH	Nicotinamide adenine dinucleotide phosphate
NCIC	Radiotherapy Groups and the National Cancer Institute of Canada
NEU	Human epidermal growth factor receptor 2
NP	Nanoparticle
NTAP	Non-thermal atmospheric plasma
OES	Optical Emission Spectroscopy
ON	Oligonucleotide
p21	21-kDa protein
P53	Protein 53
PAM	Plasma activated medium
PBS	Phosphate buffer solution
pDNA	Plasmid DNA
PEG	Polyethylene glycol
PEGylated	Polyethylene glycol-coated
PEI	Polyethylenimine
PHAs	Polyhydroxyalkanoates
PI	Propidium iodide
PI3K	Phosphatidylinositol 3-kinase
PIP3	Phosphatidylinositol-3,4,5-trisphosphate
PLGA	Poly- lactide-co-glycolic acid
POD	Peroxidase

PSLs	pH-sensitive liposomes
PTEN	Phosphatase and tensin homolog
PVA	Polyvinyl alcohol
rhTNF	Recombinant human Tumour Necrosis Factor
RNS	Reactive Nitrogen Species
ROS	Reactive Oxygen Species
RS	Reactive species
RT	Radiotherapy
S.E.M	Standard error of the mean
SBA-15	Santa Barbara Amorphous-15
siRNA	Small interfering RNA
SPR	Surface plasmon resonance
SPS	Second positive system
TBA	Thiobarbituric acid
TBARS	Thiobarbituric Acid Reactive Substances
TMZ	Temozolomide
TP53	Tumour suppressor protein 53
TPPMS	Triphenylphosphine monosulfonate
TRX	Thioredoxins
TSLs	Thermo-sensitive liposomes
WHO	World Health Organization

Table of Contents

Table of Figures

Table of Tables

CHAPTER 1. INTRODUCTION

Part of this introduction has been published (Book Chapter).

See Appendix I

1.1 Brain Cancer

As technology improves, the survival rates of certain types of cancer, such as lung and breast cancer, have changed dramatically during recent years. However, only small improvements were made in brain cancer treatment. Brain cancers are divided in two types, primary brain cancer and secondary brain cancer (Young *et al.*, 2015). Primary brain cancer originates in brain cells, forms in the central nervous system (CNS) and usually does not metastasize to the outside of the CNS. Secondary brain malignancy is formed by tumours cells metastasized from outside of CNS, such as lung cancer and breast cancer (Young *et al.*, 2015). Although secondary brain cancer is more common, primary brain cancer is more deadly, which is the third leading cause of cancer deaths in age 15-34 adults and the most common cause of neoplasm deaths in children (Mladenov *et al.*, 2007). Primary brain cancer can be classified as gliomas and nongliomas according to the origination (as described in Table 1 below).

Table 1. Main types of primary brain cancer

Gliomas	Astrocytomas, Oligodendrogliomas, Ependymomas
Nongliomas	Menigiomas, Medulloblastomas

Gliomas are developed from glial cells, including astrocytes, oligodendrocytes and ependymal cells or mixed of the above (Parsons *et al.*, 2008). Glial cells are non-neuronal cells in CNS and the peripheral nervous system which mainly provide protection and support for neurons (Jessen and Mirsky, 1980). Most common types of nongliomas include meningiomas, tumours that are developed in the meninges (Marta, Correa and Teixeira, 2011), and medulloblastomas, primitive neuroectodermal tumour that is raised in the cerebellum and commonly represents in childhood brain tumours (Schroeder and Gururangan, 2014).

Astrocytomas are the most common type (representing approximately 50%) in the above primary brain cancer. According to the World Health Organization (WHO), astrocytomas are classified into 4 types, including pilocytic astrocytoma (Grade 1), low-grade astrocytoma (Grade 2), anaplastic astrocytoma (Grade 3), glioblastoma (Grade 4) (Young *et al.*, 2015). Grade 1 pilocytic astrocytomas glow slowing and typically can be cured by surgical excision (Louis *et al.*, 2016). Low-grade astrocytomas, also known as diffuse astrocytomas, have higher possibility to recur and may further progress to higher grade astrocytomas, thus regarded as malignant tumours (Louis *et al.*, 2016). WHO grade 3 and 4 astrocytomas grow much faster compared to the previous tumours mentioned above, when surgical excision is more difficult to be performed completely (Young *et al.*, 2015). Thus, radiation therapy and chemotherapy are typically applied to control the progress of malignancy and extend survival.

1.2   Glioblastoma Multiforme

Glioblastoma, also known as glioblastoma multiforme (GBM), is the most invasive brain malignancy and the most common primary brain cancer among the previous tumours mentioned in section 1.1, accounts for 60-75% of astrocytic tumours and 15% of intracranial tumours in adults (Young *et al.*, 2015). The term glioblastoma multiforme was first defined by Harvey Cushing and Percival Bailey in 1926, as the name implies, GBM is developed from glial cells, and presents highly various morphologies, as well as variable levels of cellular and nuclear polymorphism, which also is able to induce multiple symptoms, including cysts, haemorrhage and necrosis (Møller *et al.*, 2013). Even "multiforme" is currently not used in WHO classification, GBM is still commonly accepted in the literature as abbreviation synonymous with glioblastoma.

The most common symptoms of GBM include changes to personality, headaches, localized neurological problems, memory loss, mood or concentration, nausea, seizure

and vomiting (Alifieris and Trafalis, 2015). However, the type of symptoms induced has no specificity and mainly depends on the location of the neoplasm. Computed tomography (CT), Magnetic resonance imaging (MRI), Magnetic resonance spectroscopy (MRS) are commonly used to view suspected GBM. Craniotomy with tumour resection, stereotactic biopsy and pathology are typically required for definitive diagnosis. Furthermore, based on histological confirmation and genetic analysis, GBM can be divided into primary and secondary subtype. Primary GBM directly originates from glial cells (*de novo*), and develops faster, presenting much worse prognosis compared to secondary GBM. Secondary GBM is progressed from lower-grade (WHO Grade 2) astrocytoma which has been previously clinical identified. It should be noted that, as mentioned in section 1.1, all primary and secondary subtypes of GBM originate in brain cells, which are all primary brain cancer. Due to the difference between primary and secondary GBM, it is crucial to distinguish these two subtypes, especially identify primary glioblastoma to determine tumour therapy and prognosis. Although, primary and secondary GBM cannot be differentiate morphologically, clinical statistic presented that primary GBM was frequently diagnosed in patients older than 60 years, whereas secondary GBM more commonly occurred in patients younger than 45 years. The genetic make-up of primary and secondary GBM can be distinguished. The genetic alternation in primary GBM more commonly (40-50%) presents as over expression of Epidermal Growth Factor Receptor (EGFR), whereas tumour suppressor protein (TP53) mutations were usually (~60%) identified in secondary GBM (Riemenschneider *et al.*, 2010). However, the current common chemotherapy agents showed little efficacy in the treatment of primary GBM which develops faster and has worse prognosis compared to secondary GBM (Clarke, Butowski and Chang, 2010; Tabunoki *et al.*, 2012). Therefore, efficient novel therapy for primary GBM is urgently needed. The following sections will

focus on primary GBM treatment. U373MG glioma cell line was used for investigation of the treatment against primary GBM in this project. In the following sections, the term 'GBM' was used to present primary GBM.

Surgery typically is applied after diagnosis of GBM to remove the tumour as much as possible, followed by aggressive treatment, including radiotherapy or chemotherapy or combining of them (Gallego, 2015). TMZ is commonly used in chemotherapy, which is considered having relatively efficient killing effect to GBM cells compared with other drugs, therefore is used in standard treatment following maximal surgical resection (75 mg/m^2 TMZ daily, together with 60 Gy radiotherapy for 6 weeks) (Hart *et al.*, 2013; Khosla, 2016). However, even when aggressive treatment was applied after operation, the neoplasm usually will recur and the prognosis is very dismal (Gallego, 2015). The length of survival is 12-15 month following diagnosis in most cases, and only less than 3%-5% of patients survived longer than 5 years. The median survival without treatment is merely 3-4 months (Omuro and DeAngelis, 2013; Gallego, 2015).

The largest cause of treatment failure is the strong resistance of GBM tumours to conventional therapies, including radiotherapy and chemotherapy. Tumour hypoxia is that tumour cells alter their metabolism to survival under oxygen deficit situation. As tumours grow, the insufficient blood supply and rapid proliferating of tumour cells limit the oxygen diffusing further into core area of the tumour. Therefore, to survive and proliferate under low oxygen condition, those hypoxic tumour cells dramatically changed their signalling pathway and following behaviour, which can lead to the resistance to radiotherapy compared to well-oxygenated cells (Gilkes, Semenza and Wirtz, 2014). Hypoxia is well known to exhibit in portions of GBM tumours. Spontaneous necrosis was frequently found in GBM tumours and considered as result of hypoxia (Brat *et al.*, 2004). In 1994, Rampling et al. proved that hypoxic regions are present in glioblastomas via

directly measuring the oxygen level (varies from 9.5% to 68.5%, pO_2) in tumours from 10 patients (Rampling *et al.*, 1994). Oxygen plays the key role in the cytotoxicity of ionizing radiation. The free electron of the free radical in DNA caused by ionizing radiation, can aggressively react with oxygen then causes covalent modification of DNA leading to damage of tumour cells and alteration of the sensitivity of tumour cells to other DNA damaging agents.

However, under hypoxic conditions, the radical in DNA can be 'neutralized' when obtained hydrogen from non-protein sulfhydryls in tumour cells, which gives glioblastomas strong resistance to ionizing radiation (Brown, 1999). The alteration of signalling pathways in the absence of oxygen, such as hypoxia-inducible factor (HIF-1) and following pathways, also have been indicated that induce resistance to radiotherapy. At present, TMZ has been approved by the US Food and Drug Administration (FDA) and used as standard chemotherapy in GBM treatment. TMZ can alkylate the guanine base of DNA, thus leading to cell damage (Figure 1). Meanwhile, this alkylating agent can be effectively transported through the blood brain barrier (BBB) and get into GBM cells. As seen in Figure 1, TMZ acts a prodrug which is stable at acidic pH but labile above pH 7 and spontaneously breaks down to form monomethyl triazene 5-(3-methyltriazen-1-yl)-imidazole-4-carboxamide (MTIC) (Zhang *et al.*, 2011). MTIC then reacts with water to release 5-aminoimidazole-4-carboxamide (AIC) and the highly reactive methyldiazonium cation which methylates DNA (Tisdale, 1987; Zhang *et al.*, 2011). Although the extracellular pH level in the environment of cancer cells is lower than that around normal cells whereas the acidic products/protons generated during rapid metabolism of cancer cells are actively transported to the extracellular space via Na^+/H^+ exchangers, $Na^+HCO_3^-$ transporters, Cl^-/HCO_3^- exchangers and monocarboxylate transporters (MCT), etc. (Hjelmeland *et al.*, 2011). The average intracellular pH level of

brain tumours was found to be 7.31, slightly higher than normal brain cells (7.24) (Hao, Xu and Li, 2018). In this case, GBM cells possess a more alkaline pH compared with healthy tissue, therefore favouring TMZ activation preferentially within tumour tissue DNA (Rottenberg *et al.*, 1984; Zhang *et al.*, 2011).
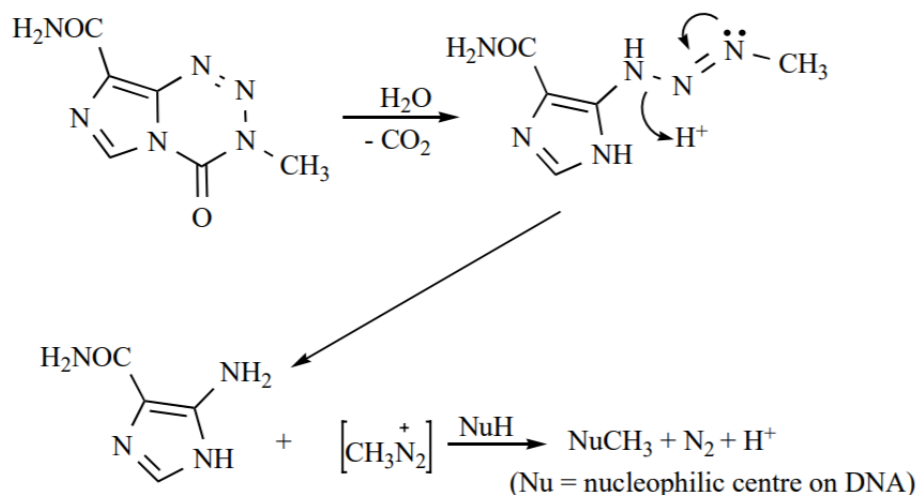
Figure 1. Structure and activation route of prodrug temozolomide (Zhang *et al.*, 2011)*.

However, it has been demonstrated that glioblastomas also present resistance to TMZ treatment (Mirimanoff *et al.*, 2007; Hegi *et al.*, 2008). The enzyme, methylguanine methyltransferase (MGMT), can attach to damaged DNA and obtain the alkyl group from guanine. The alkylated MGMT then will be detached and finally be degraded via ubiquitin/proteasomal system (Zhang *et al.*, 2011). The expression level of MGMT is increased in GBM cells, thus resulting in resistance to TMZ treatment. Meanwhile, it has been found that TMZ has little or no effect on prognosis in up to half GBM (FERNANDES *et al.*, 2017).

Various radiosensitizers, such as oxygen diffusion-enhancing compound trans sodium crocetinate, have been investigated in preclinical and clinical trials with limited success (Gainer *et al.*, 2017). More powerful techniques, molecular targeted therapy (such as HIF-1 inhibitors) and hypoxia-selective drugs, etc. were investigated to beat glioblastomas (HARADA, 2011). However, the limitations of conventional treatment in GMB therapy

haven't been overcome and novel efficient therapeutic methods with low side effects are still urgently needed.

1.3 Plasma

Plasma is one of the four fundamental states of matter which is a form of ionized gas, usually, and accounts for most of the known Universe's matter. Its early stage of biomedical applications is focus on the heat and high temperature of thermal plasma for the purpose of tissue removal, sterilization, and cauterization (Fridman *et al.*, 2008).

1.3.1 Clinical Application of Hot Plasmas

Hot plasmas, also known as high temperature/thermal plasmas, have been widely used for sterilization, blood coagulation, tissue ablation and tumour therapy, etc. The high temperature and kinetic energy generated by thermal plasmas device are utilized to coagulate, cut or ablate tissue surfaces (Heinlin *et al.*, 2010; Gibson and Suslov, 2012). In the mid-1970s, Glover et al. first reported a convenient thermal plasma device with a nozzle that was capable of generating high power density of plasma flow by a low gas flow, which was able to both coagulate and cut tissue and showed that plasma scalpel is effective in cauterizing blood vessels and causes less damage compared with steel/electrosurgical scalpels (Link, Incropera and Glover, 1976). This design rapidly gained ground in surgical operation and has been developed further to invent the PlasmaJet system.

The PlasmaJet system has been used in clinical surgery since 2004, using small scale, high-thermal and high-kinetic argon plasma jet to effectively ablate, coagulate a tissue surface (Roman *et al.*, 2013). The PlasmaJet causes slight thermal tissue damage (seldom more than 600 μm) with the formation of a filmy coagulum (Deb *et al.*, 2010). It has shown safety and high performance in plastic surgery, hepatic surgery, gastroenterology, orthopedics and thoracic surgery (Nezhat and Kho, 2009). More recently, PlasmaJet and

other thermal plasma devices have been investigated as safe and effective modalities for treatment of tumours which are untreatable by surgery (Sagawa *et al.*, 2003; Roman *et al.*, 2013). For instance, using PlasmaJet in ablation of endometrioma showed encouraging recurrence and pregnancy rates compared with the best reported results of endometrioma cystectomy, may be due to the fact that the surgeon can select appropriate degree of completeness of treatment and keep enough normal endometrial tissues by the plasma operation (Roman *et al.*, 2013). Meanwhile, electrically neutral thermal argon plasma technology has been demonstrated that can maximize cancer cell killing effects and decrease tumour burden in several cases of epithelial ovarian cancer (Renaud and Sebastianelli, 2013). In gynecological oncology cases, PlasmaJet also is used to minimize the damage to the underlying tissue when removing secondary tumour from the sensitive or vital structures, such as ureter, bowel and liver (Madhuri *et al.*, 2010).

1.3.2 Cold Atmospheric Plasma

Technological advances have allowed researchers to generate cold atmospheric plasma which possesses ambient temperatures and approximately 1.0 atmospheric pressure, compared to hot plasma. Even though hot and cold plasma are both generated by adding energy to a gas, releasing electrons from nuclei of atoms, electrons in cold plasma can be at several million K whereas the nucleus of atoms are at room temperature (thermodynamic disequilibrium state). These are known as cold (or non-thermal/low temperature) atmospheric plasmas. The application of cold atmospheric plasma allows direct treatment of cells or live tissues with ionised gases without risking thermal injury. Cold atmospheric plasma (CAP) has been investigated as a promising technique for therapies in various fields. Known biomedical applications of CAP include cancer therapy (Keidar *et al.*, 2011), sterilization (Zelzer *et al.*, 2012), wound healing (Isbary *et al.*, 2012) blood coagulation (Kalghatgi *et al.*, 2007) and viral destruction (Shi *et al.*,

2012). CAP has also been investigated as a novel method to enhance cell transfection (Leduc *et al.*, 2009) and promote cell proliferation (Kalghatgi *et al.*, 2010).

CAP generates a unique physical and chemical environment activating short- and long-lived reactive nitrogen species (RNS, e.g. peroxinitrite (ONOO-), nitric oxide radicals (NO)) and reactive oxygen species (ROS, e.g. hydroxyl radicals (OH), oxygen atoms (O), oxygen negative ions (O_2^-)), photons as well as generation of heat, pressure gradients, charged particles, and electrostatic and electromagnetic fields (Stoffels, Kieft and Sladek, 2003; Kong, Keidar and Ostrikov, 2011; Babington *et al.*, 2015), many of which are known to induce biological effects. For example, peroxinitrite (ONOO-), which also occurs naturally (Babington *et al.*, 2015), can initiate lipid peroxidation reactions and help to protect against infection during inflammation (Patel *et al.*, 1999) whereas ROS can cause damage to DNA and induce apoptosis by activating the cell death receptors in the TNF/NGF-family (Stoffels, Sakiyama and Graves, 2008). These high flux of ROS also have significant effect in inactivating fungi, virus and bacteria (Fridman *et al.*, 2008; Kong *et al.*, 2009; Park *et al.*, 2014).
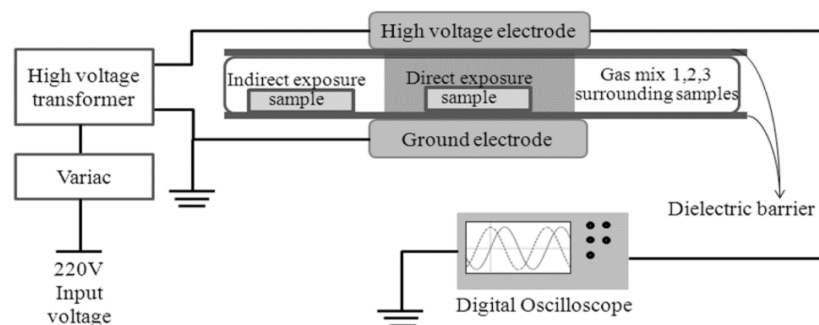
Figure 2. The dielectric barrier discharge (DBD) plasma source (Lu *et al.*, 2014)*.*

CAP can be generated by several different principles such as dielectric barrier discharge (DBD) plasma sources, atmospheric pressure plasma jet and corona discharge plasma sources (Weltmann *et al.*, 2008; Hähnel, Von Woedtke and Weltmann, 2010; Ehlbeck *et al.*, 2011; Wu *et al.*, 2011; Park *et al.*, 2012; Haertel *et al.*, 2014; Babington *et al.*, 2015).

17

Different gases such as air, argon, helium, oxygen and nitrogen can be used which alter the physical and chemical properties of the CAP (Babington *et al.*, 2015). Cold atmospheric plasmas can be divided into three types in accordance with the interaction with target cells / tissues: direct plasmas, indirect plasmas and hybrid plasmas (Kong *et al.*, 2009).

The dielectric barrier discharge (DBD) plasma source is known as the most widely used direct plasma. The electrical discharge is generated between two electrodes separated by a dielectric barrier. The dielectric cannot pass direct current and prevents the rise of arcing after breakdown (Kuchenbecker *et al.*, 2009). The prototype DIT-120, DBD plasma source used in this project, consists of two circular aluminium plate electrodes over perspex dielectric layers, a high voltage transformer and a voltage variac (Figure 2). The applied voltage to the electrode is obtained from the voltage transformer (Lu *et al.*, 2014; Pankaj *et al.*, 2014). The two electrodes are separated by a dielectric barrier and the discharge is generated between these two electrodes to ionize gas and create plasma (Babington *et al.*, 2015). The treated sample has direct contact with all agents in DBD.

The main difference between indirect plasmas and direct plasma is that the plasmas generated between two electrodes are then mixed into a gas flow to treat samples remotely in indirect plasmas devices. This technology is also called the atmospheric pressure plasma jet, Figure 3 (Cullen and Milosavljević, 2015), and has developed various devices from large 'plasma torches' to very narrow 'micro plasma jet' (Laroussi, 2002; Kieft, Laan and Stoffels, 2004; Sladek and Stoffels, 2005; H. W. Lee et al., 2009; Kong et al., 2009; Babington et al., 2015) . Corona discharge plasma source is also known as 'barrier coronal discharges (BCD)', BCD introduce a grounded wire mesh electrode and combine the current-free property of indirect plasmas and the production technique of direct plasmas (Morfill et al., 2009). As seen in Figure 4, the BCD device can be safely applied

on human body for disinfection.
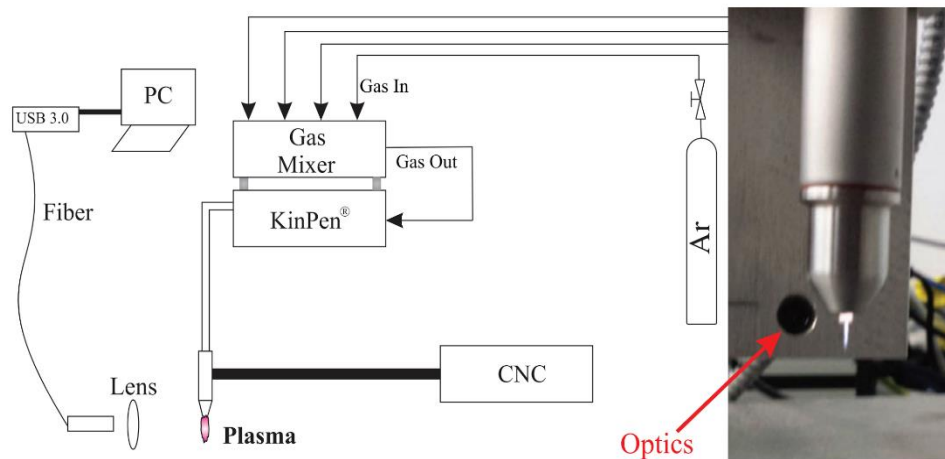
Figure 3. kINPen® MED^{TM} plasma source.

*Photograph of **kINPen® MED**^{TM} plasma source (right) with the schematic of the entire system (left). It's a commercially available plasma jet with pure argon as a carrier gas* (Cullen and Milosavljević, 2015).
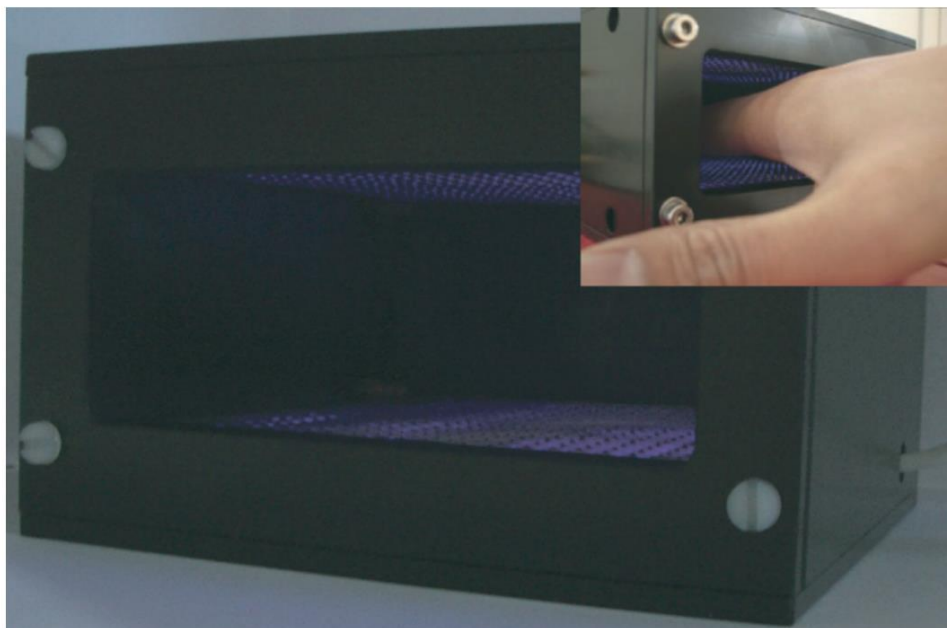
Figure 4. 'HandPlaSter', a prototype of corona discharge plasma source (Morfill *et al.*, 2009)**.**

Cold atmospheric plasmas have been proved to have various effects on mammalian cells, such as stimulating proliferation or inducing proliferation arrest, necrosis and apoptosis. All these responses are dependent on the type and dose of CAP and the type of cell being

treated (Kim et al., 2010; Kalghatgi et al., 2011). At present, it is promising that there are a great variety of CAP generating prototypes and commercial cold atmospheric plasma devices. With different devices, by alternation of gas types, voltage, frequent and current of energy input, etc., the dose and location of applied CAP can be precisely and easily controlled to induce specific reaction to targeted area (Adhikari et al., 2020). Most importantly, cancer cells are generally sensitive to low doses of CAP and can subsequently undergo apoptosis. These doses often do not produce any measurable cytotoxic effect on corresponding normal cells (Ahn et al., 2011; Keidar et al., 2011; Siu et al., 2015). As described above, the wide range and high amounts of reactive oxygen species and reactive nitrogen species (ROS/RNS) generated by plasma were proposed to play the major role in the selective cytotoxicity (Walk et al., 2013). It also showed that CAP can likely induce cancer cells to produce more of their own ROS/RNS (Keidar et al., 2011). However, the exact mechanism of CAP is not fully understood. Previous research has proposed several mechanisms for the selective toxicity of cold atmospheric plasmas, including membrane disruption, mitochondrial dysfunction, DNA damage, deregulation of signal pathways, protein up/down regulation, cell cycle arrest and finally apoptosis/necrosis/ autophagy.

CAP have been demonstrated to induce the S-nitrosylation of SH-groups in proteins and thereby cause inactivation of proteins function (Ishaq, Evans and Ostrikov, 2014). In addition, ROS can cause lipid peroxidation by interacting with unsaturated fatty acid. It has been found that CAP treatment could cause the loss of cancer cell membrane integrity, induce the leakage of cellular content (Siu *et al.*, 2015) and promote the transmission of ROS/RNS into cells by S-nitrosylation, lipid peroxidation and creating rifts in the membrane (Halliwell, 1991; Rao, Hale and Ormrod, 1995; Bestwick *et al.*, 2001; Babington *et al.*, 2015). Nina Recek et. al have studied the differential effects of CAP on

cell membrane of normal human astrocytes and human glioblastoma cells by atomic force microscopy (Recek *et al.*, 2015). CAP didn't harm E6/E7 cells but only caused temporary disappearance of microvilli structure on cell membrane, whereas plasma treatment caused selective apoptotic effect on the GBM cells along with granular elevations and bigger clusters were observed on the surface of GBM cells (Recek *et al.*, 2015). These different effects on cell membrane may indicate the potential mechanisms of selective toxicity of CAP (Recek *et al.*, 2015). In the meantime, the cold atmospheric plasma treatment has been shown to cause enhanced mitochondrial transmembrane permeability and possible release of proapoptotic factors by depolarizing the mitochondrial membrane potential via generation of free radicals. And the plasma-induced cell apoptosis has been proved to be mediated partially by mitochondria-dependent caspase cascade (Ahn *et al.*, 2011).

After CAP treatment, it was found that cellular DNA was damaged with increasing intracellular levels of ROS (Babington *et al.*, 2015). In addition, plasma treatment has been proved to selectively induce the deregulation of several genes in cancer cells. These genes are intimately associated with multiple pathways, including cell adhesion, cell proliferation, growth regulation and cell death. Some of these pathways are involved in cancer processes and their deregulation may be the potential reason of tumour ablation while treating CAP. Notably, the genes related with oxidative stress and apoptotic pathways were significantly deregulated in tumour cells by plasma treatment, which could potentially help explain the plasma-induced apoptosis mechanism (Keidar *et al.*, 2011).

At present stage, the short-lived and long-lived reactive species generated by cold atmospheric plasma are considered playing key role in selective cytotoxicity to cancer cells. In the following section, the interaction between reactive species and tumour cells

will be detailed introduced.

1.4 The Intracellular Reactive Species and Signalling Pathway Affected by CAP

Reactive oxygen species (ROS) are a group of highly reactive molecules that have been identified as important regulators of many signaling pathway. Moderate levels of ROS are generated during normal cellular metabolism progress and participate in cellular signalling and several cellular functions by reversibly oxidizing/modifying protein structure (Ray, Huang and Tsuji, 2012; Perillo *et al.*, 2020). Meanwhile, uncontrolled ROS have long been known as initiating tumourigenesis, which can cause oxidative damage to lipid, proteins and DNA or disrupt oxidative signalling to promote cancer-causing mutations and cell proliferation (Perillo *et al.*, 2020). Some epidemiological evidence exists for this, including the observation that a diet high in natural anti-oxidants is generally associated with lower incidence of various cancers. Thereby, antioxidant food and supplements have been considered as weapon to prevent cancer for a long term.

As understanding deepens, ROS were found to be a double-edged sword to cancer cells. Evidence shows that higher level of ROS were generated in cancer cells, compared to normal cells, due to higher metabolic activities and more rapid proliferation of transformed cells (Schumacker, 2006). Hence, the cellular antioxidant system works under heavier load to protect tumour cells from oxidative stress, suggesting it may be possible to selectively eliminate them with inducers of tumour ROS (Trachootham, Alexandre and Huang, 2009).

One hypothesis for the increased production of ROS in tumour cells is the difference in metabolism between normal and cancer cells. Cancer cells require more biomass synthesis per unit time due to the unregulated and relatively rapid cell growth and proliferation (Harris *et al.*, 2015). It has been found a phenomenon called "the Warburg

effect" that cancer cells rely primarily on glycolysis and lactic acid fermentation to generate energy, whereas most other nucleated cells generate adenosine triphosphate (ATP) by oxidative phosphorylation (Vander Heiden, Cantley and Thompson, 2009). To deal with higher intracellular ROS levels, tumour cells synthesise nicotinamide adenine dinucleotide phosphate (NADPH). NADPH is utilized as a reducing equivalent to reduce thioredoxins (TRX), peptides that in turn reduce oxidized proteins such as peroxiredoxins, a family of hydrogen peroxide-scavenging enzymes (Sabharwal and Schumacker, 2014). NADPH is also involved in the generation of the antioxidant glutathione (GSH), an important tripeptide in antioxidant systems (Harris *et al.*, 2015). Despite the increased expression of antioxidant systems, cancer cells generally have a higher baseline intracellular ROS which strains the antioxidant capacity of tumour cells to deal with additional oxidative stressors (Harris *et al.*, 2015). With the excessive intracellular levels of ROS, lipids, proteins and DNA can be damaged in cancer cells, leading to lipid peroxidation-initiated oxidative stress, inhibition of phosphatases, alternation of cytoplasmic and nuclear signaling, disruption of epigenetic modulators, etc., and eventually apoptosis, autophagy or ferroptosis of cancer cells (Perillo *et al.*, 2020).

Therefore, the reactive species generated by CAP can be selective toxic to tumour cells which can be exploited for efficient, specific and low side effects anticancer strategies. It has been shown that CAP treatment regulates possible signalling cascades implicated in cancer cell death, such as stress kinases pathways and growth signalling pathways, etc. Meanwhile, it also has been found that the interaction of CAP with proteins and interrupting of cell cycle play important roles in CAP-induced selective cell death, as detailed below.

1.4.1 Stress Kinase Pathways

Mitogen-activated protein kinase (MAPK or MAP kinase) is involved in the regulation

of various cellular functions, including apoptosis, differentiation, gene expression, mitosis and proliferation. c-Jun N-terminal kinase (JNK) is also involved in multiple pathways which are responsive to apoptosis, differentiation and stress stimulation, including ROS, ultraviolet radiation, heat and osmotic shock. (Tobiume *et al.*, 2001). Elevated accumulation of intracellular ROS was found to activate p38α MAPK/JNK by the activity of Apoptosis signalling regulating kinase 1 (ASK1) (Elenitoba-Johnson *et al.*, 2003; S. P. Li *et al.*, 2003). ASK1 is one of the regulators of pathways involving p38α MAPK and JNK. Then p38α MAPK results in the activation of several tumour suppressors, including protein 53 (P53) (Bulavin and Fornace, 2004), Cdc25 phosphatases (Manke *et al.*, 2005) and pro-apoptotic members of B-cell lymphoma 2 (Bcl2) family (Ishaq, Evans and Ostrikov, 2014), leading to caspases-dependent apoptosis of cancer cells (Figure 5). Inhibitory members of Bcl-2 family are capable of inhibiting the release of cytochrome c from mitochondria and in turn lead to the inhibition of caspases in the apoptosis pathway (Küpper *et al.*, 2014). P53 is able to downregulate the production of anti-apoptotic Bcl-2 members   promote phosphorylation of the inhibitory Bcl-2, then stimulate caspases pathway (Ling *et al.*, 2002) (Figure 5). Phosphorylation of inhibitory Bcl-2 members has been observed after CAP treatment in a study using Hela and lung cancer cells (Ahn *et al.*, 2014).
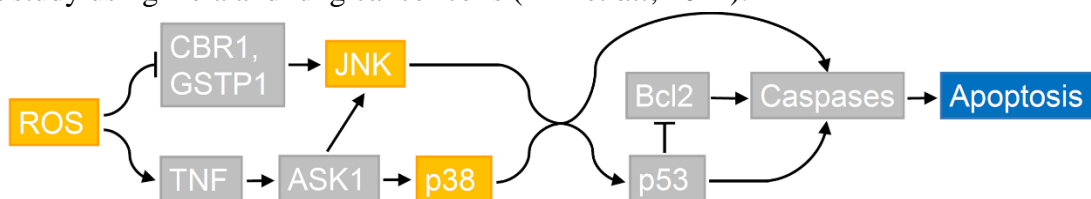
Figure 5. *CAP affected stress kinase pathway.*

Excessive intracellular ROS generated by plasma can stimulate TNF pathway and inhibit CBR1 and GSTP1, leading to the activation of downstream JNK or p38α MAPK, which finally induces caspase-dependent tumour cell apoptosis.

Similarly, the signalling cascade of the stress-activated protein kinase JNK is important

and involved in cellular environment adaptiveness and several physiological processes, including inflammation, proliferation and apoptosis (Ishaq, Evans and Ostrikov, 2014). The augmented level of intracellular ROS also has been indicated that may activate JNKs by blocking stress-response proteins such as Glutathione S-transferase pi 1 (GSTP1) and carbonyl reductase 1 (CBR1), leading to tumour cells suppression and growth arrest by stabilizing p53 and stimulating the caspase cascade (Ishaq, Evans and Ostrikov, 2014) (Figure 5). There's evidence that pre-treatment of HeLa cells with antioxidants, JNK and p38 inhibitors, and JNK and p38 siRNA inhibits mitochondrial membrane depolarization and reduced plasma-induced cancer cell death (Ahn *et al.*, 2014).

The exact mechanisms for activation of JNK and P38 is not fully clear, although in a study using melanoma cells, upregulation of TNFR1 and TNFα was observed when incubated with CAP. This was accompanied by an increase in active caspases and could be reversed using TNFR1 blocking antibodies. Interestingly, increased expression of TNFR1 and TNFα was only observed in malignant melanoma cells and not in melanocytes (Ishaq *et al.*, 2014).

1.4.2 Growth Signalling Pathways

CAP can directly interact with growth signalling pathways. For example, the 21-kDa protein (p21), known as a tumour suppressor encoded by gene WAF1/CIP1, was found to inhibit the activities of cyclin-dependent kinase which is required for progression of the cell cycle (Wade Harper *et al.*, 1993). The expression of p21 provided another pathway to inhibit tumour growth whilst normal p53 function is lost in half of all tumours. It has been found that excessive level of intracellular ROS induces the expression of p21 as a consequence of oxidative damage, which is independent of p53 (Russo *et al.*, 1995). Secondary GBM often shows p53 mutation whereas primary GBM mainly contain EGFR amplification as the principal mutation and rarely present p53 genetic alteration

(Watanabe *et al.*, 1996). The EGFRvIII, a ligand-independent constitutively active mutant of EGFR which is often associated in primary GBM, is keeping activating the phosphatidylinositol 3-kinase (PI3K)/v-akt murine thymoma viral oncogene homolog (AKT) signaling pathway, thus promotes the survival of primary GBM cells (Li *et al.*, 2004; Tabunoki *et al.*, 2012). PI3K/AKT pathway is known as a oncogenic signalling disturbed in many human tumours, which plays an important role in tumour development and affect the response of cancer cells to tumour treatment (Fresno Vara *et al.*, 2004). PI3K binds to the growth factor receptors on cell membrane while the receptor is activated, and then converted to phosphatidylinositol-3,4,5-trisphosphate (PIP3). PIP3 induces the activation of several signalling proteins, including PKB/AKT, subsequently leading to survival, growth and proliferation of cells via various signalling pathways (Fresno Vara *et al.*, 2004). AKT phosphorylates and inhibits p21 by sequestering it in the cytoplasm (Zhou *et al.*, 2001). Therefore, excessive intracellular ROS generated by plasma can potentially activate p21, counteract the PI3K/AKT pathway and control tumour cell growth (Ishaq, Evans and Ostrikov, 2014) (Figure 6).
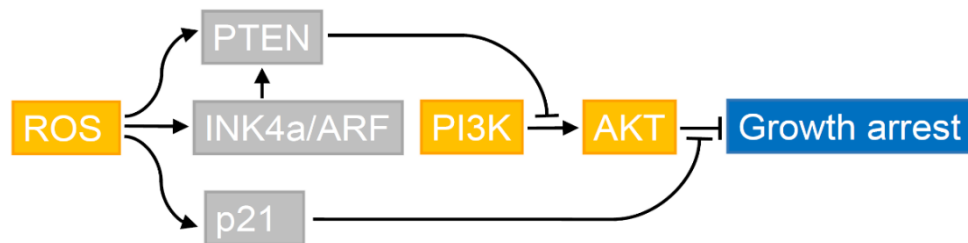
Figure 6. Cold plasma affected growth signalling pathway.

The induced generation of ROS can counteract PI3K/AKT pathway and induce growth arrest of cancer cells via activation of p21, PTEN and INK4a/ARF.

Intracellular ROS is also capable of inhibiting PI3K/AKT by activating several other tumour suppressors, including phosphatase and tensin homolog (PTEN) and INK4a/ARF (Ishaq, Evans and Ostrikov, 2014). PTEN downregulates the level of PIP3 by dephosphorylating it and inhibits the phosphorylation/activity of AKT(Stambolic *et al.*,

1998). INK4a/ARF encodes two proteins p16 and p14 respectively, which are required for the activation of PTEN (Maehama and Dixon, 1999; Uhrbom *et al.*, 2002).

1.4.3 Protein Interactions

CAP can directly modify cellular enzymes and structural proteins. For instance, CAP are able to enhance lipase activity (Li *et al.*, 2011), inactivate lysozyme in aqueous solution (Takai *et al.*, 2012), decrease peroxidase (POD) activity in fruits and vegetables (Pankaj, Misra and Cullen, 2013), and inactivate lactate dehydrogenase (LDH) in the phosphate buffer solution (PBS) (Zhang *et al.*, 2015). The changes of protein activity could be mainly due to the interaction between protein and the long-lived reactive species (RS) generated by CAP. These long-lived RS, such as ozone (O_3) and hydrogen peroxide (H_2O_2) can modify many amino acids (Cataldo, 2005) and denature proteins by oxidizing them (Nordberg and Arnér, 2001). Therefore, the modification of amino acids can lead to the secondary structure changes or protein-protein cross-linkage. The structure changes in the active centre will significantly affect protein activity and protein-protein cross-linkage may cause the molecular aggregation between proteins and then decrease the amount of viable exposed active sites (Zhang *et al.*, 2015). Especially, cysteine was found to be the most sensitive of the 20 amino acids to oxidizer. The oxidation of thiol group on the cysteine residue can affect the function of proteins, including several antioxidant small molecules or enzymes, including thioredoxin, peroxiredoxin and glutathione peroxidase, which further reduces the capacity of the antioxidant system of targeted cancer cells and facilitates the cytotoxicity of extracellular ROS generated by CAP treatment (Yan *et al.*, 2015).

1.5   Nanoparticles in Cancer Therapy

Cancer treatment can be affected by a combination of physical, chemical and biological technologies. Due to the considerable variation between types and status of tumours and

individual patients, the efficiency of cancer therapy is difficult to guarantee and commonly associated with side effects and off-target toxicity can be daunting (Chen *et al.*, 2017). However, recent technological advances have led to the development of new nanotechnological approaches for cancer therapies, which promise high-precision ways to beat cancer. Nanotechnology can be combined with chemotherapy to facilitate targeted delivery into cancer tissue with high specificity and efficacy (Ferrari, 2005). Nanoplatforms allow more accurate, non-invasive and real-time cancer diagnosis and monitoring during therapy using magnetic resonance imaging, ultrasonography, etc. (Alexis *et al.*, 2008; Baetke, Lammers and Kiessling, 2015; Zaimy *et al.*, 2017) Adjuvant nanotechnological devices are used in cancer interventions such as radiotherapy (Wu *et al.*, 2016), photodynamic therapy (Clement *et al.*, 2017) and sonodynamic therapy (H. Xu *et al.*, 2016), which are capable of achieving considerably higher precision of treatment and reduced side effects. After decades of developing the understanding of nanotechnology, cancer-related nano-treatments have undergone extensive preclinical and clinical-trial studies and shown promising results (Chen *et al.*, 2017). Bregoli et al. have summarised the current state of the art of nanomedicines undergoing clinical trial and clinically-approved nanomedicines for cancer therapies (Bregoli *et al.*, 2016).

The traditional definition of a nanotechnological device for cancer treatment is that the essential components of the device or the device itself are artificial, and have at least one dimension in the 1-100 nm range (Whitesides, 2003; Ferrari, 2005). It has been suggested that there should be less emphasis on the exact definition of size which could be extended to a range of 1–1,000 nm, and define the approaches to bionanotechnology according to their function and purpose (Ferrari, 2005). According this definition, nanotechnologies used in cancer treatment include drug-delivery, therapeutic nanovectors, nano-sensitizers, diagnostic agents and macroscopic devices with essential nanocomponents such as

microarrays/ 'nanoarrays', nanocantilever arrays and silicon nanowires for highly-specific and highly-efficient molecular detection and diagnostic (Ferrari, 2005). The recent advances and use of these emerging nanotechnological treatments for cancer is briefly reviewed in this section with an emphasis on nanotechnologies used for drug-delivery.

The applications of nanoparticles in pharmacology have been investigated over the last three decades and a new generation of vehicles for delivery of biomedical compounds has emerged (Couvreur and Vauthier, 2006). Nano-scale carriers have been exploited for drug delivery, drug targeting, histological engineering, tissue targeting and labelling (Kong, Keidar and Ostrikov, 2011). The evolution of nanotechnology enables researchers to synthesize a wide variety of nanoparticles with distinct functions and characteristics. Such nanomaterials can be functionalised with molecular and imaging probes or bioactive compounds which can be conjugated, linked, coated or adsorbed to them, in order to implement specific functions (Kong, Keidar and Ostrikov, 2011).

For cancer therapy, nanoparticles have been demonstrated to provide site-specific delivery by incorporation of various targeted ligands to bind to the desired site or utilizing stimuli-responsive strategies. Targeted ligands can include various compounds (e.g. antibodies, peptides, hormones, receptor ligands, nucleic acids and lipid derivatives) (Eckmann *et al.*, 2014). Functionalized nanoparticles are capable of responding to one or more physical, chemical, biochemical or environmental stimuli, including osmotic pressure, hydrodynamic pressure, vapor pressure, mechanical force, magnetics, sonophoresis, iontophoresis, hydration, electricity, pH, salt concentration, hydrolysis, enzyme, temperature, light and hypoxia, etc. (Bennet and Kim, 2014) In addition, nanocarriers can prolong circulation time and are incapable of diffusing across non-fenestrated endothelium, thus enabling accumulation in the tumour tissues, resulting in

enhanced permeation and retention (EPR). Notably, however, it has been pointed out that precise prognosis should be based on comprehensive characterisation of an individual tumour, rather than broadly on the EPR effect (Chen *et al.*, 2017).

The term nanoparticle can encompass a variety of materials, including liposomes, nanogels and polymer-based nanoparticles, silicon and silica nanoparticles, dendrimers, metal-based nanoparticles, and combinations of the above. This section reviews the recent developments of nanoparticles for effective cancer treatment and provides related content that can be used for reference.

1.5.1 Liposomes

Liposome platforms have attracted considerable attention from the academic and clinical arenas and have become one of the most studied biomaterial nanoparticles, due to the fact that liposomes can significantly improve the efficiency of a drug by increasing its solubility, overcoming resistance, controlling its targeted release and modifying its biocompatibility, bioavailability and safety profile. There have been several clinically approved liposome-based nanomedicines for cancer therapies, such as Doxil, Myocet, Mepact, Dauno Xome, Depocyt, Marqibo and MEPACT (Bregoli *et al.*, 2016). Moreover, advances in liposome research have led to the emergence of hundreds, even thousands, of different functional liposomes for various tumours, which have been tested in preclinical research and clinical trials (Ferrari, 2005; Bregoli *et al.*, 2016). According to their number of bilayer membranes, liposomes are grouped into unilamellar and multilamellar vesicles (Zununi Vahed *et al.*, 2017). Unilamellar vesicles have a single lipid bilayer, while multilamellar vesicles consist of several unilamellar vesicles surrounded by lipid bilayers. On the another hand, according to the formulation, liposomes can be grouped into several types, including PEGylated stealth liposomes (Couvreur and Vauthier, 2006), immunoliposomes (Tila *et al.*, 2015), lipoplexes (Lonez,

Vandenbranden and Ruysschaert, 2008), fusogenic liposomes (Yuba *et al.*, 2010), stimuli-responsive liposomes (Zununi Vahed *et al.*, 2017) and combinations of the above. (Couvreur and Vauthier, 2006)

Nanoparticles, including liposomes, can be rapidly cleared from the bloodstream by the mononuclear phagocytic system (MPS), significantly decreasing in-vivo circulation half-life and the delivery efficiency of drugs (Bregoli *et al.*, 2016). Therefore, for a longer circulation time, it is critical to protect liposomes from MPS detection. Doxil, the first clinical approved nanomedicine for cancer therapy, is made of polyethylene glycol-coated (PEGylated) liposomes containing anti-cancer drug doxorubicin (Bregoli *et al.*, 2016). Coating liposomes with polyethylene glycol, which is a class of biocompatible, inert and hydrophilic polymer, results in significant increases of the circulation half-life, from several hours to around 45 h, achieving sustained and prolonged drug delivery, and promoting tumour accumulation of liposomes (Couvreur and Vauthier, 2006). PEGylated stealth liposomes have been widely applied in the clinic and are easily functionalised with other functional features, such as stimuli-responses and ligand targeting (Tila *et al.*, 2015). Alternatively, sustained release of a drug from MPS cells, more complex liposomal formulations (e.g. small size, net neutral charge, incorporation of cholesterols and lipids), or drug release into specific areas, such as the cerebrospinal fluid, non-PEGylated liposomes have been demonstrated to result in an increase in the tumour exposure to the drug (Bregoli *et al.*, 2016).

Attaching targeting ligands to the liposome surface is now a well-established and widely used feature in liposome design. Liposomes functionalised with antibodies, also known as immunoliposomes, can carry a drug dose and selectively bind to a chosen tumour site, whilst antibody fragments, glycoproteins, peptides, vitamins and oligonucleotide aptamers can also be used as targeting ligands (Zalipsky *et al.*, 1996; Park *et al.*, 1997;

Mastrobattista, Koning and Storm, 1999; Gunawan and Auguste, 2010; Tila *et al.*, 2015). Gene therapies have been considered as a novel and promising method for cancer treatment. Lipoplexes (cationic liposomes) have been investigated as an attractive gene delivery system that are simple to synthesize and control, have high delivery efficiency and can enhance the stability of nucleic acid therapeutics (Tila *et al.*, 2015). Cationic lipids used in lipoplexes are comprised of a cationic head and hydrophobic domain and have the capacity to form particulate complexes in the liposomal membrane by interacting with nucleic acids therapeutics (negatively charged), including plasmid DNA (pDNA), small interfering RNA (siRNA) or micro-RNA (Tila *et al.*, 2015).

Fusogenic liposomes are able to fuse with cellular membranes and directly release encapsulated drugs into the cytoplasm or targeted cell organelles, significantly enhancing the cellular uptake of drugs, avoiding lysosomal degradation, and counteracting the drug resistance of cancer cells (Kunisawa *et al.*, 2005; Tila *et al.*, 2015). Membrane fusion is achieved by the specific interactions between the membrane receptors and the liposomes or the membrane-associated proteins or peptides that are contained within the liposomes. Moreover, negatively charged phospholipids promote the fusion in the presence of calcium in some types of fusogenic liposomes (Malaekeh-Nikouei *et al.*, 2008; Yuba *et al.*, 2010; Watarai *et al.*, 2014). The formation of lipid bilayers and incorporation of special lipids (e.g. dioleoyl phosphatidylethanolamine (DOPE)) also promote the membrane fusion reaction and enhance the release of the encapsulated drugs (Tila *et al.*, 2015).

Functional liposomes have been used for the improvement of circulation time and stability of drugs, specifically targeting cancer cells, and promoting drug delivery. More recently, the maturation of stimuli-responsive liposome technologies has yielded precise control of drug release, which provides greater individualised treatment with lower

undesirable side effects (Deshpande, Biswas and Torchilin, 2013). Several types of drug release triggers have been used in liposome-based delivery systems, including temperature, pH level, enzymes, light, ultrasound, electromagnetic waves and magnetic fields. (Zununi Vahed *et al.*, 2017)

Tumor cells are efficient at maintaining plasmalemmal pH gradients, whereas the protons generated during the metabolism of cancer cells are exported to the extracellular space efficiently and the extracellular bicarbonate is taken up by cancer cells, following re-export of CO_2, for increasing intracellular pH (Chiche *et al.*, 2012). Therefore, the extracellular pH level in the environment of cancer cells is lower than that around normal cells (pH 6.2-6.8 vs pH 7.35-7.45). Additionally, in endosomal vesicles, the pH is lower than 5 (Moussa, Martins and Husseini, 2015). pH-sensitive liposomes (PSLs) are stable at the neutral pH of blood and healthy tissues, but are designed to become destabilized and release encapsulated drugs in the vicinity of cancer cells and/or in endosomes (Karanth and Murthy, 2007). The most developed class of PSLs are designed to be triggered after endocytosis and several mechanisms may be involved: direct release of drugs into the cytosol due to the fusion of the endosome and liposome membranes which is induced via pH changes; drug leakage into the cytosol because of the pH-induced destabilization of liposomal membranes which will cause the destabilization of endosomal membranes; release of drugs inside the endosomes due to the pH-induced destabilisation of the liposomes, followed by the diffusion of the molecules into the cytosol (Moussa, Martins and Husseini, 2015). There are several classes of materials used in the formulation of different PSLs, including polymorphic lipids combined with amphiphilic compounds that contain an acidic group, lipid derivatives that have pH-sensitive chemical bond (e.g. N-acylated aminophospholipid derivatives and plasmalogens), reconstituted fusion proteins or peptides that are pH-sensitive and able to

destabilise the membrane of liposomes in acidic environments, and pH-titratable polymers, which change conformations at low pH, as recently reviewed by Moussa et al. (Moussa, Martins and Husseini, 2015)

Thermo-sensitive liposomes (TSLs) are sensitive to temperature, due to their specific chemical composition. For example, some types of liposomes consist of lipids (e.g. dipalmitoyl phosphatidylcholine) that begin to melt when the temperature exceeds their thermal threshold, whereupon the surface of the liposomes becomes porous and the encapsulated drug is released (Moussa, Martins and Husseini, 2015). The increase of local temperature, known as hyperthermia, can be induced via pathological status or external triggers such as light, ultrasound, microwave or magnetic fields (Moussa, Martins and Husseini, 2015; Tila *et al.*, 2015). Optimisation of the hyperthermic effect allows precise control over the amplitude and location of the temperature rise in targeted cancer tissues. Therefore, TSLs which are stable at the temperature of the human body (37°C on average), can be triggered to release the encapsulated molecules at targeted sites by hyperthermia (about 39-43°C) to achieve greater therapeutic effect and reduced side effects (Ta and Porter, 2013; Moussa, Martins and Husseini, 2015).

Moreover, liposomes can be designed to be sensitive to certain enzymes that only have high activity at the tumour site, such as lipases, cancer-associated proteases and phospholipases (de la Rica, Aili and Stevens, 2012; Arouri *et al.*, 2013; Moussa, Martins and Husseini, 2015). There are several classes of enzyme-sensitive liposomes, chemically modified with different molecules (e.g. lipopolymers (Arouri *et al.*, 2013), small peptides and phosphorylated synthetic estrogen, etc.(Bibi *et al.*, 2012)) that can specifically respond to certain enzyme levels above a threshold.

Some types of liposomes are capable of absorbing the energy of certain external triggers (e.g. light, ultrasound, electromagnetic waves or magnetic fields, etc.) and subsequently

converting it to heat, causing a localised hyperthermia that effects the liposomes and induces the release of drugs (Moussa, Martins and Husseini, 2015). These external triggers also can be used to directly affect the liposomes. For instance, light can induce changes in the form of photosensitive lipids, which are chemically modified, and change the membrane permeability (Anderson and Thompson, 1992). Ultrasound is able to induce the rupture of microbubbles at target sites, known as transient cavitation. The collapse of microbubbles produces enormous localised heat and pressure waves, which can cause the disruption of the liposomal and/or cell membranes, consequently allowing the release and permeation of drugs (Hernot and Klibanov, 2008).

Additionally, liposomal platforms which are capable of co-delivering combinatorial drugs bring a paradigm shift in tumour therapy (Hu, Aryal and Zhang, 2010). Several classes of liposome-based drug combinations have been reported, including the co-delivery of chemotherapeutic drugs, the co-delivery of chemosensitizers and chemotherapies, and the co-delivery of siRNA and chemotherapies (Mayer *et al.*, 2006; Saad, Garbuzenko and Minko, 2008; Hu and Zhang, 2010). The combination of drugs can achieve greater synergistic activity by loading them into liposomes at optimised molar ratios and selecting appropriate encapsulation schemes (Hu, Aryal and Zhang, 2010). For example, multiple hydrophilic drugs can be encapsulated in liposomes; lipophilic drugs can be partitioned into the membrane of liposomes; and negatively charged oligonucleotide drugs (e.g. siRNA) are able to bind to the positively charged liposomal surface (Hu, Aryal and Zhang, 2010).

1.5.2 Nanogels and Polymeric Nanoparticles

Polymeric nanoparticles are nano-sized colloidal particles and have been extensively explored for drug delivery for cancer therapies. Among the various materials, designs and synthesis methods, the polymeric nanoparticles studied most commonly consist of a

hydrophobic polymer-based core containing anticancer drugs and a hydrophilic outer shell, which ultimately enabled longer persistence and systemic circulation time in the bloodstream, leading to further accumulation of nanoparticles in cancer tissue (Masood, 2016). Alternatively, there has also been increasing interest in using nanosized hydrophilic cross-linked polymer networks, also termed as nanogels, for drug delivery (Sivaram *et al.*, 2015; Chan and Almutairi, 2016).

Polyhydroxyalkanoates (PHAs) (Li and Loh, 2017), cyclodextrins (CDs) (Duchene, Cavalli and Gref, 2016) and poly-(lactide-co-glycolic acid) (PLGA) (Katiyar *et al.*, 2016) are the most commonly used polymer materials for the core fabrication (Masood, 2016). Meanwhile, nontoxic hydrophilic outer shells provide outstanding blood biocompatibility, such as , polyvinyl alcohol (PVA), PEG and monomethoxy poly-(ethylene glycol) (mPEG), which has also been widely applied in surface modification of other kinds of nanoparticles, such as liposomes and gold nanoparticles (Masood, 2016). The reader is referred to (Duchene, Cavalli and Gref, 2016; Masood, 2016; Li and Loh, 2017) for an in-depth investigation and discussion of recent advanced PHAs, CDs and PLGA-based polymeric nanoparticles used for cancer treatment.

Nanogels are hydrophilic nanosized cross-linked polymer networks, also called hydrogel nanoparticles (Lux *et al.*, 2013; Sivaram *et al.*, 2015; Chan and Almutairi, 2016). In the last decade, there has been increasing interest in the applications of nanogels as drug carriers and imaging agents (Maya *et al.*, 2013; Sultana *et al.*, 2013; Sivaram *et al.*, 2015). Nanogels have unique utilities and properties including:

1. high biocompatibility on account of the high water content and living tissue-like physical properties and they are easily biodistributed by intravenous injection (Chan and Almutairi, 2016; Soni and Yadav, 2016).

2. the ability to selectively respond to stimulation, including changes of pH, ionic

content, biomolecules, magnetic field, light and temperature, which is important in specific drug delivery and responsive imaging (Stuart *et al.*, 2010; Eckmann *et al.*, 2014).

3. highly efficient loading capacity of a wide range of drugs due to the prolonged residence time provided by muco-adhesive polymers (Sivaram *et al.*, 2015).

The release of the drugs and other molecules is easy to control by varying the nanogel properties, for example by incorporating stimulus-responsive crosslinkers or changing crosslinking density (Sivaram *et al.*, 2015).

Nanogels are capable of generating appropriately sized complexes with molecules and keeping their configuration and activity, and even encapsulating fragile compounds to increase their stability (Bae *et al.*, 2008; Sasaki *et al.*, 2010; Singh, Gill and Gill, 2013; Sivaram *et al.*, 2015). Like other nanomaterials, nanogels have nanoscale physical properties, such as size (20~200 nm) and large surface area (Maya *et al.*, 2013; Soni and Yadav, 2016). Meanwhile, the production of nanogels enables versatile formulation and it is facile to chemically modify nanogels for specific purposes, including triggered drug release and targeted drug delivery (Vinogradov, Bronich and Kabanov, 2002; Maya *et al.*, 2013). These properties of nanogels make them promising for applications in anti-skin disease, anti-inflammatory, ocular, transdermal and protein/peptide drug delivery and therapy, cancer drug delivery and imaging (Sivaram *et al.*, 2015).

For cancer therapy, nanogels demonstrate site-specific delivery by incorporating various targeted ligands to bind to a desired site, or utilising the stimuli-responsive ability (Eckmann *et al.*, 2014). Targeting ligands can include various compounds, such as antibodies, peptides, hormones, receptor ligands, nucleic acids and lipid derivatives, etc. In addition, nanogel carriers have prolonged circulation time and are incapable of diffusing across non-fenestrated endothelium, and thus are able to accumulate in tumour

tissues. For instance, Liang et, al. described a novel self-assembled nanogel consisting of hyaluronic acid-epigallocatechin gallate conjugates (HA–EGCG), cytotoxic protein Granzyme B (GzmB) and linear polyethylenimine (PEI) (Liang *et al.*, 2016). HA is known to have the ability of targeting CD44, which is overexpressed in many cancer cells types and EGCG is used to facilitate the formation of stable nanogels. After endocytosis, PEI is able to change the pH in endosomes and rupture the membrane to release drugs into the cytosol (Boussif *et al.*, 1995). It has been observed that this nanogel efficiently kills CD44-overexpressing cancer cells and shows little toxic effect to normal cells (Liang *et al.*, 2016).

After accumulating in tumour tissues via the EPR effect, pH-responsive nanogels are triggered to release drugs either in the extracellular fluids (pH 6.8) or, after cellular uptake, in the acidic endosomes and lysosomes (pH 4.5-6.5) in cancer cells (Manchun, Dass and Sriamornsak, 2012; Manchun *et al.*, 2015). In recent research, hybrid nanogels have been applied to photothermal cancer therapy. Hui Wang et al. fabricated drug loaded core-shell hybrid nanogels that have the function of both tumour imaging, local hyperthermia, temperature sensing and triggered drug release (Wang *et al.*, 2014). These multifunctional nanoparticles have high photoluminescence, photostability, magnetic/NIR-heat conversion ability and drug accumulation potential due to the composite structure consisting of fluorescent carbon dots, a porous carbon shell and superparamagnetic iron oxide nanocrystals. Meanwhile, the hydrogel shell can control the release of drug and fluorescence intensity by varying environmental temperature, which is based on the thermo-responsive poly (N-isopropylacrylamide-co-acrylamide) (Wang *et al.*, 2014). Therefore, NIR light and magnetic field are able to induce localised heating and trigger the release of drugs. In addition, they demonstrated that these hybrid nanogels are capable of overcoming cellular barriers to exert effects in mouse melanoma B16-F10 cells (Wang

et al., 2014).

1.5.3 Silicon and Silica Nanoparticles

As emerging nanomaterials, nanosized porous silicon (silicon-based nanoparticles) and silicon oxide (silica)-based nanoparticles have attracted great attention for cancer treatment applications. Compared to other types of nanoparticles, silicon and silica based nanoparticles have uniquely mesoporous structures, strong hydrophobicity and other distinct material characteristics which make them a promising nanomaterial for cancer therapy applications (Feng *et al.*, 2016). Due to the biocompatibility, porous structures/volume and high active surface area of silicon-based nanoparticles, they have been demonstrated to be one of the outstanding candidate nanovectors for targeted drug delivery, diagnosis and sensitisations of sonodynamic, photodynamic and thermal therapies, etc. (Ferrari, 2005; Stojanovic *et al.*, 2016) Silicon is one of the most fundamental trace materials in the human body, and silicon-based nanoparticles are completely degradable in the living organism. The generated free silicon atoms can be converted to a nontoxic bioavailable form and be excreted efficiently, which illustrates the biocompatibility of silicon-based nanoparticle (Stojanovic *et al.*, 2016). It was observed using Raman spectroscopy that silicon nanoparticles can be completely biodegraded in breast cancer cells after 13-days incubation (Tolstik *et al.*, 2016). The surface modifications of silicon-based nanoparticles for stabilisation, targeted delivery, controlled drug release or immunotherapy can be accomplished due to the porous structures/volume and high surface area (Stojanovic *et al.*, 2016). Meanwhile, the pores inside silicon-based nanoparticles and their structure allow high-efficiency loading of varied compounds for cancer treatment, including both hydrophilic and hydrophobic compounds (Salonen *et al.*, 2005; Kinsella *et al.*, 2011; Kaasalainen *et al.*, 2015; Stojanovic *et al.*, 2016).

Coating silicon nanoparticles with PEG (Putnam, 2008) or serum albumin (Xia *et al.*, 2013) is capable of increasing the solubility and stability of silicon nanoparticles in aqueous environments and results in a much longer circulation time and EPR, similar to other nanoparticles. Simultaneously, silicon nanoparticles can target tumour tissue and enter cancer cells by recognising the receptors on the cell membrane and anchoring via multiple functionalised components, such as carbohydrates, antibodies and peptides (Godin *et al.*, 2011; Secret *et al.*, 2014; Stojanovic *et al.*, 2016). A variety of silicon nanoparticle-delivered drugs have been examined, such as methotrexate, SFN (Wang *et al.*, 2015), indomethacin (Liu *et al.*, 2013), PTX (Liu *et al.*, 2015), DOX (Xu *et al.*, 2015) and siRNA (Osminkina *et al.*, 2012), etc.

Silicon oxide, also known as silica, is well-known as a bio-safe and widely applied natural material. Due to the large internal surface area, controllable porous structure and other material properties of silica-based nanoparticles, they have been investigated as imaging agents, drug vectors and sensitisers as well as silicon-based nanoparticles (Feng *et al.*, 2016). The most commonly studied structures of silica nanoparticles for drug delivery are mesoporous silica based nanoparticles based on Mobil Composition of Matter No. 41 (MCM-41) and/or Santa Barbara Amorphous-15 (SBA-15) (Feng *et al.*, 2016). By altering the temperature, solution composition and concentrations of the synthesis system, the size, shape, surface area and pore size of the hexagonal porous MCM-41 structure can be easily controlled. SBA-15 type silica nanoparticles are synthesized using a polymeric template, which is able to provide mesostructural ordering properties for silica nanoparticles (Zhao *et al.*, 1998). MCM-41 type and SBA-15 type have both been extensively explored for targeted drug delivery (Feng *et al.*, 2016). Controlled-release drug delivery systems based on silica nanoparticles have also attracted increasing attention. The stimuli used for triggered drug release from silica nanoparticles include pH

(Casasús *et al.*, 2004), temperature (Yang *et al.*, 2014), redox potential (Giri *et al.*, 2005), enzyme (Radhakrishnan *et al.*, 2015) and light (Tang *et al.*, 2015), etc. For instance, Chang et al. fabricated a pH-sensitive drug delivery system by modifying the surface of silica nanoparticles with polydopamine. The anti-cancer drug desipramine contained in pH-triggered silica nanoparticles can be released in low-pH cellular conditions (Chang *et al.*, 2016). Compared to free desipramine, pH-sensitive silica nanoparticles showed significantly higher toxicity and inhibitory effects to cancer cells. Lipid-coated silica nanoparticles, a lipid bilayer surrounding silica nanoparticles containing anti-cancer drugs, have been investigated recently, and less drug leakage, slower rate of drug release, and more substantial in vivo therapeutic effects where observed (Meng *et al.*, 2015; Choi *et al.*, 2016; Liu *et al.*, 2016) .

1.5.4 Dendrimers

Dendrimers are 3-dimensional, highly branched monodispersed nanoscale macromolecules (Sharma *et al.*, 2017). Generally, dendrimers consist of an initiator core, branches which emanate from the core and functional end groups on the outermost layer (Gupta *et al.*, 2010). Dendrimers have been considered as a promising nanomaterial for targeted delivery and diagnostic imaging agents, due to their unique properties, such as the monodispersity, internal cavities and modifiable functional end groups (Sharma *et al.*, 2017). The cavity in the hydrophobic core and the multivalent surface allow dendrimers to effectively load hydrophobic and hydrophilic compounds, respectively (Hu, Aryal and Zhang, 2010). Varied dendrimer-based MRI, X-ray and CT contrast agents have been developed by linking contrast agents to dendrimers with design formulations (Sharma *et al.*, 2017). In addition to diagnostic agents, functionalized and ligand-anchored dendrimers have shown outstanding ability to target drug delivery. The ligands that have been used with dendrimers include folic acid (Hilgenbrink and Low, 2005), biotin (Yang

et al., 2009), N-acetyl-glucosamine (Vannucci *et al.*, 2014) and riboflavin, etc. (Sharma *et al.*, 2017) Due to the definition of dendrimers, the formulations of dendrimers are various, such as PAMAM (Buczkowski *et al.*, 2011), polyglycerol (Lee and Ooya, 2012), PPI (Jain *et al.*, 2015), polyester (Morgan *et al.*, 2006) and nucleic acid (Taghdisi *et al.*, 2016), etc. (Sharma *et al.*, 2017) For instance, Taghdisi et al. fabricated an aptamer-base DNA dendrimer containing the anti-cancer drug epirubicin, and targeted drug delivery and considerable in vivo tumour inhibiting effects were observed (Taghdisi *et al.*, 2016). Several major types of nanovectors, including liposomes, polymeric, metal-based, silicon and silica-based nanoparticles, and dendrimers which have been applied in clinical or preclinical trials for targeted delivery of anti-cancer drugs, have been briefly introduced above. Moreover, oceans of novel nanoparticles are currently under study and the systematically combination of varied nanomaterial will provide a very large number of options for selecting highly specific and highly efficient therapeutic nanovectors according to individual patient. On the other hands, to develop more selective and less toxic cancer therapies, nanoparticles have been applied to combine several therapeutic interventions, including photodynamic (Chatterjee, Fong and Zhang, 2008; Roblero-Bartolon and Ramon-Gallegos, 2015; Agostinis P, Berg K, Cengel K., 2017), sonodynamic (H. Xu *et al.*, 2016; Rengeng *et al.*, 2017) and radiotherapy (Hainfeld *et al.*, 2010), etc., as sensitisers or imaging agent or both. The following sections will review the recent advance in the combination of nanoparticles with existing anti-cancer interventions.

1.5.5 Metal-based Nanoparticles

Metal-based nanoparticles used for drug delivery include gold (Cooper, Bekah and Nadeau, 2014), iron oxide (Sharma *et al.*, 2015), zinc oxide (Rasmussen *et al.*, 2010) and titanium oxide (Bakhshizadeh *et al.*, 2017) based nanoparticles. For instance, Sun et al.

fabricated iron oxide nanoparticles conjugated with anti-cancer drug methotrexate and targeting ligand chlorotoxin, and enhanced cytotoxicity was observed both *in vitro* and *in vivo* (Sun *et al.*, 2008). Meanwhile, due to the superparamagnetic properties of iron oxide nanoparticles, they can also be used as MRI contrast agents for diagnosing and monitoring the effects of tumour treatment at the same time (Sun *et al.*, 2008). To enhance the loading capacity of metal-based nanoparticles, polymer (Bakhshizadeh *et al.*, 2017), lipid (Kong *et al.*, 2012) or other customized shells have been used to coat the metal cores, which also provide high stability and biocompatibility. For instance, Bakhshizadeh et al. assembled core-shell molecularly imprinted polymer for drug delivery by coating titanium oxide nano-cores with diacrylated polycaprolctone as cross-linkers and methacrylic acid or 4-vinylpyridin as the functional modification, and superior loading capacity, higher amount of drug release and considerable cytotoxicity in vitro were observed (Bakhshizadeh *et al.*, 2017).

On the other hand, metal-based nanoparticles, including copper, copper oxide (Studer *et al.*, 2010; Akhtar *et al.*, 2016), titanium oxide (Park *et al.*, 2008), silver (Foldbjerg *et al.*, 2009) have been demonstrated to be able to induce the generation of reactive oxygen species inside cells and ultimately lead to oxidative stress, DNA damage and apoptosis of targeted cells, which provide the therapeutic potential as anti-cancer agents themselves. Among those nanoparticles, gold nanoparticles (AuNPs) are the most studied metal-based nanoparticles for anti-cancer drug delivery and have been demonstrated to be promising and effective imaging labels and contrast agents on account of their strong surface plasmon resonance (SPR) effect. Electromagnetic radiation of specific resonant frequencies can induce a coherent oscillation of the free electrons on the nanoparticle surface, when the diameter (1-100 nm) of the metal nanoparticles is less than the wavelength of light. The oscillation is called the SPR. The SPR can cause an intensely

enhanced absorption and scattering of electromagnetic radiation in resonance with the metal nanoparticles (Jain, ElSayed and El-Sayed, 2007). Furthermore, AuNPs have high stability and can be easily manufactured in controllable size, shape and functionalised by bioconjugations and biomodifications, which make them an outstanding nanomaterial for drug delivery. AuNPs are facile to be bio-conjugated and bio-modified on account of the strong binding affinity towards amines, disulphides and thiols of their surface. This strong affinity allows AuNPs to conjugate a variety of peptides, proteins, DNA and other biomedical compounds (Niemeyer, 2001; Katz and Willner, 2004; Jain, ElSayed and El-Sayed, 2007). Cancer specific antibodies (such as anti-FAK antibody and anti-EGFR antibody), biomolecules (which can be eagerly taken up by cancer cells) and viruses etc. can be conjugated to AuNPs to selectively target cancer cells (El-Sayed, Huang and El-Sayed, 2005; Jain, ElSayed and El-Sayed, 2007; Kim *et al.*, 2008; Cheng *et al.*, 2014). Therefore, antibody-conjugated gold nanoparticles are widely used in cancer diagnosis and therapy. It is also known that AuNPs with strong surface-plasmon-enhanced absorption can convert the absorbed light into localized heat expeditiously and therefore can be utilised for selective photothermal cancer therapy (El-Sayed, Huang and El-Sayed, 2006).

AuNPs are generally considered relatively nontoxic to normal cells (Connor *et al.*, 2005; Shukla *et al.*, 2005; Alkilany and Murphy, 2010; Villiers *et al.*, 2010), but non-functionalized AuNPs have been reported to show selective cytotoxicity to certain cell lines, especially cancer cells. Hirak K. Patra and colleagues found that citrate-capped AuNPs (13 nm in diameter) can specifically induce death in the human carcinoma lung cell line (A549), while leaving two other cell lines, baby hamster kidney and human hepatocellular liver carcinoma, unaffected at the same dosage (Patra *et al.*, 2007). AuNPs have been implicated in detrimental effects on various important cellular components,

such as mitochondria and membrane, damage to DNA, generation of reactive chemical species, hindrance of cell function and ultimately induction of cell death (Alkilany and Murphy, 2010). Triphenylphosphine monosulfonate (TPPMS) capped AuNPs (1.4 nm in diameter) were found to be toxic to HeLa cervical carcinoma epithelial cells (IC_{50} = 48 μM）as a result of oxidative stress and mitochondrial damage leading to necrosis (Pan *et al.*, 2009). Metal nanoparticles can capture electrons from O_2, owing to their high surface/volume ratio and the specific electronic configuration of surface atoms (Nel *et al.*, 2006). Jia et Al. reported that AuNPs (13 nm in diameter) can catalyse the production of nitric oxide (NO) from endogenous S-nitroso adducts with thiol groups (RSNOs) in blood serum, resulting in the formation of Au-thiolate on the surface. It is known that NO can effectively interact with superoxide to generate a toxic peroxinitrite ($ONOO^-$) (Jia *et al.*, 2009).

Cellular responses to AuNPs depend on their chemical/physical properties, such as surface charge, size and shape (Alkilany and Murphy, 2010). For instance, Goodman and colleagues found that cationic (aminated) AuNPs (size 2 nm) are able to cause membrane disruption and cell death, while anionic (carboxylated) AuNPs with similar size and shape show no toxicity to cells. It suggests that the binding of the AuNPs to the negatively charged cell membrane can be a potential mechanism of the cytotoxicity of cationic AuNPs (Goodman *et al.*, 2004).

Recent nanoparticles-cancer research has led to the development of special functional nanosized gold-based particles that conjugate drugs, antibodies or bioactive ligands which are designed to target or kill cancer cell (Service, 2005; Kong, Keidar and Ostrikov, 2011; Cheng *et al.*, 2014). Branch et al. reported aurimmune CYT-6091, constructed by concurrently binding polyethylene glycol (PEG) and recombinant human Tumour Necrosis Factor (rhTNF) to AuNPs. It was tested in a phase I dose escalation clinical trial.

It was demonstrated that the rhTNF plays a role in targeting and killing cancer cells (Libutti *et al.*, 2010). Anil Kumar et al. successfully investigated a kind of peptide functionalized AuNPs which consists of a therapeutic peptide, PMI and neuropilin-1(Nrp-1) receptor-targeted peptide on ultrasmall AuNPs (2 nm). Since nrp-1 is highly expressed by a variety of human cancer cell lines and PMI is a potent inhibitor of suppressive protein, p53, these AuNPs can target cancer cells and show strong anti-cancer activity (Kumar *et al.*, 2012).

1.5.6 Combination of Gold Nanoparticles and CAP Treatment

The combination of CAP treatment and nanoparticles, especially gold nanoparticles, has been a new approach in the therapies of cancer. There are few studies reported that CAP treatment has anti-cancer synergy with various types of nanoparticles, including iron nanoparticles (Jalili, Irani and Mirfakhraie, 2016), iron oxide-based magnetic nanoparticles (Li *et al.*, 2019), silver nanoparticles (Manaloto *et al.*, 2020), paclitaxel loaded core-shell magnetic nanoparticles (Yu *et al.*, 2018). However, the related studies were mainly focused on the combination therapy between CAP treatment and AuNPs due to the unique properties and various advantages of AuNPs.

Kim *et al.* first reported their study about synergistic effect between CAP and antibody-conjugated AuNPs on G361 human melanoma skin cell (Kim *et al.*, 2008). The authors achieved five-fold enhancement in G361 cell death over the case of the CAP alone by using CAP with AuNPs conjugated to anti-phospho-focal adhesion kinase (FAK) antibodies (Kim *et al.*, 2008). In this study, melanoma cancer cells were placed 2 mm from the touch-safe CAP source and treated for 40s. The CAP temperature remained less than 38°C even after radiating for 10 min (Kim *et al.*, 2008). FAK was more expressed in melanoma cells than in normal cells and crucial for melanoma cells' survival, growth and metastasis. So anti-FAK antibody-conjugated AuNPs (FAK-AuNPs) can target

melanoma cells and enter into cytoplasm to bind to FAK (Kim *et al.*, 2008). In the research, there were three groups cultured in: (1) only medium (control); (2) medium containing AuNPs; (3) medium containing FAK-AuNPs. FAK-AuNPs (30 nm) and AuNPs (30 nm) did not show to toxicity to G361 compared with the control group. After these groups of cells were exposed to CAP for 40s, the cell death rate was 74% (FAK-AuNPs), 36% (AuNPs) and 14% (control) (Kim *et al.*, 2008). It seems that CAP stimulated nanoparticles induced deactivation of FAK and led to increased cell death rate. This study first demonstrated that a low-dose CAP treatment can combine AuNPs located inside cells to effectively kill cancer cells. The synergy of CAP and AuNPs suggested a promising novel method to against cancer which is low-dose, safe, selective and effective (Kim *et al.*, 2008).

More recently, using CAP plus various cancer specific antibody-conjugated AuNPs has been reported that has significant cancer selective lethal effect, such as anti-epidermal growth factor receptor (EGFR) antibody conjugated AuNPs (AuNPs-EGFR). EGFR has been demonstrated to be overexpressed in multiple cancer types and can promote solid tumor growth (Nicholson, Gee and Harper, 2001). It was shown that AuNPs coated with EGFR binding immunoglobulins can bind selectively to EGFR on cancer cells membrane and inactivate them with CAP stimulating, consequently causing the destruction of cancer cell membrane and cell death while leaving normal cells significantly less affected (Choi *et al.*, 2012).

A similar approach was taken by the same authors (Choi BB et al.) using anti-human epidermal growth factor receptor 2 (NEU) antibody labelled AuNPs and CAP to treat melanoma cells. The NEU protein is usually over-expressed in melanoma cells and the anti-NEU antibody labelled AuNPs can preferentially target melanoma cells rather than other normal cells (Choi *et al.*, 2015). It was shown that the NEU protein was selectively

destroyed, leading a downstream effector after the synergistic treatment. These effects finally caused significantly higher death rate of melanoma cells compared with other control groups (Choi *et al.*, 2015).

Unconjugated AuNPs also display synergistic effects when used in combination with CAP against cancer. Chen et al. studied the synergistic effect of non-attached AuNPs and CAP on human brain glioblastoma U87 cell line, which takes a larger CAP lethal dose than other brain glioblastoma cancer cell lines and is resistant to AuNPs (Cheng *et al.*, 2014). The synergy can induce up to 30% more cell death with an optimal concentration of AuNPs compared to control groups (Cheng *et al.*, 2014). The unconjugated AuNPs in the cell culture medium may potentially promote the absorption of extracellular ROS and RNS generated by CAP into cells (Cheng *et al.*, 2014). The absorption may help accumulation of intracellular ROS and RNS and theoretically leads to oxidative stress, which further affects the cellular pathways and causes damage to the DNA, lipids and proteins. This strengthened effect on CAP treatment varies with the concentration, incubation time of AuNPs and cancer cell lines (Cheng *et al.*, 2014). The exact mechanism has yet to be studied further.

In the study by Irani S et al. higher concentration of AuNPs showed stronger cytotoxicity to Human colorectal cancer cells (HCT-116). The authors used highest concentration of AuNPs (375 ppm) and CAP (exposure time: 60, 90, 120 and 180 s) to treat HCT-116 cells, longer CAP treatment time led to more apoptotic cell death synergistically combined with AuNPs treatment (Irani *et al.*, 2015). The endocytosis of AuNPs plays an important role in their application, and indicated that CAP may promote the uptake of AuNPs into cancer cells. X. Cheng et al. found that CAP induced the formation of small pores on cell membrane of Glioblastoma cells (U87) and made the membrane become uneven, while leaving immortalized normal human astrocytes (E6/E7) unaffected. The

cancer cell morphology was changed by CAP treatment which may explain the accelerated uptake of AuNPs by CAP (Cheng *et al.*, 2015).

The combination of low doses of AuNPs and CAP was indicated to inhibit PI3K/AKT pathway in cancer cells (Kaushik *et al.*, 2016). AKT activation has been demonstrated to obstruct the function of p53 protein and inhibit the activity of caspase-9 (Cardone *et al.*, 1998; Jeong *et al.*, 2005). Caspase cleavage plays a crucial role in apoptosis (Jia *et al.*, 2015) and is known as reliable marker of apoptotic cell death with PARP cleavage together (Kaushik *et al.*, 2016). Moreover, CASP9, p53, and CASP3 mRNA expression were observed that were enhanced by the co-treatment with AuNPs and CAP (Kaushik *et al.*, 2016). Epithelial-mesenchymal transition (EMT) is known as a cellular mechanism that contributes to normal embryonic development and generally is responsible for the initiation of metastasis in solid tumors (Roizen, 2012; Kaushik *et al.*, 2016). It has also been indicated that EMT can stimulate the cancer stem cells (CSCs) potential of cancer cells. CSCs are the only cells that can initiate and drive tumor growth, resulting metastasis, tumor recurrence and clinical relapse (Mani *et al.*, 2008; Morel *et al.*, 2008). A growing amount of evidence indicates that these cells are resistant to radiation therapy and chemotherapy. Hence, it is highly promising that co-treatment with AuNPs and CAP can effectively block EMT and inhibit CSCs. It has also been found that low dose of AuNPs combined with CAP induce the increase of epithelial markers, such as E-cadherin, with decrease in mesenchymal markers, such as N-cadherin (Kaushik *et al.*, 2016). Co-treatment also can enhance the expression levels of some EMT-associated transcription proteins, such as N-Cad, Zeb-1 and Slug which can block cell cycle and are related with the loss of N-Cadherin (Kajita, McClinic and Wade, 2004; Vega *et al.*, 2004; Kaushik *et al.*, 2016). Besides, it has been shown that co-treatment with AuNPs and CAP can significantly reduce the population of glioma stem-like cells (GSCs) in vivo and vitro

model and thus avoid drug resistance, recurrence and metastasis (Kaushik *et al.*, 2016). However, the effects of combination therapy of CAP treatment and AuNPs can vary due to the wide range of different AuNPs, CAP-generating devices and cell lines. More importantly, the exact and detailed mechanism behind the synergistic cytotoxicity, especially, accelerated uptake of AuNPs into cancer cells by CAP, has yet been to be discovered. Therefore, considering all the advantage of AuNPs and the unsolved research questions, this project used AuNPs to investigate the synergistic anti-cancer effects combined with CAP treatment.

1.6   Combination of Chemotherapy with CAP Treatment

A number of studies have investigated the possible additive, or synergic effect of CAP with traditional chemotherapeutic agents. The chemical and physical effects (i.e. production of reactive oxygen and nitrogen species, generation of heat and electromagnetic fields) of CAP treatment induced cell permeability (Leduc *et al.*, 2009), disruption of cell membrane (Chen, Cheng and Cheng, 2018), enhanced endocytosis (He *et al.*, 2018) and cell apoptosis (Tanaka *et al.*, 2015). Therefore, the cancer cells treated by CAP could increase their uptake of chemotherapeutic agents and present higher sensitivity to chemotherapy. Additive or synergic effects have been described in a number of studies and several mechanisms of action are beginning to emerge (Brullé *et al.*, 2012; Kaushik *et al.*, 2015; Conway *et al.*, 2016; Zhu *et al.*, 2016). For instance, Conway GE et. al first reported the enhanced ROS-, JNK-, and caspase-independent mechanism of cell inactivation in human glioma cell line U373MG by the combination of CAP with TMZ (Conway *et al.*, 2016). CAP was observed to overcome chemoresistance of the GBM cell line LN18 which has unfavourable MGMT status and displays resistance to TMZ. Pre-treatment with CAP induced cytotoxicity and restored cell cycle arrest in G2/M Phase when co-treated with TMZ (Köritzer *et al.*, 2013). In a myeloma cell line model,

CAP was found to increase bortezomib sensitivity and induce myeloma cell apoptosis (D. Xu *et al.*, 2016). Interestingly, low frequency, low intensity alternating current electrical stimulation has also been shown to enhance chemotherapeutic efficacy in MDR1 drug resistant brain, lung, prostate, ovary, fibrosarcoma and tumour cells (Janigro *et al.*, 2006). Due to the alterations of metabolism of cancer cells, a specific microenvironment with high reactive species level is created both inside of cancer cells and in the tumour tissues. The increased reactive species level provide an attractive target for developing anticancer therapy, especially as it seems a common feature among various types of cancer (Marzenell *et al.*, 2013). Several anticancer drugs targeting this feature have been developed to further increase reactive species level in cancer cells beyond their tolerable allowance to trigger cancer cell death, including fenretinide (Sun *et al.*, 1999), nitric oxide-donating aspirin (Gao, Liu and Rigas, 2005), imexone (Hersh *et al.*, 1992), motexafin gadolinium (Evens *et al.*, 2005), menadione (Beck *et al.*, 2009), β-lapachone (Y. Li *et al.*, 2003) and others (Trachootham, Alexandre and Huang, 2009). However, those drugs also can increase the reactive species level in healthy cells, which may induce secondary malignancies as a dangerous side effect (Marzenell *et al.*, 2013). Therefore, prodrugs, which were developed in an alternative strategy against the specific high reactive species level in tumours, are only activated to be cytotoxic after exposure to rich reactive species, which should lack this side effect and be more specific.

The majority of prodrugs were developed to be activated in cells by oxidation induced by ROS. CAP has been demonstrated to generate ROS and RNS in specific area and treat tumour tissues with controllable dose (Welz *et al.*, 2015), therefore it can be a promising intervention for combination therapy with ROS-activated pro-drugs, especially, increasing the therapeutic efficiency of pro-drugs.

In this project, we have acquired four types of prodrug candidates, including ferrocene-

based prodrugs provided by Prof. Andriy Mokhir (Marzenell *et al.*, 2013) and Prof. Gérard Jaouen (Jaouen, Vessières and Top, 2015), matrix metalloproteinase proinhibitors and thiazolidinone-based prodrugs provided by Prof. Seth M. Cohen (Perez *et al.*, 2015), and pyrazolopyrimidines derivatives provided by Prof. John Stephens (Kelada *et al.*, 2018).

As seen from Appendix V Supplementary Table S1 and S3, ferrocene ($C_5H_5FeC_5H_5$) consists of two cyclopentadienyl rings and a central iron atom. Ferrocene itself has high stability but reacts with reactive oxygen species which induces alternations of their derivatives. Prof. Gérard Jaouen and his group have investigated and reported a series of compounds based on ferrocene derivatives, [3] ferrocenophane and ferrocifen derivatives. [3] ferrocenophane consists of a central iron atom and two cyclopentadienyl rings linked by a three-carbon atom bridge. Ferrocifen is also known as ferrocene derivative hydroxyferrocifen. So, based on those ferrocene derivatives and analogues, Prof. Jaouen's group has developed a series of compounds which are capable of being activated in cancer cells by their relative high ROS level with the formation of alkylating agents and other cytotoxic agents, which inhibit the cellular antioxidative system and induce antiproliferative effects against cancer cells (Plazuk *et al.*, 2009; Görmen *et al.*, 2010; Top *et al.*, 2013; Jaouen, Vessières and Top, 2015). A series of compounds that have been tested and approved to be antiproliferative against MDA-MB-231 breast cancer cell line were provided to us for investigating the combination treatment with CAP against GBM U373MG cell line. Meanwhile, we also received two aminoferrocene-based prodrugs from Prof. Andriy Mokhir which are active against primary chronic lymphocytic leukemia cells and found to not affect mononuclear cells and representative bacterial cells (Marzenell *et al.*, 2013). And those aminoferrocene-based prodrugs also contain boronic acid ester residue, which has been well-developed as oxidation trigger group, therefore

will be cleaved in the presence of ROS, leading to the formation of two types of anti-cancer agents: redox-active iron-containing species (aminoferrocenes and iron(II) ions) that induce the catalytic generation of ROS and a quinone methide that inhibits the cellular antioxidative system (Marzenell *et al.*, 2013).

The matrix metalloproteinase pro-inhibitors provided by Prof. Cohen contain boronic acid esters or benzylic ether as ROS trigger groups which can liberate the active compounds while being oxidised by high level of ROS (Rouffet and Cohen, 2011). The pro-inhibitors were designed to inhibit matrix metalloproteinase at high ROS level therefore could apply for the treatment of ischemic injury whereas increasing level of ROS and ROS activated matrix metalloproteinases break down the blood brain barrier (Major Jourden and Cohen, 2010; Rouffet and Cohen, 2011). Therefore, they were not designed for cancer treatment, but it is interesting to treat brain cancer cells with those matrix metalloproteinase pro-inhibitors in combination with CAP treatment. Meanwhile, Prof. Cohen provided few thiazolidinone-based prodrugs, in which thiazolidinone group can reveal carboxylic acid groups after activation by hydrogen peroxide (Perez *et al.*, 2015).

The last group of compounds were provided by Prof. John Stephens, which are pyrazolopyrimidine derivates, not usually considered as prodrugs, but have found use as various bioactive molecules in the battle against cancer, infections, obesity and cystic fibrosis (Kelada *et al.*, 2018). It also has been reported that pyrazolopyrimidines derivatives present notable inhibiting effects to the activity or function of several kinases, including the PI3 kinase, glycogen synthase kinase -3 (GSK-3) and others, which are involved in and even play key roles in a variety of cellular activities including cell differentiation, motility, cell growth, proliferation, survival and intracellular trafficking, and therefore involved in cancer cells (Peat *et al.*, 2004; Folkes *et al.*, 2008; Venkatesan

et al., 2010; Martina Ferrari *et al.*, 2015). Therefore, it is promising to find novel drugs in pyrazolopyrimidine derivates for cancer treatment which may possess synergistic anti-cancer effects in combination with CAP treatment.

1.7 Aims & Objectives

GBM neoplasms usually recur and the prognosis is highly dismal. The length of survival is commonly 12-15 month, whereas 5-year survival rate is only less than 3%-5% (Gallego, 2015). Meanwhile, even with aggressive treatment, application of radiosensitizer or many chemotherapeutic agents, high amount of GBM tumours present high resistance to conventional therapies, and the therapeutic effects of chemotherapeutics are limited when they are blocked by the blood-brain barrier. Novel therapies are urgently needed and the understanding of molecular signalling processes of GBM also needs to be further investigated. The aim of this project is to investigate novel therapies for glioblastomas by combining cold atmospheric plasma, gold nanoparticles and chemotherapy, to enhance the knowledge of the reaction of GBM to cold atmospheric plasma and provide the basis to further develop efficient novel clinical treatment for GBM tumour. More specifically, we aimed to investigate the synergistic anti-cancer effects between low dose CAP treatment, AuNPs and discover new prodrug candidates that possess strong synergy with CAP treatment. Our research questions are 'How does low dose CAP treatment accelerate the uptake of non-toxic AuNPs into GBM U373MG cells and lead to synergistic cytotoxicity?' and 'Identify potential leading prodrug candidates that can be activated and induce synergistic anti-cancer effects in combination with low dose CAP treatment.'

There are 4 Chapters in this PhD thesis. In Chapter 1, the objective is completing a literature review, which has been presented above in section 1.1-1.6, to introduce brain cancer, especially GBM, therapeutic cold and hot plasma, the intracellular reactive species and related signalling pathways, nanoparticles in cancer therapy and

chemotherapy agents, especially, prodrugs that have potential synergistic anti-cancer effects combined with CAP treatment. The literature review has been published as a book chapter. In Chapter 2, the objective was identifying the synergistic cytotoxicity of CAP treatment and AuNPs against U373MG cells and investigating the mechanism of CAP-accelerated uptake of AuNPs, which leads to the synergistic cytotoxicity. For deliverables: (1) The study was published (He *et al.*, 2018); (2) We preliminary determined the mechanism of the synergistic effects between CAP and AuNPs. The further studies about signalling pathway and detailed mechanism of CAP-accelerated uptake is being carrying out and is presented in Chapter 3. In Chapter 3, the objective was determining the possible endocytosis pathways activated by low dose CAP treatment. For deliverables: (1) The study described above was published (He *et al.*, 2020); (2) For the first time, we discovered the membrane repairing clathrin-dependent endocytosis was activated after being treated with CAP, whereas it increases the accumulation of AuNPs inside cells and eventually leads to cell death. This mechanism of RONS-induced endocytosis will also be of relevance to other cancer therapies that induce an increase in extracellular RONS. In Chapter 4, the objective was screening all prodrug candidates and identify possible leading candidates that have significant synergy with CAP treatment. For deliverables: (1) Screening of all 47 prodrug candidates was carried out and the alamar blue assay was used for all compounds to determin their dose response curves against U373MG cells with or with CAP treatment; (2) The manuscript is in preparation and will be submitted for publication soon; (3) We have indentified two leading candidates and the possible mechanism of the activation of prodrug JW-04-061 by CAP treatment.

CHAPTER 2. COLD ATMOSPHERIC PLASMA PROMOTE THE UPTAKE AND ACCUMULATION OF GOLD NANOPARTICLES IN U373MG CELLS

See Appendix I

2.1   Introduction

Gold nanoparticles (AuNPs) can be used as diagnostic agents, radiosensitizers and drug delivery vehicles, due to their specific physical and chemical properties, such as strong surface plasmon resonance effect, high stability and low cytotoxicity (Jain, ElSayed and El-Sayed, 2007; Cheng *et al.*, 2011; Joh *et al.*, 2013). AuNPs can be readily manufactured in various controllable shapes, sizes and monodispersity. Though non-functionalized AuNPs can show selective cytotoxicity to certain cell lines, especially cancer cells (Patra *et al.*, 2007), AuNPs are generally considered nontoxic to normal cells (Connor *et al.*, 2005; Alkilany and Murphy, 2010). Cytotoxicity of AuNPs is size dependent, small AuNPs elicit higher cytotoxicity than larger AuNP. AuNPs of ~20 nm diameter elicit relatively low cytotoxicity in both normal and cancer cells (Pan *et al.*, 2007) and are optimal for traversing the blood brain barrier to enter the brain (Shilo *et al.*, 2015). The surface chemistry of AuNPs enables bio-conjugation and bio-modification, for example, conjugation of antibodies to assist in targeting or conjugation of chemotherapeutic or detection agents (Cheng *et al.*, 2011; Joh *et al.*, 2013). These properties underpin the emergence of gold nanoparticles as promising therapeutic and diagnostic administration systems to treat neoplasms.

Plasma, a form of ionized gas, is one of the four fundamental states of matter and by far the most common form of matter in the universe. Initially, biomedical applications of plasma concentrated on heat and high temperature, i.e. thermal plasmas, for tissue removal, sterilization, and cauterization (Fridman *et al.*, 2008). Technological advances have allowed researchers to generate plasmas at ambient temperatures and at approximately 1.0 atmospheric pressure, allowing safer application to biological samples and tissues without risking thermal injury. These are known as non-thermal atmospheric plasma (NTAP) or Cold Atmospheric Plasma (CAP). CAP has been investigated as a

promising technique for various biomedical applications including tumour therapies, sterilization, wound healing and local viral and microbial infection control (Isbary *et al.*, 2012; Shi *et al.*, 2012; Zelzer *et al.*, 2012; Yan *et al.*, 2015). CAP generates a unique physical and chemical environment for exposure of biological tissues, eliciting effects such as activation of short and long lived reactive nitrogen species (RNS, e.g. N_2^+, NO_3 and NO, etc.) and reactive oxygen species (ROS, e.g. OH•, O and O_2•, etc.), photons as well as generation of heat, pressure gradients, charged particles, and electrostatic and electromagnetic fields (Kong, Keidar and Ostrikov, 2011; Babington *et al.*, 2015), many of which are known to induce effective death pathways in cancer cells (Yan *et al.*, 2015). Synergistic anti-cancer effects between AuNPs and CAP have emerged as a promising potential approach in cancer therapy studies. Kim et al. first reported that cytotoxicity of CAP to melanoma cells was significantly increased (near five-fold) by combining with antibody-conjugated AuNPs (Kim *et al.*, 2008). Zhu et al. showed that CAP coupled with drug loaded core-shell AuNPs led to a significant enhancement in growth inhibition of breast cancer cells compared with control groups (Zhu *et al.*, 2016). Other studies have also suggested that AuNPs have synergistic cytotoxicity when combined with CAP in cancer treatment (Cheng *et al.*, 2014; Irani *et al.*, 2015). However, the effects of CAP and AuNPs can vary due to the wide range of different AuNP, CAP-generating devices and cell lines.

The current research uses an experimental dielectric barrier discharge (DBD) plasma device, DIT 120, with a maximum voltage output of 120 kV at 50 Hz generated between two 15 cm diameter aluminium disk electrodes (Figure 7a, b) (Ziuzina *et al.*, 2013; Patange *et al.*, 2017). We have previously characterised biological activities in cancer cells that are dependent and independent of reactive species generation using this system (Boehm *et al.*, 2016; Conway *et al.*, 2016). We wished to explore the mechanism of CAP

and AuNPs induced cytotoxicity in cancer cells using our system. Using various analytical chemistry, biochemistry and microscopy to characterise the effects of CAP on AuNP, we provide evidence that direct exposure to CAP induces increased AuNPs endocytosis and trafficking to lysosomes, which could be the mechanism of the synergistic cytotoxic effects observed in GBM U373MG cells.
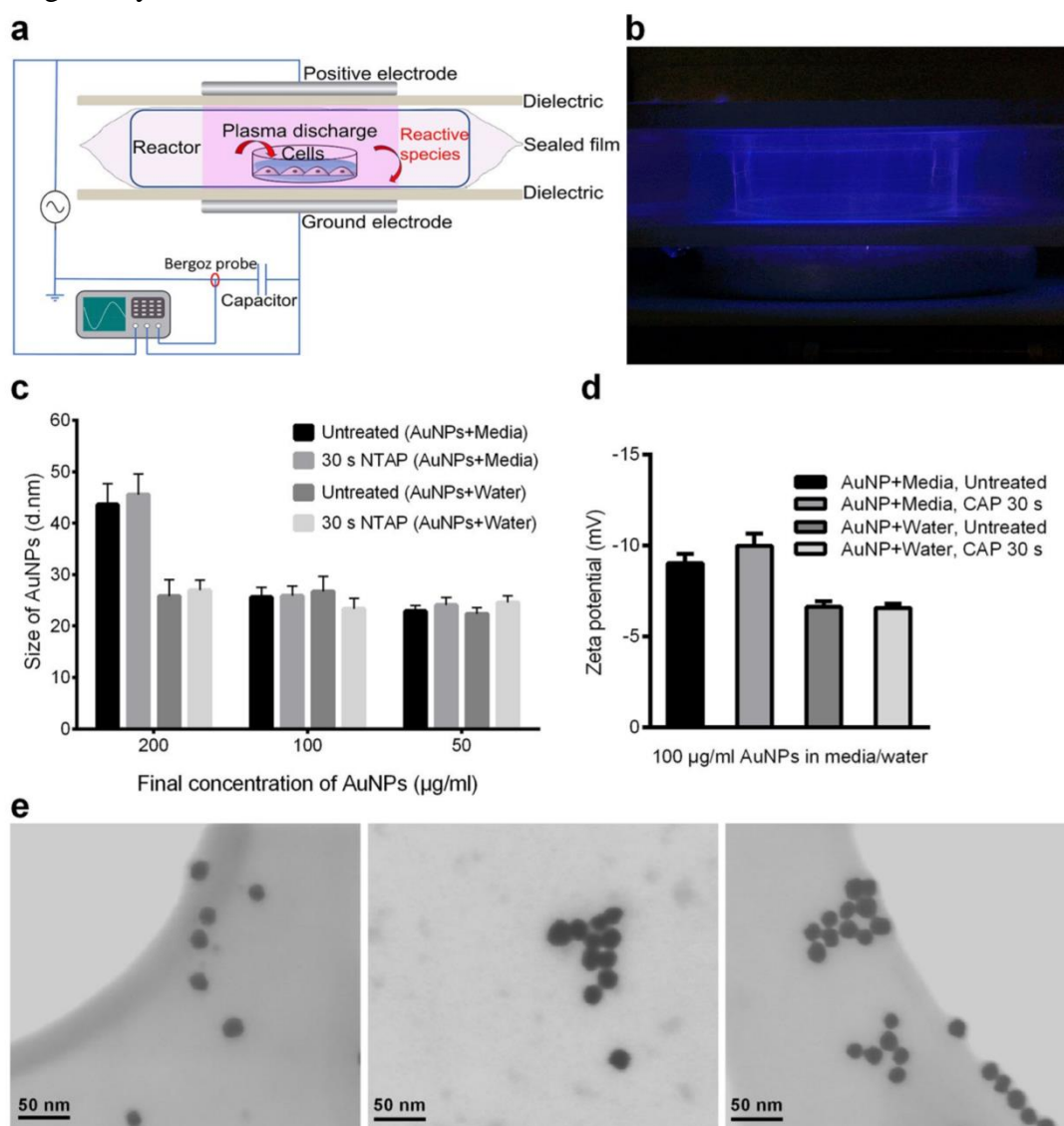
Figure 7. CAP demonstrates no significant effect on AuNPs (≤100μg/ml) within culture medium or water.

(a) Schematic of the DIT120 Plasma Device used in this study. (b) A photograph showing plasma generation (blue) and treatment on cell samples. (c) 20nm AuNPs were diluted to different concentrations with cell culture medium or water. The mixed solutions were

treated with CAP (75 kV, 30 s), incubated for 24h, then measured the sizes by Zetasizer.

(d) AuNPs were diluted in cell culture medium or water to 100μg/ml and treated with

CAP at 75 kV for 0, 30 s. Zeta potential was then measured by Zetasizer. (e) STEM of

AuNP, from left to right: mixed with water; mixed with culture media; mixed with culture

medium then exposed to CAP for 75 kV, 30 s, AuNPs concentrations are 100μg/ml. For

Fig. 1c and d, Zetasizer measurements were repeated in six replicates. Statistical analysis

was carried out using one-way ANOVA with Bonferroni's multiple comparisons post-test.

2.2 Materials &Methods

2.2.1 Cell Culture.

The human brain glioblastoma cancer cell line U-251 MG (formerly known as U-373 MG) (ECACC 09063001) were obtained from Dr Michael Carty (Trinity College Dublin). The stock held as U-373MG in ECACC was found to be identical by STR-PCR profiling to U-251, so now has been re-named as 'U-251 MG (formerly known as U-373 MG)'. The new deposit of U-373 MG is named as U-373 MG (Uppsala) (ECACC catalogue number 08061901). However, the U-373MG cell line used in this project is considered as a subclone of U-251 and has been demonstrated to display variations in phenotypic marker expression as well as differences in growth characteristics, which may explain that various laboratories reported different results from U-373MG and U251 cell lines (Torsvik *et al.*, 2014). Therefore, we used term U373MG in this thesis and only added explanation in all Method Sections to distinguish it from the U-251 and U-373MG (Uppsala) cell lines. Cells were cultured in Dulbecco's Modified Eagle's Media-high glucose (Sigma-Aldrich) supplemented with 10% foetal bovine serum (Sigma-Aldrich) and 1% penicillin and streptomycin mixture (Thermo Fisher Scientific) in TC flask T25, standard for adherent cells (Sarstedt). The cultures were maintained under a condition of 5% (v/v) CO_2 and 37 °C in a humidified incubator. Culture medium was changed every

2 days until reaching around 80% confluency. Cells were then brought into suspension using 0.25% trypsin solution (Thermo Fisher Scientific) and subcultured in new flasks.

2.2.2 CAP Configuration and Treatment.

The CAP-DBD device used (Figure 7a, b) is an experimental atmospheric low temperature plasma generator (Conway *et al.*, 2016). It consists of two aluminium disc-electrodes (diameter 15 cm) with a polypropylene sheet in the middle, which is used as dielectric barrier and holder for the reactor and cell samples. The thickness of the dielectric barrier is 1.2mm, and the distance between the two electrodes was 26.6 mm. Samples were placed in a sealed reactor and treated inside or outside the plasma discharging area. The CAP was generated between two disc-electrodes when the high voltage was applied. Voltage was monitored using an InfiniVision 2000 X-Series Oscilloscope (Agilent Technologies Inc., Santa Clara, CA, USA). TC dish 35 standard (35x10mm, Sarstedt) was used as the cell container for CAP treatment. U373MG cells were seeded into the dishes at a density of 1×10^5 cells/ml and incubated overnight to allow a proper adherence (70-80% confluency). For direct treatment, culture medium was removed from the dishes before the CAP treatment, then the cell culture dishes were put between the two electrodes and treated at 75 kV for 0-40 s. The fresh culture medium containing 100 μg/ml AuNPs or inhibitors was added after exposing to CAP. For CAP-activated culture medium, the fresh culture medium were contained in TC dish 35, standard and treated with CAP at 75 kV for 30 s and stored overnight to remove short-lived reactive species. AuNPs were added into CAP-activated medium to 100 μg/ml. The CAP-untreated cells were then incubated with CAP-activated medium containing AuNPs for 24 and 48 h. The indirect CAP treatment was used to determine the role of direct physical effects. To indirectly treat cells with CAP, the sample was treated in the reactor without the dish lid on it, and culture medium was removed before the treatment. The cell

culture dish was placed on the corner of the reactor, outside the plasma discharging area. During the treatment (75 kV, 30 s), the reactor was sealed in a high barrier polypropylene bag (B2630; Cryovac Sealed Air Ltd, Dunkan, SC, USA) to keep the CAP inside the reactor, and to make sure the cells were only affected by the short-lived and long-lived reactive species generated in air (Han *et al.*, 2016). Fresh culture medium containing 100 µg/ml AuNPs was then added after indirect CAP treatment.

2.2.3 Gold Nanoparticles Synthesis and Characterization.

20 nm AuNPs used in this study are synthesised by trisodium citrate ($Na_3C_6H_5O$) reduction of auric acid ($HAuCl_4$). The typical method of AuNPs synthesis as follows. $HAuCl4$ was dissolved in water at a concentration of 0.25 mM in a clean glass flask and heated with magnetic stirring and brought to boiling. The corresponding amount of 5% (w/v) sodium citrate solution was quickly added to final 3.5:1 molar ratio of citrate to $Au3+$ while being keep heating and stirring. The reaction was completed until the colour of solution was changed from dark purple to wine red and keep stable. The gold colloid was then centrifuged at 10000 g for 10 min to concentrate the AuNPs stock solution to 2500 µg/ml. The size, absorbance curve and zeta potential of AuNPs was then determined by UV-Vis spectrometer (Shimadzu, UV-1800), Zetasizer (Malvern, Nano ZS) and scanning transmission electron microscopy (STEM). The AuNPs stock solution was diluted in water or culture medium to corresponding concentration as indicated in the relevant figures.

2.2.4 Cell Viability Assays.

Cell viability was analysed using the Alamar blue assay (Thermo Fisher Scientific), which used a redox indicator that can generate fluorescent signal by the metabolic reduction. U373MG cells were plated into 96-well plates (Sarstedt) at a density of 1×104 cells/well (100 µl culture medium per well) and were incubated overnight to allow a

proper adherence. The cells were then directly treated with CAP at 75 kV for 0- 30 s at 70-80% confluency, and culture medium containing 0-100 µg/ml AuNPs was added post CAP treatment. Forty-eight hours late, the cells were rinsed once with phosphate buffered saline (Sigma-Aldrich), incubated for 3 h at 37 ℃ with a 10% Alamar blue/90% culture medium solution. The fluorescence was then measured (excitation, 530 nm; emission, 595 nm) by a Victor 3V 1420 microplate reader (Perkin Elmer).

2.2.5 Atomic Absorption Spectroscopy.

U373MG cells were seeded into 60 mm dishes (Sarstedt) at a density of 1×10^5 cells/ml and incubated for 2 days to achieving 90-100% confluency. The culture medium was removed, and cells were directly exposed to CAP at 75 kV for corresponding time. The fresh culture medium containing 100 µg/ml AuNPs or 0.1% (w/v) NaN_3 was then replaced and incubated for 0.5-48 h at 37 ℃ or 4 ℃ as indicated. After treatment, cells were washed thrice with phosphate buffered saline to remove the AuNPs outside cells. Cells were then dissociated and collected from the culture dish using prewarmed (37 ℃) 0.25% trypsin solution. The cell suspension was counted using hemocytometer, then transferred to 15 ml tube (Sarstedt) to measure the gold atomic absorbance in AAS. To verify the Au amount of the samples, five-point standard curve were first established using 1-5 ppm standard gold colloid. The concentrations of AuNPs in samples were then calibrated by the standard curve as described elsewhere (Trono *et al.*, 2009).

2.2.6 Inhibitor Studies.

To determine the uptake of AuNPs, NaN_3 was used as metabolic inhibitor to inhibit the energy-dependent endocytosis. 20% (w/v) NaN_3 stock solution was prepared in phosphate buffered saline. The cells were pre-incubated with 0.1% (w/v) NaN_3 in prewarmed (37 ℃) culture medium for 1h. The culture medium was then removed during CAP treatment, then fresh medium containing 0.1% (w/v) NaN_3 and 100 µg/ml AuNPs

was added into the cell culture and incubated at 37 °C as indicated. 4 °C incubation was used to inhibit endocytosis as a standard experiment. Cells were incubated at 4 °C for 1h before the CAP treatment, pre-chilled culture medium containing 100 μg/ml AuNPs was then replaced post CAP treatment and incubated at 4 °C for 0.5-6 h as indicated. N-Acetyl Cysteine (NAC) was used as antioxidant to remove long-lived reactive species. 4 M NAC stock solution was prepared in water. The cells were pre-incubated with 4 mM NAC in culture medium for 1 h at 37 °C. The culture medium was then removed during CAP treatment. Afterward, cells were incubated in fresh medium with 4 mM NAC and 100 μg/ml AuNPs for 24 and 48 h.

2.2.7 Fluorescent Dyes and Cell Imaging.

Lysosomes was demonstrated using the LysoTracker™ Green DND-26 (Thermo Fisher Scientific). Cells were seeded in 35 mm glass-bottom dishes (Greiner Bio-One) at a density of 1×10^5 cells/ml overnight and treated with CAP for 0-40 s at 70-80% confluency, the fresh medium containing 0-100 μg/ml AuNPs was then replaced and incubated for 24h or 48 h at 37 °C as indicated. After treatment, the cells were rinsed thrice with phosphate buffered saline and incubated with prewarmed (37 °C) LysoTracker-containing (50 nM) medium for 5 min at 37 °C. Cells were then washed once with phosphate buffered saline and loaded with fresh phosphate buffered saline and observed using Zeiss LSM 510 confocal laser scanning microscope fitted with the corresponding filter settings as follows. LysoTracker™ Green DND-26, excitation wavelength: 488 nm, emission filter: 505-530 nm; AuNPs, excitation wavelength: 633 nm, reflection filter: 649-799 nm. Plan-Apochromat 63x/1.4 Oil Ph3 was used as objective for all samples. To determine the level of AuNPs reflection, around 50 cells were randomly imaged for each treatment condition and the levels of reflection was analysed using the ImageJ and compared with other groups.

2.2.8 Statistical Analysis.

All data points were from at least triplicate independent samples and are presented and/or pooled as mean ± S.E.M unless indicated otherwise. Curve fitting and statistical analysis were carried out using Prism 6 (GraphPad Software). The Alpha for all tests is 0.05 and two-tailed P values were used. One-way ANOVA and two-way ANOVA was used to verify the significance between data points as indicated in figures (*$P<0.05$, **$P<0.01$, ***$P<0.001$, ****$p<0.0001$).

2.3   Results

2.3.1 The effects of CAP on the physical properties of AuNP.

CAP has been used to fabricate metal nanoparticles (e.g. gold and silver) without adding reducing agents (Tseng *et al.*, 2009). Moreover, AuNPs are known to agglomerate upon stresses such as repeated centrifugation, dilution, dialysis, and upon contact with biological medium (Articles and Results, 2012). We first explored whether exposure of 20 nm AuNPs to our experimental plasma device DIT 120 altered their physical parameters (size, shape, surface (zeta) potential, or extent of agglomeration) in water and biological cell culture medium. A concentration range of AuNPs (20 nm, 50-200 µg/ml) in water or culture medium was treated with CAP (75 kV, 30s), or untreated and incubated for 24 hours prior to analysis. As evident in Figure 7c, agglomeration was evident at higher concentrations (>100 µg/ml) in culture medium and no agglomeration of AuNPs was evident even at 200 µg/ml in water. CAP did not induce any significant change in particle size and there is no evidence of agglomeration either in water or in culture medium (Figure 7c, $P=0.1160$ in medium group, >0.9999 in water group). We also confirmed that dilution of AuNPs in culture medium to 100 µg/ml and exposure to CAP (75 kV, 30 s) has no significant change in relation to other physical properties such as zeta potential (Figure 7d, $P>0.05$) or optical absorption (see Figure S1 in the *Appendix*

III). Moreover, no discernible change in physical parameters was evident using Scanning Transmission Electron Microscopy, nanoparticles remaining spherical with an average diameter of 20 nm and displaying similar degrees of dispersion across the surface of the gird (Figure 7e). As AuNPs were not observed to agglomerate in culture medium for concentrations AuNPs ≤ 100 μg/ml and no changes in physical parameters were detected in response to CAP, culture medium containing up to 100 μg/ml AuNPs were used in subsequent experiments exploring uptake kinetics of AuNP.

2.3.2 Synergistic cytotoxicity when CAP and AuNPs are combined.
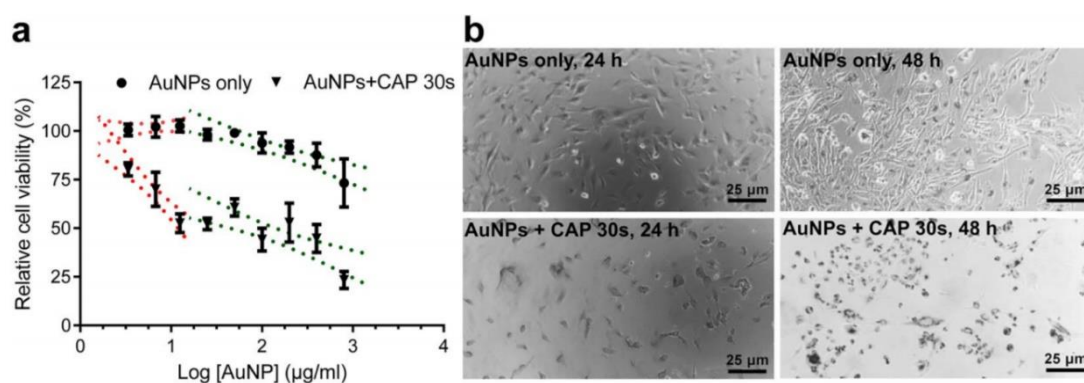
Figure 8. Cytotoxic synergy observed between CAP and AuNP.

(*a*) *U373MG cells were treated with different concentrations of AuNPs (0-800 μg/ml). After incubation for 48 h, cell viability was analysed using the Alamar Blue assay. The cell viabilities were divided into two phases (red and green) and non-linear regression was carried out. The 95% confidence bands are displayed using dotted lines. Significant differences in the slope (p<0.05) are evident using non-toxic AuNPs concentrations (0-12.5 μg/ml) which was further confirmed using Pearson's Correlation test (p<0.05). All experiments were repeated in five replicates. (*b*) After CAP treatment (75 kV, 0, 30s) U373MG cells were incubated with 100 μg/ml AuNPs for 24 h, 48 h, then observed under optical microscope.*

In our previous study, U373MG cells were exposed to CAP for between 3 and 300 s at 75 kV and the IC_{50} value of CAP treatment was determined to be 74.26 s (95% confidence

range of 47.24–116.8 s) (Conway *et al.*, 2016). The toxicity measured in U373MG cells exposed to 30 s CAP is low (18.52%, SEM=5.41%) (see Table S1 in the *Appendix III*). Figure 8a shows the results of non-linear regression analysis used to calculate IC_{50} values and confidence ranges for cells treated with AuNPs alone and AuNPs combined with CAP (75 kV, 30 s) (see Table S1 in the *Appendix III*). The IC_{50} value for AuNPs alone was 2125 μg/ml (95% confidence range: 1294-3491 μg/ml) (Inverse IC_{50}=~0.471 μl/μg), which is in agreement with other reports that ~20 nm spherical gold nanoparticles have very low cytotoxicity to healthy or cancerous cells (Connor *et al.*, 2005; Pan *et al.*, 2007). The IC_{50} value for AuNPs combined with CAP was 81.71 μg/ml (95% confidence range: 53.83-124.16 μg/ml) (Inverse IC_{50}=~12.238 μl/μg), ~26 times more toxic by comparing their inverse IC_{50}. The dose response curve was divided into two phases of toxicity (Figure 8a) to demonstrate synergy between CAP and AuNP. In the first phase, using low concentrations of AuNPs (0-12.5 μg/ml), a sharp and significant drop in viability was observed only when cells were incubated with both CAP and increasing AuNPs concentrations. The 95% confidence intervals of the slope of CAP and AuNPs treated cells during first phase (-63.57 to -33.43) was significantly different to AuNPs only treated cells (-5.573 to 12.71). We believe this provides evidence that CAP and AuNPs have a synergistic cytotoxicity to U373MG cells and the uptake of AuNPs could reach to a threshold with increase concentration of AuNP.

Morphological assessment using bright-field microscopy confirmed the accumulation of AuNPs in cells, but this was significantly greater when cells were pretreated with CAP (Figure 8b). We therefore hypothesised that CAP can accelerate the uptake and accumulation of AuNPs into U373MG cells, thereby causing higher cytotoxicity. To explore the mechanism of synergistic cytotoxicity of CAP and AuNPs, we used 100 μg/ml AuNPs which is close to the IC_{50} value, at which no discernible physical changes to

AuNPs was observed.

2.3.3 Role of active (ATP-dependent) and passive (ATP-independent) transport mechanisms.

To confirm the hypothesis that CAP affects enhanced AuNPs uptake, and to investigate the mechanisms, Atomic Absorption Spectroscopy (AAS) was used to quantify the total amount of gold in cells. Intracellular AuNPs accumulated over time and followed a similar overall non-linear relationship for cells with or without exposure to CAP. We observed that CAP significantly increased both the initial rate of uptake and total amount of AuNPs accumulated in cells (Figure 9a).

To confirm whether active transport or passive diffusion mechanisms were involved, we used the mitochondrial decoupler, NaN_3, to identify endocytosis, in which ATP is the rate limiting component. Meanwhile, cold temperature incubation (4 °C) was used to inhibit all energy-dependent uptake in cells. NaN_3 inhibited AuNPs uptake by about 50% when compared with controls (Figure 9a). Interestingly, NaN_3 treatment inhibited the uptake of AuNPs in both CAP-treated cells and untreated cells. No significant difference was observed between these two groups between 4 and 48 hours (Figure 9a), indicating that CAP-stimulated uptake of AuNPs is mainly ATP-dependent. On the other hand, NaN_3 can act as a RONS scavenger, which may lead to different conclusions. In Chapter 3, AuNPs have been demonstrated to be uptake into cells mainly via endocytosis when the cell membrane remains intact. We have demonstrated that the membrane lipids were partly peroxidised by the membrane got repaired rapidly and remains intact. Therefore, we can confirm that NaN_3 mainly inhibited the ATP-dependent endocytosis pathway. Cells were then incubated at 4 °C for 0.5, 1, 4, 6 h (cell viability was affected at longer time points). As expected, uptake of AuNPs was significantly inhibited compared with controls (Figure 9a). Together, we believe this provides evidence that an active transport

mechanism, most likely endocytosis, is the major route of uptake of AuNPs in cells, which occurred between 0 and 16 hours after incubation with AuNP, and which was stimulated by CAP exposure. We could not rule out other transport mechanisms playing a minor role. For example, we observed a small fraction (i.e. 10%) of CAP-stimulated AuNPs accumulation in cells that was not inhibited in either NaN_3 or 4 ℃-incubated cells. This second, minor CAP-dependent uptake mechanism occurs within 1-hour exposure to NaN_3 (Figure 9b) and 4 hours of exposure to 4 ℃-incubated cells (Figure 9c). Plasma-activated culture medium (PAM) containing AuNPs was used to treat cells to determine the role of long-lived reactive species (Judée *et al.*, 2016). As seen in Figure 9d, the uptake of AuNPs in PAM showed no significant difference when compared with the control after 24 and 48 h incubation.
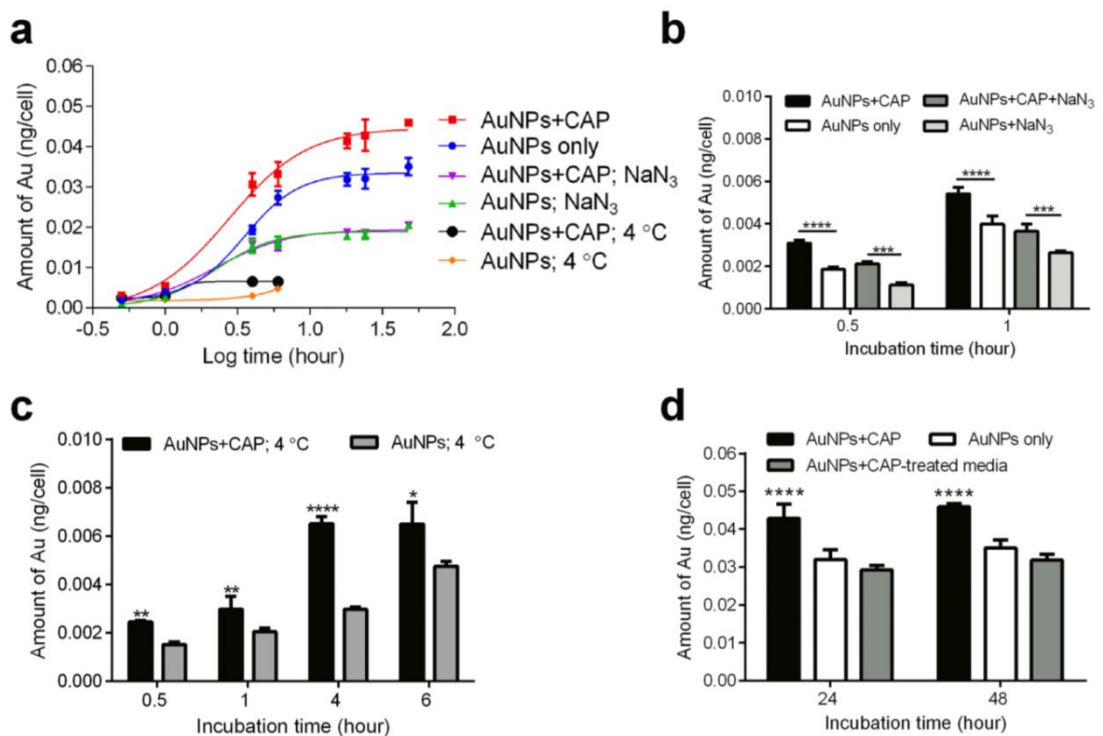
Figure 9. AAS analysis demonstrate the accelerated uptake of AuNPs into cells.

*(**a**) After CAP treatment (75 kV, 0, 30s), U373MG cells were treated with 100 μg/ml AuNPs together with 1% NaN_3 or without to inhibit endocytosis, then incubated at 37 ℃ or 4 ℃ as indicated before calculating the average amount of Au per cell using AAS. The*

2.3.4 Subcellular localization of AuNPs endocytosed in response to CAP treatment.

Despite the accuracy of using AAS to quantify to total amount of Au in a sample, one limitation with the technique is the difficulty in differentiating between AuNPs that are loosely associated with the plasma membrane compared with intracellular AuNP. To verify the uptake of intracellular AuNP, investigate the subcellular location and quantify the rate of uptake, we used confocal microscopy (Figure 10). Unlabelled, citrate-capped AuNPs were visualised using reflection of laser light from the colloid gold (red dots) and lysosomes were counterstained using LysoTracker Green, as shown in Figure 10a. The absorption spectrum of 20nm AuNPs confirmed that the absorption peak is around 520 nm, and that there is minimal absorbance above 600 nm (see Figure S1 in the *Appendix III*). The reflection filter setting for AuNPs was set at 649-799 nm and the emission filter for LysoTracker Green was set at 505-530 nm. This allowed us to confirm that the green fluorescence signal is from LysoTracker Green (excited with argon laser) and red reflection is from AuNPs (reflected light from HeNe laser). A significant fraction of intracellular colocalization was evident (yellow), indicating that the lysosomal compartment was the major destination of AuNPs following CAP-stimulated uptake (Figure 10a). Interestingly, some AuNPs were not located in lysosomes, suggesting that

these AuNPs remained in early endosomes or had entered the cytosol, either by passive diffusion, transport mechanisms through the cell membrane or released from lysosomes subsequent to endocytosis. Significantly higher levels of intracellular AuNPs in cells were observed following CAP treatment (Figure 10b), in agreement with our AAS data. Moreover, varying the dose of CAP confirmed a significant, strong and positive correlation exists between exposure to CAP and subsequent AuNPs uptake (Figure 10c), Pearson's correlation, $r=0.9359$, $P=0.0193$.

Z-stacked images were obtained to ensure that only intracellular AuNPs were quantified. Stacked, deconvoluted confocal images were next reconstructed using rendering software (Imaris 8.0. Bitplane) to generate 3 dimensional reconstructions of individual cells. The presence of AuNPs (red) inside lysosomes (green) was confirmed by rotating and sectioning the cells around the three spatial axes and projecting sections from the x, y and z planes of the reconstructions (Figure 11a, b. Taken together, our data confirm that CAP induces synergistic cytotoxicity while-stimulating the uptake of citrate capped 20nm AuNPs through a predominantly endocytic mechanism, leading to trafficking of the AuNPs into acidic (lysosomal) compartments of U373MG cells.
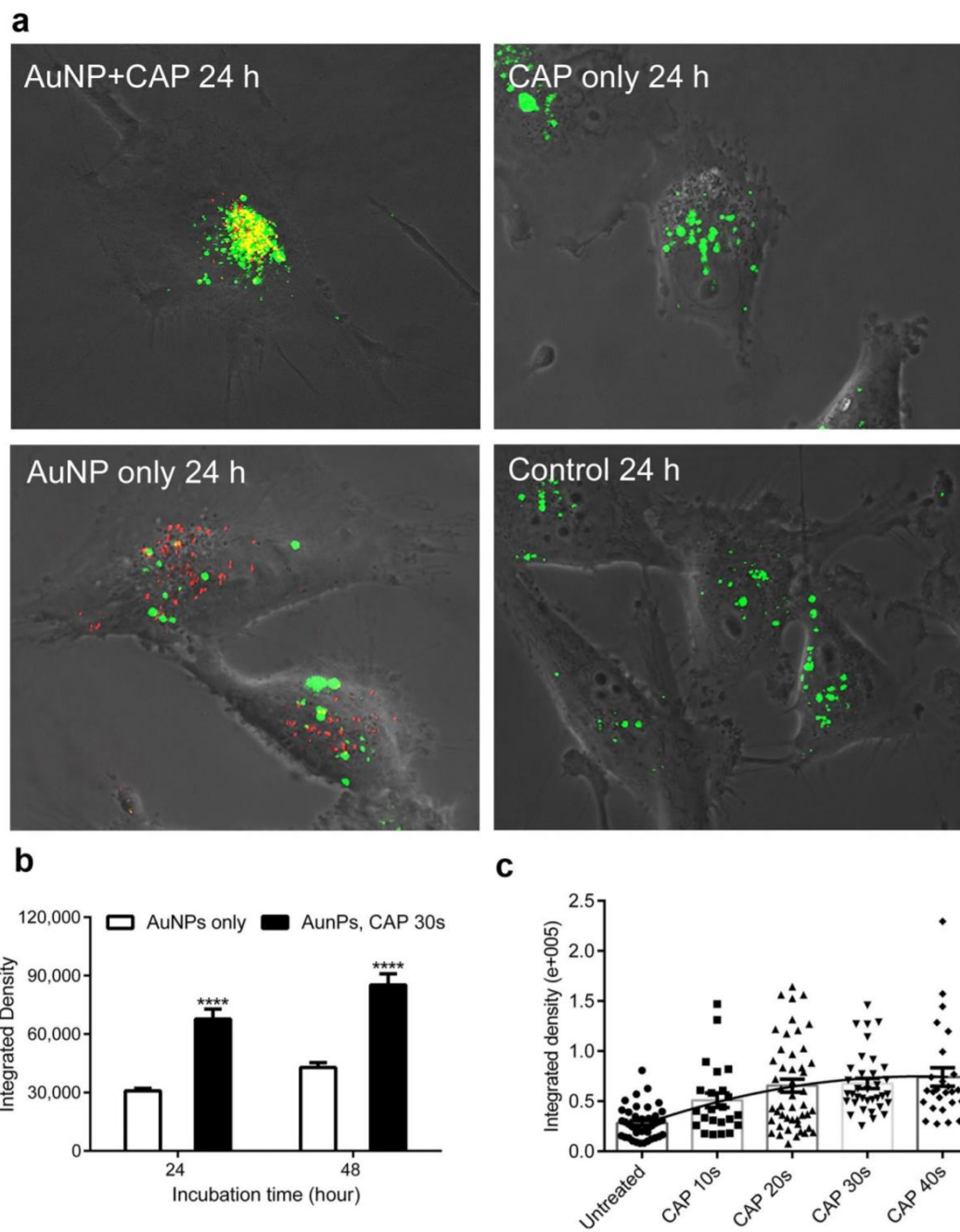
Figure 10. Uptake and subcellular localization of AuNPs observed by confocal microscopy.

*(**a**) After CAP treatment (75 kV, 0, 30 s), U373MG cells were incubated with 100 µg/ml AuNPs for 24 h. Cell lysosomes were stained using 50 nM LysoTracker™ Green DND-26. The reflection of AuNPs was measured by confocal microscopy. (**b**) After CAP treatment (75 kV, 0, 30 s), U373MG cells were incubated with 100 µg/ml AuNPs for 24 h, 48 h. Cells were then measured by confocal microscopy, the level of reflection of AuNPs was quantified using ImageJ. The statistical significance was assessed by two-way ANOVA with Tukey's multiple comparison post-test (*P<0.05, **P<0.01, ***P<0.001, ****p<0.0001), n≥20. (**c**) After exposure to CAP for increasing time (75 kV, 0-40 s), U373MG cells were incubated with 100 µg/ml AuNPs for 24 h. Cells were then measured by confocal microscopy, the level (Integrated Density) of reflection of AuNPs was quantified using the software, ImageJ. Statistical analysis was carried out using Pearson's correlation, r=0.9359, *P (two-tailed) =0.0193, n≥20.*

2.3.5 Role of physical and chemical effects of CAP on AuNPs uptake.

Our data indicated that long-lived reactive species present in plasma activated medium (PAM) did not play a major role in enhanced uptake of AuNPs (Figure 9d). We wished to further investigate effects of CAP on AuNPs endocytosis. Due to the set-up of the DBD plasma device, samples can either be placed directly in the plasma discharging area (direct exposure) or outside the plasma-discharging area (indirect exposure). Plasma sources for direct or indirect plasma treatment were previously distinguished by Fridman et, al. (Fridman *et al.*, 2008) and more recently by Von Woedtke et, al. (2013) (von Woedtke *et al.*, 2013). In indirect plasma treatment, the electrodes are part of the plasma-generating device, only and there is no significant electrical contact to the targeted structures, whereas in direct plasma treatment, the biological samples serve as one of the two electrodes. In both cases, samples are contained within a sealed reactor. Direct exposure results in direct interaction with UV, electric fields, electron beams, charged

particles, whereas indirect exposure does not result in any interaction with these physical species. However, the sealed reactor system still allows the exposure of reactive species to cells. It has been demonstrated that ozone concentration and reactive oxygen species generated are not significantly different during direct or indirect CAP exposure (Ziuzina *et al.*, 2013; Han *et al.*, 2016). We investigated the difference between direct and indirect CAP treatment on AuNPs uptake to differentiate between direct physical effects and chemical (oxidation) effects. Our results demonstrated that AuNPs uptake was significantly higher when cells were treated with indirect CAP exposure compared with untreated cells, suggesting that chemical effects were important in promoting endocytosis (Figure 11c, d). The enhanced AuNPs uptake was consistently slightly lower compared with direct CAP exposure although we were not able to determine a significant difference, suggesting that any physical effects only play a minor role in the increased uptake of AuNP. We used N-Acetyl Cysteine (NAC), a synthetic precursor of intracellular cysteine and glutathione (GSH) that replenishes intracellular GSH and scavenges reactive species as a redox buffer (Deneke, 2001) to remove long-lived ROS *in situ* during CAP treatment. This was ineffective in significantly reducing AuNPs uptake enhanced by CAP (Figure 11c, d), suggesting that either the oxidising environment generated by CAP overwhelms GSH and other intracellular anti-oxidant defences, or that NAC-insensitive chemicals produced by both direct and indirect contained CAP fields are the primary cause of enhanced AuNPs uptake.
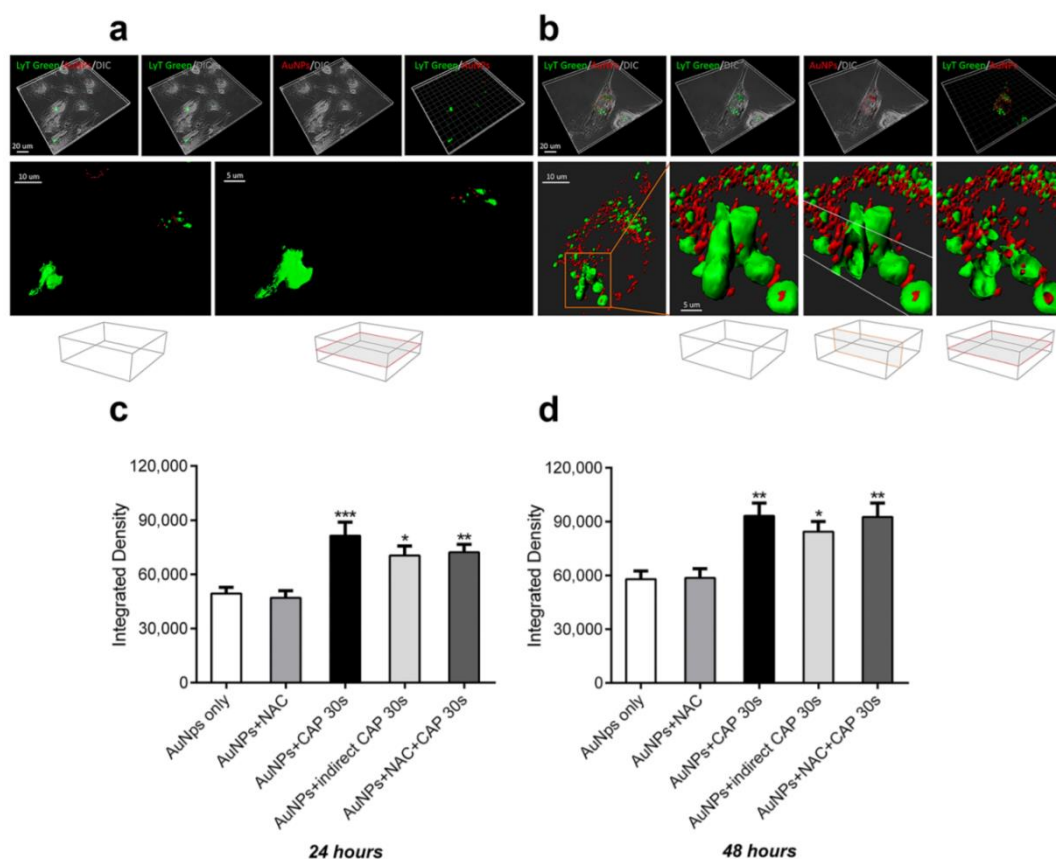
Figure 11. AuNPs are incorporated within lysosomes in glioma cells.

(**a**) 3D reconstruction of the CAP-treated glioma cells visualized with dichroic channel (grey), incorporating AuNPs (red) within lysosomes (LysoTracker green). U373MG cells were incubated with 100 µg/ml AuNPs for 24 h, after CAP treatment (75 kV, 0, 30 s) and a significant increase of AuNPs was observed in the entire cells but being part located inside lysosomes. High magnifications in bottom panel show lysosomes evidenced with green isosurface. Vertical and horizontal clipping planes reveal red AuNPs nanoparticles inside lysosomes. Boxes at the bottom indicate the orientation of the clipping planes (**b**)

*Analogous 3D reconstruction of CAP-untreated cells, demonstrated low incorporation of AuNPs inside the cells. High magnification at the bottom panel shows lysosomes rendered with green isosurface. Horizontal clipping plane revealed no red material inside lysosomes. (**c, d**) The role of short and long-lived reactive species generated by CAP on endocytosis in U373MG cells was determined by pretreating cells with 4 mM anti-oxidant N-Acetyl Cysteine (NAC) for 1 h before CAP treatment (75 kV, 30 s) or by indirect CAP treatment (see detail in Method). The level of reflection of AuNPs was quantified using the ImageJ after incubated for 24 (c) or 48 hours (d). The statistical significance was assessed by two-way ANOVA with Tukey's multiple comparison post-test (*P<0.05, **P<0.01, ***P<0.001), n ≥ 20..*

2.4   Discussion

AuNPs have been developed as promising theranostic agents for brain cancer therapy in diverse applications, such as *in vivo* tumour imaging, inducing radiosensitization and targeted delivery of chemotherapeutics across blood-brain barrier (BBB) to brain cancer cells (Joh *et al.*, 2013; Setua *et al.*, 2014). As an emerging platform for drug delivery, the toxic effect of AuNPs to normal cells can be minimized or eliminated by altering the size. (Pan *et al.*, 2007) However, the proportion of AuNPs that penetrate the BBB is usually no more than 1% (Dykman and Khlebtsov, 2012). To date, efforts to enhance AuNPs crossing of the BBB have been mainly focused on targeting AuNPs to the surface receptors of endothelial cells (Kumar, Zhang and Liang, 2013) and the limited success means that there is still need for further studying the mechanisms of crossing BBB and blood-tumour barriers, etc. The permeability, targeting capacity and uptake of AuNPs into targeted cancer cells are the key to successful clinical application of AuNP. CAP treatment has been extensively investigated in cancer therapy, due to its promising selective capacity of killing a wide range of cancer cells (Yan *et al.*, 2015), such as

carcinomas, glioblastomas, melanomas and hematopoietic malignancies (Kim *et al.*, 2008; H. J. Lee *et al.*, 2009; Yan *et al.*, 2012). In recent years, CAP has been successfully and safely used in a prospective clinical trial for head and neck cancer treatment and chronic wound healing, demonstrating significant benefits and no side-effects. Meanwhile, the synergistic anti-cancer effects between AuNPs and CAP were reported in several previous studies (Kim *et al.*, 2008; Cheng *et al.*, 2014; Irani *et al.*, 2015; Kaushik *et al.*, 2016; Zhu *et al.*, 2016).

Although cancer cells are generally reported to be favourably sensitive to CAP induced cytotoxicity when compared with normal cells or tissues (Babington *et al.*, 2015), U373MG GBM cells have significantly higher resistance to CAP treatment compared to other cancer cell lines (Conway *et al.*, 2016). GBM cells also show high aggressiveness and resistance to radiation therapy and most chemotherapies (Candolfi *et al.*, 2007). There is evidence in the literature that AuNPs have synergistic cytotoxicity combined with CAP, although the mechanisms remain to be elucidated. Therefore, we chose to study the mechanism of CAP, combined with AuNP, as a possible future chemotherapy delivery vehicle. In this study, we confirmed that combining CAP with AuNPs increased around 25-fold of U373MG cell death compared to AuNPs only. We also demonstrated that CAP treatments accelerate the endocytosis of U373MG cells by temporarily increaseing membrane permeabilisation or turnover, thereby increasing uptake and cytotoxicity of AuNP. These effects will be useful to induce higher selective cytotoxicity against cancer cells while increasing drug delivery efficiency and/or imaging diagnostics for cancer therapy.

In this study, we used 20 nm citrate capped AuNPs, which not only have optimal BBB permeability and low toxicity, but also can rapidly enter cells, mostly by receptor-mediated endocytosis (Gao, Shi and Freund, 2005; Pan *et al.*, 2007; Shilo *et al.*, 2015).

77

Therefore, 20 nm AuNPs can be the optimal candidate for drug delivery across BBB. We were able to confirm that the observation of the uptake of 20 nm citrate capped AuNPs are consistent with endocytosis and a large proportion of them were trapped in lysosomes in both CAP-treated and untreated U373MG cells (Figure 9, 4 and 5). We confirmed that CAP did not discernibly alter the physical properties of AuNP, although we did see evidence that CAP could stimulate low levels of non-active uptake through an ATP-independent mechanism, which may indicate some level of surface modification or other physical change to AuNPs and/or cell membranes. Although we were unable to detect physical changes to AuNPs exposed to CAP, significant alterations in cell membranes after exposure to CAP were previously observed by others (Recek *et al.*, 2015). Our observation that synergistic cytotoxicity occurs in parallel with enhanced uptake suggests the two processes are linked in U373MG cells. Although, there have been no studies reported to date on the relative sensitivity of normal and GBM cells to CAP-induced endocytosis, it has been demonstrated that the significant alterations in cell membrane of GBM cells induced by CAP treatment is maintained, whereas the membrane alteration in normal human astrocytes E6/E7 is weaker and reversible (Recek *et al.*, 2015). More detailed mechanisms regulating the uptake of nanoparticles in normal and GBM cells will be investigated in a follow-on study. A controllable, directable CAP treatment, which is directly applied to diseased tissue, also is expected to be included to present the in vivo experiment in the follow-on study. At this stage, we provided a likely hypothesis as follows.

It is possible that enhanced uptake of AuNPs may underpin the synergistic cytotoxicity observed, in combination with other effects such as the higher load of reactive species carried by CAP-treated AuNP. For example, it has been reported that AuNPs are capable of trapping reactive species and extending their half-life, and thus helping the delivery of

CAP generated reactive species into cancer cells (Kong, Keidar and Ostrikov, 2011). It is also likely that the enhanced accumulation of AuNPs is caused by one of three effects attributed to CAP, i.e. reactive species, direct physical effects and cellular mechanism (mainly endocytosis).

Considering the potential role of reactive species, hydrogen peroxide (H_2O_2) was found to be capable of facilitating the endocytosis of polyethylenimine /oligonucleotide (PEI/ON) complexes, involving a cytoplasmic [Ca^{2+}]-independent activation of calcium/calmodulin-dependent protein kinase II (CaMKII), which stimulates cytoskeleton contractions and transportation (Ma, Sun and Wang, 2014). It was also found that the ROS generated in mitochondria mediate the hypoxia-induced endocytosis in alveolar epithelial cells (Dada *et al.*, 2003). It is considered that CAP is capable of influencing cell behaviour by generating intracellular ROS and RNS (Conway *et al.*, 2016). These studies imply that the CAP-generated intracellular ROS could have an impact on the enhanced endocytosis. Meanwhile, reactive species are capable of inducing membrane damage and increasing the permeability of cell membrane (Djordjević, 2004). The reactive species generated in the cytoplasm or in the medium can induce lipid peroxidation in membranes by oxidizing the polyunsaturated fatty acids. Reactive species are also able to attack membrane proteins, causing the membrane damage (Djordjević, 2004). It has been found that the membrane lesions are capable of activating rapid endocytosis to remove damage parts and preserve and repair the integrity of cell membrane (Idone *et al.*, 2008). Therefore, it is possible that the chemical and physical membrane damage caused by CAP could activate the membrane repair response, thus accelerating the endocytosis of AuNPs. Although we found that long-lived reactive species have little effect on the uptake of AuNPs (Figure 9d), the short-lived, highly reactive species may play a role in the stimulated uptake, which will need to be further

elucidated.

Considering the direct physical effects, which are mainly electrical factors in DBD CAP treatment, Jinno, M et, al. has described the roles of chemical (reactive species) and electrical effects of CAP in the CAP gene transfection in L-929, mouse fibroblast cells (Jinno *et al.*, 2016). It was found that reactive species alone do not work, but need to be combined with electrical effects. Electroporation effects, which can last for a few minutes, were also found to play a role in gene transfection (Jinno *et al.*, 2016). Computational modelling was used to determine that large pore formation in spherical cell membranes (i.e. 15-25 nm) can be induced in strong electric fields *in silico* (Krassowska and Filev, 2007), a notion which has since been confirmed for 20 nm AuNPs *in vitro* (Zu *et al.*, 2014). Meanwhile, it was observed that the treatment of CAP in GBM cells results in an uneven membrane and development of membrane pores (Cheng *et al.*, 2015). Nina Recek et. al. have studied the differential effects of CAP on cell membranes of normal human astrocytes (E6/E7) and GBM cells by atomic force microscopy. CAP treatment causes a temporary disappearance of microvilli in E6/E7, and unrecoverable partial cell membranes and cell components damage of GBM cells. The temporary pores created in membranes and membrane damage could be the ATP-independent mechanism that stimulates low levels of non-active uptake of AuNPs during the first few hours after treatment with NaN_3 or under low-temperature incubation (Figure 9b, c). Moreover, it is also known that CAP is capable of temporarily changing the polarity/potential of the membrane, which also could play a role in stimulating endocytosis (Dong, Liu and Xiong, 2017). As seen in Figure 11c, d, the indirect treatment, which removes the direct physical effects caused by CAP, showed only slightly decreased accumulation of AuNPs and no significant difference evident compared with direct treatment. It confirmed that the temporary direct physical influence caused by DBD CAP treatment plays only a minor

role in the increased uptake of AuNP.

It is considered that the endocyosis of cells can be stimulated by CAP via reactive species and other mechanisms such as membrane damage, as indicated above (Idone *et al.*, 2008; Ma, Sun and Wang, 2014; Jinno *et al.*, 2016). In gene transfection, the clathrin-dependent endocytosis stimulated by CAP was found to be dominant in the uptake, while synergistically combining with electrical effects (Jinno *et al.*, 2016). We observed two phases to the enhanced uptake of AuNP. Over the first one hour, we observed both increased endocytosis and possibly also increased passive diffusion through damaged or otherwise permeable membranes (Figure 9b, c). We then observed a second phase, between 4 and 18 hours, where AuNPs uptake was further accelerated by CAP primarily though endocytosis with no evidence for further passive mechanisms before reaching a maximum accumulated threshold (Figure 9a).

Taken together, we report that the synergistic cytotoxicity of AuNPs and CAP is a result of enhanced endocytosis and trafficking to the lysosomal compartment as well as temporarily increased membrane permeability, due to CAP treatment. This contributes understanding to the mechanisms of synergistic cytotoxic effects between CAP and nanotechnologies and identifies strategies that may be employed for the release of drugs when used in a drug-delivery capacity.

CHAPTER 3. COLD ATMOSPHERIC PLASMA STIMULATES CLATHRIN-DEPENDENT ENDOCYTOSIS TO REPAIR OXIDISED MEMBRANE AND ENHANCE UPTAKE OF NANOMATERIAL IN GLIOBLASTOMA MULTIFORME CELLS

Part of this Chapter has been published.

See Appendix I

3.1 Introduction

Cold atmospheric plasma (CAP) is increasingly studied in a growing number of clinical trials for cancer treatment (Fridman *et al.*, 2008; Guerrero-Preston *et al.*, 2014) and research is ongoing to explore the combination of CAP with other therapies, including nanoparticles, radiotherapy and chemotherapy (Kim *et al.*, 2008; Collet *et al.*, 2014; He *et al.*, 2020).

Gold nanoparticles (AuNPs) are known to be weakly-toxic to human cells and be readily manufactured and designed for targeting delivery of various therapeutic compounds into cells. Citrate-capped cationic AuNPs may adsorb serum proteins onto their surface and thereby stimulate receptor-mediated endocytosis(Alkilany and Murphy, 2010). Without special surface functionalisation, AuNPs enter cells and become trapped in vesicles (Chithrani, Ghazani and Chan, 2006; Alkilany and Murphy, 2010; Freese *et al.*, 2012) or enter the nucleus, depending on their size/shape (Tsoli *et al.*, 2005; Ryan *et al.*, 2007). Meanwhile, AuNPs with functionalised surface chemistries/ligands can directly penetrate the membrane and enter the cytoplasm (Verma *et al.*, 2008).

Recently, AuNPs have emerged as a promising reagent, combined with CAP, for anti-cancer therapy (Kim *et al.*, 2008; Irani *et al.*, 2015; Zhu *et al.*, 2016). CAP generates a unique physical and chemical environment, including generating short- and long-lived reactive nitrogen species (RNS, e.g. excited N_2, N_2^+, $ONOO^-$ and $NO^{\bullet}$, etc.) and reactive oxygen species (ROS, e.g. $^{\bullet}OH$, O, $^{\bullet}O_2^-$ and O_3, etc.), photons as well as heat, pressure gradients, charged particles, and electrostatic and electromagnetic fields, many of which are known to induce biological effects (Stoffels, Kieft and Sladek, 2003; Kong, Keidar and Ostrikov, 2011; Babington *et al.*, 2015). Parallels to this can be found in phagocytes of the immune system. Enzymatic production of RONS along with various hypohalous acids, especially hypochlorite, play a significant role in respiratory bursts, also known as

oxidative bursts, which are used in the clearance of tumour cells by phagocytic immune cells including neutrophils, macrophages and monocytes (Reuter *et al.*, 2010). Anti-cancer cytotoxicity induced by respiratory bursts has been shown to induce spontaneous regression in mouse tumour models (Chao *et al.*, 1994; Hicks *et al.*, 2006; Zivkovic *et al.*, 2007).

Reactive species can induce a free radical chain reaction in membrane lipids leading to lipid peroxidation, oxidative degradation of the lipids, disruption of membrane function and induced injury and disorder in cells. Peroxidated lipid products can induce further propagation of free radical reactions (Halliwell *et al.*, 1992). Several ROS and RNS generated by CAP can induce cell injures via lipid peroxidation (Leopold and Loscalzo, 2009), for instance, hydroxyl radicals ($^{\bullet}OH$) react with various cellular components, including membrane lipid (Adibhatla and Hatcher, 2008) while superoxide ($^{\bullet}O_2^-$) can form peroxynitrite ($ONOO^-$), which is able to initiate lipid peroxidation, after reacting with nitric oxide (NO) (Adibhatla and Hatcher, 2008). RNS, such as NO_2 and ONOOH, also interact with lipids to form nitrated lipids, which have been demonstrated to play roles in vascular and inflammatory cellular signalling pathways (Leopold and Loscalzo, 2009).

Independent application of AuNPs and CAP for cancer therapy has been widely investigated. Recent studies have shown that combination of AuNPs and CAP is emerging as a novel and promising therapeutic approach against malignant tumours, resulting in synergistic anti-cancer effects. Synergistic cytotoxicity has been demonstrated for various AuNPs when combined with CAP against several cancer cell lines including melanoma (Kim *et al.*, 2008), breast cancer (Zhu *et al.*, 2016), glioblastoma (Cheng *et al.*, 2014), alveolar basal epithelial cancer (Kim *et al.*, 2017) and colorectal cancer cells (Irani *et al.*, 2015).

In our previous study, we demonstrated CAP in combination with AuNPs shows promising synergistic cytotoxicity to U373MG Glioblastoma multiforme (GBM) cells and ATP-dependent uptake mechanism (He *et al.*, 2018). Kim et al. demonstrated that epidermal growth factor-conjugated AuNPs combined with CAP induced DNA damage and selective apoptosis of A549 human cancer cells after uptake via receptor-mediated endocytosis (Kim *et al.*, 2017). Shi et al found that CAP treatment can induce iron-dependent oxidative stress to stimulate fluid-phase endocytosis in in mesothelioma cells (Shi *et al.*, 2017).

However, the precise route of uptake requires further investigation. Herein, we demonstrate, for the first time, that synergistic effects of nonfunctionalised AuNPs combined with CAP is via clathrin-mediated endocytosis pathway and is triggered as part of the CAP-induced membrane repair process in GBM cells. Numerical modelling of the uptake of AuNPs, confirmed that CAP treatment stimulated a new uptake route separate from normal cellular processes and in response to lipid peroxidation. Meanwhile, our use of CAP as an alternative novel tool to trigger and understand membrane oxidative damage and repair mechanisms is outlined.

3.2   Methods

3.2.1 Cell Culture and Gold Nanoparticle Treatment.

U-251 MG (formerly known as U-373 MG) (ECACC 09063001), human brain glioblastoma cancer cells (Obtained from Dr Michael Carty, Trinity College Dublin) were cultured in DMEM-high glucose medium (Merck, Arklow, Ireland) supplemented with 10% FBS (Merck) and maintained in a 37 °C incubator within a humidified 5% (v/v) CO_2 atmosphere. Gold nanoparticles were synthesised by trisodium citrate reduction of auric acid. 20nm sphere citrate-capped AuNPs were used to treat cells whose properties were determined in a previous study (He *et al.*, 2018). The gold colloid was concentrated to

2500 μg/ml then diluted in culture medium to 100 μg/ml.

3.2.2 CAP Configuration and Treatment.

The current research uses an experimental atmospheric dielectric barrier discharge (DBD) plasma reactor, which has been described and characterised in detail (Moiseev *et al.*, 2014; Conway *et al.*, 2016). Unless otherwise stated, all U373MG cells were treated within containers, which were placed in between two electrodes, at a voltage level of 75 kV for 30 s. The culture medium was removed prior to CAP treatment then replaced with fresh culture medium afterwards.

3.2.3 H_2DCFDA Assay and Optical Emission Spectroscopy (OES) and Ozone measurement.

H_2DCFDA (Thermo Fisher Scientific, Ballycoolin, Ireland) was used to detect ROS induced by CAP treatment. U373MG cells were seeded into the TC dish 35 standard (Sarstedt, Belfast, UK) at a density of 2×10^5 cells/ml and incubated overnight to allow adherence. After washing twice with PBS, cells were incubated with 25 μM H_2DCFDA in serum-free medium for 30 min at 37 °C. Cells were then washed with PBS twice, culture medium once and treated with CAP at 75 kV for 30s. The fluorescence of H_2DCFDA was measured using flow cytometry 30 minutes later.

Optical emission spectroscopy was carried out using an Edmund Optics CCD spectrometer with a spectral resolution of between 0.6 nm to 1.8 nm. The spectra was measured using BWSpec[TM] software with a spectral range between 200 and 850 nm and was acquired every 7.5 s with an integration time of 1500 ms. Total relative intensity of each emission line was calculated using the integral of the area under each peak. EEDF was calculated using a line ratio method (N_2 at 337 nm and N_2^+ at 391 nm) (Begum, Laroussi and Pervez, 2013). O_3 was sampled using a standard Gastec sampling pump in conjunction with a Gastec detection tubes immediately after plasma discharge had ceased.

3.2.4 Measurement of Hydrogen Peroxide, Nitrite and Nitrate Concentrations.

The concentrations of hydrogen peroxide, nitrite and nitrate were quantitatively measured in CAP-treated culture medium without phenol red. Concentrations of hydrogen peroxide, nitrite and nitrate were determined employing the $TiSO_4$ assay, Griess reagent and 2,6-dimethylphenol assay, respectively. The quantitative methods have been described in detail elsewhere (Lu *et al.*, 2017). To eliminate the effect of the culture medium on photometrical measurements, the results of CAP-treated groups were standardised with untreated culture medium.

3.2.5 Lipid Peroxidation.

For TBARS assay, thiobarbituric acid (TBA), trichloroacetic acid, MDA were purchased from Merck. U373MG cells were seeded into TC Dish 150 (Sarstedt) at a density of 1×10^5 cells/ml and incubated until confluence. After CAP treatment, cells were further incubated for 24 h, and collected by trypsinisation, centrifuged (100 g for 5 min), and homogenized by sonication. 100 μl homogenate was mixed with 200 μl ice cold 10% trichloroacetic acid and incubated on ice for 15 min to precipitate protein, then centrifuged (2200 g for 15 min at 4 ℃). 200 μl of each supernatant was then mixed with 200 μl 0.67% (w/v) TBA and incubate at 100 ℃ for 10 min. After cooling, samples were measured at 532 nm for MDA.

Lipid peroxidation sensor, C11-BODIPY (581/591) (Thermo Fisher Scientific) was used for *in-situ* detection and localization of the lipid peroxidation induced by CAP treatment. Cells were incubated in fresh culture medium containing 5 μM of the probe at 37 ℃ for 30 min in advance. Then the cells were washed with PBS twice and culture medium once. After CAP treatment, cells were further incubated with fresh medium for 30 min at 37 ℃ and observed using flow cytometry and confocal microscope as described later.

3.2.6 Flow Cytometry.

BD Accuri™ C6 Plus flow cytometry (BD Bioscience, Allschwil, Switzerland) was used in this study. Cells were loaded with C11-BODIPY and treated with CAP as described above (Lipid peroxidation). To prepare aliquots, all floating and attaching cells were collected by trypsinisation and then washed twice with PBS. For the measurement, a 488 nm laser was used for excitation, and 10,000 gated events were collected. Green fluorescence (oxidised dye) and red fluorescence (non-oxidised dye) was measured using an FL1 standard filter (533/30 nm) and FL2 standard filter (585/40 nm), respectively.

For Propidium iodide (PI) staining, cells were exposed to CAP 75kV for 30s and incubated at 37 °C for 30 minutes afterwards, then collected by trypsinisation, resuspended into 1ml PBS. Resuspended cells were stained with 1μg/ml PI for 5 minutes. The fluorescence of PI was then measured at FL2 (585/40nm) standard filter.

3.2.7 Inhibitor Studies.

To inhibit various endocytic pathways, cells were pre-incubated with Pitstop (12.5 μM, 5 min) chlorpromazine (10 μg/ml, 10 min), filipin (5 μg/ml, 30 min), genistein (200 μM, 30 min), amiloride (50 μM, 30 min) and methyl-β-cyclodextrin (10 mM, 30 min) in culture medium for the time indicated, at 37 °C. After inhibiting treatment, the culture medium was removed during CAP treatment, prewarmed fresh culture medium containing 100 μg/ml AuNPs was then added immediately to the dishes and incubated for 3 h before observing using a Zeiss LSM 510 confocal laser scanning microscope.

Transferrin conjugated with Alexa Fluor™ 546 was used to determine the change of early endosomes induced by CAP combining various endocytosis inhibitors. After the inhibiting and CAP treatments indicated above, the cells were incubated in prewarmed fresh medium for 0 or 3 h, then incubated with 25 μg/ml transferrin in medium for 5 min. Afterwards, cells were fixed with 4% PFA and then observed using confocal microscopy. The details of the confocal microscope are described in following section.

3.2.8 Clathrin Silencing.

MISSION® esiRNA (human CLTC) and MISSION® siRNA transfection reagents were purchase from Merck. 50,000 U373MG cells were seeded into each 35 mm glass-bottom dishes (Greiner Bio-One, Lörrach, Germany) and incubated overnight. 1.2 ul esiRNA stock was mixed with 20 ul of transfection reagent in 400 μl serum-free medium and incubated for 15 minutes at room temperature. In glass-bottom dishes, previous medium was replaced with 1 ml of prewarmed fresh medium with serum. The siRNA/transfection reagent solution was then added onto the cells and homogenized to final volume of 1.2 ml. Afterwards, U373MG cells were incubated at 37 °C for 24 h and then incubated with fresh medium containing 100 μg/ml AuNPs for 3 h before observing using confocal microscopy.

3.2.9 Endocytosis Tracking and Cell Imaging.

Early endosomes, late endosomes, lysosomes were demonstrated using the CellLight™ Early Endosomes-RFP, BacMam 2.0, the CellLight™ Late Endosomes-RFP, BacMam 2.0 and the LysoTracker™ Green DND-26, respectively (Thermo Fisher Scientific). 35 mm glass-bottom dishes (Greiner Bio-One) were used as containers for confocal imaging. For early and late endosome marker, 2 μl of BacMan 2.0 reagent per 10,000 cells was added in fresh medium and incubated with cells at 37 °C for 16 h. Then the cells were treated with CAP for 30s and incubated with fresh medium containing 100 μg/ml AuNPs for 3 h at 37 °C. Before observing under a Zeiss LSM 510 confocal laser scanning microscope, cells were washed twice with PBS and incubated with fresh medium containing 50 nM LysoTracker for 5 min at 37 °C. The corresponding filter settings were as follows. AuNPs, excitation 633 nm, reflection 649-799 nm; Transferrin conjugated with Alexa Fluor™ 546, excitation 568 nm, emission 580-630 nm; CellLight™ Early Endosomes-RFP, BacMam 2.0, excitation 568 nm, emission 580-630 nm; CellLight™

Late Endosomes-RFP, BacMam 2.0, excitation 568 nm, emission 580-630 nm; LysoTracker™ Green DND-26, excitation 488 nm, emission 505-530 nm; C11-BODIPY (581/591), excitation 1: 488 nm, emission 1: 500-560 nm; excitation 2: 568 nm, emission 2: 560-620 nm. Plan-Apochromat 63x/1.4 Oil Ph3 was used as objective for all samples. The integrated density of fluorescence in the confocal images was quantified using ImageJ software. The confocal images were unscaled, the quantified integrated density being the sum of the pixel values in the selection, which is the selected fluorescent area.

3.2.10 Statistical Analysis.

At least triplicate independent tests were carried out for each data point, unless indicated otherwise. Error bars of all figures are presented using the standard error of the mean (S.E.M). Prism 6 (GraphPad Software) was used to carry out curve fitting and statistical analysis. Two-tailed P values were used and the Alpha for all experiments is 0.05. The significance between data points was verified using one-way ANOVA and two-way ANOVA with Tukey's multiple comparison post-test, as indicated in figures ($*P<0.05$, $**P<0.01$, $***P<0.001$, $****p<0.0001$).

3.3 Results

3.3.1 Numerical Modelling of the Uptake of AuNPs by GBM Cells
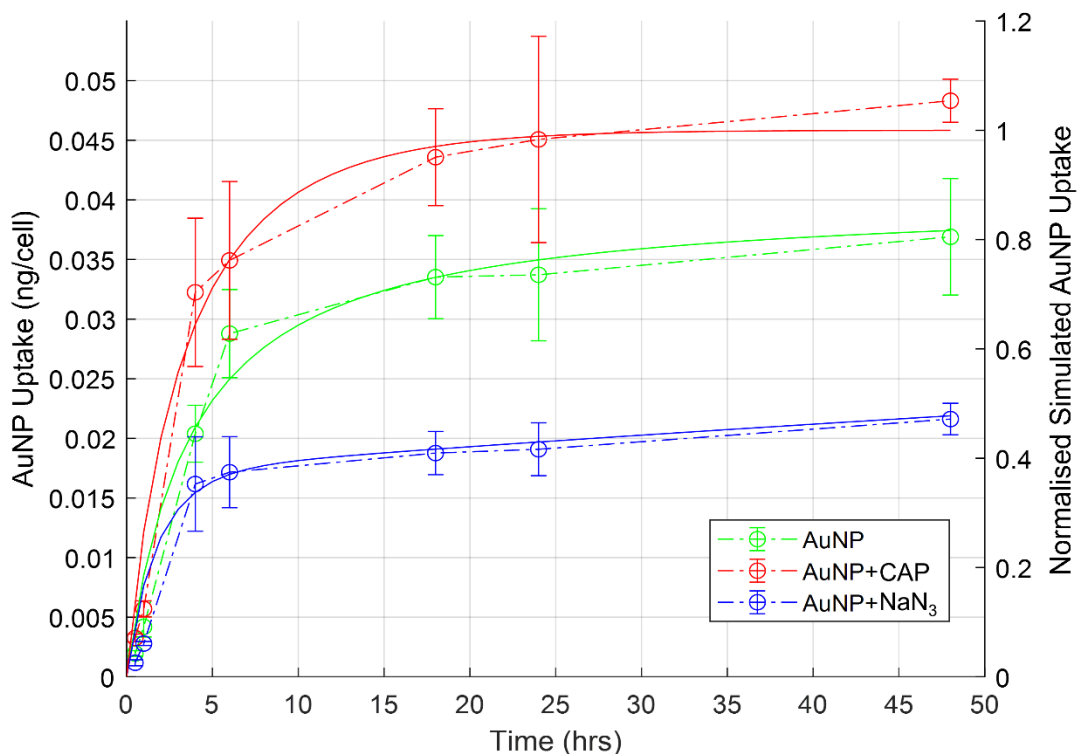
Figure 12. Modelling uptake of AuNPs.

Numerical modelling of experimental data from our previous uptake study (He *et al.*, *2018) (shown with open circles and dashed lines) was carried out for simulated AuNPs uptake (green solid line), AuNPs uptake quenched by incubation of the cells with NaN3 (blue solid line), AuNPs uptake on application of low dose CAP (red solid line). The simulated uptake of AuNPs has been normalised to the maximum calculated value.*

The accumulation of AuNPs inside U373MG cells was monitored using atomic absorption spectroscopy and the dose response curve of AuNPs with or without CAP treatment has been presented in previous study (He *et al.*, 2018). The experimental results reproduced in Figure 12 (open circles/dashed lines) were further analysed according to a simulated uptake model to better understand the possible mechanism of CAP-stimulated AuNPs uptake. Uptake of nanoparticles by cell populations *in vitro* has previously been

91

modelled according to a phenomenological rate equation approach (Maher *et al.*, 2014; Souto *et al.*, 2016; Byrne and Maher, 2019), which was extended here to further investigate the role of CAP in AuNPs uptake.

The rate of uptake of AuNPs into a cell can be described by the equation:

$$dN_{AuNP}/dt = (D-N_{AuNP}) *(1+k_{doub}) *(N_1*R_1+N_2*R_2+N_3*R_3) \qquad (1)$$

where N_{AuNPs} is the number of internalised AuNPs, D is the initial dose of AuNPs, (D-N_{AuNP}) allows for the depletion of the applied AuNPs dose, and k_{doub} is the doubling time of the cells. N_1/R_1, N_2/R_2 and N_3/R_3 allow for three different principle uptake pathways, with respective limiting capacities of N and rates R. The first two terms describe independent active and passive uptake mechanisms, respectively, with limiting cellular capacities $N_1(0) = N_{1max}$ and $N_2(0) = N_{2max}$, such that:

$$dN_1dt = -N_1*(D-N_{AuNP}) *R_1 \qquad (2)$$

$$dN_2dt = -N_2*(D-N_{AuNP}) *R_2 \qquad (3)$$

Figure 12 (solid green line) shows the simulated uptake of AuNPs, normalised to the maximum uptake observed for AuNPs + CAP, for the case of $R_1 = 3 \times 10^{-3}$ hr^{-1}, $R_2 = 2.5 \times 10^{-5}$ hr^{-1}, $R_3 = 0$, which faithfully reproduces the experimentally observed behaviour. Quenching of the active uptake of AuNPs by NaN$_3$ is best simulated by addition of a further term in equation 2, such that

$$dN_1dt = -N_1*(D-N_{AuNP}) *R_1-N_1*NaN_3*R_4 \qquad (4)$$

where NaN$_3$ is the effective dose of sodium azide, and R_4 allows for the rapid depletion of the active uptake pathway. The experimentally observed uptake was well simulated (solid blue line) by a value of $R_4 = 3 \times 10^{-5}$ hr^{-1}, keeping all other rates as before.

In simulating the increased uptake of AuNPs upon CAP treatment, it was noted that the enhancement of a single pathway described by equations (2-4) by CAP treatment, by increasing a single uptake rate, did not faithfully reproduce the experimentally observed

behaviour, as the uptakes were limited by the parameters N_{1max} and N_{2max}. Rather, faithful reproduction of the observed behaviour required the introduction of independent uptake mechanisms for untreated and CAP treated AuNPs uptake, an observation which was critical to the interpretation of the effects of CAP treatment on the cells. Such a pathway can be represented by:

$$dN_3/dt = -N_3*(D-N_{AuNP})*R_3 \tag{5}$$

such that $N_3(0) = N_{3max}$. Upon the application of CAP, the enhanced uptake was well fitted (solid red line) by $R_3 = 2.5 \times 10^{-4}$ hr^{-1}, keeping all other rates as before.

The modelling process indicates that CAP treatment increases the capacity of the U373MG cells to uptake AuNPs by introducing a third uptake route distinct from passive uptake and normal active uptake processes. The modelling parameters employed are detailed in Table 1. Note that the parameters relating to the limiting cell uptake, N_{nmax}, were determined by the definition of the dose as 100 mg/mL. Furthermore, the process was one of simulation, rather than a mathematical fitting, so the parameters should be considered within ~10% confidence.

Table 2: The modelling parameters employed in Figure 12.

	N_{1max}	N_{2max}	N_{3max}	NaN_3	R_1 hr^{-1}	R_2 hr^{-1}	R_3 hr^{-1}	R_4 hr^{-1}
AuNP	75	150	400	8500	3×10^{-3}	2.5×10^{-5}	0	0
AuNPs + NaN₃	75	150	400	8500	3×10^{-3}	2.5×10^{-5}	0	3×10^{-5}
AuNPs + CAP	75	150	400	8500	3×10^{-3}	2.5×10^{-5}	2.5×10^{-4}	0

3.3.2 Reactive Species Generated by CAP Treatment.

To identify the possible uptake pathways implicated by the numerical modelling of our data, ROS generation of 30 s, 75 kV CAP treatment was first investigated. Several RONS were measured using optical emission spectroscopy (OES) and Gastec gas detector tubes, including N_2, N_2^+, ${}^{\bullet}OH$, and O_3. OES emission intensities from the N_2 second positive system (SPS) were measured at 315, 337, 357, and 377 nm, the N_2^+ first negative system (FNS) at 391 nm, and ${}^{\bullet}OH$ at 310 nm were measured. The data demonstrated a relatively constant RONS production throughout the 30 s treatment (Figure 13a).
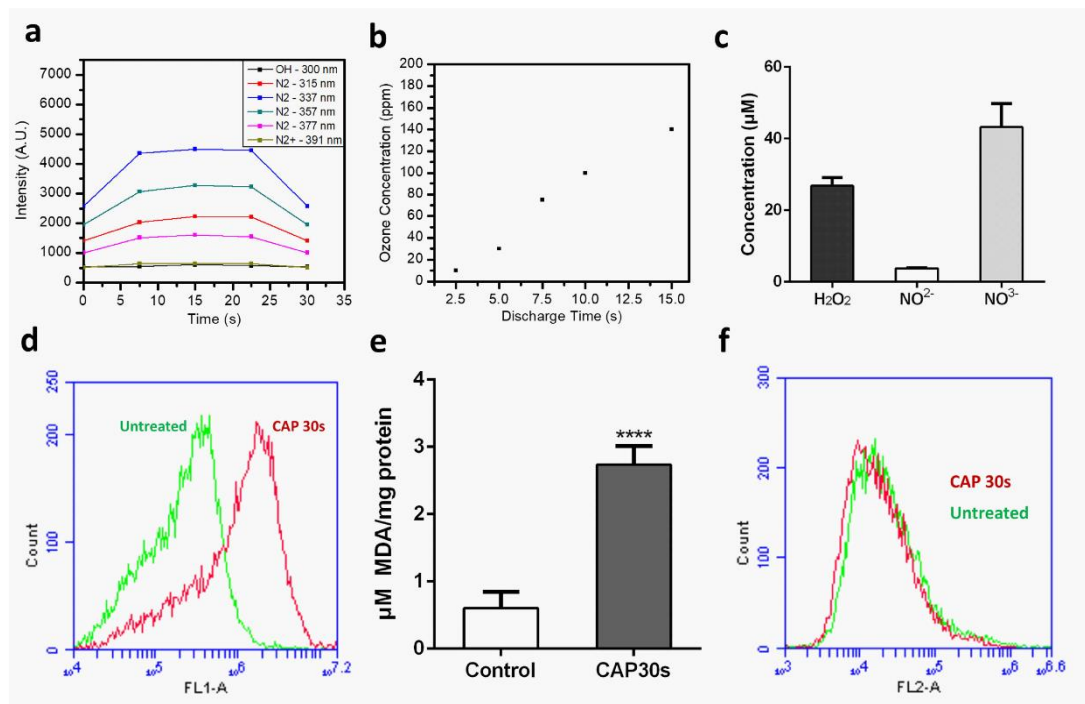
Figure 13. Measurement of reactive species generated by CAP treatment by OES and H₂DCFDA, TBARS assay and PI staining.

(a) Emission intensities of excited N_2 molecules, N_2^+ and ${}^{\bullet}OH$. (b) Concentration of O_3 measured during CAP treatment. (c) The concentrations of hydrogen peroxide, nitrite and nitrate were measured in CAP-treated culture medium. (d) Fluorescence level of intracellular oxidised H₂DCFDA was measured via Flow cytometry, left curve (green, untreated cells), right curve (red, CAP-treated cells). (e) U373MG cells were incubated for 24 hours after CAP treatment (0-30 s, 75 kV) and then collected and analysed to detect cellular MDA level using TABARS assay. (f) 30 mins after CAP treatment, cells were

stained with PI for 5 min, then measured with Flow cytometry.

The electron energy distribution function (EEDF) of the plasma was also determined. As seen in Appendix IV Supplementary Figure S1a, EEDF remained close to a ratio of 7 during CAP treatment, which indicated that the electron energies were distributed more so on the lower end of the energy scale (11 - 12 eV) than the higher energy levels (18.8 eV). The low variability of the EEDF indicated that the electric field was stable, and that the formation of the reactive species was in a steady state manner. Using Gastec ozone detector tubes, the concentrations of generated O_3 in the extracted gas were measured post-discharge of CAP treatment (Figure 13b), revealing significantly increasing levels of O_3 recorded over the discharge time, which became saturated at the maximum labelled value of O_3 detection tube after 15 s. High levels of ozone generation may give explanation why no detectable or low emission of NO, O, NO_x (NO_2, NO_3, N_2O_2, N_2O_3, and N_2O_4), $^{\bullet}OH$ and N_2^+ were measured in air using OES (Schmidt-Bleker *et al.*, 2015) (Appendix IV Supplementary Table S1).

Hydrogen peroxide (H_2O_2), nitrite (NO_2^-) and nitrate (NO_3^-) were measured and detected in culture medium (Figure 13c). Comparing with previous results (Tsoukou, Bourke and Boehm, 2018), CAP treatment of culture medium for 30 s generated very low amounts of H_2O_2 (~20 μM), NO^{2-}(~5 μM), and NO^{3-}(~30 μM) which are at least 15-fold and 200-fold lower than the IC_{50} cytotoxicity values we measured previously for U373MG cells (315 μM, >1200 μM and >600 μM respectively) and therefore are essentially non-toxic (Lu *et al.*, 2017). Intracellular H_2O_2 was significantly elevated 30 minutes after CAP treatment when measured using H2DCFDA by flow cytometry (Figure 13d). Mean fluorescence was observed to significantly increase by 4-5-fold above untreated controls (Appendix IV Supplementary Figure S1b).

3.3.3 CAP Treatment Induces Lipid Peroxidation.

ROS induces lipid peroxidation of the cell membrane (Leutner, Eckert and Müller, 2001; Schuessel *et al.*, 2006). The level of the lipid peroxidation indicator malondialdehyde (MDA), measured using the Thiobarbituric acid reactive substances (TBARS) assay, was significantly higher in U373MG cells 24 h after CAP treatment compared with the control group (Figure 13e), indicating a high level of lipid peroxidation is induced by CAP treatment. In our previous study, the IC_{50} of CAP treatment (75 kV) was determined to be 74.26 s (95% confidence range of 47.24–116.8 s) for U373MG cells (Conway *et al.*, 2016) and we demonstrated that 60 s CAP treatment induces rapid permeabilisation of U373MG cell membranes (Conway *et al.*, 2019). Here, we confirm that no significant increase of PI uptake is evident following 30 s CAP treatment compared to the control (Figure 13f), indicating that membrane integrity was not significantly affected by 30 s CAP treatment and CAP-induce lipid peroxidation. This is in agreement with our previous findings, where 30 s CAP treatment induces very low, non-significant levels of toxicity in U373MG cells 48 hours post treatment (18.52%, SEM=5.41%)(He *et al.*, 2018).

CAP induced lipid peroxidation was further analysed and visualised using the lipid peroxidation fluorescent sensor C11-BODIPY (581/591). C11-BODIPY (581/591) is a lipophilic fluorescent dye that remains membrane bound, can react with various RONS and oxidation leads to a shift of the emission peak from around 590 nm (Orange) to around 510 nm (Green) (Drummen *et al.*, 2004). To determine the level of lipid peroxidation, more than 60 cells were analysed using ImageJ software for each group. A significantly stronger emission of the oxidised green fluorescence was observed in CAP-treated cells compared to the untreated cells (****$p<0.0001$, Figure 14a, 2nd panel and Figure 14b), which was accompanied by a significant decrease in the non-oxidised orange fluorescence (Figure 14a, 1st panel and Appendix IV Supplementary Figure S2).

Furthermore, Figure 14c demonstrated a 3-fold significantly greater level of the oxidised green fluorescence in CAP-treated cells (****p<0.0001) with a focus on green fluorescent vesicle-like structures (Figure 14a, 3rd panel), likely caused by concentrated oxidised lipid membranes internalised in endosomes or lysosomes. CAP-induced oxidation of lipid membranes was confirmed using flow cytometry (Figure 14d). When cells were counterstained with LysoTracker™ Deep Red (red), examples of colocalization of oxidised membranes and acidic vesicular organelles (such as lysosomes, late endosomes, etc.) were clearly evident in CAP treated cells (Appendix IV Supplementary Figure S3, middle& right).
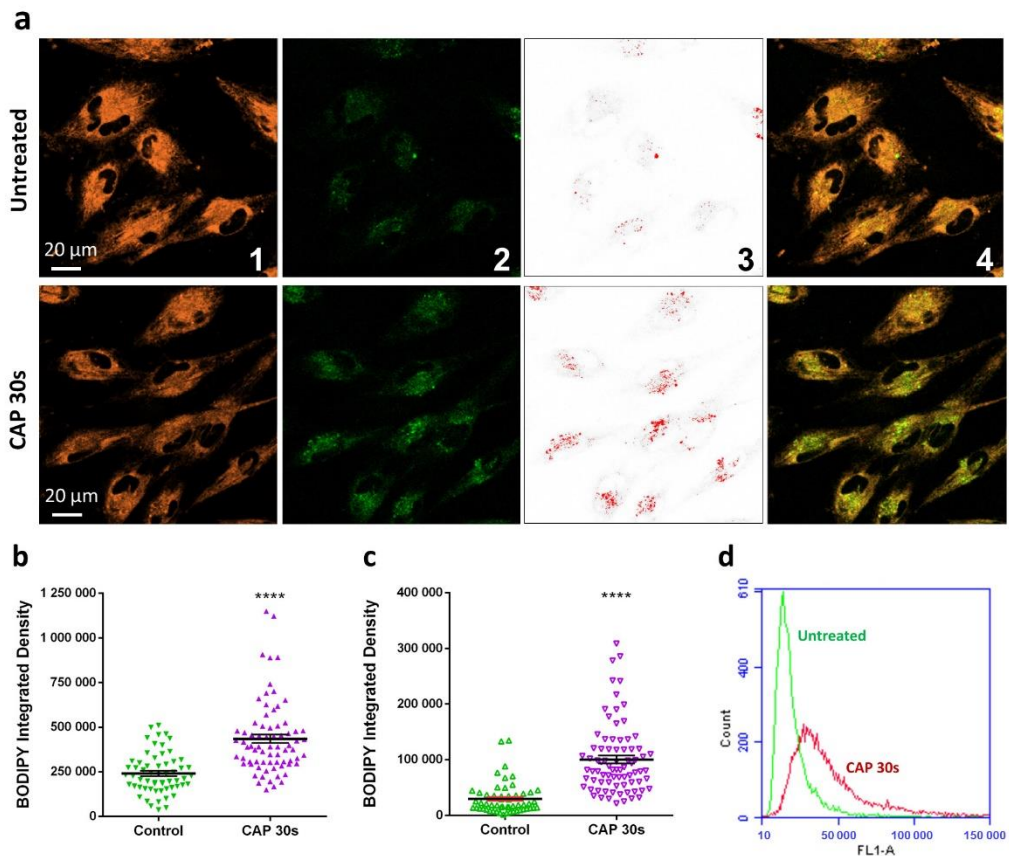
Figure 14. C11-BODIPY (581/591) staining shows lipid peroxidation and membrane trafficking inside the cell to lysosomes.

(a) Confocal imaging of C11-BODIPY loaded cells, from 1st to 4th panel: Orange, reduced form of C11-BODIPY; Green, oxidised form of C11-BODIPY; Red, vesicle-like structures was highlighted from green fluorescence using high threshold setting in

97

*ImageJ; Merged images (orange and green channels). (**b**) The total fluorescent integrated density of oxidised BODIPY was quantified using ImageJ. (**c**) With high threshold setting, the fluorescence integrated density of oxidised BODIPY was quantified with a focus on green fluorescent vesicle-like structures. The statistical significance (**b, c**) assessed by unpaired T-test. (*P<0.05, **P<0.01, ***P<0.001, ****p<0.0001), n≥50, see Appendix IV Supplementary Table S2 for original data. (**d**) Fluorescence level of intracellular oxidised BODIPY was measured via Flow cytometry, left curve (green, untreated cells), right curve (red, CAP-treated cells).*

3.3.4 Effects of CAP Treatment on Endocytosis of AuNPs.

A membrane repair mechanism has been described where cells can quickly remove damaged regions of membranes from the cell surface through rapid endocytosis (Idone, Tam and Andrews, 2008; Andrews and Corrotte, 2018). These impaired membranes can be trafficked into endosomes and finally into lysosomes. We wished to determine whether rapid endocytosis may contribute to the increased uptake of AuNPs and other materials into cells following CAP treatment. To test this hypothesis, CellLight™ Early Endosomes-RFP, BacMam 2.0 and CellLight™ Late Endosomes-RFP, BacMam 2.0 were used to further visualise the route of uptake of AuNPs after CAP treatment. Rab5a and Rab7a chimeras tagged with RFP were transfected and expressed inside cells. Following overnight incubation, Rab5a-RFP and Rab7a-RFP specifically tracked early endosomes and late endosomes, respectively (Dolman, Kilgore and Davidson, 2013). Cells were then incubated with AuNPs for 3 h after CAP treatment. In Appendix IV Supplementary Figure S4, the white arrows identify examples of co-localisation of AuNPs (red) with early (left) and late (right) endosomes (orange). Lysosomes (green) were also counterstained. We have previously demonstrated that AuNPs accumulate in lysosomes 24 hours after 30 s, 75 kV CAP treatment using confocal imaging and 3D-

image construction (He *et al.*, 2018). We demonstrate here that that AuNPs enter CAP-treated U373MG cells mainly through endocytosis and colocalise with Rab5a and Rab7a chimeras corresponding to early and late endosomes respectively, eventually accumulating in lysosomes (Appendix IV Supplementary Figure S4).

Transferrin conjugated with Alexa Fluor™ 546, is used as an early endosome marker. To investigate the immediate uptake route, CAP treated U373MG cells were incubated with Alexa546-Transferrin for 5 min, then fixed with 4% PFA. As seen from confocal imaging, within 5 mins after CAP treatment, the number of transferrin-containing endosomes was greater compared to the control group (Figure 15a). Quantification of transferrin uptake confirmed a significant increase of endosomes 5 min after CAP treatment (Figure 15b, $p<0.0001$).

Endocytosis is typically subdivided into four types, including clathrin-mediated endocytosis (CME), caveolae-mediated endocytosis, macropinocytosis and phagocytosis. We used a panel of inhibitors (Iversen, Skotland and Sandvig, 2011) to delineate the specific endocytic pathway activated by CAP (see Table 2). Clathrin-inhibitors and MβCD-induced cholesterol depletion decreased the number of transferrin labelled endosomes and AuNP-uptake 3 h following CAP treatment (Figure 15c, d) whereas caveolae-specific inhibitors and an inhibitor of micropinocytosis did not lead to any significant inhibition of Transferrin or AuNPs endocytosis in cells 3 h after CAP treatment (Figure 15e, f). Original data for quantification can be viewed in Appendix IV Supplementary Table S4.

To further confirm that clathrin-mediated endocytosis played the main role in CAP-accelerated cellular uptake, MISSION® Endoribonuclease-prepared siRNA (esiRNA) against human Clathrin heavy chain 1 (CLTC) was used to disrupting endocytosis mediated by clathrin coated pit formation. As seen in Figure 16, AuNPs uptake was much

lower in clathrin-silenced cells and no increase in AuNPs uptake was observed 3 h after

CAP treatment (p<0.0001, see Appendix IV Supplementary Table S5 for original data).

Together, our data confirms that clathrin-mediated endocytosis played an important role

in AuNPs uptake, and accelerated endocytosis following CAP treatment was clathrin

dependent.

Table 3: Inhibitors used to inhibit endocytosis in this research.

Agent	Effect	Targeting endocytosis
Pitstop	Small molecular that target and disfunction clathrin (Robertson *et al.*, 2014)	Clathrin-mediated endocytosis
CPZ	Inhibits Rho GTPase. (Wang, Rothberg and Anderson, 1993)	Clathrin-mediated endocytosis
MβCD	Extracts cholesterol from membrane. (Iversen, Skotland and Sandvig, 2011)	CME, caveolae and micropinocytosis
Filipin	Interacts with cholesterol (Iversen, Skotland and Sandvig, 2011)	A few caveolae and cholesterol-dependent mechanisms
Genistein	Inhibitor of few tyrosine kinases (Pelkmans, Püntener and Helenius, 2002)	Caveolae pinching
Amiloride	Lowers the submembraneous pH and blocks Rac1 and Cdc42 signalling (Koivusalo *et al.*, 2010)	Micropinocytosis
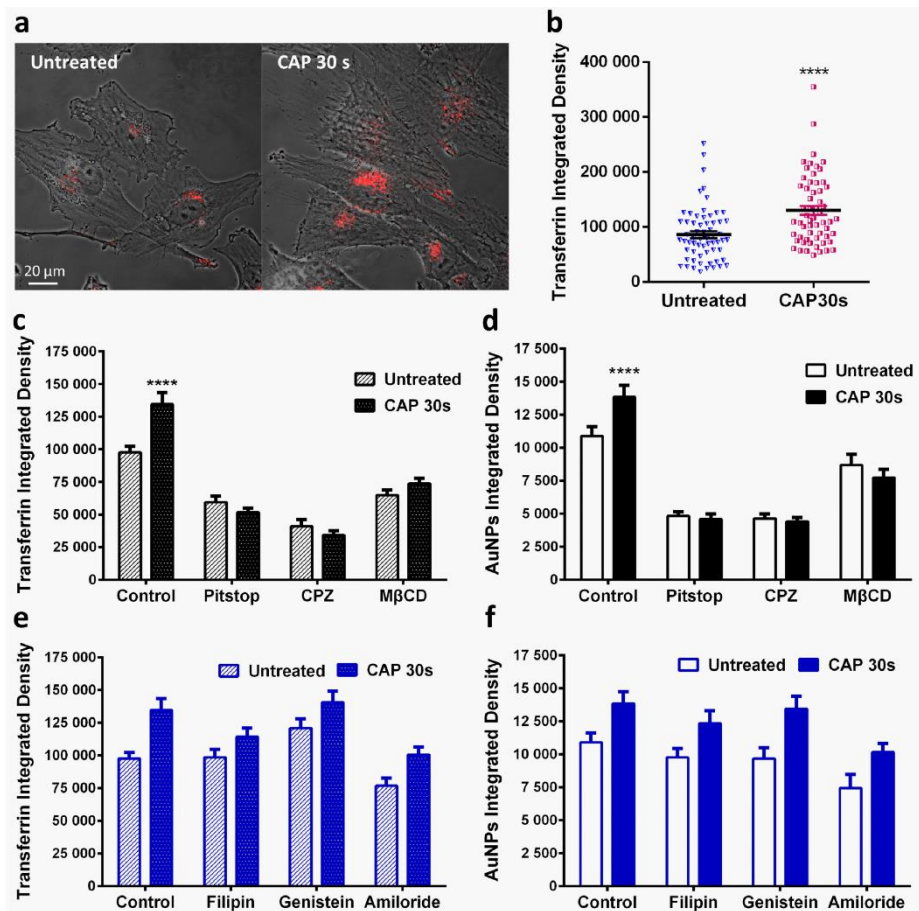
Figure 15. The CAP-induced endocytosis is clathrin-dependent.

*(**a**) After CAP treatment (0, 30 s), cells were loaded with transferrin-conjugated with Alexa Fluor™ 546 (red) for 5 min and fixed before observing with a confocal microscope. (**b**) The fluorescence level of transferrin was quantified using ImageJ, see Appendix IV Supplementary Table S3 for original data. (**c, d, e, f**) After incubation with various inhibitors as indicated, U373MG cells were treated with CAP for 0, 30 s at 75 kV and then loaded with transferrin for 5 min or 100 µg/ml AuNPs for 3 h respectively before observing using confocal microscopy, with the fluorescence integrated densities quantified using ImageJ. The statistical significance in (**b, c, d, e, f**) was assessed by one-way ANOVA with Tukey's multiple comparison post-test (*P<0.05, **P<0.01, ***P<0.001, ****p<0.0001), n≥50.*
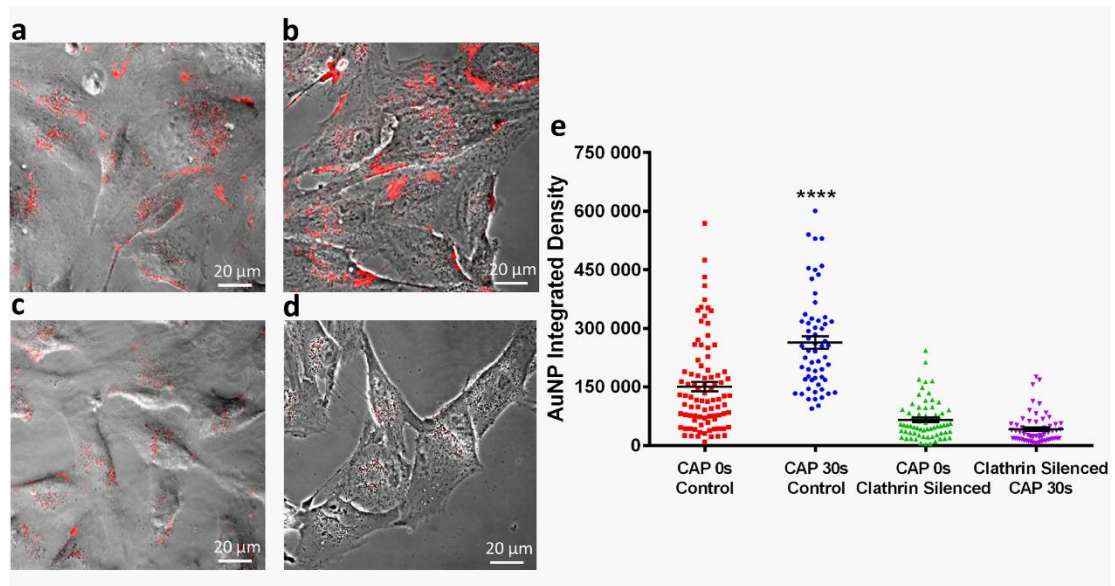
Figure 16. Clathrin silencing inhibits AuNPs uptake and CAP-induced endocytosis.

After incubation with esiRNA, targeting expression of clathrin heavy chain, U373MG cells were treated with CAP for 0, 30 s at 75 kV and then loaded with 100 µg/ml AuNPs for 3 h before observation by confocal microscopy, in comparison with unsilenced groups. (a) CAP-untreated cells without silencing, (b) CAP-treated cells without silencing, (c) CAP-untreated cells with silencing of clathrin heavy chain, (d) CAP-treated cells with silencing of clathrin heavy chain. AuNPs are identifiable as red fluorescence inside cells. (e) The fluorescence level was quantified using ImageJ and presented as integrated density. The statistical significance was assessed by one-way ANOVA with Tukey's multiple comparison post-test (*P<0.05, **P<0.01, ***P<0.001, ****p<0.0001), n≥50.

3.4   Discussion

The cytoplasmic membrane separates and protects the cellular interior from the exterior environment and provides specific and efficient exchange channels for the remaining intracellular balance and cell viability. Therefore, the integrity of the membrane is vital for all cells. Mammalian cells have developed efficient membrane repair mechanisms that can recover and reseal an injured cytoplasm membrane quickly to retain cell viability. Although investigations of the precise membrane repairing mechanisms have been

limited, four possible mechanisms, including patch, tension reduction and exocytosis/endocytosis and budding repair mechanisms have been proposed (Andrews and Corrotte, 2018). The study of cytoplasmic membrane repair usually employs bacterial pore-forming toxins, such as Streptolysin O, to create mechanical injuries on membranes (Andrews and Corrotte, 2018). Meanwhile, lipid peroxidation is a complex process that damages cellular membrane structure and function, which is believed to link to numerous human diseases and aging, including Alzheimer diseases, dementia, Huntington, Parkinson, and traumatic injuries, under presence of oxidative stress (Stockwell *et al.*, 2017; Feng and Stockwell, 2018). Many studies have shown that lipid peroxidation have various significant effects to cellular membranes, such as increased membrane permeability (Goldstein and Weissmann, 1977; Chatterjee and Agarwal, 1988; Van Der Paal *et al.*, 2016), alteration of the lipid order and membrane fluidity (Chatterjee and Agarwal, 1988; Borchman *et al.*, 1992; Petrescu *et al.*, 2001; Jacob and Mason, 2005) and activity change of membrane proteins (Mattson, 1998; Mattson *et al.*, 1999; Sevanian and Ursini, 2000; Jacob and Mason, 2005). However, there remains a paucity of literature identifying mechanisms of lipid peroxidation-related membrane damage repair, and the mechanisms of oxidised membrane repair remain unknown.

CAP is known to generate reactive species and thereby cause lipid peroxidation of cells. In this research, we explored CAP-induced lipid peroxidation using a low, relatively non-toxic dose of CAP and studied the possible mechanisms of accelerated cellular uptake of AuNPs following CAP-induced oxidative membrane damage.

As seen in Figure 12, the uptake and accumulation of AuNPs into U373MG cells was first modelled. To faithfully reproduce the experimentally observed results in our mathematical model, a new independent uptake rate was necessary in the model (equation 5). This numerical model indicates that CAP treatment may introduce a new uptake route.

Following a detailed experimental analysis, we can confirm this occurs and is due to a CAP-triggered, membrane repairing, clathrin-dependent, pathway of endocytosis.

As seen in Figure 13, we observed a relatively high level of reactive species generated in air during CAP treatment such as $^\bullet OH$, $ONOO^-$ and O_3. This was also evident in medium, cells, and ultimately in lipid membranes with the detection of RONS including hydrogen peroxide, nitrite and nitrate and detection of peroxidated lipids and by-products. Interestingly, the low doses of CAP treatment used generate non-toxic levels of RONS but still are induce significant lipid peroxidation.

CAP treatment has been shown to alter membrane structures, which may be partly due to the reactive species-caused lipid peroxidation (Adibhatla and Hatcher, 2010; Cheng *et al.*, 2014; Recek *et al.*, 2015; Conway *et al.*, 2019). However, in our study, cell membranes remain PI impermeable and therefore intact after exposing to 75 kV CAP for 30 s. Interestingly, not only did we observe a significant increase in oxidised lipids using C11-BODIPY following CAP treatment, but there was also a clear and significant increase in vesicle-like structures with high levels of oxidised C11-BODIPY, suggesting that peroxidised membrane lipids were trafficked inside cells via endocytosis (Figure 14a). An immediate (within 5 minutes) increase in endosomes was also confirmed using transferrin conjugated with Alexa Fluor™ 546.

Therefore, we propose that low, sub-toxic doses of CAP can cause cytoplasmic membrane oxidation which triggers a rapid membrane repair system. The increased endocytosis induced by membrane repair is initiated within 5 minutes and accelerates the uptake of AuNPs into U373MG cells.

To further explore the route of uptake, AuNPs were tracked in cells counterstained with Rab5a-RFP, Rab7a-RFP, and LysoTracker™ Green DND-26. Co-localisation of AuNPs with early and late endosomes and lysosomes were observed. AuNPs uptake displayed a

tendency to enter the periphery region of the cells through endocytosis, then gather at the central zone of the cells via endosome trafficking into lysosomes. This demonstrates that CAP treatment of U373MG cells triggers uptake and trafficking of AuNPs through early endosomes into late endosomes and ultimately accumulation lysosomes.

Our inhibitor studies and RNA interference studies demonstrate a primary role for clathrin-dependent endocytosis of AuNPs, and no other routes of endocytosis in CAP-triggered uptake. We compared uptake of AuNPs with Transferrin, an essential iron-binding protein that facilitate iron-uptake in cells via transferrin receptors. Uptake of Transferrin is well characterised and involves Clathrin-mediated, receptor dependent endocytosis (Lakadamyali, Rust and Zhuang, 2006). Interestingly, Shi et al found that CAP treatment decreased transferrin receptor-1 but could induce iron-dependent oxidative stress to stimulate significant increase in fluid-phase endocytosis, lysosome biogenesis and autophagy in mesothelioma cells (Shi *et al.*, 2017). In contrast to this, as seen in Figure 15a, b, our data demonstrates that the uptake of transferrin was significantly increased just 5 min after CAP treatment, which may due to the diversity of cell lines or CAP generation devices. Similar to AuNPs, formation of transferrin-trafficking endosomes was inhibited in both groups with 0 and 30 s CAP treatment, after exposure to specific/non-specific clathrin inhibitors, including pitstop, CPZ and MβCD. Tracking the accumulation of AuNPs demonstrates the long-term CAP-triggered uptake via a single, clathrin-dependent endocytosis route are retained for at least 24 hours post CAP treatment. Jinno M et al. demonstrated in a CAP-induced gene transfection model using mouse fibroblasts that a clathrin specific inhibitor showed 60% decrease in the gene transfection efficiency and that both clathrin-dependent endocytosis and electroporation played a role in enhanced transfection efficiency (Jinno *et al.*, 2016). The work of Jinno M et al. supports our investigation that clathrin may play key roles in CAP-

induced cellular uptake mechanisms in response to different materials.

Our data indicate that oxidised lipids can be seen to colocalise with endosomes and lysosomes demonstrating the intracellular sites where the repair of peroxidised lipid membranes is taking place. Further investigation of these mechanisms and sites of membrane repair following CAP-stimulated oxidative damage is ongoing, to identify novel therapeutic targets that can augment CAP cytotoxicity and to fully understand the cellular mechanisms governing oxidative membrane repair.

In summary, we report that the enhanced uptake of AuNPs induced by CAP can be as a result of ROS-caused lipid peroxidation, leading to rapid plasma membrane repair via clathrin-dependent endocytosis. This contributes to our understanding of the cellular effects induced by CAP, especially membrane damage and endocytosis activation, which can be employed for efficient uptake of nanomaterials and pharmaceuticals into cells when combining CAP with cancer therapies. This mechanism of RONS-induced endocytosis will also be of relevance to researchers optimizing other cancer therapies that induce an increase in extracellular RONS.

CHAPTER 4. SYNERGISTIC CYTOTOXICITY BETWEEN PRO-DRUGS AND CAP AGAINST GLIOBLASTOMA CELLS

Manuscript in preparation.

4.1 Introduction

Extensive efforts have been made in the war against cancer in the past decades, however, the treatment of cancer is challenging due to the tumour heterogeneity and varied patient characteristics. Widespread application of advanced stage cancer treatment and early diagnosis of cancer are still the highest aspirations.

Reactive oxygen species (ROS), as natural products generated during normal metabolism pathways, play key roles in a variety of cellular activities, but also are considered as carcinogenic factors as high levels of ROS are capable of inducing damage and mutation of intracellular DNA and therefore cause malignancy (Metelmann *et al.*, 2015). However, as understanding deepened, ROS were found to be a double-edged sword to cancer cells (von Woedtke *et al.*, 2013). Evidence showed that higher levels of ROS are generated in cancer cells by comparison with normal cells, which is attributed to the higher metabolic activities and more rapid proliferation of transformed cells (von Woedtke *et al.*, 2013). Hence, the cellular antioxidant system works under heavier load to protect tumour cells from oxidative stress, which is a common feature in many types of tumours that can be targeted for development of efficient therapies. There have been reported various anticancer drugs which can induce extra generation of tumour ROS to kill cancer cells, however, they also increase the ROS level in healthy cells, which may induce DNA damage and cause secondary malignancies (Peng and Gandhi, 2012). Cold atmospheric plasma (CAP) can induce generation of ROS to adjustable levels in controllable area (Welz *et al.*, 2015). Meanwhile, prodrugs, which only have cytotoxicity after being activated by high level of ROS, have less side effects and are more specific to cancer cells (Görmen *et al.*, 2010). Therefore, combining prodrugs with CAP to locally increase tumour ROS and activate cytotoxicity only in tumour tissue may provide a novel promising combination therapy against most, if not all, cancers.

We have acquired in total 47 various types of prodrug candidates from our collaborators, who are experts in discovery of novel drugs, including aminoferrocene-based prodrugs provided by Prof. Andriy Mokhir (Marzenell *et al.*, 2013), ferrocene, [3] ferrocenophane and ferrocifen derivatives provided by Prof. Gérard Jaouen (Jaouen, Vessières and Top, 2015), matrix metalloproteinase pro-inhibitors and thiazolidinone-based prodrugs provided by Prof. Seth M. Cohen (Perez *et al.*, 2015), and a series of pyrazolopyrimidines derivatives provided by Prof. John Stephens (Kelada *et al.*, 2018) as described in section 1.6 (Appendix V Supplementary Table S1, S2, S3, S4 and S5).

In this chapter, we have screened those 47 candidates for their potential synergistic anti-cancer effect combined with CAP treatment and identified two leading prodrug candidates JW-04-057a and JW-04-061, which were both pyrazolopyrimidine derivates provided by Prof. John Stephens. In combination with low dose CAP treatment, which had little or no toxicity on cancer cells, the cytotoxicity of leading prodrug candidates was synergistically enhanced more than 10 times. The synergistic cytotoxicity between JW-04-061 and CAP treatment has been further demonstrated and investigated as described in following sections. The ROS generated in culture medium by CAP treatment has been determined to play the main role in the activation of prodrug JW-04-061.

4.2   Methods

4.2.1 Cell Culture

U-251 MG (formerly known as U-373 MG) (ECACC 09063001), human brain glioblastoma cancer cells (Obtained from Dr Michael Carty, Trinity College Dublin) were cultured in DMEM-high glucose medium containing pyruvate (Merck) supplemented with 10% FBS (Merck) and maintained in a 37 °C incubator within a humidified 5% (v/v) CO_2 atmosphere. For prodrug treatment, DMEM-high glucose medium without pyruvate (Merck) was used to make up culture medium for all groups to avoid the antioxidant

effects of pyruvate (O'donnell-Tormey *et al.*, 1987).

4.2.2 H₂DCFDA Assay

H₂DCFDA (Thermo Fisher Scientific, Ballycoolin, Ireland) was used to detect ROS induced by CAP treatment. U373MG cells were seeded into the TC dish 35 standard (Sarstedt, Belfast, UK) (for flow cytometry) at a density of 2×10^5 cells/ml, or 35 mm glass-bottom dishes (Greiner Bio-One) (for confocal imaging) at a density of 1×10^5 cells/ml and incubated overnight to allow adherence. After washing twice with PBS, cells were incubated with 25 μM H₂DCFDA in serum-free medium for 30 min at 37 °C. 30 minutes before measuring the fluorescence of H₂DCFDA using flow cytometry, cells were then washed with PBS twice, culture medium once and treated with CAP at 75 kV for 30s. For confocal imagining, cells were washed with PBS twice, culture medium once and treated with CAP at 75 kV for 30s, then were observed under a Zeiss LSM 510 confocal laser scanning microscope 30 min later (excitation 488 nm, emission 505-530 nm).

4.2.3 CAP Configuration and Prodrug Treatment.

The current research uses an experimental atmospheric dielectric barrier discharge (DBD) plasma reactor, which has been described and characterised in detail (Moiseev *et al.*, 2014; Conway *et al.*, 2016). Unless otherwise stated, all U373MG cells were treated within containers, which were placed in between two electrodes, at a voltage level of 75 kV for 10-40 s. The culture medium was removed prior to CAP treatment then replaced with fresh culture medium afterwards. An optimized prodrug treatment protocol was developed and applied in this project as described below. U373MG cells were plated into 96-well plates (Sarstedt) at a density of 1×10^4 cells/well (100 μl normal culture medium per well) and were incubated overnight to allow a proper adherence. Unless otherwise stated, the plating map was 6×10 wells, for 10 different concentrations, negative and

positive control groups (5 replicates for each group). All pro-drugs were dissolved and prepared in 100% DMSO (Merck) for stock solution, which were then series diluted in culture medium to different concentrations as indicated. Afterwards, 10 μl of prodrug non-pyruvate culture medium solution was added into each well after fully removing previous medium and the rest of prodrug culture medium solution was added into empty wells in the plate (300 μl per well). The plate then was treated with CAP at 75 kV for 10-40 s as indicated. 90 μl of CAP-treated prodrug culture medium solution was then add to corresponding wells with cells to final volume 100 μl immediately after CAP treatment. Cell viability assays were then carried out after incubation for indicated time.

4.2.4 Cell Viability Assays.

Cell viability was analysed using the Alamar blue assay (Thermo Fisher Scientific), which used a redox indicator that can generate fluorescent signal by the metabolic reduction. After CAP and prodrug treatment, plates were incubated in a 37 °C incubator within a humidified 5% (v/v) CO_2 atmosphere for forty-eight hours. Afterwards, the cells were rinsed once with phosphate buffered saline (Sigma-Aldrich), incubated for 3 h at 37 °C with a 10% Alamar blue/90% culture medium solution. The fluorescence was then measured (excitation, 530 nm; emission, 595 nm) by a Victor 3V 1420 microplate reader (Perkin Elmer).

4.2.5 CAP-activated medium/prodrug/cells and Inhibitor Study.

We have investigated the effects of CAP on prodrugs alone to determine the mechanism of synergistic cytotoxicity to U373MG cells. Prodrugs were treated with CAP at 75 kV for 10 s to 10 min in DMSO stock solution or culture medium solution using 96-well plates as container as indicated. The CAP-treated prodrug solution was then added into 96-well plates to incubate with U373MG cells for 48 hours before cell viability assays. For CAP-activated medium, the culture medium was treated with CAP at 75 kV for 30

sec in 96-well plate and incubated overnight to remove short-lived reactive species. Then prodrug stock solution was series-diluted in the overnight storage CAP-activated medium and incubated with U373MG cells in 96-well plates for 48 hours before cell viability assays.

For CAP-activated cells, the U373MG cells were treated with CAP for 30 sec in 96-well plates with 10 µl culture medium without pyruvate covered in each well, while culture medium was added into empty wells in the plate (300 µl per well). Then the CAP-treated culture medium was added to each well to 100 µl. Those CAP-activated cells were then incubated in the CAP-activated medium for 0-5 hours as indicated in the figures. Afterwards, the previous medium was replaced with fresh medium containing corresponding concentrations of prodrugs. The U373MG cells were then further incubated for 48 hours before cell viability assays.

Meanwhile, N-Acetyl Cysteine (NAC) was used as antioxidant to investigate the roles of reactive species in activation of prodrugs. 4 M NAC stock solution was prepared in water. 4 M NAC solution was then diluted in culture medium till final concentration 4 mM before adding prodrugs and CAP treatment. The CAP treated culture medium containing prodrugs and 4 mM NAC was then added into 96-well plates to incubate with U373MG cells for 48 hours before cell viability assays.

Catalase stock solution (1 mg/ml) was fresh prepared with PBS, then diluted in culture medium to 0.1mg/ml for inhibition of H_2O_2 production. 10 µl of culture medium containing 0.1mg/ml catalase and corresponding concentrations of pro-drugs was added into each well of 96-well plates to treat U373MG cells with CAP, the rest of culture medium containing catalase and pro-drugs was treated in the empty wells of the same plates (300 µl per well). After CAP treatment, 90 µl of CAP-treated culture medium containing catalase and pro-drugs was added into each well and the U373MG cells were

then incubated with in total 100 µl of the culture medium containing catalase and pro-drugs for 48 hours before cell viability assays.

4.2.6 Statistical Analysis.

At least triplicate independent tests were carried out for each data point, unless indicated otherwise. Error bars of all figures are presented using the standard error of the mean (S.E.M). Prism 6 (GraphPad Software) was used to carry out curve fitting and statistical analysis. The isobologram and synergistic analysis were carried out using CompuSyn software (Available for free download from www.combosyn.com) according to the detail mentioned in Figure 25d legend (Chou and Martin, 2005). Two-tailed P values were used and the Alpha for all experiments is 0.05. The significance between data points was verified using one-way ANOVA and two-way ANOVA with Tukey's multiple comparison post-test, as indicated in figures (*$P<0.05$, **$P<0.01$, ***$P<0.001$, ****$p<0.0001$).

4.3 Results

The majority of prodrugs were developed to be activated in cells by oxidation induced by ROS. CAP has been well known as inducing generation of ROS (Babington *et al.*, 2015; Conway *et al.*, 2016; He *et al.*, 2018). We have demonstrated the generation of ROS by CAP in Chapter 3. In Chapter 4, besides flow cytometry, we have used confocal microscope and ROS indicator H_2DCFDA to demonstrate the ROS generated by 30 s of CAP treatment (Figure 17).
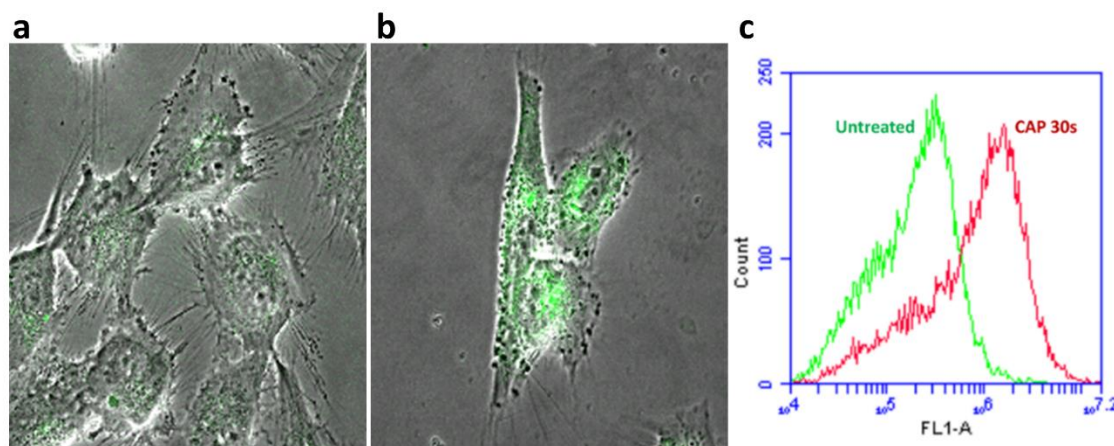
Figure 17. Measurement of reactive species generated by CAP treatment by H₂DCFDA. *Confocal imaging of H2DCFDA loaded cells: (**a**) untreated U373MG cells; (**b**) 30 s CAP treated U373MG cells. (**c**) Fluorescence level of intracellular oxidised H2DCFDA was measured via Flow cytometry, left curve (green, untreated cells), right curve (red, 30 s CAP treated cells).*

As seen in Figure 13 and 14 in Chapter 3, we have also quantified the ROS generation in cells and culture medium after 30 s of CAP treatment and measured the level of lipid peroxidation in CAP-treated U373MG cells as well. Therefore, 30 s of CAP treatment has been demonstrated to be effective on ROS generation and can be used to test the synergistic effects with prodrugs. In total four different types of prodrugs have been tested in this Chapter, including ferrocene-based prodrugs, pyrimidone bicycle family compounds, matrix metalloproteinase pro-inhibitors and thiazolidinone-based prodrugs. Due to high amount of work, and to identify leading candidates as soon as possible, all compounds were preliminarily tested in CAP-treated and control groups once to acquire dose response curves to determine the synergistic cytotoxicity. The relative IC75 values of each compounds have been summarised in Figure 18, except low or non-toxic compounds (Cmpd1, Cmpd2 and MK2, as seen in Figure 22 and 23, and Table 7 and 8). The IC75 values of control groups were separately normalised to 1 together with

corresponding CAP-treated groups. The 95% confident ranges were used to present the error bars. As see in Figure 18, the difference between control and CAP-treated groups, which presents possible synergistic cytotoxicity, was only significant with compounds 1e, PY-2-Benzyl, JW-04-057a and JW-04-061. However, according to corresponding dose response curves (Figure 19 and 22), there was no significant synergy effect between CAP treatment and compounds 1e, PY-2-Benzyl separately. Therefore, JW-04-057a and JW-04-061 have been determined as the only two leading candidates after repeating the dose response curves for two more times. Furthermore, the investigation of the synergistic effects between CAP treatment and JW-04-061 and the mechanisms behind it has been carried out and presented.
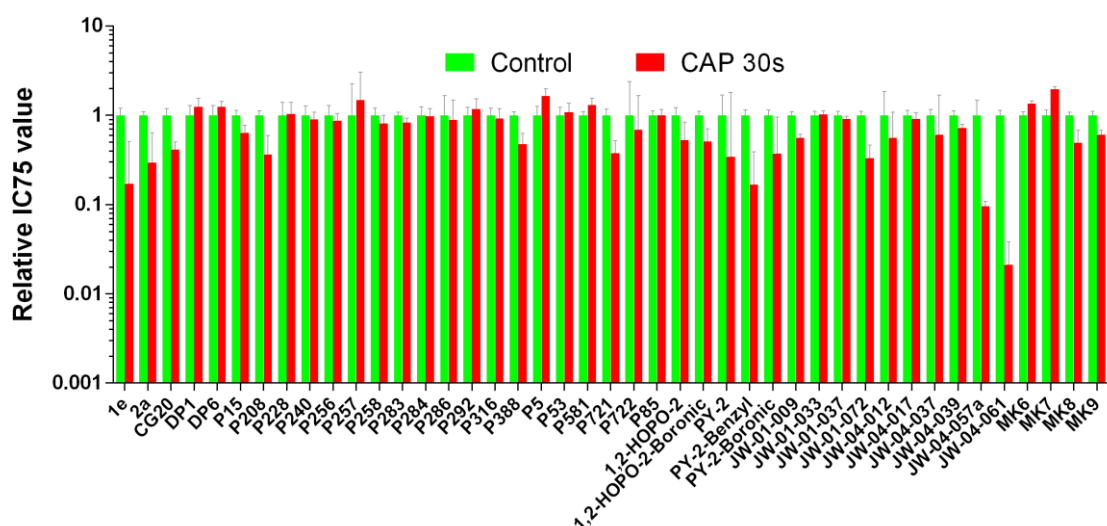
Figure 18. Summary of relative IC75 values of all available compounds.

The IC75 values were calculated using IC50 values and corresponding hillslopes, and then all control groups were normalised to 1 along with corresponding CAP-treated groups and 95% confident interval as error bar.

4.3.1 Ferrocene-based Prodrugs.
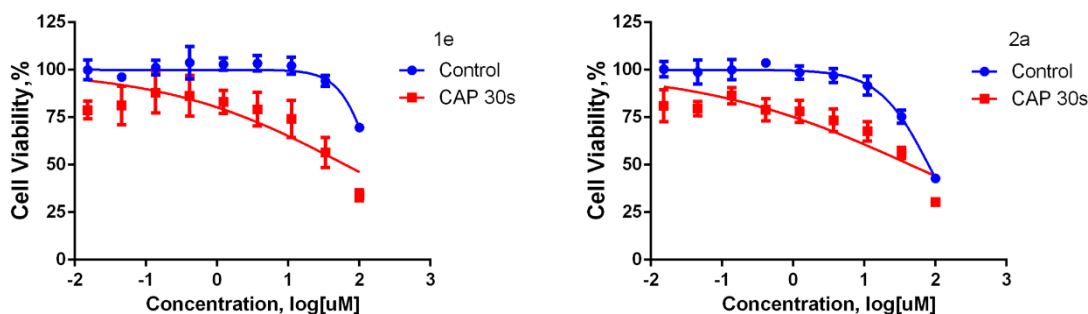
Figure 19. Dose response curves of compounds 1e and 2a, provided by Prof. Andriy Mokhir, Friedrich Alexander University, Germany.

We have acquired and received a variety of ferrocene-based prodrugs from Prof. Andriy Mokhir and Prof. Gérard Jaouen. Two aminoferrocene-based prodrugs were provided by Prof. Andriy Mokhir. As seen in Figure 19, compounds 1e and 2a had no significant synergistic cytotoxicity but additive cytotoxicity with 30 s CAP treatment. The CAP treatment decreased the IC50 values of 1e and 2a (Table 5), but the cell viabilities decreased nearly 20% in all CAP treated groups therefore same trends were presented in both dose response curves treated with or without CAP.

Table 4. IC50 values of compounds 1e and 2a, provided by Prof. Andriy Mokhir.

	Control		CAP 30s	
	IC50 (μM)	95% Confidence Intervals	IC50 (μM)	95% Confidence Intervals
1e	153	121.4 to 192.9	63.9	28.42 to 143.7
2a	80.07	72.40 to 88.55	44.56	23.46 to 84.62

Meanwhile, a series of ferrocene, [3] ferrocenophane and ferrocifen derivatives provided by Prof. Gérard Jaouen were tested with U373MG cells (Figure 20 and 21). There was no significant synergy observed between those compounds and CAP treatment. Ferrocene, [3] ferrocenophane and ferrocifen derivatives usually present strong reaction to ROS. They could be already fully activated by the relatively high ROS level in U373MG cells instead of CAP treatment, therefore, leading to no synergistic effects with CAP.

As seen in Table 6, there were highly toxic candidates, P257 (IC50: 62.64 nM, 95%

confidence intervals: 20.05 to 195.7 nM), P286 (IC50: 77.75 nM, 95% confidence intervals: 39.15 to 154.4 nM), P686 (IC50: 4.1 nM, 95% confidence intervals: 2.134 to 8.116 nM), P722 (IC50: 29.06 nM, 95% confidence intervals: 8.561 to 98.65 nM), which could be further tested both in cancer cell lines with high ROS levels and health cell lines with normal ROS levels for drug discovery for GBM treatment as a future project. It is interesting that P686 presented significantly lowed cytotoxicity when combining with CAP treatment (Figure 21), which might due to chemical or physical effects generated by CAP treatment against the structure of P686, thus deactivating the cytotoxicity of P686.

Table 5. IC50 values of compounds provided by Prof. Gérard Jaouen.

	Control		CAP 30s	
	IC50 (μM)	95% Confidence Intervals	IC50 (μM)	95% Confidence Intervals
CG20	0.233	0.1899 to 0.2859	0.1041	0.08296 to 0.1305
DP1	0.7197	0.5216 to 0.9929	0.8853	0.6660 to 1.177
DP6	5.772	4.220 to 7.894	6.697	5.556 to 8.071
P15	3.188	2.754 to 3.691	2.376	1.928 to 2.927
P208	5.746	4.991 to 6.614	3.001	1.871 to 4.815
P228	0.486	0.3139 to 0.7523	0.5175	0.3606 to 0.7426
P240	1.176	0.8729 to 1.583	1.093	0.8713 to 1.370
P256	1.626	1.180 to 2.240	1.531	1.253 to 1.872
P257	0.06264	0.02005 to 0.1957	0.09171	0.03351 to 0.2510
P258	0.5966	0.4794 to 0.7424	0.5094	0.4016 to 0.6462
P283	5.303	4.802 to 5.857	5.225	4.679 to 5.835
P284	1.396	1.073 to 1.817	1.403	1.113 to 1.768
P286	0.07775	0.03915 to 0.1544	0.07017	0.03573 to 0.1378
P292	14.56	11.28 to 18.79	18.05	13.15 to 24.77
P316	4.756	3.796 to 5.957	4.491	3.268 to 6.170
P388	21.16	18.94 to 23.63	17.17	13.92 to 21.17
P5	1.739	1.304 to 2.320	2.668	2.096 to 3.396
P53	0.229	0.1782 to 0.2944	0.2526	0.1895 to 0.3368
P581	6.813	6.099 to 7.611	8.139	6.512 to 10.17
P686	0.00416	0.002134 to 0.008116	0.3142	0.1376 to 0.7175
P721	2.104	1.721 to 2.573	0.8811	0.6000 to 1.294
P722	0.02906	0.008561 to 0.09865	0.01991	0.005744 to 0.06901
P85	5.389	4.685 to 6.199	5.773	4.893 to 6.810
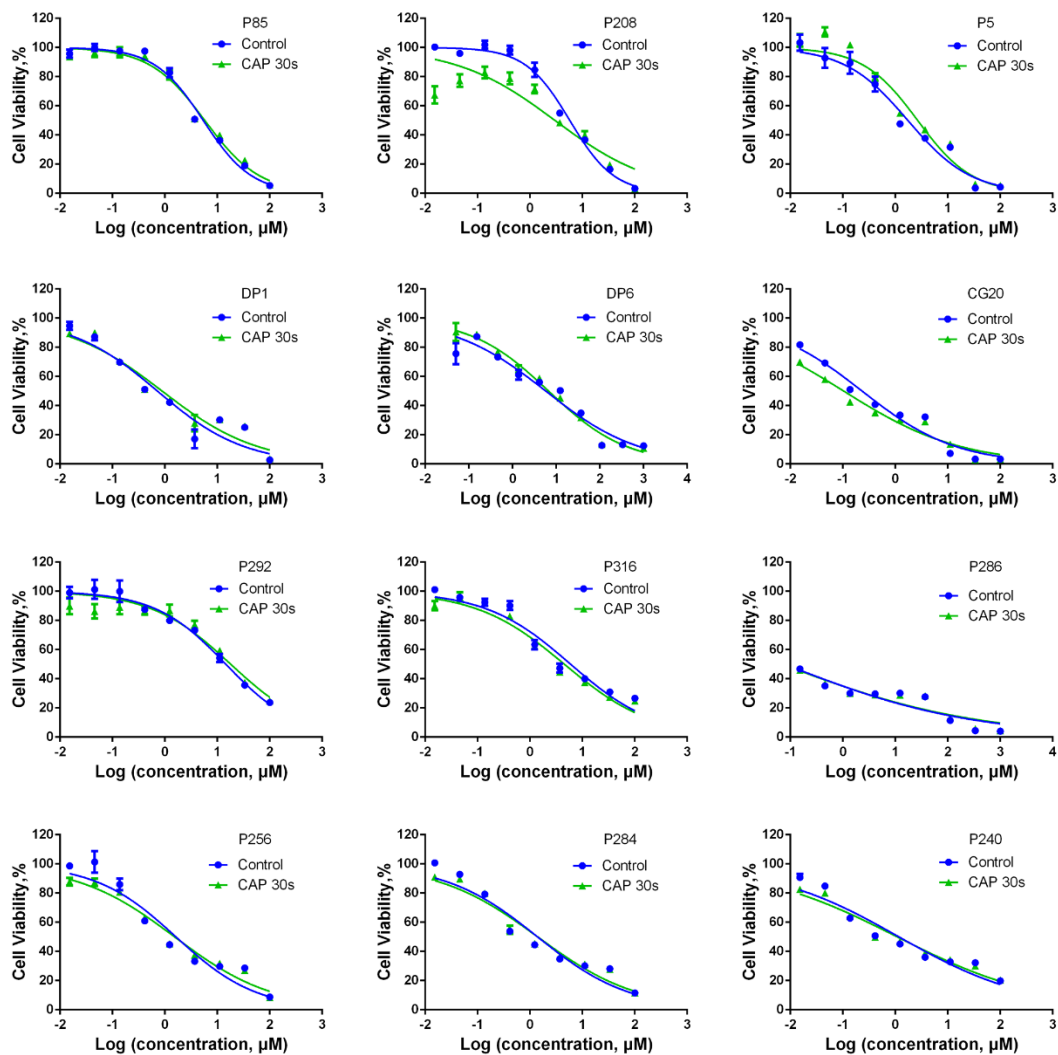
Figure 20. Dose response curves of compounds provided by Prof. Gérard Jaouen, Chimie ParisTech, France, Part 1.
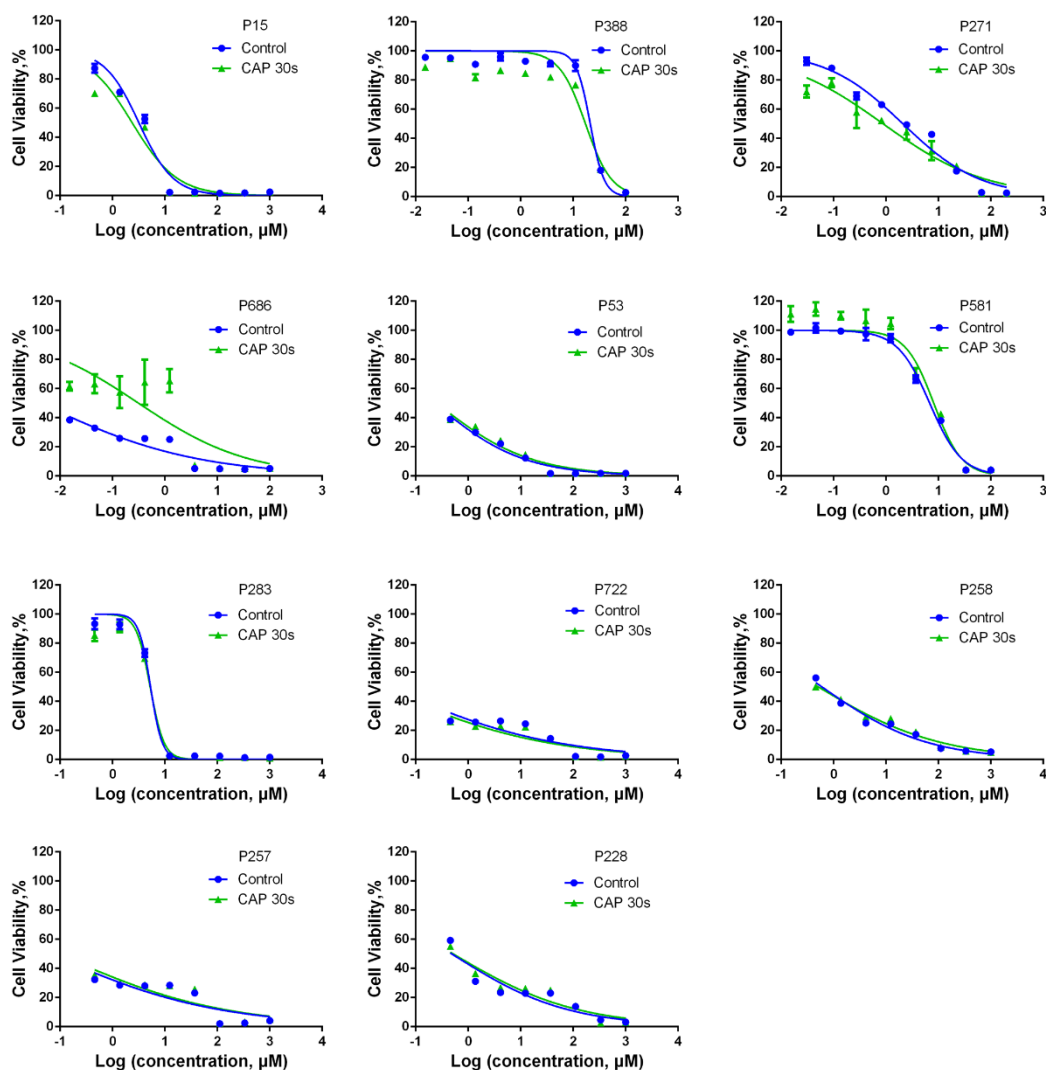
Figure 21. Dose response curves of compounds provided by Prof. Gérard Jaouen, Chimie ParisTech, France, Part 2.

4.3.2 Matrix Metalloproteinase Pro-Inhibitors and Thiazolidinone-Based Prodrugs.

Several hydrogen peroxides activated matrix metalloproteinase inhibitors and hydrogen peroxide responsive thiazolidinone-based compounds were provided by Prof. Seth M. Cohen. In our previous study, IC_{50} value of CAP treatment to U373MG cells was determined to be 74.26 s (95% confidence range of 47.24–116.8 s)(Conway *et al.*, 2016). The toxicity measured in U373MG cells exposed to 30 s CAP is 18.52%, SEM=5.41% (He *et al.*, 2018). As seen from Figure 22, the majority of the compounds presented no synergistic effects with CAP treatment. There was only additive decrease of nearly 20%

119

cell viability when U373MG cells were treated with compounds in combination with 30

s CAP treatment.

Table 6. IC50 values of compounds provided by Prof. Seth M. Cohen.

	Control		CAP 30s	
	IC50 (μM)	95% Confidence Intervals	IC50 (μM)	95% Confidence Intervals
1,2-HOPO-2	118.3	93.12 to 150.3	78.11	47.32 to 128.9
1,2-HOPO-2-Boronic	55.39	49.11 to 62.46	36.67	26.32 to 51.08
PY-2	1008	497.0 to 2045	489.9	71.38 to 3363
PY-2-Benzyl	51.83	43.88 to 61.21	17.07	8.523 to 34.18
PY-2-Boronic	47.41	40.05 to 56.12	29.19	11.60 to 73.44
Cmpd1	Not converged	Not converged	203.6	141.4 to 293.3
Cmpd2	Not converged	Not converged	4391	195.1 to 98790
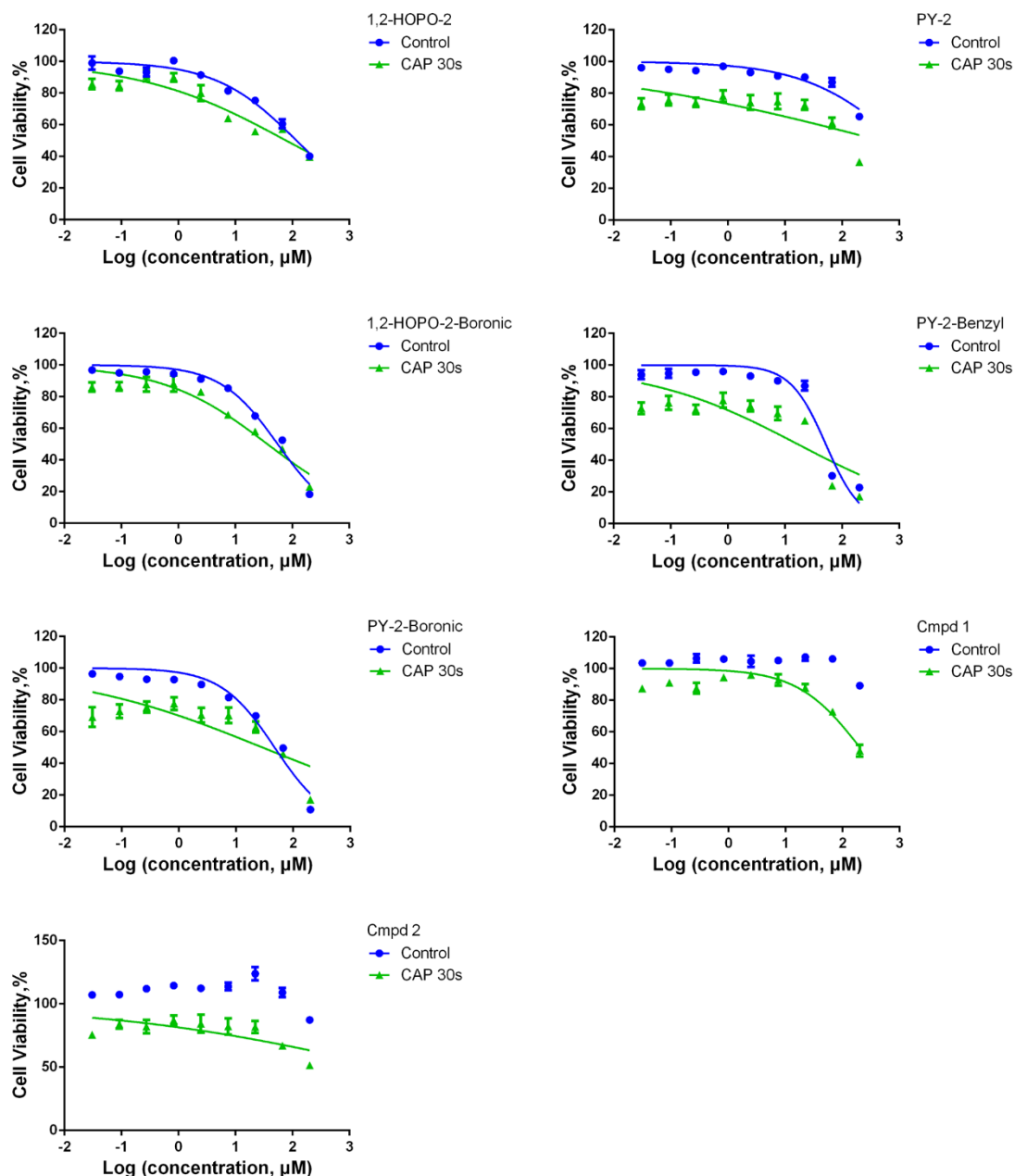
Figure 22. Dose response curves of compounds provided by Prof. Seth M. Cohen, University of California San Diego, US.

4.3.3 Pyrimidone Bicycle Family Compounds

A series of pyrazolopyrimidines derivatives, also as known as compounds from pyrimidone bicycle family, provided by Prof. John Stephens were tested using U373MG cell line. As seen in Figure 24, the majority of pyrazolopyrimidines derivatives had no synergistic cytotoxicity in combination with CAP treatment, the dose response curves of

CAP-treated groups presented high comparability and similar trends with untreated groups. The CAP treatment didn't change the IC50 values of the majority of tested compounds (Table 8).

However, the leading candidates of CAP-activated prodrugs were determined in this pyrimidone bicycle family. As seen in Figure 23, JW-04-061 and JW-04-057a presented great synergistic cytotoxicity with 30 s of CAP treatment. The CAP treatment induced a pronounced descent of dose response curves with the increasing of concentrations of prodrugs. As seen in Table 8, CAP treatment induced significant decreases of IC50 values of JW-04-061 (from 610.8 μM to 55.37 μM) and JW-04-057a (from 940.6 μM to 62.41 μM) while presenting low cytotoxicity themselves.

Therefore, among all 47 candidates of prodrugs, JW-04-061 and JW-04-057a were determined as the only two leading candidates of CAP-activated prodrugs. The dose response curves of JW-04-061 and JW-04-057a with or without 30 s CAP treatment have been repeated to further confirm the synergistic cytotoxicity (Appendix V Supplementary Figure S2). JW-04-061 has been chosen to be the research focus to save time and budget and lay the foundation for future projects.

Table 7. IC50 values of compounds provided by Prof. John Stephens.

	Control		CAP 30s	
	IC50 (μM)	95% Confidence Intervals (μM)	IC50 (μM)	95% Confidence Intervals (μM)
JW-01-009	25.51	22.84 to 28.50	12.92	11.53 to 14.48
JW-01-033	11.32	10.09 to 12.70	11.4	10.34 to 12.57
JW-01-037	197	174.3 to 222.7	126.8	113.0 to 142.4
JW-01-072	42.9	37.75 to 48.74	19.04	13.75 to 26.38
JW-04-012	13372	5733 to 31190	5670	1831 to 17555
JW-04-017	77.68	66.55 to 90.67	73.62	60.59 to 89.44

JW-04-037	366.8	306.1 to 439.5	462.1	197.3 to 1082
JW-04-039	137.2	120.2 to 156.6	86.27	76.20 to 97.68
JW-04-057a	940.6	564.2 to 1568	62.41	49.58 to 78.56
JW-04-061	610.8	523.0 to 713.4	55.37	44.94 to 68.21
MK2	Not converged		Not converged	
MK6	502.2	452.4 to 557.4	608.6	561.0 to 660.2
MK7	23.34	19.82 to 27.49	38.23	34.96 to 41.80
MK8	74.59	67.68 to 82.20	44.42	31.39 to 62.85
MK9	148.1	131.7 to 166.6	86.7	75.02 to 100.2
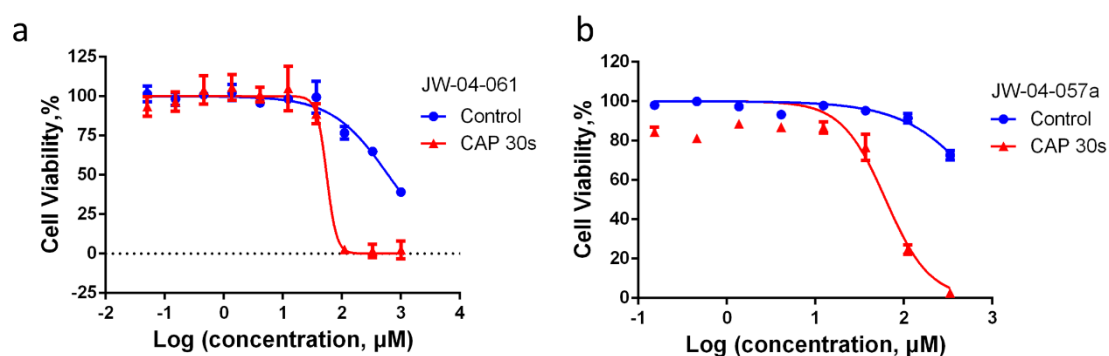
Figure 23. Dose response curves of compounds provided by Prof. John Stephens, Maynooth University, Ireland, part 1.

(*a*) *Dose response curves of JW-04-061 with or without CAP treatment.* (*b*) *Dose response curves of JW-04-057a with or without CAP treatment.*
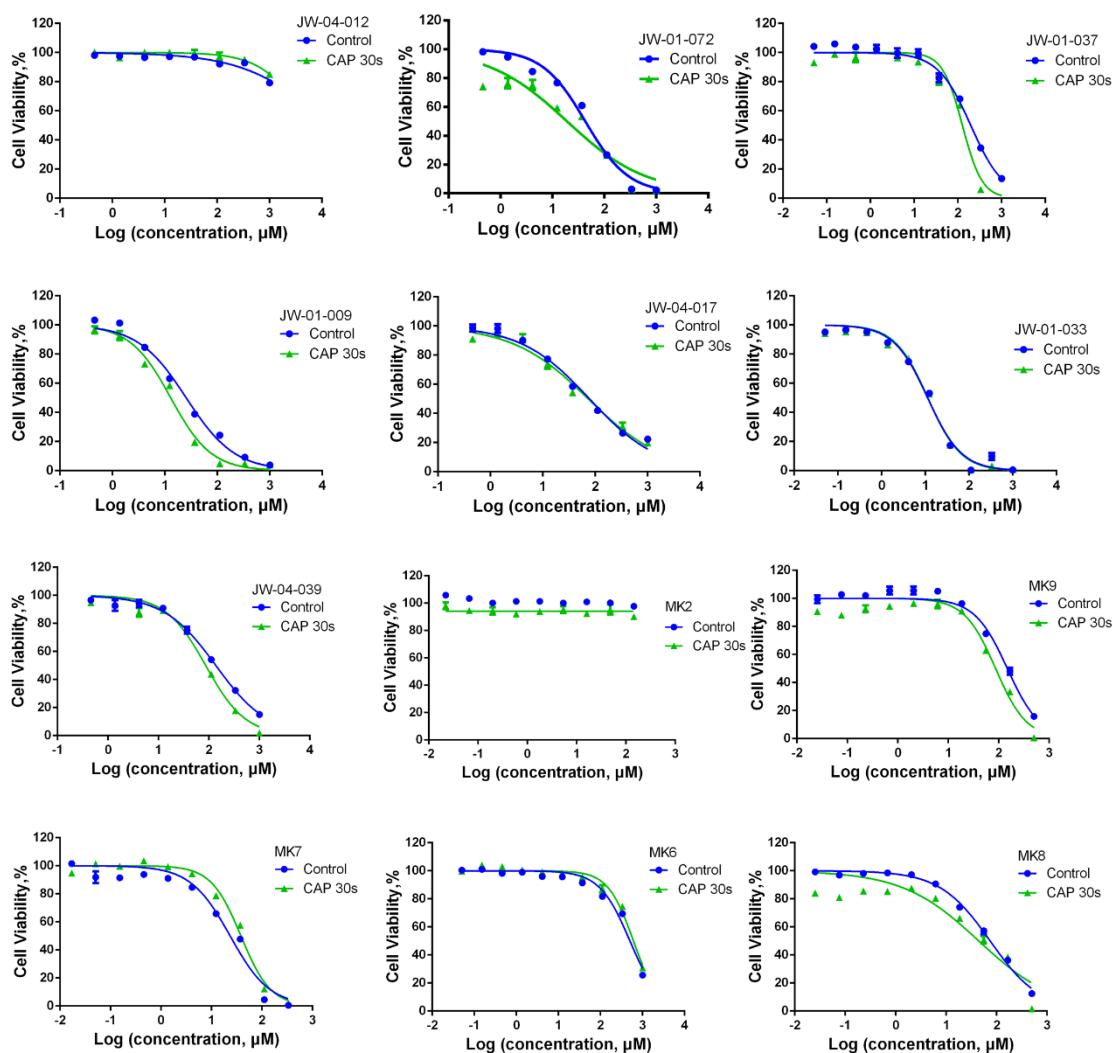
Figure 24. Dose response curves of compounds provided by Prof. John Stephens, Maynooth University, Ireland, part 2.

4.3.4 Investigate the Mechanism behind the Synergistic Cytotoxicity Between Leading Prodrug Candidate JW-04-061 and CAP Treatment.

JW-04-061 has been used to further investigate the synergistic anti-cancer effects in combination with CAP treatment. To determine the mechanism of CAP activation of JW-04-061, JW-04-061 was first dissolved in 100% DMSO and then treated with 30 s and 10 min CAP in DMSO solution. Afterwards, CAP-treated JW-04-061 DMSO solution was diluted in culture medium to 1000 μM (DMSO final concentration 1%) and series diluted to lower concentrations to incubate with U373MG cells for 48 h before Alamar Blue

assay. As seen from Figure 25c, CAP-10 min treated DMSO (series diluted concentrations starting from 1%) had no significant cytotoxicity on U373MG cells, and untreated JW-04-061, CAP 30s treated JW-04-061 in DMSO, CAP 10 min treated JW-04-061 in DMSO presented similar dose response curves and IC50 values (Table 9). This may due to the lack of ROS generation in 100% DMSO solvent, whereas the generation of reactive species relies on the present of reactants in treated liquid (Tanaka *et al.*, 2011), and the DMSO may function as scavenger of OH radicals (Eberhardt and Colina, 1988). Hence, 30 s and 10 min CAP-treated JW-04-061 DMSO solution demonstrated likely non or weak synergistic cytotoxicity in combination with CAP treatment.

To further confirm the synergistic effects between JW-04-061 and CAP, JW-04-061 was diluted in culture medium in different concentration then treated with CAP for 0-40 s. The CAP-treated JW-04-61 culture medium solution was subsequently incubated with U373MG cells for 48 h before Alamar Blue assay. As seen in Figure 25a, b, CAP 10-40 s treated JW-04-061 culture medium solution induced a pronounced decreasing of cell viability with concentrations higher than 10 μM compared with CAP untreated group, when CAP treatment alone had low cytotoxicity (~20% decrease of cell viability).

Table 8. IC50 values of JW-04-061 treated by CAP 0-30s in DMSO solution.

	Untreated JW-04-061	CAP 30s treated JW-04-061 in DMSO	CAP 10 min treated JW-04-061 in DMSO	CAP 10 min treated DMSO
IC50 (μM)	120.3	107.6	123	2279
95% Confidence Intervals (μM)	85.37 to 169.4	84.72 to 136.8	117.7 to 128.5	1228 to 4233

Meanwhile, NAC was applied as antioxidant to further investigate the mechanism. 4 M NAC solution was diluted in culture medium till final concentration 4 mM before adding JW-04-061 and 40 s CAP treatment. As seen in Figure 25a, b, the NAC treated group

presented much higher cell viability and relatively gentle decrease of dose response curve compared to CAP treated group, which demonstrated that ROS generated by CAP treatment played key roles in the activation of anti-cancer effects of JW-04-061. The normalized isobologram also have been analysed and presented in Figure 25d, which further confirm the synergistic effects between CAP treatment and JW-04-061 treated in culture medium. Using CompuSyn software, the synergistic analysis was carried out and combination index (CI) values have been calculated. The CI values of JW-04-061 with 10 s CAP were 0.31099, 0.33520 with 20s, 0.47561 with 30s, and 0.57796 with 40 s, which were all less than 1.00 and confirmed the significant synergistic cytotoxicity between CAP treatment and JW-04-061 (Figure 25d).

Taken together, we have demonstrated that JW-04-061 was mainly activated by the reactive species generated during CAP treatment, therefore presented significant synergistic cytotoxicity to U373MG cells in combination with CAP treatment.

Before the COVID-19 situation and closure of the research buildings, we acquired additional preliminary results which have been included in Appendix V, which can be used to further determine the detailed mechanism behind the synergistic cytotoxicity between CAP treatment and prodrug JW-04-061. Overnight storage CAP-activated medium, CAP-activated cells and catalase (hydrogen peroxide decomposition) have been used to study the dose response of U373MG cells to JW-04-061.

As seen in Appendix V Supplementary Figure S3a, when cells were treated with overnight storage CAP-activated medium and prodrug, no synergistic cytotoxicity was observed. Meanwhile, the U373MG cells have been activated and incubated for 0-5 hours after CAP treatment, then incubated with fresh medium containing prodrug. There was no significant synergistic cytotoxicity observed between CAP-activated cells and prodrug comparing to direct combination of CAP treatment and prodrug, but the CAP-activated

cells presented relative lower cell viability at low prodrug concentration comparing to direct combination of CAP treatment and prodrug (as seen in Appendix V Supplementary Figure S3b). On the other hand, as seen in Appendix V Supplementary Figure S3c, there was no significant synergistic effects between CAP treatment and prodrug JW-04-061 to catalase treated cells.

Table 9. IC50 values of JW-04-061 treated by CAP 0-40s in culture medium solution.

	IC50 (µM)	95% Confidence Intervals (µM)
JW-04-061 Control	270.9	218.6 to 335.6
JW-04-061 CAP10s treated medium +drug	54.37	47.56 to 62.15
JW-04-061 CAP20s treated medium +drug	31.05	26.71 to 36.10
JW-04-061 CAP30s treated medium +drug	39.21	31.27 to 49.16
JW-04-061 CAP40s treated medium +drug	37.06	31.18 to 44.04
JW-04-061 CAP40s treated medium +drug +NAC	95.65	79.08 to 115.7
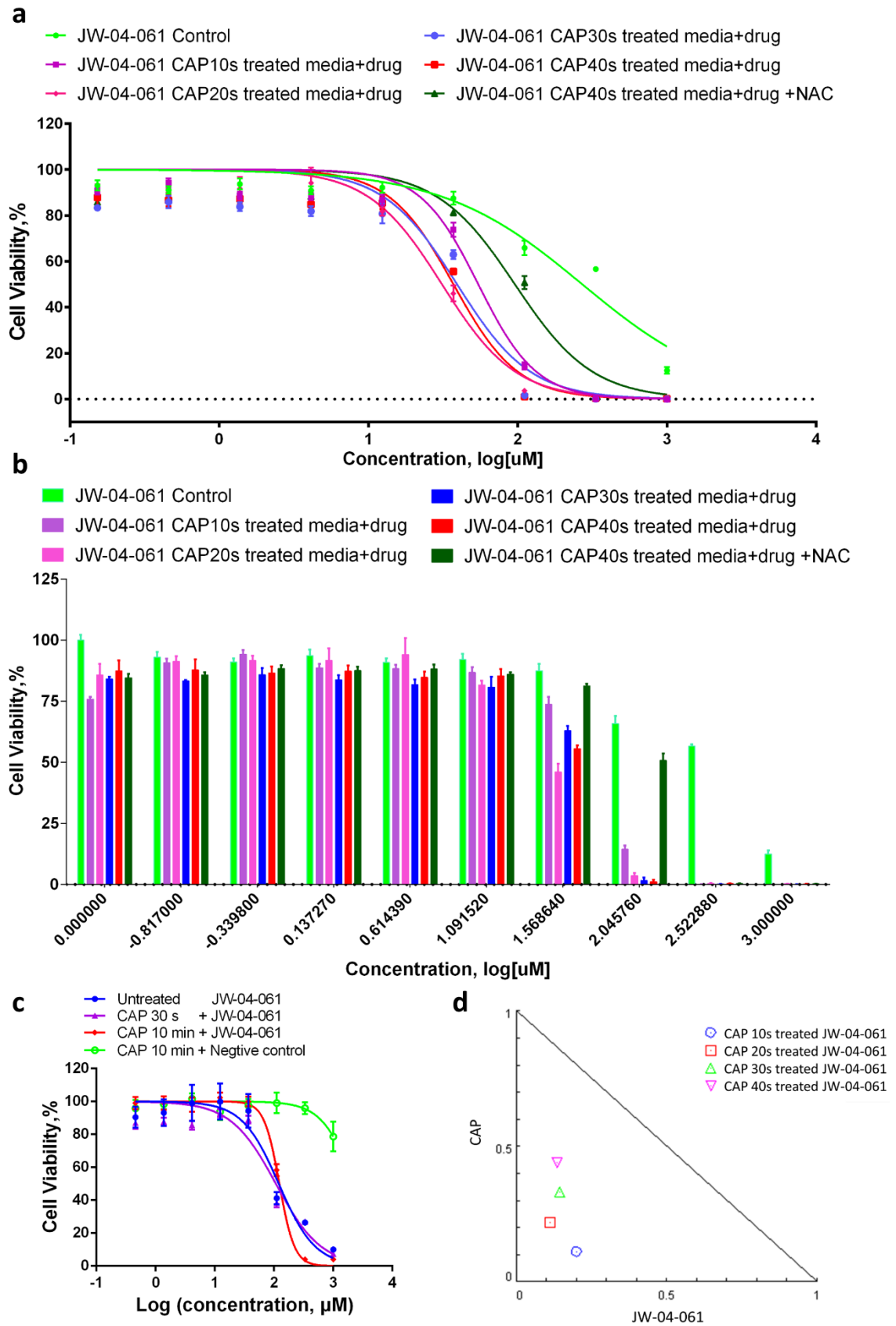
Figure 25. Dose responses of U373MG cells to JW-04-061 treated by CAP in culture medium solution or DMSO stock solution.

128

*JW-04-061 has been added into culture medium to corresponding concentrations then treated with CAP for 0-40 s with or without NAC. Then the CAP treated medium containing JW-04-061 was added in 96-well plates to incubate with U373MG cells for 48 hours and the dose response was presented using nonlinear regression (**a**) and bar chart (**b**). (**c**) JW-04-061 was prepared in DMSO stock solution and treated with CAP for 30s and 10 min, then series diluted in fresh culture medium and incubated with U373MG cells for 48 hours and compared with control groups (Untreated JW-04-061 and vehicle (equivalent volume of pure DMSO) treated with CAP for 10 min).(**d**) Isobologram analysis of the combinational effect of JW-04-061 and CAP. The single doses CAP on y-axis and JW-04061 on x-axis were used to draw the line of additivity. Four combination points were indicated in the isobologram (CAP 10-40s and corresponding IC50 values of CAP-treated JW-04-061). The localisation of combined JW-04-061 and CAP at different time exposures can be translated to synergism CI < 1, additivity CI=1 or antagonism CI>1.*

4.4   Discussion

With development of technique and revolution of knowledge, we are capable of performing precise surgery, targeted and focused chemotherapy and radiotherapy after quick and accurate diagnosis of tumours. However, current treatments still present several side effects, including poor patient experience, secondary malignancy and a variety of long-term sequelae (Triesscheijn *et al.*, 2006; Tachibana, Feril and Ikeda-Dantsuji, 2008; von Woedtke *et al.*, 2013; Murray and Robinson, 2016). Meanwhile, researchers are exploring novel therapies based on different techniques, including sonodynamic therapy (Maeda *et al.*, 2017), photodynamic therapy (Kawczyk-Krupka *et al.*, 2015), CAP therapy (Ratovitski *et al.*, 2014), gene therapy (Naldini, 2015) and immunotherapy (Pardoll, 2012) and some of them have achieved great outcome in clinical trials and even been

successfully applied in practice. However, novel therapies are also very limited with the high requirement of technique, expensive cost and unknow side effects. In this case, combination therapy has been considered as a promising way to solve the problem in a short time while generating less side effects. Usually patients are treated with combination of surgery, radiotherapy and chemotherapy based on the type and progress of the tumours. However, those treatments usually present no synergistic therapeutic effects but increase additive anti-cancer effects to improve the survival of patients along with more side effects. The purpose of investigating combination therapy in this chapter is to improve the anti-cancer effects synergistically and therefore to reduce the dose and side effects of the treatment.

We have tested a total of 47 prodrug candidates from 4 collaborators, including aminoferrocene-based prodrugs provided by Prof. Andriy Mokhir (Marzenell *et al.*, 2013), ferrocene, [3] ferrocenophane and ferrocifen derivatives provided by Prof. Gérard Jaouen (Jaouen, Vessières and Top, 2015), matrix metalloproteinase pro-inhibitors and thiazolidinone-based prodrugs provided by Prof. Seth M. Cohen (Perez *et al.*, 2015), and a series of pyrazolopyrimidines derivatives provided by Prof. John Stephens (Kelada *et al.*, 2018), in combination with low dose CAP treatment using culture medium without pyruvate. We have identified only two leading candidates with synergistic cytotoxicity in combination with CAP treatment, which are JW-04-061 and JW-04-057a provided by Prof. Stephens.

As seen in Figure 19, 20, 21 and 22, all candidates provided by Prof. Andriy Mokhir, Prof. Gérard Jaouen and Prof. Seth M. Cohen which contain typical ROS-trigger groups presented no significant synergistic cytotoxicity in combination with low dose CAP treatment. However, there were few prodrug candidates which presented significant anti-cancer effects just themselves. This might be due to the relatively high ROS level in

U373MG cancer cells caused by their rapid proliferation and altered metabolism. Subsequently, the relatively high cellular ROS level in U373MG cells was already rich enough to trigger the activation of those prodrug candidates without extra ROS generated by low dose CAP treatment. Therefore, the CAP treatment didn't activate those prodrug candidates in U373MG cells and thus presented no synergistic cytotoxicity in combination with those prodrugs. However, those high cytotoxic prodrug candidates, including P286, P686, P53, P722, P258, P257 (as seen IC50 values in Table 6, dose response curves in Figure 20 and 21), can be used in future projects to test their cytotoxicity and specificity in healthy cells and cancer cells, which may contribute to the discovery of novel efficient anti-cancer prodrugs.

Furthermore, as seen in Figure 25, we have investigated the synergistic effects between JW-04-061 and CAP treatment. To distinguish the effects induced by CAP to cells and to prodrugs, we have investigated the cytotoxicity of CAP-treated prodrugs without direct and immediate effects from CAP treatment to cells.

To remove the direct and immediate effects from CAP to U373MG cells, we first treated JW-04-061 in DMSO for 30 sec or 10 min then series diluted the CAP-treated JW-04-061 DMSO solution in fresh medium to corresponding final concentrations, subsequently, U373MG cells were incubated with CAP treated JW-04-061 culture medium solution (from CAP-treated DMSO solution) to investigate if the CAP treatment induced direct changes to prodrugs in DMSO solution. However, there's no significant synergistic cytotoxicity observed when the CAP treatment was performed to prodrug DMSO solution (Figure 25c). We have realized that 100% DMSO contains no H_2O in the solution, therefore it could be one of the reasons that the CAP treatment could not induce enough generation of ROS in JW-04-061 DMSO solution without substrate (Lu *et al.*, 2017). DMSO has been demonstrated to be a scavenger of OH radicals (Eberhardt and Colina,

1988). Therefore, alternatively, JW-04-061 was first diluted in fresh culture medium to corresponding concentrations, then was exposed to CAP treatment for 10-40 s at 75 kV. The CAP-treated JW-04-061 culture medium solution was subsequently incubated with U373MG cells for 48 h before Alamar Blue assay. As seen in Figure 25a, b, significant synergistic effects were observed in combination of CAP treatment and JW-04-061 treated in culture medium solution. The synergistic cytotoxicity was also analysed using isobologram (Figure 25d). Meanwhile, we have applied NAC as antioxidant to investigate the roles of ROS. As seen from Figure 25a, b, with protection from NAC, the cytotoxicity of CAP-treated JW-04-061 in culture medium was significantly decreased. Although, the NAC may decrease the intracellular ROS level of U373MG cells then lead to the decreased cytotoxicity. The lower dose of CAP treatment induced less increasement of cytotoxicity of JW-04-061, which supported that the ROS generated in culture medium played the main role in the activation of drug. Taken together, we can determine that, without direct and immediate effects from CAP to U373MG cells, JW-04-061 still has significant synergistic cytotoxicity in combination with CAP treatment when there is normal generation of ROS in culture medium. However, we could not fully determine the roles of CAP-induced ROS played in the synergistic effects yet. The high level of ROS in culture medium may affect U373MG cells via a variety of activities, including lipid peroxidation, oxidation of protein/DNA/RNA, and intracellular ROS signalling pathways, then trigger the synergistic cytotoxicity with JW-04-061. We acquired additional preliminary results which may explain more mechanism behind the synergistic cytotoxicity between JW-04-061 and CAP treatment.

Overnight storage CAP-activated medium, CAP-activated cells and catalase (hydrogen peroxide decomposition) have been used to study the dose response of U373MG cells to JW-04-061 and investigate the mechanism behind the synergistic cytotoxicity between

JW-04-06 and CAP treatment. As seen in Appendix V Supplementary Figure S3a, JW-04-061 was added into overnight storage CAP-activated medium just before incubation with cells, no synergistic cytotoxicity was observed when cells were treated with overnight storage CAP-activated medium containing JW-04-061 compared to control groups. Yan et al. reported that short-lived reactive species were removed by overnight storage as well as most of long-lived reactive species, such as hydrogen peroxides in the CAP-activated medium (Yan *et al.*, 2016). However, the DIT-120 system investigated in this project has been shown to generate high concentrations of hydrogen peroxides which were stable in various liquids over storage time (Boehm *et al.*, 2017). Therefore, this is yet to be further determined for prodrug treatment. So far, we can determine that the oxidised components in CAP-activated medium have no effect on the synergistic cytotoxicity between CAP-treatment and prodrug JW-04-061. For the record, the fresh CAP-activated medium should have been used to compare with the overnight storage CAP-activated medium for prodrug series dilutions and treatment. As seen in Figure 25, the fresh CAP-treated medium containing prodrugs presented significant synergy, which may be comparable with overnight storage CAP-activated medium. Meanwhile, as seen from Appendix V Supplementary Figure S3c, catalase has been used to decompose hydrogen peroxides, and the prodrug only has been exposed to other reactive species generated by CAP, which demonstrated no significant synergistic cytotoxicity. It demonstrated that the hydrogen peroxides generated by CAP in culture medium may play a main role in the activation of JW-04-061 during and after CAP treatment.

On the other hand, CAP-activated U373MG cells have been applied to investigate the possible synergy between prodrugs and cellular responses to CAP treatment, such as peroxidised cellular membrane, accelerated cellular uptake and oxidation stress response (He *et al.*, 2020). U373MG cells were activated together with medium by CAP for 30 sec

and then incubated for 0-5 hours. Afterwards, fresh medium containing prodrug JW-04-061 was used to test cellular dose response and the possible synergistic effects. As we can see in Appendix V Supplementary Figure S3b, there was no significant synergistic cytotoxicity observed between CAP-activated cells and JW-04-061 compared to direct combination of CAP treatment and prodrug. However, it presented lower cell viability (around 25% decrease) in CAP-activated cells, which may be due to changing of culture medium 0-5 hours after CAP treatment causing extra loss of cells. However, it demonstrated that the synergistic cytotoxicity is mainly from CAP-activated prodrug instead of CAP-activated cells. The experiments discussed above, including treating cells with CAP only, incubating cells with prodrugs only, treating cells and prodrugs with CAP at the same time, incubating CAP-untreated cells with CAP-treated prodrugs (prodrugs were treated with CPA in culture medium solution or DMSO stock solution), incubating CAP-untreated cells with prodrugs dissolved in overnight storage CAP-activated medium, incubating CAP-treated cells with CAP-untreated prodrugs, were performed with same volumes, same concentrations of prodrugs and same types of culture medium without pyruvate. NAC and catalase were used as scavengers of reactive species in inhibiting study. The preliminary conclusion is that the JW-04-061 presents significant synergistic cytotoxicity against U373MG cells after being activated by low doses of CAP treatment in culture medium, whereas the ROS, specifically hydrogen peroxides, may play a main role in the activation of JW-04-061.

All in all, investigating combination therapy is a promising way to develop efficient anti-cancer therapies with as little as possible side effects, especially if there are significant synergistic anti-cancer effects which can be specifically and precisely targeted to tumour tissue. Various compounds and nanoparticles were investigated as sensitizers for radiotherapy, photodynamic therapy and others. However, the majority of sensitizers only

promote the efficiency of the therapy itself or present extra diagnosis function but have no extra therapeutic effect. Therefore, in this chapter, we discovered and demonstrated new compounds that can synergistically kill cancer cells in combination with low dose CAP treatment, which have not been reported before. The JW-04-061 and JW-04-057a can be further investigate for future trials. This research has contributed to the foundation of CAP/ROS-trigger prodrugs research and will inspire the development of more efficient prodrugs that can be combined with targeted and precise CAP treatment for cancer therapy.

5. GENERAL DISCUSSION

In the development of successful interventions to cure cancer, nanomaterials have played key roles. In last two decades, a variety of nanomaterials have been greatly expanded as well as highly diversified and multi-functionalized. Some of these nanomaterials were determined as lead candidates to delivery chemotherapeutics to tumours and have passed preclinical trials and successfully applied to the clinic. Enhanced permeation and retention-based tumour targeting and then, especially, active targeting was introduced, which highly increased the efficiency and specificity of drug delivery into tumours. Due to the excellent loading capacity of nanocarriers and multifunctionality of their ligand or themselves, nanoparticles can be applied in cancer treatments, as both carriers, sensitisers and imaging agents, which can provide advanced diagnosis as well as diversified treatments.

AuNPs, as one of the most commonly investigated and used nanomaterials for cancer treatment, can be readily manufactured in a variety of specific shapes, size and monodispersity with different functions, therefore can be used as diagnostic agents, carriers and/or sensitizers for cancer therapy. The AuNPs we used in this project were synthesised by trisodium citrate ($Na_3C_6H_5O$) reduction of auric acid ($HAuCl_4$) and therefore were not functionalized and only capped with citrate and manufactured in spherical shape and ~20 nm diameter by controlling the ratio between $Na_3C_6H_5O$ and $HAuCl_4$. Non-functionalized AuNPs have shown selective cytotoxicity to cancer cells, are generally consider nontoxic to healthy cells whereas small AuNPs usually elicit higher cytotoxicity than larger AuNPs (Connor *et al.*, 2005; Patra *et al.*, 2007; Alkilany and Murphy, 2010). The AuNPs of ~20 nm diameter we used have been demonstrated to have elicit relatively low cytotoxicity in both normal and cancer cells and are optimal for permitting BBB compared with non-functionalized AuNPs of other sizes (Pan *et al.*, 2007; Shilo *et al.*, 2015). Therefore, 20 nm citrated capped spherical AuNPs were applied in

this study for investigation of the combination therapy with CAP treatment, which also can be the optimal candidate for drug delivery across BBB.

As emerging technology, it has been clinically shown that cold atmospheric plasma can be safely and directly applied on patients for disinfection and promoting the healing of wounds and ulcerations (Weltmann *et al.*, 2008; von Woedtke *et al.*, 2013; Mai-Prochnow *et al.*, 2014; O'Connor *et al.*, 2014). CAP is showing strong potential in cancer treatment as well. Recently, it has been repetitively demonstrated that CAP have significant and selective cytotoxicity to multiple tumour lines in vitro and in animal models (Walk *et al.*, 2013; Ratovitski *et al.*, 2014; Park *et al.*, 2015; Recek *et al.*, 2015; Yan *et al.*, 2015; Conway *et al.*, 2016; Zhu *et al.*, 2016). Moreover, as additional treatment, a prospective clinical trial for head and neck cancer treatment has been carried out, Metelmann et al. presented that CAP treatment not only reduced contamination of ulcerations caused by head and neck cancer and may have inhibited tumour growth and caused visible local destruction after two weeks of treatment. Meanwhile, during the trial, CAP treatments presented low side effects and benefits to patients in various aspects, such as easy to handle treatment, easing cancer pain, gain of weight and likely prolonged survival. (Metelmann *et al.*, 2015). Most recently, for the first time, a CAP device, Canady Helios™ Cold Plasma Scalpel, has been approved for human clinical cancer treatment trials by the FDA to evaluate its safety in patients with solid tumours with carcinomatosis scheduled to undergo surgical resection for cytoreduction ('Canady Helios Cold Plasma Scalpel Treatment at the Surgical Margin and Macroscopic Tumor Sites', 2020). In this study, cold plasma is sprayed in the area of the resected tumour margins after removing gross solid tumour via surgery ('Canady Helios Cold Plasma Scalpel Treatment at the Surgical Margin and Macroscopic Tumor Sites', 2020). Cold plasma also has been successfully evaluated in many non-cancer related trials (e.g. Chronic wounds treatment

(Isbary *et al.*, 2012), symptomatic knee osteoarthritis treatment (Sánchez *et al.*, 2012), herpes treatment (Isbary *et al.*, 2014), treatment of lesions in Hailey-Hailey disease (Isbary *et al.*, 2011)). For instance, for chronic wounds treatment, a randomized controlled trial presented a significant reduction in bacterial load in plasma-treated wounds (Isbary *et al.*, 2012). The CAP treatment for patient with chronic wounds was well tolerated and no side-effects occurred (Isbary *et al.*, 2012).

A promising synergistic anti-cancer effect between CAP and AuNPs which we observed was that the uptake of AuNPs into U373MG cells was significantly enhanced with CAP treatment, and the cytotoxicity of the AuNPs to U373MG cells was also significantly increased combined with CAP treatment. There have been reports that CAP treatment can induce pore formation on cell membrane that may increase delivery of agents into cells, and had synergistic cytotoxicity combined with nanoparticles especially gold nanoparticles. Jinno et al. has described that the electrical effects of CAP combined with reactive species helped the gene transfection into L-929, mouse fibroblast cells (Jinno *et al.*, 2016). Krassowska et al., simulated that strong electric fields, which exist during CAP treatment, can induce formation of large pore in spherical cell membranes (i.e. 15-25 nm) (Krassowska and Filev, 2007). Cheng et al., observed that uneven membrane and membrane pores were induced in U87 cells after treatment of CAP (Cheng *et al.*, 2015). Nina et al., also described the unrecoverable partial cell membranes and cell components damage induced by CAP treatment in U87 cells. The direct membrane damage and pore formation induced by CAP treatment described in these studies may explain that we observed low levels of non-active uptake of AuNPs during the first few hours after CAP treatment, which was not inhibited by NaN_3 or low-temperature (4 °C) incubation. NaN_3 was used as metabolic inhibitor to inhibit the energy-dependent endocytosis, and low-temperature incubation was used to inhibit endocytosis as a standard experiment.

However, we mainly observed that active uptake of AuNPs was stimulated after low dose CAP treatment which was inhibited by NaN_3 and low-temperature incubation. This has not been reported before. Furthermore, we also observed the significant enhancement of AuNPs uptake with indirect CAP treatment which removes the direct physical effects. It confirmed that pore formation and direct membrane damage plays only a minor role in the increased uptake of AuNPs induced by low dose CAP treatment compared to previous studies. It should be noted that each of these studies were carried out using different cancer cell lines and various dose of CAP generated by different devices with distinct input voltage, frequent, current and therefore cause different response of cancer cells to CAP treatment.

On the other hand, several studies to date have reported the synergistic anti-cancer effect between CAP treatment and AuNPs. Kim et al., first demonstrated that cytotoxicity of CAP to G361 human melanoma skin cancer cells was significantly increased (near five-fold) by combining with anti-FAK antibody-conjugated AuNPs (FAK-AuNPs) (Kim *et al.*, 2008). In this study, the adopted 30nm AuNPs didn't present any observable cytotoxic effect on the proliferation of G361 cells while applied alone, but increased the cell death rate from 14% (CAP only) to 36% (CAP and unconjugated AuNPs) and 74% (CAP and FAK-AuNPs) (Kim *et al.*, 2008). It is interesting that Kim et al., noted that the cell morphology was maintained, even in dead cells, after combination treatment of CAP and FAK-AuNPs, whereas cells dying from CAP usually undergo anoikis. (Kim *et al.*, 2008). In another study, fluorouracil, a DNA synthesis inhibitor chemotherapeutic that has been widely used in clinical treatment of breast, gastrointestinal and gynaecological cancers, was loaded in core (gold)-shell (PLGA) nanoparticles for combination treatment with CAP against human breast cancer MDA-MB-231 cell line (Zhu *et al.*, 2016). Synergistic cytotoxicity between the drug loaded core-shell AuNPs and CAP treatment and enhanced

cellular internalization of the drug loaded core-shell AuNPs by CAP treatment were observed (Zhu *et al.*, 2016). Similarly, X. Cheng et al., described that 100 nm uncoated AuNPs presented synergistic cytotoxicity to U87 cells combined with CAP treatment, which was also dose dependent (Cheng *et al.*, 2014). At the optimal concentration, AuNPs induced U87 cell death up to a 30% overall increase compared to the control group with the same plasma dosage only (Cheng *et al.*, 2014). Highest intracellular ROS intensity induced by CAP was measured at this optimal concentration as well (Cheng *et al.*, 2014). The exact mechanism has yet to be discovered but they concluded that the AuNPs in the medium may accelerate the absorption of exogenous ROS and RNS generated by CAP into cells (Cheng *et al.*, 2014). A study was carried out by Irani et al. which demonstrated that the cell death of HCT-116 cells (human colorectal cancer cells) was increased significantly by CAP treatment in the present of ~55 nm citrate-capped AuNPs (Irani *et al.*, 2015). However, despite all the evidences for the synergistic anti-cancer effects between CAP treatment and AuNPs, the underlying mechanism of this synergistic cytotoxicity was yet to be well understood.

To date and to the best of our knowledge we are the first to demonstrate the detailed mechanism behind the synergistic anti-cancer effects between CAP treatment and AuNPs and gave a strong hypothesis with regards to CAP facilitated permeability of drugs. As described in Chapter 2, we have successfully determined that CAP treatment promotes the uptake of AuNPs into U373MG cells via ATP-dependent active pathway and eventually accumulated in lysosomes, and published a peer-reviewed paper based on this work (He *et al.*, 2018). The enhanced accumulation of AuNPs in U373MG cells was first observed under optical microscope. Then we have tracked the accumulation and uptake of AuNPs into cells with or without CAP treatment using a variety of technique and devices, including AAS, confocal microscope, flow cytometry, electron microscope and

Zetasizer, combined with a panel of inhibitors and fluorescent probes, including ATP inhibitor sodium azide, antioxidant NAC, lysosomes tracker. Using AAS, we have successfully tracked the accumulation of AuNPs inside U373MG cells and demonstrated that the uptake of AuNPs enhanced by CAP treatment was an active pathway. Using confocal microscope, the majority of intracellular AuNPs has been confirmed to located in lysosomes which presented significant greater accumulation with CAP treatment. It should be noted that antioxidant NAC didn't significantly decrease the stimulated uptake of AuNPs by CAP, which may demonstrate that short-lived species or NAC-insensitive reactive species played the main role in the stimulation of cellular uptake. Using indirect CAP treatment also demonstrated that physical effects induced by CAP also didn't play main role in the increased uptake of AuNPs into U373MG cells.

However, we didn't fully answer the questions behind the synergistic cytotoxicity between CAP treatment and AuNPs. It is worth to understand the mechanism behind the synergy which will be useful for developing more efficient deliveries of nanoparticles and pharmaceuticals into cancer cells for tumour therapy and diagnosis and other relevant cancer therapies that induce an increase in extracellular ROS. Therefore, we continued the investigation of the synergistic effects between CAP treatment and AuNPs and tried to precisely identify the CAP-affected cellular pathways involved in the enhanced uptake of AuNPs.

The current study of Chapter 3 demonstrated, for the first time, that the synergistic effects of nonfunctionalised AuNPs combined with CAP, to glioblastoma cancer cells, is via the clathrin-mediated endocytosis stimulated by CAP-induced membrane repair processes. In Chapter 3, numerical modelling of the uptake of gold nanoparticles into U373MG glioma cells predicted that CAP may introduce a new uptake route. We have demonstrated that cell membrane repair pathways play the main role in the stimulated

new uptake route, following non-toxic doses of CAP treatment (30 s, 75 kV). CAP treatment induced cellular membrane damage, mainly via lipid peroxidation as a result of ROS and RNS generation. Membranes rich in peroxidised lipids were then trafficked into cells via membrane repairing endocytosis. We confirmed that the enhanced uptake of nanomaterials is clathrin-dependent using a batch of specific chemical inhibitors and silencing of gene expression. Therefore, we have hypothesised that CAP-stimulated membrane repair increases endocytosis and accelerates the uptake of gold nanoparticles into U373MG cells after CAP treatment. In Chapter 3, our data has demonstrated the utility of CAP to model membrane oxidative damage in cells and characterised a previously unreported mechanism of membrane repair to trigger nanomaterial uptake. This research article has been published in the peer-reviewed journal 'Scientific Report' (He *et al.*, 2020).

Although there has been study hypothesis that after uptake via receptor-mediated endocytosis, epidermal growth factor (EGF)-conjugated AuNPs combined with CAP induced DNA damage and selective apoptosis of A549 human alveolar basal epithelial cancer cells (Kim *et al.*, 2017). This hypothesis was based on the decreased uptake of the EGF-conjugated AuNPs when incubated at 29.5 °C compared to 37 °C, and that the EGF ligand usually triggers recruitment of the EGF receptor to clathrin-coated pits which has been demonstrated to be the endocytosis pathway of uptake of EGFR-ligand complex, as well as that AuNPs are mainly internalized via clathrin/ caveolar-mediated endocytosis, phagocytosis, macropinocytosis, and pinocytosis (Kim *et al.*, 2017). However, this study didn't directly demonstrate that the increased uptake of AuNPs was via receptor-media endocytosis and also used ligand-conjugated nanoparticles which is different compared to our study. There is another study demonstrating that iron-dependent cold plasma-induced oxidative stress can stimulate significant increase in fluid-phase endocytosis,

lysosome biogenesis and autophagy, therefore inducing highly selective anti-proliferative activity against rat SM2 (sarcomatoid subtype) malignant mesothelioma cells (Shi *et al.*, 2017). However, the study presented that the CAP treatment decreased transferrin receptor-1 which is in contrast with our study. We used transferrin conjugated with Alexa Fluor™ 546, an early endosome marker, and confocal microscope to investigate the endocytosis enhanced by CAP treatment and demonstrated that the quantification of transferrin uptake was significantly increased within 5 min after CAP treatment compared to control group. The contrast may be due to the variety of different cell lines and different dose of CAP generated from distinct devices.

As seen in Chapter 2 and 3, the ROS and RNS induced lipid peroxidation played an important role in the CAP-induced endocytosis and oxidization stress. It should be noted that ROS and RNS play important roles in many other anti-cancer interventions, including phototherapy (Zhou *et al.*, 2016), ultrasonic therapy (Yu, Wang and Mason, 2004), as well as some types of chemotherapy (Kasiappan and Safe, 2016), as especially in this most common cancer treatment, radiotherapy (RT) (Manda, Nechifor and Neagu, 2009). As mentioned in Chapter 1, the reactive species is a double-edged sword for cancer cells and can be utilised for developing efficient therapeutic strategies against cancer cells. ROS-inducing chemotherapy agents and radiation therapy are now the most common anti-cancer innovation involved with reactive species.

Radiation therapy is one of the primary treatments for neoplasm using high-energy ionizing radiation (IR). The acting mechanisms of RT include the generation of free radicals or the direct deposition of energy by IR. Due to photoelectric effects and Compton effects, the energy track of IR is composed by electrons in matters, which induce ionization and excitation (Rehman *et al.*, 2015). In cells, the electrons interact with water and generate free radicals, including ROS and RNS (Mikkelsen and Wardman,

144

2003). Damage is induced by the ROS/RNS-caused oxidative stress and lesions of cellular macromolecules, including DNA, protein and lipids (Nikitaki *et al.*, 2016). Meanwhile, the cell killing effect is also related to the direct deposition of energy by IR, which is highly penetrating and able to cause irreparable damage to genetic materials even at low dose (Rothkamm and Löbrich, 2003). However, due to the high cytotoxicity and non-targeted effects of radiation, the radiation must be accurately delivered to tumour tissue while sparing normal tissue to improve PFS, OS and life quality of patients (Nikitaki *et al.*, 2016). Although ionizing radiation induces the generation of intracellular ROS and free radicals (Magné *et al.*, 2006; Graves, 2012), the cytotoxicity of radiation is mainly owing to the photons-directly-caused DNA damage (Mikkelsen and Wardman, 2003; Graves, 2012), even at low doses, resulting in irreparable damage to cellular genetic material and cell death (Rothkamm and Löbrich, 2003). Compared to radiation, CAP can produce longer lived reactive species, selectively inducing apoptosis to cancer cells through signalling pathways, generating low-energy species which is relatively low-toxic to normal cells. Due to the regular ROS level in normal cells, the antioxidant system in normal cells present higher resistant to CAP treatment compared with cancer cells. However, it has been demonstrated that CAP treatment can induce proliferation arrest, DNA damage and a senescence phenotype to healthy cells without killing them. Therefore, the dose of CAP treatment should be carefully controlled on targeted cancerous tissue.

CAP devices are low cost, easy to control and the field is undergoing a rapid pace of innovation and advancement (Ishaq, Evans and Ostrikov, 2014). Therefore, the potential of CAP for developing more efficient and lower side-effects human healthcare is significant and promising. On the other side, there are many research questions related with CAP treatment awaiting to be solved for the clinical application of CAP for cancer

therapy. For instance, there are a variety of CAP devices which have been investigated in research. Due to high diversity (voltage, currency, frequency, gas types, various components and designs of devices), the comparability between CAP devices is yet to be further improved. Meanwhile, the doses of CAP generated from disparate devices are difficult to be precisely identified by time of treatment. The identification of exact reactive species, especially short-lived reactive species, have not been solved yet. CAP only has been investigated for cancer therapy recently, thus the long-term effects of CAP treatment are yet to be fully explored. Those are the challenges facing the field of plasma medicine and require more efforts to eventually implement the CAP therapy in the clinic. In Chapter 2 and 3, the focus of the project was investigation of the synergy between AuNPs and CAP to understand the mechanism behind CAP and AuNPs synergy. In Chapter 4, the focus was brought to prodrugs and CAP treatment. We first screened all prodrug candidates using culture medium with pyruvate but didn't observed leading candidates with significant synergistic cytotoxicity. We have realized that pyruvate, a common component of culture medium, may present negative effects in our experiments as antioxidant (Ramos-Ibeas *et al.*, 2017). Therefore, in Chapter 4, we screened all 47 prodrug candidates again and successfully identified that two compounds, JW-04-061 and JW-04-057a, provided by Prof. John Stephen, have significant synergistic cytotoxicity in combination with low dose CAP treatment, using culture medium without pyruvate. The synergistic effects between JW-04-061 and CAP treatment was further investigated and will be published as peer-reviewed article in collaboration with Prof. John Stephen. Other prodrugs, provided by Prof. Andriy Mokhir, Prof. Gérard Jaouen and Prof. Seth M. Cohen, all contain typical ROS-trigger groups but presented no significant synergistic cytotoxicity in combination with low dose CAP treatment, which may be due to the natural ROS level in U373MG cancer cells being high enough for

prodrug activation without CAP treatment. But we still have identified that few prodrug candidates, including P286, P686, P53, P722, P258, P257, present high anti-cancer effects on their own. Thus, those candidates can be used in future research to test their cytotoxicity and specificity in healthy cells and cancer cells to discover new prodrugs.

In conclusion, we investigated the mechanism behind the synergistic anti-cancer effect between CAP and AuNPs and provided solid evidence that the membrane oxidation damage induced clathrin-dependent endocytosis played main role in the accelerated uptake of AuNPs into U373MG cells by CAP treatment. In Chapter 4, we screened all prodrug candidates and have identified two leading candidates that possess most significant synergistic cytotoxicity to U373MG cells in combination with CAP treatment. We also have provided preliminary evidence that reactive species generated in CAP-treated culture medium did play the main role in the activation of the leading prodrug candidate JW-04-061, which leads to the synergistic cytotoxicity. This thesis provides evidence to understand how CAP treatment induces a variety of responses of glioma cells, especially stimulated endocytosis, which can be also applied in enhancing permeability and tumour accumulation of other therapeutic and diagnostic agents for development of efficient cancer therapies and diagnosis. Meanwhile, two novel prodrugs that have synergy with CAP treatment have been identified and investigated. However, new research questions have been brought to light by this study. Further studies are required to fully elucidate what cell death pathways are involved in the synergistic cytotoxicity of AuNPs and CAP. Investigation of this novel combination therapy using prodrug-loaded AuNPs and CAP treatment *in vitro,* in 3-dementional cancer sphere model, and *in vivo* also can be investigated in future projects for development of practical innovations in clinical therapy. For *in vivo* treatment, alternative CAP devices, such as plasma jet or plasma needle, are required to deliver CAP to targeted area. The cell death pathways

involved in the anti-cancer effects of prodrug leading candidates combined with CAP have yet to be explored.

6. Bibliography

Adhikari, M. *et al.* (2020) 'Cold Atmospheric Plasma as a novel therapeutic tool for the treatment of brain cancer', *Current Pharmaceutical Design*. doi: 10.2174/1381612826666200302105715.

Adibhatla, R. M. and Hatcher, J. F. (2008) 'Phospholipase A2, reactive oxygen species, and lipid peroxidation in CNS pathologies', *Journal of Biochemistry and Molecular Biology*, 41(8), pp. 560–567. doi: 10.5483/bmbrep.2008.41.8.560.

Adibhatla, R. M. and Hatcher, J. F. (2010) 'Lipid oxidation and peroxidation in CNS Health and disease: From molecular mechanisms to therapeutic opportunities', *Antioxidants and Redox Signaling*, 12(1), pp. 125–169. doi: 10.1089/ars.2009.2668.

Agostinis P, Berg K, Cengel K., et al. (2017) 'Republic of Yemen Ministry of Public Health and Population Nutrition and Mortality Survey Report Ibb Governorate , Yemen', *Ca Cancer J Clin*. Wiley Subscription Services, Inc., A Wiley Company, 61(April), pp. 250–281. doi: 10.3322/caac.20114.Available.

Ahn, H. J. *et al.* (2011) 'Atmospheric-pressure plasma jet induces apoptosis involving mitochondria via generation of free radicals', *PLoS ONE*, 6(11), pp. 6–12. doi: 10.1371/journal.pone.0028154.

Ahn, H. J. *et al.* (2014) 'Targeting cancer cells with reactive oxygen and nitrogen species generated by atmospheric-pressure air plasma', *PLoS ONE*, 9(1). doi: 10.1371/journal.pone.0086173.

Akhtar, M. J. *et al.* (2016) 'Dose-dependent genotoxicity of copper oxide nanoparticles stimulated by reactive oxygen species in human lung epithelial cells', *Toxicology and Industrial Health*. SAGE PublicationsSage UK: London, England, 32(5), pp. 809–821. doi: 10.1177/0748233713511512.

Alexis, F. *et al.* (2008) 'New frontiers in nanotechnology for cancer treatment', *Urologic Oncology: Seminars and Original Investigations*, 26(1), pp. 74–85. doi:

10.1016/j.urolonc.2007.03.017.

Alifieris, C. and Trafalis, D. T. (2015) 'Glioblastoma multiforme: Pathogenesis and treatment', *Pharmacology and Therapeutics*, 152, pp. 63–82. doi: 10.1016/j.pharmthera.2015.05.005.

Alkilany, A. M. and Murphy, C. J. (2010) 'Toxicity and cellular uptake of gold nanoparticles: What we have learned so far?', *Journal of Nanoparticle Research*, 12(7), pp. 2313–2333. doi: 10.1007/s11051-010-9911-8.

Anderson, V. C. and Thompson, D. H. (1992) 'Triggered release of hydrophilic agents from plasmologen liposomes using visible light or acid', *BBA - Biomembranes*, 1109(1), pp. 33–42. doi: 10.1016/0005-2736(92)90183-M.

Andrews, N. W. and Corrotte, M. (2018) 'Plasma membrane repair', *Current Biology*, 28(8), pp. R392–R397. doi: 10.1016/j.cub.2017.12.034.

Arouri, A. *et al.* (2013) 'Lipases, liposomes and lipid-prodrugs', *Current Opinion in Colloid and Interface Science*, pp. 419–431. doi: 10.1016/j.cocis.2013.06.001.

Articles, C. and Results, R. (2012) 'Web of Knowledge [v . 5 . 5] - All Databases Citing Articles Web of Knowledge [v . 5 . 5] - All Databases Citing Articles', *Chemical Reviews*, 7641(0), pp. 1–5. doi: 10.1021/cr030698.

Babington, P. *et al.* (2015) 'Use of cold atmospheric plasma in the treatment of cancer', *Biointerphases*, p. 029403. doi: 10.1116/1.4915264.

Bae, K. H. *et al.* (2008) 'Synthesis, characterization, and intracellular delivery of reducible heparin nanogels for apoptotic cell death', *Biomaterials*, 29(23), pp. 3376–3383. doi: 10.1016/j.biomaterials.2008.04.035.

Baetke, S. C., Lammers, T. and Kiessling, F. (2015) 'Applications of nanoparticles for diagnosis and therapy of cancer', *British Journal of Radiology*, 88(1054). doi: 10.1259/bjr.20150207.

Bakhshizadeh, M. *et al.* (2017) 'TiO2-based Mitoxantrone Imprinted Poly (Methacrylic acid-co-polycaprolctone diacrylate) Nanoparticles as a Drug Delivery System', *Current Pharmaceutical Design*, 23(18), pp. 1–1. doi: 10.2174/1381612823666170214122413.

Beck, R. *et al.* (2009) 'Menadione reduction by pharmacological doses of ascorbate induces an oxidative stress that kills Breast Cancer cells', *International Journal of Toxicology*, 28(1), pp. 33–42. doi: 10.1177/1091581809333139.

Begum, A., Laroussi, M. and Pervez, M. R. (2013) 'Atmospheric pressure He-air plasma jet: Breakdown process and propagation phenomenon', *AIP Advances*, 3(6). doi: 10.1063/1.4811464.

Bennet, D. and Kim, S. (2014) 'Polymer Nanoparticles for Smart Drug Delivery', in *Application of Nanotechnology in Drug Delivery*. InTech. doi: 10.5772/58422.

Bestwick, C. S. *et al.* (2001) 'Characterisation of and changes to pro- and anti-oxidant enzyme activities during the hypersensitive reaction in lettuce (Lactuca sativa L.)', *Plant Science*, 161(3), pp. 497–506. doi: 10.1016/S0168-9452(01)00427-7.

Bibi, S. *et al.* (2012) 'Trigger release liposome systems: Local and remote controlled delivery?', *Journal of Microencapsulation*, 29(3), pp. 262–276. doi: 10.3109/02652048.2011.646330.

Boehm, D. *et al.* (2016) 'Cytotoxic and mutagenic potential of solutions exposed to cold atmospheric plasma', *Scientific Reports*, 6(1), p. 21464. doi: 10.1038/srep21464.

Boehm, D. *et al.* (2017) 'Hydrogen Peroxide and Beyond-the Potential of High-voltage Plasma-activated Liquids Against Cancerous Cells', *Anti-Cancer Agents in Medicinal Chemistry*, 18(6), pp. 815–823. doi: 10.2174/1871520617666170801110517.

Borchman, D. *et al.* (1992) 'The dual effect of oxidation on lipid bilayer structure', *Lipids*, 27(4), pp. 261–265. doi: 10.1007/BF02536472.

Boussif, O. *et al.* (1995) 'A versatile vector for gene and oligonucleotide transfer into

cells in culture and in vivo: Polyethylenimine', *Proceedings of the National Academy of Sciences of the United States of America*, 92(16), pp. 7297–7301. doi: 10.1073/pnas.92.16.7297.

Brat, D. J. *et al.* (2004) 'Pseudopalisades in Glioblastoma Are Hypoxic, Express Extracellular Matrix Proteases, and Are Formed by an Actively Migrating Cell Population', *Cancer Research*, 64(3), pp. 920–927. doi: 10.1158/0008-5472.CAN-03-2073.

Bregoli, L. *et al.* (2016) 'Nanomedicine applied to translational oncology: A future perspective on cancer treatment', *Nanomedicine: Nanotechnology, Biology, and Medicine*. Elsevier Inc., 12(1), pp. 81–103. doi: 10.1016/j.nano.2015.08.006.

Brown, J. M. (1999) 'The hypoxic cell: A target for selective cancer therapy - Eighteenth Bruce F. Cain Memorial Award Lecture', in *Cancer Research*, pp. 5863–5870.

Brullé, L. *et al.* (2012) 'Effects of a Non Thermal Plasma Treatment Alone or in Combination with Gemcitabine in a MIA PaCa2-luc Orthotopic Pancreatic Carcinoma Model', *PLoS ONE*, 7(12), pp. 1–10. doi: 10.1371/journal.pone.0052653.

Buczkowski, A. *et al.* (2011) 'Interaction between PAMAM-NH2 G4 dendrimer and 5-fluorouracil in aqueous solution', *International Journal of Pharmaceutics*. Elsevier, 408(1–2), pp. 266–270. doi: 10.1016/j.ijpharm.2011.02.014.

Bulavin, D. V. and Fornace, A. J. (2004) 'p38 MAP kinase's emerging role as a tumor suppressor', *Advances in Cancer Research*, 92, pp. 95–118. doi: 10.1016/S0065-230X(04)92005-2.

Byrne, H. J. and Maher, M. A. (2019) 'Numerically modelling time and dose dependent cytotoxicity', *Computational Toxicology*, 12. doi: 10.1016/j.comtox.2019.100090.

'Canady Helios Cold Plasma Scalpel Treatment at the Surgical Margin and Macroscopic Tumor Sites' (2020) *Case Medical Research*. doi: 10.31525/ct1-nct04267575.

Candolfi, M. *et al.* (2007) 'Intracranial glioblastoma models in preclinical neuro-oncology: Neuropathological characterization and tumor progression', *Journal of Neuro-Oncology*, 85(2), pp. 133–148. doi: 10.1007/s11060-007-9400-9.

Cardone, M. H. *et al.* (1998) 'Regulation of cell death protease caspase-9 by phosphorylation', *Science*, 282(5392), pp. 1318–1321. doi: 10.1126/science.282.5392.1318.

Casasús, R. *et al.* (2004) 'Toward the development of ionically controlled nanoscopic molecular gates', *Journal of the American Chemical Society*. American Chemical Society, 126(28), pp. 8612–8613. doi: 10.1021/ja048095i.

Cataldo, F. (2005) 'Ozone degradation of ribonucleic acid (RNA)', *Polymer Degradation and Stability*, 89(2), pp. 274–281. doi: 10.1016/j.polymdegradstab.2004.10.020.

Chan, M. and Almutairi, A. (2016) 'Nanogels as imaging agents for modalities spanning the electromagnetic spectrum', *Materials Horizons*. Royal Society of Chemistry, 3(1), pp. 21–40. doi: 10.1039/c5mh00161g.

Chang, D. *et al.* (2016) 'Polydopamine-based surface modification of mesoporous silica nanoparticles as pH-sensitive drug delivery vehicles for cancer therapy', *Journal of Colloid and Interface Science*. Academic Press, 463, pp. 279–287. doi: 10.1016/j.jcis.2015.11.001.

Chao, C. C. *et al.* (1994) 'Priming effect of morphine on the production of tumor necrosis factor-α by microglia: Implications in respiratory burst activity and human immunodeficiency virus-1 expression', *Journal of Pharmacology and Experimental Therapeutics*, 269(1), pp. 198–203.

Chatterjee, D. D. K., Fong, L. L. S. and Zhang, Y. (2008) 'Nanoparticles in photodynamic therapy: An emerging paradigm', *Advanced Drug Delivery Reviews*. Elsevier B.V., 60(15), pp. 1627–1637. doi: 10.1016/j.addr.2008.08.003.

Chatterjee, S. N. and Agarwal, S. (1988) 'Liposomes as membrane model for study of lipid peroxidation', *Free Radical Biology and Medicine*, pp. 51–72. doi: 10.1016/0891-5849(88)90011-1.

Chen, C. Y., Cheng, Y. C. and Cheng, Y. J. (2018) 'Synergistic effects of plasma-activated medium and chemotherapeutic drugs in cancer treatment', *Journal of Physics D: Applied Physics*. doi: 10.1088/1361-6463/aaafc4.

Chen, H. *et al.* (2017) 'Rethinking cancer nanotheranostics', *Nature Reviews Materials*, 2(7), p. 17024. doi: 10.1038/natrevmats.2017.24.

Cheng, X. *et al.* (2014) 'Synergistic effect of gold nanoparticles and cold plasma on glioblastoma cancer therapy', *Journal of Physics D: Applied Physics*, 47(33), p. 335402. doi: 10.1088/0022-3727/47/33/335402.

Cheng, X. *et al.* (2015) 'Cold Plasma Accelerates the Uptake of Gold Nanoparticles into Glioblastoma Cells', *Plasma Processes and Polymers*, 12(12), pp. 1364–1369. doi: 10.1002/ppap.201500093.

Cheng, Y. *et al.* (2011) 'Addressing brain tumors with targeted gold nanoparticles: A new gold standard for hydrophobic drug delivery?', *Small*, 7(16), pp. 2301–2306. doi: 10.1002/smll.201100628.

Chiche, J. *et al.* (2012) 'In vivo pH in metabolic-defective Ras-transformed fibroblast tumors: Key role of the monocarboxylate transporter, MCT4, for inducing an alkaline intracellular pH', *International Journal of Cancer*. doi: 10.1002/ijc.26125.

Chithrani, B. D., Ghazani, A. A. and Chan, W. C. W. (2006) 'Determining the size and shape dependence of gold nanoparticle uptake into mammalian cells', *Nano Letters*, 6(4), pp. 662–668. doi: 10.1021/nl052396o.

Choi, B. B.-B. *et al.* (2012) 'Nonthermal Plasma-Mediated Cancer Cell Death; Targeted Cancer Treatment', *Journal of Thermal Science and Technology*, 7(2), pp. 399–404. doi:

10.1299/jtst.7.399.

Choi, B. B. *et al.* (2015) 'Targeting NEU protein in melanoma cells with non-thermal atmospheric pressure plasma and gold nanoparticles', *Journal of Biomedical Nanotechnology*, 11(5), pp. 900–905. doi: 10.1166/jbn.2015.1999.

Choi, J. Y. *et al.* (2016) 'PEGylated lipid bilayer-supported mesoporous silica nanoparticle composite for synergistic co-delivery of axitinib and celastrol in multi-targeted cancer therapy', *Acta Biomaterialia*, 39, pp. 94–105. doi: 10.1016/j.actbio.2016.05.012.

Chou, T. C. and Martin, N. (2005) 'CompuSyn for drug combinations', *A Computer Software for Quantitation of Synergism and Antagonism, and the Determination of IC50, ED50 and LD50 Values.[PC software and user's guide.](ComboSyn, Paramus, NJ)*.

Clarke, J., Butowski, N. and Chang, S. (2010) 'Recent advances in therapy for glioblastoma', *Archives of Neurology*. doi: 10.1001/archneurol.2010.5.

Clement, S. *et al.* (2017) 'Nanoparticle-mediated singlet oxygen generation from photosensitizers', *Journal of Photochemistry and Photobiology A: Chemistry*. Elsevier B.V., 332, pp. 66–71. doi: 10.1016/j.jphotochem.2016.08.009.

Collet, G. *et al.* (2014) 'Plasma jet-induced tissue oxygenation: Potentialities for new therapeutic strategies', *Plasma Sources Science and Technology*, 23(1). doi: 10.1088/0963-0252/23/1/012005.

Connor, E. E. *et al.* (2005) 'Gold nanoparticles are taken up by human cells but do not cause acute cytotoxicity', *Small*, 1(3), pp. 325–327. doi: 10.1002/smll.200400093.

Conway, G. *et al.* (no date) 'Ursolic acid inhibits cell migration and promotes JNK-dependent lysosomal associated cell death in Glioblastoma multiforme cells', *Biorxiv.Org*. doi: 10.1101/2020.03.11.987578.

Conway, G. E. *et al.* (2016) 'Non-thermal atmospheric plasma induces ROS-independent

cell death in U373MG glioma cells and augments the cytotoxicity of temozolomide',
British Journal of Cancer, 114(4), pp. 435–443. doi: 10.1038/bjc.2016.12.

Conway, G. E. *et al.* (2019) 'Cold Atmospheric Plasma induces accumulation of
lysosomes and caspase-independent cell death in U373MG glioblastoma multiforme
cells', *Scientific Reports*, 9(1), pp. 1–29. doi: 10.1038/s41598-019-49013-3.

Cooper, D. R., Bekah, D. and Nadeau, J. L. (2014) 'Gold nanoparticles and their
alternatives for radiation therapy enhancement', *Frontiers in Chemistry*, 2(October), pp.
1–13. doi: 10.3389/fchem.2014.00086.

Couvreur, P. and Vauthier, C. (2006) *Nanotechnology: intelligent design to treat complex
disease*, *Pharmaceutical Research*. doi: 10.1007/s11095-006-0284-8.

Cullen, P. J. P. and Milosavljević, V. (2015) 'Spectroscopic characterization of a radio-
frequency argon plasma jet discharge in ambient air', *Progress of Theoretical and
Experimental Physics*, 2015(6), pp. 0–17. doi: 10.1093/ptep/ptv070.

Dada, L. A. *et al.* (2003) 'Hypoxia-induced endocytosis, of Na,K-ATPase in alveolar
epithelial cells is mediated by mitochondrial reactive oxygen species and PKC-ζ', *Journal
of Clinical Investigation*, 111(7), pp. 1057–1064. doi: 10.1172/JCI16826.

Deb, S. *et al.* (2010) 'Histological quantification of the tissue damage caused by
PlasmaJet[TM] coagulator', *Gynecological Surgery*, 7(4), pp. 441–446. doi:
10.1007/s10397-010-0582-3.

Deneke, S. M. (2001) 'Thiol-based antioxidants', *Current Topics in Cellular Regulation*,
36(C), pp. 151–180. doi: 10.1016/S0070-2137(01)80007-8.

Deshpande, P. P., Biswas, S. and Torchilin, V. P. (2013) 'Current trends in the use of
liposomes for tumor targeting', *Nanomedicine*, 8(9), pp. 1509–1528. doi:
10.2217/nnm.13.118.

Djordjević, V. B. (2004) 'Free radicals in cell biology', *International Review of Cytology*,

pp. 57–89. doi: 10.1016/S0074-7696(04)37002-6.

Dolman, N. J., Kilgore, J. A. and Davidson, M. W. (2013) 'A review of reagents for fluorescence microscopy of cellular compartments and structures, part I: BacMam labeling and reagents for vesicular structures', *Current Protocols in Cytometry*, (SUPPL.65). doi: 10.1002/0471142956.cy1230s65.

Dong, X., Liu, T. and Xiong, Y. (2017) 'A novel approach to regulate cell membrane permeability for ATP and NADH formation in Saccharomyces cerevisiae induced by air cold plasma', *Plasma Science and Technology*, 19(2), p. 024001. doi: 10.1088/2058-6272/19/2/024001.

Drummen, G. P. C. *et al.* (2004) 'Mass spectrometric characterization of the oxidation of the fluorescent lipid peroxidation reporter molecule C11-BODIPY581/591', *Free Radical Biology and Medicine*, 36(12), pp. 1635–1644. doi: 10.1016/j.freeradbiomed.2004.03.014.

Duchene, D., Cavalli, R. and Gref, R. (2016) 'Cyclodextrin-based Polymeric Nanoparticles as Efficient Carriers for Anticancer Drugs', *Current Pharmaceutical Biotechnology*. Bentham Science Publishers, 17(3), pp. 248–255. doi: 10.2174/1389201017666151030104944.

Dykman, L. and Khlebtsov, N. (2012) 'Gold nanoparticles in biomedical applications: Recent advances and perspectives', *Chemical Society Reviews*, 41(6), pp. 2256–2282. doi: 10.1039/c1cs15166e.

Eberhardt, M. K. and Colina, R. (1988) 'The reaction of OH radicals with dimethyl sulfoxide. A comparative study of fenton's reagent and the radiolysis of aqueous dimethyl sulfoxide solutions', *Journal of Organic Chemistry*, 53(5), pp. 1071–1074. doi: 10.1021/jo00240a025.

Eckmann, D. M. *et al.* (2014) 'Nanogel Carrier Design for Targeted Drug Delivery', *J.*

Mater. Chem. B, 2(46), pp. 8085–8097. doi: 10.1039/C4TB01141D.

Ehlbeck, J. *et al.* (2011) 'Low temperature atmospheric pressure plasma sources for microbial decontamination', *Journal of Physics D: Applied Physics*, 44(1), p. 013002. doi: 10.1088/0022-3727/44/1/013002.

El-Sayed, I. H., Huang, X. and El-Sayed, M. A. (2005) 'Surface plasmon resonance scattering and absorption of anti-EGFR antibody conjugated gold nanoparticles in cancer diagnostics: Applications in oral cancer', *Nano Letters*, 5(5), pp. 829–834. doi: 10.1021/nl050074e.

El-Sayed, I. H., Huang, X. and El-Sayed, M. A. (2006) 'Selective laser photo-thermal therapy of epithelial carcinoma using anti-EGFR antibody conjugated gold nanoparticles', *Cancer Letters*, 239(1), pp. 129–135. doi: 10.1016/j.canlet.2005.07.035.

Elenitoba-Johnson, K. S. J. *et al.* (2003) 'Involvement of multiple signaling pathways in follicular lymphoma transformation: p38-mitogen-activated protein kinase as a target for therapy', *Proceedings of the National Academy of Sciences of the United States of America*, 100(12), pp. 7259–7264. doi: 10.1073/pnas.1137463100.

Evens, A. M. *et al.* (2005) 'Motexafin gadolinium generates reactive oxygen species and induces apoptosis in sensitive and highly resistant multiple myeloma cells', *Blood*, 105(3), pp. 1265–1273. doi: 10.1182/blood-2004-03-0964.

Feng, H. and Stockwell, B. R. (2018) 'Unsolved mysteries: How does lipid peroxidation cause ferroptosis?', *PLoS Biology*, 16(5). doi: 10.1371/journal.pbio.2006203.

Feng, Y. *et al.* (2016) 'The application of mesoporous silica nanoparticle family in cancer theranostics', *Coordination Chemistry Reviews*. Elsevier B.V., 319, pp. 86–109. doi: 10.1016/j.ccr.2016.04.019.

FERNANDES, C. *et al.* (2017) 'Current Standards of Care in Glioblastoma Therapy', in *Glioblastoma*, pp. 197–241. doi: 10.15586/codon.glioblastoma.2017.ch11.

Ferrari, M. (2005) 'Cancer nanotechnology: Opportunities and challenges', *Nature Reviews Cancer*, 5(3), pp. 161–171. doi: 10.1038/nrc1566.

Foldbjerg, R. *et al.* (2009) 'PVP-coated silver nanoparticles and silver ions induce reactive oxygen species, apoptosis and necrosis in THP-1 monocytes', *Toxicology Letters*. Elsevier, 190(2), pp. 156–162. doi: 10.1016/j.toxlet.2009.07.009.

Folkes, A. J. *et al.* (2008) 'The identification of 2-(1H-indazol-4-yl)-6-(4-methanesulfonyl-piperazin-1-   ylmethyl)-4-morpholin-4-yl-thieno[3,2-d]pyrimidine (GDC-0941) as a potent, selective, orally bioavailable inhibitor of class I PI3 kinase for the treatment of cancer', *Journal of Medicinal Chemistry*. doi: 10.1021/jm800295d.

Freese, C. *et al.* (2012) 'Uptake and cytotoxicity of citrate-coated gold nanospheres: Comparative studies on human endothelial and epithelial cells', *Particle and Fibre Toxicology*, 9. doi: 10.1186/1743-8977-9-23.

Fresno Vara, J. Á. *et al.* (2004) 'P13K/Akt signalling pathway and cancer', *Cancer Treatment Reviews*, 30(2), pp. 193–204. doi: 10.1016/j.ctrv.2003.07.007.

Fridman, G. *et al.* (2008) 'Applied plasma medicine', *Plasma Processes and Polymers*, pp. 503–533. doi: 10.1002/ppap.200700154.

Gainer, J. L. *et al.* (2017) 'Trans sodium crocetinate with temozolomide and radiation therapy for glioblastoma multiforme', *Journal of Neurosurgery*, 126(2), pp. 460–466. doi: 10.3171/2016.3.JNS152693.

Gallego, O. (2015) 'Nonsurgical treatment of recurrent glioblastoma', *Current Oncology*, pp. e273–e281. doi: 10.3747/co.22.2436.

Gao, H., Shi, W. and Freund, L. B. (2005) 'Mechanics of receptor-mediated endocytosis', *Proceedings of the National Academy of Sciences of the United States of America*, 102(27), pp. 9469–9474. doi: 10.1073/pnas.0503879102.

Gao, J., Liu, X. and Rigas, B. (2005) 'Nitric oxide-donating aspirin induces apoptosis in

human colon cancer cells through induction of oxidative stress', *Proceedings of the National Academy of Sciences of the United States of America*, 102(47), pp. 17207–17212. doi: 10.1073/pnas.0506893102.

Gibson, P. and Suslov, N. (2012) 'The design of the plasmaJet® thermal plasma system and its application in surgery', *Plasma Medicine*, 2(1–3), pp. 115–126. doi: 10.1615/PlasmaMed.2013006357.

Gilkes, D. M., Semenza, G. L. and Wirtz, D. (2014) 'Hypoxia and the extracellular matrix: Drivers of tumour metastasis', *Nature Reviews Cancer*, pp. 430–439. doi: 10.1038/nrc3726.

Giri, S. *et al.* (2005) 'Stimuli-responsive controlled-release delivery system based on mesoporous silica nanorods capped with magnetic nanoparticles', *Angewandte Chemie - International Edition*. WILEY-VCH Verlag, 44(32), pp. 5038–5044. doi: 10.1002/anie.200501819.

Godin, B. *et al.* (2011) 'Multistage nanovectors: From concept to novel imaging contrast agents and therapeutics', *Accounts of Chemical Research*. American Chemical Society, pp. 979–989. doi: 10.1021/ar200077p.

Goldstein, I. M. and Weissmann, G. (1977) 'Effects of the generation of superoxide anion on permeability of liposomes', *Biochemical and Biophysical Research Communications*, 75(3), pp. 604–609. doi: 10.1016/0006-291X(77)91515-7.

Goodman, C. M. *et al.* (2004) 'Toxicity of gold nanoparticles functionalized with cationic and anionic side chains', *Bioconjugate Chemistry*, 15(4), pp. 897–900. doi: 10.1021/bc049951i.

Gormen, M. *et al.* (2010) 'Comparative toxicity of [3]ferrocenophane and ferrocene moieties on breast cancer cells', *Tetrahedron Letters*, 51(1), pp. 118–120. doi: 10.1016/j.tetlet.2009.10.102.

Görmen, M. *et al.* (2010) 'Synthesis, cytotoxicity, and COMPARE analysis of ferrocene and [3]ferrocenophane tetrasubstituted olefin derivatives against human cancer cells', *ChemMedChem*, 5(12), pp. 2039–2050. doi: 10.1002/cmdc.201000286.

Graves, D. B. (2012) 'The emerging role of reactive oxygen and nitrogen species in redox biology and some implications for plasma applications to medicine and biology', *Journal of Physics D: Applied Physics*, 45(26), p. 263001. doi: 10.1088/0022-3727/45/26/263001.

Guerrero-Preston, R. *et al.* (2014) 'Cold atmospheric plasma treatment selectively targets head and neck squamous cell carcinoma cells', *International Journal of Molecular Medicine*, 34(4), pp. 941–946. doi: 10.3892/ijmm.2014.1849.

Gunawan, R. C. and Auguste, D. T. (2010) 'The role of antibody synergy and membrane fluidity in the vascular targeting of immunoliposomes', *Biomaterials*, 31(5), pp. 900–907. doi: 10.1016/j.biomaterials.2009.09.107.

Gupta, U. *et al.* (2010) 'Ligand anchored dendrimers based nanoconstructs for effective targeting to cancer cells', *International Journal of Pharmaceutics*. Elsevier, 393(1–2), pp. 186–197. doi: 10.1016/j.ijpharm.2010.04.002.

Haertel, B. *et al.* (2014) 'Non-thermal atmospheric-pressure plasma possible application in wound healing', *Biomolecules and Therapeutics*, 22(6), pp. 477–490. doi: 10.4062/biomolther.2014.105.

Hähnel, M., Von Woedtke, T. and Weltmann, K. D. (2010) 'Influence of the air humidity on the reduction of Bacillus spores in a defined environment at atmospheric pressure using a dielectric barrier surface discharge', *Plasma Processes and Polymers*, 7(3–4), pp. 244–249. doi: 10.1002/ppap.200900076.

Hainfeld, J. F. *et al.* (2010) 'Gold nanoparticles enhance the radiation therapy of a murine squamous cell carcinoma', *Physics in Medicine and Biology*, 55(11), pp. 3045–3059. doi: 10.1088/0031-9155/55/11/004.

Halliwell, B. (1991) 'Reactive oxygen species in living systems: Source, biochemistry, and role in human disease', *The American Journal of Medicine*, 91(3), pp. S14–S22. doi: 10.1016/0002-9343(91)90279-7.

Halliwell, B. *et al.* (1992) 'Drug derived radicals: Mediators of the side effects of anti-inflammatory drugs?', *Annals of the Rheumatic Diseases*, 51(11), pp. 1261–1263. doi: 10.1136/ard.51.11.1261.

Han, L. *et al.* (2016) 'Mechanisms of inactivation by high-voltage atmospheric cold plasma differ for Escherichia coli and Staphylococcus aureus', *Applied and Environmental Microbiology*, 82(2), pp. 450–458. doi: 10.1128/AEM.02660-15.

Hao, G., Xu, Z. P. and Li, L. (2018) 'Manipulating extracellular tumour pH: An effective target for cancer therapy', *RSC Advances*, pp. 22182–22192. doi: 10.1039/c8ra02095g.

HARADA, H. (2011) 'How Can We Overcome Tumor Hypoxia in Radiation Therapy?', *Journal of Radiation Research*, 52(5), pp. 545–556. doi: 10.1269/jrr.11056.

Harris, I. S. *et al.* (2015) 'Glutathione and Thioredoxin Antioxidant Pathways Synergize to Drive Cancer Initiation and Progression', *Cancer Cell*, 27(2), pp. 211–222. doi: 10.1016/j.ccell.2014.11.019.

Hart, M. G. *et al.* (2013) 'Temozolomide for high grade glioma', *Cochrane Database of Systematic Reviews*. doi: 10.1002/14651858.CD007415.pub2.

He, Z. *et al.* (2018) 'Cold Atmospheric Plasma Induces ATP-Dependent Endocytosis of Nanoparticles and Synergistic U373MG Cancer Cell Death', *Scientific Reports*. Springer US, 8(1), pp. 1–11. doi: 10.1038/s41598-018-23262-0.

He, Z. *et al.* (2019) 'Combination Strategies for Targeted Delivery of Nanoparticles for Cancer Therapy', in *Applications of Targeted Nano Drugs and Delivery Systems*, pp. 191–219. doi: 10.1016/b978-0-12-814029-1.00008-9.

He, Z. *et al.* (2020) 'Cold Atmospheric Plasma Stimulates Clathrin-Dependent

Endocytosis to Repair Oxidised Membrane and Enhance Uptake of Nanomaterial in Glioblastoma Multiforme Cells', *Scientific Reports*, 10(1). doi: 10.1038/s41598-020-63732-y.

Hegi, M. E. *et al.* (2008) 'Correlation of O6-methylguanine methyltransferase (MGMT) promoter methylation with clinical outcomes in glioblastoma and clinical strategies to modulate MGMT activity', *Journal of Clinical Oncology*, pp. 4189–4199. doi: 10.1200/JCO.2007.11.5964.

Vander Heiden, M., Cantley, L. and Thompson, C. (2009) 'Understanding the Warburg effect: The metabolic Requiremetns of cell proliferation', *Science*, 324(5930), pp. 1029–1033. doi: 10.1126/science.1160809.Understanding.

Heinlin, J. *et al.* (2010) 'Plasma medicine: possible applications in dermatology', *JDDG: Journal der Deutschen Dermatologischen Gesellschaft*, 8(12), pp. 968–976. doi: 10.1111/j.1610-0387.2010.07495.x.

Hernot, S. and Klibanov, A. L. (2008) 'Microbubbles in ultrasound-triggered drug and gene delivery', *Advanced Drug Delivery Reviews*, 60(10), pp. 1153–1166. doi: 10.1016/j.addr.2008.03.005.

Hersh, E. M. *et al.* (1992) 'Antiproliferative and antitumor activity of the 2-cyanoaziridine compound imexon on tumor cell lines and fresh tumor cells in vitro', *Journal of the National Cancer Institute*. doi: 10.1093/jnci/84.16.1238.

Hicks, A. M. *et al.* (2006) 'Effector mechanisms of the anti-cancer immune responses of macrophages in SR/CR mice', *Cancer Immunity*, 6(October 2017).

Hilgenbrink, A. R. and Low, P. S. (2005) 'Folate receptor-mediated drug targeting: From therapeutics to diagnostics', *Journal of Pharmaceutical Sciences*. Wiley Subscription Services, Inc., A Wiley Company, pp. 2135–2146. doi: 10.1002/jps.20457.

Hjelmeland, A. B. *et al.* (2011) 'Acidic stress promotes a glioma stem cell phenotype',

Cell Death and Differentiation, 18(5), pp. 829–840. doi: 10.1038/cdd.2010.150.

Hu, C.-M. and Zhang, L. (2010) 'Therapeutic Nanoparticles to Combat Cancer Drug Resistance', *Current Drug Metabolism*, 10(8), pp. 836–841. doi: 10.2174/138920009790274540.

Hu, C. M. J., Aryal, S. and Zhang, L. (2010) 'Nanoparticle-assisted combination therapies for effective cancer treatment', *Therapeutic Delivery*, 1(2), pp. 323–334. doi: 10.4155/tde.10.13.

Idone, V. *et al.* (2008) 'Repair of injured plasma membrane by rapid Ca2+ dependent endocytosis', *Journal of Cell Biology*, 180(5), pp. 905–914. doi: 10.1083/jcb.200708010.

Idone, V., Tam, C. and Andrews, N. W. (2008) 'Two-way traffic on the road to plasma membrane repair', *Trends in Cell Biology*, pp. 552–559. doi: 10.1016/j.tcb.2008.09.001.

Irani, S. *et al.* (2015) 'Induction of growth arrest in colorectal cancer cells by cold plasma and gold nanoparticles', *Archives of Medical Science*, 11(6), pp. 1286–1295. doi: 10.5114/aoms.2015.48221.

Isbary, G. *et al.* (2011) 'Cold atmospheric plasma: A successful treatment of lesions in hailey-hailey disease', *Archives of Dermatology*. doi: 10.1001/archdermatol.2011.57.

Isbary, G. *et al.* (2012) 'Successful and safe use of 2 min cold atmospheric argon plasma in chronic wounds: Results of a randomized controlled trial', *British Journal of Dermatology*, 167(2), pp. 404–410. doi: 10.1111/j.1365-2133.2012.10923.x.

Isbary, G. *et al.* (2014) 'Randomized placebo-controlled clinical trial showed cold atmospheric argon plasma relieved acute pain and accelerated healing in herpes zoster', *Clinical Plasma Medicine*. doi: 10.1016/j.cpme.2014.07.001.

Ishaq, M. *et al.* (2014) 'Atmospheric gas plasma-induced ROS production activates TNF-ASK1 pathway for the induction of melanoma cancer cell apoptosis.', *Molecular biology of the cell*, 25(9), pp. 1523–31. doi: 10.1091/mbc.E13-10-0590.

Ishaq, M., Evans, M. and Ostrikov, K. (2014) 'Effect of atmospheric gas plasmas on cancer cell signaling', *International Journal of Cancer*, 134(7), pp. 1517–1528. doi: 10.1002/ijc.28323.

Iversen, T. G., Skotland, T. and Sandvig, K. (2011) 'Endocytosis and intracellular transport of nanoparticles: Present knowledge and need for future studies', *Nano Today*. Elsevier Ltd, 6(2), pp. 176–185. doi: 10.1016/j.nantod.2011.02.003.

Jacob, R. F. and Mason, R. P. (2005) 'Lipid peroxidation induces cholesterol domain formation in model membranes', *Journal of Biological Chemistry*, 280(47), pp. 39380–39387. doi: 10.1074/jbc.M507587200.

Jain, N. K. *et al.* (2015) 'The development, characterization and in vivo anti-ovarian cancer activity of poly(propylene imine) (PPI)-antibody conjugates containing encapsulated paclitaxel', *Nanomedicine: Nanotechnology, Biology, and Medicine*. Elsevier, 11(1), pp. 207–218. doi: 10.1016/j.nano.2014.09.006.

Jain, P. K., ElSayed, I. H. and El-Sayed, M. A. (2007) 'Au nanoparticles target cancer', *Nano Today*, 2(1), pp. 18–29. doi: 10.1016/S1748-0132(07)70016-6.

Jalili, A., Irani, S. and Mirfakhraie, R. (2016) 'Combination of cold atmospheric plasma and iron nanoparticles in breast cancer: Gene expression and apoptosis study', *OncoTargets and Therapy*. doi: 10.2147/OTT.S95644.

Janigro, D. *et al.* (2006) 'Alternating current electrical stimulation enhanced chemotherapy: a novel strategy to bypass multidrug resistance in tumor cells.', *BMC cancer*, 6, p. 72. doi: 10.1186/1471-2407-6-72.

Jaouen, G., Vessières, A. and Top, S. (2015) 'Ferrocifen type anti cancer drugs.', *Chemical Society reviews*, 44(24), pp. 8802–17. doi: 10.1039/c5cs00486a.

Jeong, S. J. *et al.* (2005) 'Activated AKT regulates NF-κB activation, p53 inhibition and cell survival in HTLV-1-transformed cells', *Oncogene*, 24(44), pp. 6719–6728. doi:

10.1038/sj.onc.1208825.

Jessen, K. R. and Mirsky, R. (1980) 'Glial cells in the enteric nervous system contain glial fibrillary acidic protein', *Nature*, 286(5774), pp. 736–737. doi: 10.1038/286736a0.

Jia, H. Y. *et al.* (2009) 'Potential oxidative stress of gold nanoparticles by induced-NO releasing in serum', *Journal of the American Chemical Society*, 131(1), pp. 40–41. doi: 10.1021/ja808033w.

Jia, J. *et al.* (2015) 'Caspases shutdown nonsense-mediated mRNA decay during apoptosis.', *Cell death and differentiation*, 22(11), pp. 1–10. doi: 10.1038/cdd.2015.18.

Jinno, M. *et al.* (2016) 'Investigation of plasma induced electrical and chemical factors and their contribution processes to plasma gene transfection', *Archives of Biochemistry and Biophysics*. Elsevier Inc, 605, pp. 59–66. doi: 10.1016/j.abb.2016.04.013.

Joh, D. Y. *et al.* (2013) 'Selective Targeting of Brain Tumors with Gold Nanoparticle-Induced Radiosensitization', *PLoS ONE*, 8(4). doi: 10.1371/journal.pone.0062425.

Judée, F. *et al.* (2016) 'Short and long time effects of low temperature Plasma Activated Media on 3D multicellular tumor spheroids.', *Scientific reports*, 6(October 2015), p. 21421. doi: 10.1038/srep21421.

Kaasalainen, M. *et al.* (2015) 'Electrostatic interaction on loading of therapeutic peptide GLP-1 into porous silicon nanoparticles', *Langmuir*. American Chemical Society, 31(5), pp. 1722–1729. doi: 10.1021/la5047047.

Kajita, M., McClinic, K. N. and Wade, P. A. (2004) 'Aberrant Expression of the Transcription Factors Snail and Slug Alters the Response to Genotoxic Stress', *Molecular and Cellular Biology*, 24(17), pp. 7559–7566. doi: 10.1128/mcb.24.17.7559-7566.2004.

Kalghatgi, S. *et al.* (2010) 'Endothelial cell proliferation is enhanced by low dose non-thermal plasma through fibroblast growth factor-2 release', *Annals of Biomedical Engineering*, 38(3), pp. 748–757. doi: 10.1007/s10439-009-9868-x.

Kalghatgi, S. *et al.* (2011) 'Effects of non-thermal plasma on mammalian cells', *PLoS ONE*, 6(1), pp. 1–11. doi: 10.1371/journal.pone.0016270.

Kalghatgi, S. U. *et al.* (2007) 'Mechanism of blood coagulation by nonthermal atmospheric pressure dielectric barrier discharge plasma', *IEEE Transactions on Plasma Science*, 35(5 II), pp. 1559–1566. doi: 10.1109/TPS.2007.905953.

Karanth, H. and Murthy, R. S. R. (2007) 'pH-Sensitive liposomes-principle and application in cancer therapy', *Journal of Pharmacy and Pharmacology*, 59(4), pp. 469–483. doi: 10.1211/jpp.59.4.0001.

Kasiappan, R. and Safe, S. (2016) 'ROS-Inducing Agents for Cancer Chemotherapy', *Reactive Oxygen Species*, 1(1). doi: 10.20455/ros.2016.805.

Katiyar, S. S. *et al.* (2016) 'Co-delivery of rapamycin- and piperine-loaded polymeric nanoparticles for breast cancer treatment', *Drug Delivery*. Taylor & Francis, 23(7), pp. 2608–2616. doi: 10.3109/10717544.2015.1039667.

Katz, E. and Willner, I. (2004) 'Integrated nanoparticle-biomolecule hybrid systems: Synthesis, properties, and applications', *Angewandte Chemie - International Edition*, 43(45), pp. 6042–6108. doi: 10.1002/anie.200400651.

Kaushik, N. K. N. *et al.* (2015) 'Non-thermal plasma with 2-deoxy-D-glucose synergistically induces cell death by targeting glycolysis in blood cancer cells', *Scientific Reports*, 5, p. 8726. doi: 10.1038/srep08726.

Kaushik, N. K. N. N. K. N. N. K. *et al.* (2016) 'Low doses of PEG-coated gold nanoparticles sensitize solid tumors to cold plasma by blocking the PI3K/AKT-driven signaling axis to suppress cellular transformation by inhibiting growth and EMT', *Biomaterials*. Elsevier Ltd, 87, pp. 118–130. doi: 10.1016/j.biomaterials.2016.02.014.

Kawczyk-Krupka, A. *et al.* (2015) 'Photodynamic therapy in colorectal cancer treatment: The state of the art in clinical trials', *Photodiagnosis and Photodynamic Therapy*, 12(3),

pp. 545–553. doi: 10.1016/j.pdpdt.2015.04.004.

Keidar, M. *et al.* (2011) 'Cold plasma selectivity and the possibility of a paradigm shift in cancer therapy.', *British journal of cancer*. Nature Publishing Group, 105(9), pp. 1295–301. doi: 10.1038/bjc.2011.386.

Kelada, M. *et al.* (2018) 'Synthesis of pyrazolopyrimidinones using a "one-pot" approach under microwave irradiation', *Beilstein Journal of Organic Chemistry*, 14, pp. 122–1228. doi: 10.3762/bjoc.14.104.

Khosla, D. (2016) 'Concurrent therapy to enhance radiotherapeutic outcomes in glioblastoma', *Annals of Translational Medicine*, 4(3). doi: 10.3978/j.issn.2305-5839.2016.01.25.

Kieft, I. E., Laan, E. P. V. D. and Stoffels, E. (2004) 'Electrical and optical characterization of the plasma needle', *New Journal of Physics*, 6(149), pp. 1–14. doi: 10.1088/1367-2630/6/1/149.

Kim, G. C. J. C. *et al.* (2008) 'Air plasma coupled with antibody-conjugated nanoparticles: a new weapon against cancer', *Journal of Physics D: Applied Physics*, 42(3), p. 032005. doi: 10.1088/0022-3727/42/3/032005.

Kim, G. J. *et al.* (2010) 'DNA damage and mitochondria dysfunction in cell apoptosis induced by nonthermal air plasma', *Applied Physics Letters*, 96(2), pp. 2010–2013. doi: 10.1063/1.3292206.

Kim, W. *et al.* (2017) 'Selective uptake of epidermal growth factor-conjugated gold nanoparticle (EGF-GNP) facilitates non-Thermal plasma (NTP)-mediated cell death', *Scientific Reports*. Springer US, 7(1), pp. 1–9. doi: 10.1038/s41598-017-11292-z.

Kinsella, J. M. *et al.* (2011) 'Enhanced magnetic resonance contrast of Fe 3O 4 nanoparticles trapped in a porous silicon nanoparticle host', *Advanced Materials*. WILEY-VCH Verlag, 23(36). doi: 10.1002/adma.201101877.

Koivusalo, M. *et al.* (2010) 'Amiloride inhibits macropinocytosis by lowering submembranous pH and preventing Rac1 and Cdc42 signaling (Journal of Cell Biology (2010) 188, (547-563))', *Journal of Cell Biology*, p. 385. doi: 10.1083/jcb.20090808620100331c.

Kong, M. G. *et al.* (2009) 'Plasma medicine: An introductory review', *New Journal of Physics*, 11. doi: 10.1088/1367-2630/11/11/115012.

Kong, M. G., Keidar, M. and Ostrikov, K. (2011) 'Plasmas meet nanoparticles-where synergies can advance the frontier of medicine', *Journal of Physics D: Applied Physics*, 44(17), p. 174018. doi: 10.1088/0022-3727/44/17/174018.

Kong, W. H. *et al.* (2012) 'Cationic lipid-coated gold nanoparticles as efficient and non-cytotoxic intracellular siRNA delivery vehicles', *Pharmaceutical Research*. Springer US, 29(2), pp. 362–374. doi: 10.1007/s11095-011-0554-y.

Köritzer, J. *et al.* (2013) 'Restoration of Sensitivity in Chemo - Resistant Glioma Cells by Cold Atmospheric Plasma', *PLoS ONE*. Public Library of Science, 8(5), p. e64498. doi: 10.1371/journal.pone.0064498.

Krassowska, W. and Filev, P. D. (2007) 'Modeling electroporation in a single cell', *Biophysical Journal*, 92(2), pp. 404–417. doi: 10.1529/biophysj.106.094235.

Kuchenbecker, M. *et al.* (2009) 'Characterization of DBD plasma source for biomedical applications', *Journal of Physics D: Applied Physics*. doi: 10.1088/0022-3727/42/4/045212.

Kumar, A. *et al.* (2012) 'Gold nanoparticles functionalized with therapeutic and targeted peptides for cancer treatment', *Biomaterials*, 33(4), pp. 1180–1189. doi: 10.1016/j.biomaterials.2011.10.058.

Kumar, A., Zhang, X. and Liang, X. J. (2013) 'Gold nanoparticles: Emerging paradigm for targeted drug delivery system', *Biotechnology Advances*. Elsevier Inc., 31(5), pp.

593–606. doi: 10.1016/j.biotechadv.2012.10.002.

Kunisawa, J. *et al.* (2005) 'Fusogenic liposome delivers encapsulated nanoparticles for cytosolic controlled gene release', *Journal of Controlled Release*. Elsevier, 105(3), pp. 344–353. doi: 10.1016/j.jconrel.2005.03.020.

Küpper, D. S. *et al.* (2014) 'Expression of apoptosis mediators p53 and caspase 3, 7, and 9 in chronic rhinosinusitis with nasal polyposis', *American Journal of Rhinology and Allergy*, 28(3), pp. 187–191. doi: 10.2500/ajra.2014.28.4022.

de la Rica, R., Aili, D. and Stevens, M. M. (2012) 'Enzyme-responsive nanoparticles for drug release and diagnostics', *Advanced Drug Delivery Reviews*, pp. 967–978. doi: 10.1016/j.addr.2012.01.002.

Lakadamyali, M., Rust, M. J. and Zhuang, X. (2006) 'Ligands for clathrin-mediated endocytosis are differentially sorted into distinct populations of early endosomes', *Cell*, 124(5), pp. 997–1009. doi: 10.1016/j.cell.2005.12.038.

Laroussi, M. (2002) 'Nonthermal decontamination of biological media by atmospheric-pressure plasmas: Review, analysis, and prospects', *IEEE Transactions on Plasma Science*, 30(4 I), pp. 1409–1415. doi: 10.1109/TPS.2002.804220.

Leduc, M. *et al.* (2009) 'Cell permeabilization using a non-thermal plasma', *New Journal of Physics*, 11(March). doi: 10.1088/1367-2630/11/11/115021.

Lee, H. J. *et al.* (2009) 'Degradation of adhesion molecules of G361 melanoma cells by a non-thermal atmospheric pressure microplasma', *New Journal of Physics*, 11. doi: 10.1088/1367-2630/11/11/115026.

Lee, H. and Ooya, T. (2012) '19F-NMR, 1H-NMR, and fluorescence studies of interaction between 5-fluorouracil and polyglycerol dendrimers', *Journal of Physical Chemistry B*. American Chemical Society, 116(40), pp. 12263–12267. doi: 10.1021/jp307710b.

Lee, H. W. *et al.* (2009) 'Tooth Bleaching with Nonthermal Atmospheric Pressure Plasma', *Journal of Endodontics*, 35(4), pp. 587–591. doi: 10.1016/j.joen.2009.01.008.

Leopold, J. A. and Loscalzo, J. (2009) 'Oxidative risk for atherothrombotic cardiovascular disease', *Free Radical Biology and Medicine*, pp. 1673–1706. doi: 10.1016/j.freeradbiomed.2009.09.009.

Leutner, S., Eckert, A. and Müller, W. E. (2001) 'ROS generation, lipid peroxidation and antioxidant enzyme activities in the aging brain', *Journal of Neurology*, 248(9), pp. 955–967. doi: 10.1007/s007020170015.

Li, B. *et al.* (2004) 'Mutant epidermal growth factor receptor displays increased signaling through the phosphatidylinositol-3 kinase/AKT pathway and promotes radioresistance in cells of astrocytic origin', *Oncogene*, 23(26), pp. 4594–4602. doi: 10.1038/sj.onc.1207602.

Li, H. P. *et al.* (2011) 'Manipulation of lipase activity by the helium radio-frequency, atmospheric-pressure glow discharge plasma jet', *Plasma Processes and Polymers*, 8(3), pp. 224–229. doi: 10.1002/ppap.201000035.

Li, S. P. *et al.* (2003) 'P38 Mitogen-Activated Protein Kinase Pathway Suppresses Cell Survival By Inducing Dephosphorylation of Mitogen-Activated Protein/Extracellular Signal-Regulated Kinase Kinase1,2', *Cancer Research*, 63(13), pp. 3473–3477.

Li, W. *et al.* (2019) 'Cold atmospheric plasma and iron oxide-based magnetic nanoparticles for synergetic lung cancer therapy', *Free Radical Biology and Medicine*. doi: 10.1016/j.freeradbiomed.2018.10.429.

Li, Y. *et al.* (2003) 'Selective killing of cancer cells by β-lapachone: Direct checkpoint activation as a strategy against cancer', *Proceedings of the National Academy of Sciences of the United States of America*, 100(5), pp. 2674–2678. doi: 10.1073/pnas.0538044100.

Li, Z. and Loh, X. J. (2017) 'Recent advances of using polyhydroxyalkanoate-based

nanovehicles as therapeutic delivery carriers', *Wiley Interdisciplinary Reviews: Nanomedicine and Nanobiotechnology*. John Wiley & Sons, Inc., 9(3), pp. 19–22. doi: 10.1002/wnan.1429.

Liang, K. *et al.* (2016) 'Targeted intracellular protein delivery based on hyaluronic acid-green tea catechin nanogels', *Acta Biomaterialia*. Acta Materialia Inc., 33, pp. 142–152. doi: 10.1016/j.actbio.2016.01.011.

Libutti, S. K. *et al.* (2010) 'Phase I and pharmacokinetic studies of CYT-6091, a novel PEGylated colloidal gold-rhTNF nanomedicine', *Clinical Cancer Research*, 16(24), pp. 6139–6149. doi: 10.1158/1078-0432.CCR-10-0978.

Ling, Y. H. *et al.* (2002) 'PS-341, a novel proteasome inhibitor, induces Bcl-2 phosphorylation and cleavage in association with G2-M phase arrest and apoptosis', *Molecular Cancer Therapeutics*, 1(10), pp. 841–849. doi: 10.1158/1535-7163.MCT-11-0745.

Link, W. J., Incropera, F. P. and Glover, J. L. (1976) 'A Plasma Scalpel: Comparison of Tissue Damage and Wound Healing With Electrosurgical and Steel Scalpels', *Archives of Surgery*, 111(4), pp. 392–397. doi: 10.1001/archsurg.1976.01360220088014.

Liu, D. *et al.* (2013) 'Co-delivery of a hydrophobic small molecule and a hydrophilic peptide by porous silicon nanoparticles', *Journal of Controlled Release*. Elsevier, 170(2), pp. 268–278. doi: 10.1016/j.jconrel.2013.05.036.

Liu, D. *et al.* (2015) 'Microfluidic assisted one-step fabrication of porous silicon@acetalated dextran nanocomposites for precisely controlled combination chemotherapy', *Biomaterials*. Elsevier, 39, pp. 249–259. doi: 10.1016/j.biomaterials.2014.10.079.

Liu, K. *et al.* (2018) 'Investigating the role of gold nanoparticle shape and size in their toxicities to fungi', *International Journal of Environmental Research and Public Health*,

15(5), p. 998. doi: 10.3390/ijerph15050998.

Liu, K. *et al.* (2019) 'A novel, rapid, seedless, in situ synthesis method of shape and size controllable gold nanoparticles using phosphates', *Scientific Reports*. doi: 10.1038/s41598-019-43921-0.

Liu, X. *et al.* (2016) 'Irinotecan Delivery by Lipid-Coated Mesoporous Silica Nanoparticles Shows Improved Efficacy and Safety over Liposomes for Pancreatic Cancer', *ACS Nano*, 10(2), pp. 2702–2715. doi: 10.1021/acsnano.5b07781.

Lonez, C., Vandenbranden, M. and Ruysschaert, J. M. (2008) 'Cationic liposomal lipids: From gene carriers to cell signaling', *Progress in Lipid Research*, pp. 340–347. doi: 10.1016/j.plipres.2008.03.002.

Louis, D. N. *et al.* (2016) 'The 2016 World Health Organization Classification of Tumors of the Central Nervous System: a summary', *Acta Neuropathologica*, pp. 803–820. doi: 10.1007/s00401-016-1545-1.

Lu, H. *et al.* (2014) 'Bacterial inactivation by high-voltage atmospheric cold plasma: Influence of process parameters and effects on cell leakage and DNA', *Journal of Applied Microbiology*, 116(4), pp. 784–794. doi: 10.1111/jam.12426.

Lu, P. *et al.* (2017) 'Achieving reactive species specificity within plasma-activated water through selective generation using air spark and glow discharges', *Plasma Processes and Polymers*, 14(8), pp. 1–9. doi: 10.1002/ppap.201600207.

Lux, J. *et al.* (2013) 'Metal Chelating Crosslinkers Form Nanogels with High Chelation Stability.', *Journal of Materials Chemistry B*, 1(46), pp. 6359–6364. doi: 10.1039/C3TB21104E.

Ma, Z., Sun, W. W. and Wang, X. (2014) 'Hydrogen peroxide enhances the uptake of polyethylenimine/oligonucleotide complexes in A549 cells by activating CaMKII independent of [ca2+]c elevation', *Genetics and Molecular Research*, 13(2), pp. 2914–

2921. doi: 10.4238/2014.February.21.15.

Madhuri, T. K. *et al.* (2010) 'First clinical experience of argon neutral plasma energy in gynaecological surgery in the UK', *Gynecological Surgery*, 7(4), pp. 423–425. doi: 10.1007/s10397-010-0591-2.

Maeda, M. *et al.* (2017) 'Sonodynamic Therapy Based on Combined Use of Low Dose Administration of Epirubicin-Incorporating Drug Delivery System and Focused Ultrasound', *Ultrasound in Medicine and Biology*, 43(10), pp. 2295–2301. doi: 10.1016/j.ultrasmedbio.2017.06.003.

Maehama, T. and Dixon, J. E. (1999) 'PTEN: A tumour suppressor that functions as a phospholipid phosphatase', *Trends in Cell Biology*, pp. 125–128. doi: 10.1016/S0962-8924(99)01519-6.

Magné, N. *et al.* (2006) 'NF-κB modulation and ionizing radiation: Mechanisms and future directions for cancer treatment', *Cancer Letters*, 231(2), pp. 158–168. doi: 10.1016/j.canlet.2005.01.022.

Maher, M. A. *et al.* (2014) 'Numerical simulations of in vitro nanoparticle toxicity - the case of poly(amido amine) dendrimers', *Toxicology in Vitro*, 28(8), pp. 1449–1460. doi: 10.1016/j.tiv.2014.07.014.

Mai-Prochnow, A. *et al.* (2014) 'Atmospheric pressure plasmas: Infection control and bacterial responses', *International Journal of Antimicrobial Agents*. Elsevier B.V., 43(6), pp. 508–517. doi: 10.1016/j.ijantimicag.2014.01.025.

Major Jourden, J. L. and Cohen, S. M. (2010) 'Hydrogen peroxide activated matrix metalloproteinase inhibitors: A prodrug approach', *Angewandte Chemie - International Edition*, 49(38), pp. 6795–6797. doi: 10.1002/anie.201003819.

Malaekeh-Nikouei, B. *et al.* (2008) 'The enhancement of immunosuppressive effects of cyclosporine A on human T-cells using fusogenic liposomes', *Colloids and Surfaces B:*

Biointerfaces, 67(2), pp. 238–244. doi: 10.1016/j.colsurfb.2008.09.001.

Manaloto, A. E. *et al.* (2020) 'Cold Atmospheric Plasma induces silver nanoparticle uptake, oxidative dissolution and enhanced cytotoxicity in Glioblastoma multiforme cells', *bioRxiv*. doi: https://doi.org/10.1101/2020.02.28.969758.

Manchun, S. *et al.* (2015) 'Enhanced anti-tumor effect of pH-responsive dextrin nanogels delivering doxorubicin on colorectal cancer', *Carbohydrate Polymers*, 126, pp. 222–230. doi: 10.1016/j.carbpol.2015.03.018.

Manchun, S., Dass, C. R. and Sriamornsak, P. (2012) 'Targeted therapy for cancer using pH-responsive nanocarrier systems', *Life Sciences*, 90(11–12), pp. 381–387. doi: 10.1016/j.lfs.2012.01.008.

Manda, G., Nechifor, M. T. and Neagu, T.-M. (2009) 'Reactive Oxygen Species, Cancer and Anti-Cancer Therapies', *Current Chemical Biology*, 3(1), pp. 342–366. doi: 10.2174/187231309787158271.

Mani, S. A. *et al.* (2008) 'The Epithelial-Mesenchymal Transition Generates Cells with Properties of Stem Cells', *Cell*, 133(4), pp. 704–715. doi: 10.1016/j.cell.2008.03.027.

Manke, I. A. *et al.* (2005) 'MAPKAP kinase-2 is a cell cycle checkpoint kinase that regulates the G2/M transition and S phase progression in response to UV irradiation', *Molecular cell*, 17(1), pp. 37–48. doi: 10.1016/j.molcel.2004.11.021.

Marta, G. N., Correa, S. F. M. and Teixeira, M. J. (2011) 'Meningioma: Review of the literature with emphasis on the approach to radiotherapy', *Expert Review of Anticancer Therapy*, 11(11), pp. 1749–1758. doi: 10.1586/ERA.11.162.

Martina Ferrari, S. *et al.* (2015) 'Pyrazolopyrimidine Derivatives as Antineoplastic Agents: with a Special Focus on Thyroid Cancer', *Mini-Reviews in Medicinal Chemistry*. doi: 10.2174/1389557515666151016124208.

Marzenell, P. *et al.* (2013) 'Aminoferrocene-based prodrugs and their effects on human

normal and cancer cells as well as bacterial cells', *Journal of Medicinal Chemistry*, 56(17), pp. 6935–6944. doi: 10.1021/jm400754c.

Masood, F. (2016) 'Polymeric nanoparticles for targeted drug delivery system for cancer therapy', *Materials Science and Engineering C*. Elsevier B.V., 60, pp. 569–578. doi: 10.1016/j.msec.2015.11.067.

Mastrobattista, E., Koning, G. A. and Storm, G. (1999) 'Immunoliposomes for the targeted delivery of antitumor drugs', *Advanced Drug Delivery Reviews*, pp. 103–127. doi: 10.1016/S0169-409X(99)00043-5.

Mattson, M. P. (1998) 'Modification of ion homeostasis by lipid peroxidation: Roles in neuronal degeneration and adaptive plasticity', *Trends in Neurosciences*, 21(2), pp. 53–57. doi: 10.1016/S0166-2236(97)01188-0.

Mattson, M. P. *et al.* (1999) 'Cellular and molecular mechanisms underlying perturbed energy metabolism and neuronal degeneration in Alzheimer's and Parkinson's diseases', in *Annals of the New York Academy of Sciences*, pp. 154–175. doi: 10.1111/j.1749-6632.1999.tb07824.x.

Maya, S. *et al.* (2013) 'Smart stimuli sensitive nanogels in cancer drug delivery and imaging: A review', *Current Pharmaceutical Design*, 19(41), pp. 7203–7218. doi: 10.2174/13816128194131219124142.

Mayer, L. D. *et al.* (2006) 'Ratiometric dosing of anticancer drug combinations: Controlling drug ratios after systemic administration regulates therapeutic activity in tumor-bearing mice', *Molecular Cancer Therapeutics*, 5(7), pp. 1854–1863. doi: 10.1158/1535-7163.MCT-06-0118.

Meng, H. *et al.* (2015) 'Use of a lipid-coated mesoporous silica nanoparticle platform for synergistic gmcitabine and pclitaxel dlivery to hman pncreatic cncer in mice', *ACS Nano*, 9(4), pp. 3540–3557. doi: 10.1021/acsnano.5b00510.

Metelmann, H.-R. R. *et al.* (2015) 'Head and neck cancer treatment and physical plasma', *Clinical Plasma Medicine*. Elsevier, 3(1), pp. 17–23. doi: 10.1016/j.cpme.2015.02.001.

Mikkelsen, R. B. and Wardman, P. (2003) 'Biological chemistry of reactive oxygen and nitrogen and radiation-induced signal transduction mechanisms.', *Oncogene*, 22(37), pp. 5734–54. doi: 10.1038/sj.onc.1206663.

Mirimanoff, R. *et al.* (2007) 'Is Long-Term Survival in Glioblastoma Possible? Updated Results of the EORTC/NCIC Phase III Randomized Trial on Radiotherapy (RT) and Concomitant and Adjuvant Temozolomide (TMZ) versus RT Alone', *International Journal of Radiation Oncology*Biology*Physics*, 69(3), p. S2. doi: 10.1016/j.ijrobp.2007.07.004.

Mladenov, N. *et al.* (2007) *Chemical characterization of DOM in channels of a seasonal wetland*, *Aquatic Sciences*. doi: 10.1007/s00027-007-0905-2.

Moiseev, T. *et al.* (2014) 'Post-discharge gas composition of a large-gap DBD in humid air by UV-Vis absorption spectroscopy', *Plasma Sources Science and Technology*, 23(6). doi: 10.1088/0963-0252/23/6/065033.

Møller, H. G. *et al.* (2013) 'A systematic review of MicroRNA in glioblastoma multiforme: Micro-modulators in the mesenchymal mode of migration and invasion', *Molecular Neurobiology*, pp. 131–144. doi: 10.1007/s12035-012-8349-7.

Morel, A.-P. *et al.* (2008) 'Generation of breast cancer stem cells through epithelial-mesenchymal transition.', *PloS one*, 3(8), p. e2888. doi: 10.1371/journal.pone.0002888.

Morfill, G. E. *et al.* (2009) 'Nosocomial infections - A new approach towards preventive medicine using plasmas', *New Journal of Physics*, 11(11), p. 115019. doi: 10.1088/1367-2630/11/11/115019.

Morgan, M. T. *et al.* (2006) 'Dendrimer-encapsulated camptothecins: Increased solubility, cellular uptake, and cellular retention affords enhanced anticancer activity in vitro',

Cancer Research, 66(24), pp. 11913–11921. doi: 10.1158/0008-5472.CAN-06-2066.

Moussa, H., Martins, A. and Husseini, G. (2015) *Review on Triggered Liposomal Drug Delivery with a Focus on Ultrasound*, *Current Cancer Drug Targets*. doi: 10.2174/1568009615666150311100610.

Murray, L. J. and Robinson, M. H. (2016) 'Radiotherapy: Technical aspects', *Medicine (United Kingdom)*. Elsevier Ltd, 44(1), pp. 10–14. doi: 10.1016/j.mpmed.2015.10.013.

Naldini, L. (2015) 'Gene therapy returns to centre stage', *Nature*, pp. 351–360. doi: 10.1038/nature15818.

Nel, A. *et al.* (2006) 'Toxic potential of materials at the nanolevel', *Science*, 311(5761), pp. 622–627. doi: 10.1126/science.1114397.

Nezhat, C. and Kho, K. (2009) 'Use of Neutral Argon Plasma in the Laparoscopic Treatment of Endometriosis', *Journal of Minimally Invasive Gynecology*, 16(6), p. S55. doi: 10.1016/j.jmig.2009.08.206.

Nicholson, R. I., Gee, J. M. and Harper, M. E. (2001) 'EGFR and cancer prognosis.', *European journal of cancer*, 37 Suppl 4, pp. S9–S15. doi: 10.1016/S0959-8049(01)00231-3.

Niemeyer, C. M. (2001) 'Nanoparticles, Proteins, and Nucleic Acids: Biotechnology Meets Materials Science', *Angewandte Chemie International Edition*, 40(22), pp. 4128–4158. doi: 10.1002/1521-3773(20011119)40:22<4128::AID-ANIE4128>3.0.CO;2-S.

Nikitaki, Z. *et al.* (2016) 'Systemic mechanisms and effects of ionizing radiation: A new "old" paradigm of how the bystanders and distant can become the players', *Seminars in Cancer Biology*, 37–38, pp. 77–95. doi: 10.1016/j.semcancer.2016.02.002.

Nordberg, J. and Arnér, E. S. J. (2001) 'Reactive oxygen species, antioxidants, and the mammalian thioredoxin system', *Free Radical Biology and Medicine*, 31(11), pp. 1287–1312. doi: 10.1016/S0891-5849(01)00724-9.

O'Connor, N. *et al.* (2014) 'Cold atmospheric pressure plasma and decontamination. Can it contribute to preventing hospital-acquired infections?', *Journal of Hospital Infection.* Elsevier Ltd, 88(2), pp. 59–65. doi: 10.1016/j.jhin.2014.06.015.

O'donnell-Tormey, J. *et al.* (1987) 'Secretion of pyruvate: An antioxidant defense of mammalian cells', *Journal of Experimental Medicine*. doi: 10.1084/jem.165.2.500.

Omuro, A. and DeAngelis, L. M. (2013) 'Glioblastoma and other malignant gliomas: A clinical review', *JAMA - Journal of the American Medical Association*. doi: 10.1001/jama.2013.280319.

Osminkina, L. A. *et al.* (2012) 'Photoluminescent biocompatible silicon nanoparticles for cancer theranostic applications', *Journal of Biophotonics*. WILEY-VCH Verlag, 5(7), pp. 529–535. doi: 10.1002/jbio.201100112.

Van Der Paal, J. *et al.* (2016) 'Effect of lipid peroxidation on membrane permeability of cancer and normal cells subjected to oxidative stress', *Chemical Science*, 7(1), pp. 489–498. doi: 10.1039/c5sc02311d.

Pan, Y. *et al.* (2007) 'Size-dependent cytotoxicity of gold nanoparticles', *Small*, 3(11), pp. 1941–1949. doi: 10.1002/smll.200700378.

Pan, Y. *et al.* (2009) 'Gold nanoparticles of diameter 1.4 nm trigger necrosis by oxidative stress and mitochondrial damage', *Small*, pp. 2067–2076. doi: 10.1002/smll.200900466.

Pankaj, S. K. *et al.* (2014) 'Zein film: Effects of dielectric barrier discharge atmospheric cold plasma', *Journal of Applied Polymer Science*, 131(18), pp. 9541–9546. doi: 10.1002/app.40803.

Pankaj, S. K. S., Misra, N. N. and Cullen, P. J. P. (2013) 'Kinetics of tomato peroxidase inactivation by atmospheric pressure cold plasma based on dielectric barrier discharge', *Innovative Food Science and Emerging Technologies*, 19(July), pp. 153–157. doi: 10.1016/j.ifset.2013.03.001.

Pardoll, D. M. (2012) 'The blockade of immune checkpoints in cancer immunotherapy', *Nature Reviews Cancer*. doi: 10.1038/nrc3239.

Park, E. J. *et al.* (2008) 'Oxidative stress and apoptosis induced by titanium dioxide nanoparticles in cultured BEAS-2B cells', *Toxicology Letters*, 180(3), pp. 222–229. doi: 10.1016/j.toxlet.2008.06.869.

Park, G. Y. *et al.* (2012) 'Atmospheric-pressure plasma sources for biomedical applications', *Plasma Sources Science and Technology*, 21(4), p. 043001. doi: 10.1088/0963-0252/21/4/043001.

Park, J. W. *et al.* (1997) 'Immunoliposomes for Cancer Treatment', *Advances in Pharmacology*, 40(C), pp. 399–435. doi: 10.1016/S1054-3589(08)60146-5.

Park, S.-B. *et al.* (2015) 'Differential Epigenetic Effects of Atmospheric Cold Plasma on MCF-7 and MDA-MB-231 Breast Cancer Cells.', *PloS one*, 10(6), p. e0129931. doi: 10.1371/journal.pone.0129931.

Park, S. R. *et al.* (2014) 'Enhancement of the killing effect of low-temperature plasma on Streptococcus mutans by combined treatment with gold nanoparticles.', *Journal of nanobiotechnology*, 12, p. 29. doi: 10.1186/s12951-014-0029-5.

Parsons, D. W. *et al.* (2008) 'An integrated genomic analysis of human glioblastoma multiforme', *Science*, 321(5897), pp. 1807–1812. doi: 10.1126/science.1164382.

Patange, A. *et al.* (2017) 'Controlling Brochothrix thermosphacta as a spoilage risk using in-package atmospheric cold plasma', *Food Microbiology*, 66, pp. 48–54. doi: 10.1016/j.fm.2017.04.002.

Patel, R. P. *et al.* (1999) 'Biological aspects of reactive nitrogen species', *Biochimica et Biophysica Acta (BBA) - Bioenergetics*, 1411(2–3), pp. 385–400. doi: 10.1016/S0005-2728(99)00028-6.

Patra, H. K. *et al.* (2007) 'Cell selective response to gold nanoparticles', *Nanomedicine:*

Nanotechnology, Biology, and Medicine, 3(2), pp. 111–119. doi: 10.1016/j.nano.2007.03.005.

Peat, A. J. *et al.* (2004) 'Novel pyrazolopyrimidine derivatives as GSK-3 inhibitors', *Bioorganic and Medicinal Chemistry Letters*. doi: 10.1016/j.bmcl.2004.02.036.

Pelkmans, L., Püntener, D. and Helenius, A. (2002) 'Local actin polymerization and dynamin recruitment in SV40-induced internalization of caveolae', *Science*, 296(5567), pp. 535–539. doi: 10.1126/science.1069784.

Peng, X. and Gandhi, V. (2012) 'ROS-activated anticancer prodrugs: A new strategy for tumor-specific damage', *Therapeutic Delivery*, 3(7), pp. 823–833. doi: 10.4155/tde.12.61.

Perez, C. *et al.* (2015) 'Exploring hydrogen peroxide responsive thiazolidinone-based prodrugs', *Chemical Communications*. Royal Society of Chemistry, 51(33), pp. 7116–7119. doi: 10.1039/c4cc09921d.

Perillo, B. *et al.* (2020) 'ROS in cancer therapy: the bright side of the moon', *Experimental and Molecular Medicine*, pp. 192–203. doi: 10.1038/s12276-020-0384-2.

Petrescu, A. D. *et al.* (2001) 'Steroidogenic Acute Regulatory Protein Binds Cholesterol and Modulates Mitochondrial Membrane Sterol Domain Dynamics', *Journal of Biological Chemistry*, 276(40), pp. 36970–36982. doi: 10.1074/jbc.M101939200.

Plazuk, D. *et al.* (2009) 'A [3]ferrocenophane polyphenol showing a remarkable antiproliferative activity on breast and prostate cancer cell lines', *Journal of Medicinal Chemistry*, 52(15), pp. 4964–4967. doi: 10.1021/jm900297x.

Putnam, D. (2008) 'Drug delivery: The heart of the matter', *Nature Materials*. Nature Publishing Group, 7(11), pp. 836–837. doi: 10.1038/nmat2309.

Radhakrishnan, K. *et al.* (2015) 'Mesoporous silica - Chondroitin sulphate hybrid nanoparticles for targeted and bio-responsive drug delivery', *New Journal of Chemistry*. Royal Society of Chemistry, 39(3), pp. 1754–1760. doi: 10.1039/c4nj01430h.

Ramos-Ibeas, P. *et al.* (2017) 'Pyruvate antioxidant roles in human fibroblasts and embryonic stem cells', *Molecular and Cellular Biochemistry*, 429(1–2), pp. 137–150. doi: 10.1007/s11010-017-2942-z.

Rampling, R. *et al.* (1994) 'Direct measurement of pO2 distribution and bioreductive enzymes in human malignant brain tumors', *International Journal of Radiation Oncology, Biology, Physics*, 29(3), pp. 427–431. doi: 10.1016/0360-3016(94)90432-4.

Rao, M. V., Hale, B. A. and Ormrod, D. P. (1995) 'Amelioration of ozone-induced oxidative damage in wheat plants grown under high carbon dioxide. Role of antioxidant enzymes', *Plant Physiology*, 109(2), pp. 421–432. doi: 10.1104/pp.109.2.421.

Rasmussen, J. W. *et al.* (2010) 'Zinc oxide nanoparticles for selective destruction of tumor cells and potential for drug delivery applications', *Expert Opinion on Drug Delivery*. Taylor & Francis, 7(9), pp. 1063–1077. doi: 10.1517/17425247.2010.502560.

Ratovitski, E. A. *et al.* (2014) 'Anti-cancer therapies of 21st century: Novel approach to treat human cancers using cold atmospheric plasma', *Plasma Processes and Polymers*, 11(12), pp. 1128–1137. doi: 10.1002/ppap.201400071.

Ray, P. D., Huang, B. W. and Tsuji, Y. (2012) 'Reactive oxygen species (ROS) homeostasis and redox regulation in cellular signaling', *Cellular Signalling*, pp. 981–990. doi: 10.1016/j.cellsig.2012.01.008.

Recek, N. *et al.* (2015) 'Effect of cold plasma on glial cell morphology studied by atomic force microscopy', *PLoS ONE*, 10(3), pp. 1–14. doi: 10.1371/journal.pone.0119111.

Rehman, M. U. *et al.* (2015) 'Comparison of free radicals formation induced by cold atmospheric plasma, ultrasound, and ionizing radiation', *Archives of Biochemistry and Biophysics*. Elsevier Inc, pp. 1–7. doi: 10.1016/j.abb.2016.04.005.

Renaud, M. C. and Sebastianelli, A. (2013) 'Optimal Cytoreduction With Neutral Argon Plasma Energy in Selected Patients With Ovarian and Primitive Peritoneal Cancer',

Journal of Obstetrics and Gynaecology Canada, 35(1), pp. 49–52. doi: 10.1016/S1701-2163(15)31048-3.

Rengeng, L. *et al.* (2017) 'Sonodynamic therapy, a treatment developing from photodynamic therapy', *Photodiagnosis and Photodynamic Therapy*. Elsevier B.V., 19, pp. 159–166. doi: 10.1016/j.pdpdt.2017.06.003.

Reuter, S. *et al.* (2010) 'Oxidative stress, inflammation, and cancer: How are they linked?', *Free Radical Biology and Medicine*. Elsevier Inc., 49(11), pp. 1603–1616. doi: 10.1016/j.freeradbiomed.2010.09.006.

Riemenschneider, M. J. *et al.* (2010) 'Molecular diagnostics of gliomas: State of the art', *Acta Neuropathologica*, pp. 567–584. doi: 10.1007/s00401-010-0736-4.

Robertson, M. J. *et al.* (2014) 'Synthesis of the Pitstop family of clathrin inhibitors', *Nature Protocols*, 9(7), pp. 1592–1606. doi: 10.1038/nprot.2014.106.

Roblero-Bartolon, G. V. and Ramon-Gallegos, E. (2015) '[Use of nanoparticles (NP) in photodynamic therapy (PDT) against cancer].', *Gaceta medica de Mexico*, 151(1), pp. 85–98.

Roizen, M. F. (2012) 'Hallmarks of Cancer: The Next Generation', *Yearbook of Anesthesiology and Pain Management*, 2012, p. 13. doi: 10.1016/j.yane.2012.02.046.

Roman, H. *et al.* (2013) 'Postoperative Recurrence and Fertility after Endometrioma Ablation Using Plasma Energy: Retrospective Assessment of a 3-Year Experience', *Journal of Minimally Invasive Gynecology*, 20(5), pp. 573–582. doi: 10.1016/j.jmig.2013.02.016.

Rothkamm, K. and Löbrich, M. (2003) 'Evidence for a lack of DNA double-strand break repair in human cells exposed to very low x-ray doses', *Proceedings of the National Academy of Sciences of the United States of America*, 100(9), pp. 5057–5062. doi: 10.1073/pnas.0830918100.

Rottenberg, D. A. *et al.* (1984) 'In vivo measurement of regional brain tissue pH using positron emission tomography', *Annals of Neurology*. doi: 10.1002/ana.410150718.

Rouffet, M. and Cohen, S. M. (2011) 'Emerging trends in metalloprotein inhibition', *Dalton Transactions*, pp. 3445–3454. doi: 10.1039/c0dt01743d.

Russo, T. *et al.* (1995) 'A p53-independent pathway for activation of WAF1/CIP1 expression following oxidative stress', *Journal of Biological Chemistry*, 270(49), pp. 29386–29391. doi: 10.1074/jbc.270.49.29386.

Ryan, J. A. *et al.* (2007) 'Cellular uptake of gold nanoparticles passivated with BSA-SV40 large T antigen conjugates', *Analytical Chemistry*, 79(23), pp. 9150–9159. doi: 10.1021/ac0715524.

Saad, M., Garbuzenko, O. B. and Minko, T. (2008) 'Co-delivery of siRNA and an anticancer drug for treatment of multidrug-resistant cancer', *Nanomedicine*, 3(6), pp. 761–776. doi: 10.2217/17435889.3.6.761.

Sabharwal, S. S. and Schumacker, P. T. (2014) 'Mitochondrial ROS in cancer: Initiators, amplifiers or an Achilles' heel?', *Nature Reviews Cancer*, 14(11), pp. 709–721. doi: 10.1038/nrc3803.

Sagawa, T. *et al.* (2003) 'Argon plasma coagulation for successful treatment of early gastric cancer with intramucosal invasion', *Gut*, 52(3), pp. 334–339. doi: 10.1136/gut.52.3.334.

Salonen, J. *et al.* (2005) 'Mesoporous silicon microparticles for oral drug delivery: Loading and release of five model drugs', *Journal of Controlled Release*. Elsevier, 108(2–3), pp. 362–374. doi: 10.1016/j.jconrel.2005.08.017.

Sánchez, M. *et al.* (2012) 'A randomized clinical trial evaluating plasma rich in growth factors (PRGF-Endoret) versus hyaluronic acid in the short-term treatment of symptomatic knee osteoarthritis', *Arthroscopy - Journal of Arthroscopic and Related*

Surgery, 28(8), pp. 1070–1078. doi: 10.1016/j.arthro.2012.05.011.

Sasaki, Y. *et al.* (2010) 'Polysaccharide nanogel-cyclodextrin system as an artificial chaperone for in vitro protein synthesis of green fluorescent protein', *Polymer Journal*, 42(10), pp. 823–828. doi: 10.1038/pj.2010.73.

Schmidt-Bleker, A. *et al.* (2015) 'On the plasma chemistry of a cold atmospheric argon plasma jet with shielding gas device', *Plasma Sources Science and Technology*, 25(1), p. 015005. doi: 10.1088/0963-0252/25/1/015005.

Schroeder, K. and Gururangan, S. (2014) 'Molecular variants and mutations in medulloblastoma', *Pharmacogenomics and Personalized Medicine*, pp. 43–51. doi: 10.2147/PGPM.S38698.

Schuessel, K. *et al.* (2006) 'Aging sensitizes toward ROS formation and lipid peroxidation in PS1M146L transgenic mice', *Free Radical Biology and Medicine*, 40(5), pp. 850–862. doi: 10.1016/j.freeradbiomed.2005.10.041.

Schumacker, P. T. (2006) 'Reactive oxygen species in cancer cells: Live by the sword, die by the sword', *Cancer Cell*, pp. 175–176. doi: 10.1016/j.ccr.2006.08.015.

Secret, E. *et al.* (2014) 'Two-photon excitation of porphyrin-functionalized porous silicon nanoparticles for photodynamic therapy', *Advanced Materials*, 26(45), pp. 7643–7648. doi: 10.1002/adma.201403415.

Service, R. F. (2005) 'Nanotechnology takes aim at cancer', *Science*, 310(5751), pp. 1132–1134. doi: 10.1126/science.310.5751.1132.

Setua, S. *et al.* (2014) 'Cisplatin-tethered gold nanospheres for multimodal chemo-radiotherapy of glioblastoma', *Nanoscale*, 6(18), pp. 10865–10873. doi: 10.1039/c4nr03693j.

Sevanian, A. and Ursini, F. (2000) 'Lipid peroxidation in membranes and low-density lipoproteins: Similarities and differences', *Free Radical Biology and Medicine*, 29(3–4),

pp. 306–311. doi: 10.1016/S0891-5849(00)00342-7.

Sharma, A. K. *et al.* (2017) 'Dendrimer nanoarchitectures for cancer diagnosis and anticancer drug delivery', *Drug Discovery Today*. Elsevier Ltd, 22(2), pp. 314–326. doi: 10.1016/j.drudis.2016.09.013.

Sharma, H. *et al.* (2015) 'Metal nanoparticles: A theranostic nanotool against cancer', *Drug Discovery Today*. Elsevier Ltd, 20(9), pp. 1143–1151. doi: 10.1016/j.drudis.2015.05.009.

Shi, L. *et al.* (2017) 'Non-thermal plasma induces a stress response in mesothelioma cells resulting in increased endocytosis, lysosome biogenesis and autophagy', *Free Radical Biology and Medicine*. Elsevier B.V., 108(December 2016), pp. 904–917. doi: 10.1016/j.freeradbiomed.2017.04.368.

Shi, X. M. *et al.* (2012) 'Effect of low-temperature plasma on deactivation of hepatitis B virus', *IEEE Transactions on Plasma Science*, 40(10 PART 2), pp. 2711–2716. doi: 10.1109/TPS.2012.2210567.

Shilo, M. *et al.* (2015) 'The effect of nanoparticle size on the probability to cross the blood-brain barrier: an in-vitro endothelial cell model', *Journal of Nanobiotechnology*, 13(1), p. 19. doi: 10.1186/s12951-015-0075-7.

Shukla, R. *et al.* (2005) 'Biocompatibility of gold nanoparticles and their endocytotic fate inside the cellular compartment: A microscopic overview', *Langmuir*, 21(23), pp. 10644–10654. doi: 10.1021/la0513712.

Singh, N., Gill, V. and Gill, P. (2013) 'Nanogel Based Artificial Chaperone Technology : an Overview', *American Journal of Advanced Drug Delivery*, 1, pp. 271–276.

Siu, A. *et al.* (2015) 'Differential Effects of Cold Atmospheric Plasma in the Treatment of Malignant Glioma.', *PloS one*, 10(6), p. e0126313. doi: 10.1371/journal.pone.0126313.

Sivaram, A. J. *et al.* (2015) 'Nanogels for delivery, imaging and therapy', *Wiley*

Interdisciplinary Reviews: Nanomedicine and Nanobiotechnology. doi: 10.1002/wnan.1328.

Sladek, R. E. J. and Stoffels, E. (2005) 'Deactivation of Escherichia coli by the plasma needle', *Journal of Physics D: Applied Physics*, 38(11), pp. 1716–1721. doi: 10.1088/0022-3727/38/11/012.

Soni, G. and Yadav, K. S. (2016) 'Nanogels as potential nanomedicine carrier for treatment of cancer: A mini review of the state of the art', *Saudi Pharmaceutical Journal*. King Saud University, 24(2), pp. 133–139. doi: 10.1016/j.jsps.2014.04.001.

Souto, G. D. *et al.* (2016) 'Evaluation of cytotoxicity profile and intracellular localisation of doxorubicin-loaded chitosan nanoparticles', *Analytical and Bioanalytical Chemistry*, 408(20), pp. 5443–5455. doi: 10.1007/s00216-016-9641-6.

Stambolic, V. *et al.* (1998) 'Negative regulation of PKB/Akt-dependent cell survival by the tumor suppressor PTEN', *Cell*, 95(1), pp. 29–39. doi: 10.1016/S0092-8674(00)81780-8.

Stockwell, B. R. *et al.* (2017) 'Ferroptosis: A Regulated Cell Death Nexus Linking Metabolism, Redox Biology, and Disease', *Cell*, pp. 273–285. doi: 10.1016/j.cell.2017.09.021.

Stoffels, E., Kieft, I. E. and Sladek, R. E. J. (2003) 'Superficial treatment of mammalian cells using plasma needle', *Journal of Physics D: Applied Physics*, 36(23), pp. 2908–2913. doi: 10.1088/0022-3727/36/23/007.

Stoffels, E., Sakiyama, Y. and Graves, D. B. (2008) 'Cold atmospheric plasma: Charged species and their interactions with cells and tissues', *IEEE Transactions on Plasma Science*, 36(4 PART 2), pp. 1441–1457. doi: 10.1109/TPS.2008.2001084.

Stojanovic, V. *et al.* (2016) 'Potential of porous silicon nanoparticles as an emerging platform for cancer theranostics', *Journal of Materials Chemistry B*, 4(44), pp. 7050–

7059. doi: 10.1039/c6tb01829g.

Stuart, M. A. C. *et al.* (2010) 'Emerging applications of stimuli-responsive polymer materials', *Nature Materials*, 9(2), pp. 101–113. doi: 10.1038/nmat2614.

Studer, A. M. *et al.* (2010) 'Nanoparticle cytotoxicity depends on intracellular solubility: Comparison of stabilized copper metal and degradable copper oxide nanoparticles', *Toxicology Letters*. Elsevier Ireland Ltd, 197(3), pp. 169–174. doi: 10.1016/j.toxlet.2010.05.012.

Sultana, F. *et al.* (2013) 'An overview of nanogel drug delivery system', *Journal of Applied Pharmaceutical Science*, 3(8 SUPPL). doi: 10.7324/JAPS.2013.38.S15.

Sun, C. *et al.* (2008) 'Tumor-targeted drug delivery and MRI contrast enhancement by chlorotoxin-conjugated iron oxide nanoparticles', *Nanomedicine*. Future Medicine Ltd London, UK, 3(4), pp. 495–505. doi: 10.2217/17435889.3.4.495.

Sun, S. Y. *et al.* (1999) 'Mediation of N-(4-hydoxyphenyl)retinamide-induced apoptosis in human cancer cells by different mechanisms', *Cancer Research*.

Ta, T. and Porter, T. M. (2013) 'Thermosensitive liposomes for localized delivery and triggered release of chemotherapy', *Journal of Controlled Release*, pp. 112–125. doi: 10.1016/j.jconrel.2013.03.036.

Tabunoki, H. *et al.* (2012) 'Molecular network profiling of U373MG human glioblastoma cells following induction of apoptosis by novel marine-derived anti-cancer 1,2,3,4-tetrahydroisoquinoline alkaloids', *Cancer Cell International*. doi: 10.1186/1475-2867-12-14.

Tachibana, K., Feril, L. B. and Ikeda-Dantsuji, Y. (2008) 'Sonodynamic therapy', *Ultrasonics*, 48(4), pp. 253–259. doi: 10.1016/j.ultras.2008.02.003.

Taghdisi, S. M. *et al.* (2016) 'Double targeting and aptamer-assisted controlled release delivery of epirubicin to cancer cells by aptamers-based dendrimer in vitro and in vivo',

European Journal of Pharmaceutics and Biopharmaceutics, 102, pp. 152–158. doi: 10.1016/j.ejpb.2016.03.013.

Takai, E. *et al.* (2012) 'Protein inactivation by low-temperature atmospheric pressure plasma in aqueous solution', *Plasma Processes and Polymers*, 9(1), pp. 77–82. doi: 10.1002/ppap.201100063.

Tanaka, H. *et al.* (2011) 'Plasma-activated medium selectively kills glioblastoma brain tumor cells by down-regulating a survival signaling molecule, AKT kinase', *Plasma Medicine*, 1(3–4), pp. 265–277. doi: 10.1615/PlasmaMed.2012006275.

Tanaka, H. *et al.* (2015) 'Plasma with high electron density and plasma-activated medium for cancer treatment', *Clinical Plasma Medicine*. Elsevier, 3(2), pp. 72–76. doi: 10.1016/j.cpme.2015.09.001.

Tang, Y. *et al.* (2015) 'An aptamer-targeting photoresponsive drug delivery system using "off-on" graphene oxide wrapped mesoporous silica nanoparticles', *Nanoscale*. The Royal Society of Chemistry, 7(14), pp. 6304–6310. doi: 10.1039/c4nr07493a.

Tila, D. *et al.* (2015) 'Functional liposomes in the cancer-targeted drug delivery', *Journal of Biomaterials Applications*, 30(1), pp. 3–16. doi: 10.1177/0885328215578111.

Tisdale, M. J. (1987) 'Antitumour imidazotetrazines-XV. Role of guanine O6 alkylation in the mechanism of cytotoxicity of imidazotetrazinones', *Biochemical Pharmacology*. doi: 10.1016/0006-2952(87)90351-0.

Tobiume, K. *et al.* (2001) 'ASK1 is required for sustained activations of JNK/p38 MAP kinases and apoptosis', *EMBO Reports*, 2(3), pp. 222–228. doi: 10.1093/embo-reports/kve046.

Tolstik, E. *et al.* (2016) 'Studies of silicon nanoparticles uptake and biodegradation in cancer cells by Raman spectroscopy', *Nanomedicine: Nanotechnology, Biology, and Medicine*. Elsevier, 12(7), pp. 1931–1940. doi: 10.1016/j.nano.2016.04.004.

Top, S. *et al.* (2013) 'The Ferrocifen Family as Potent and Selective Antitumor Compounds: Mechanisms of Action', in *Advances in Organometallic Chemistry and Catalysis*, pp. 563–580. doi: 10.1002/9781118742952.ch42.

Torsvik, A. *et al.* (2014) 'U-251 revisited: Genetic drift and phenotypic consequences of long-term cultures of glioblastoma cells', *Cancer Medicine*. doi: 10.1002/cam4.219.

Trachootham, D., Alexandre, J. and Huang, P. (2009) 'Targeting cancer cells by ROS-mediated mechanisms: A radical therapeutic approach?', *Nature Reviews Drug Discovery*. Nature Publishing Group, 8(7), pp. 579–591. doi: 10.1038/nrd2803.

Triesscheijn, M. *et al.* (2006) 'Photodynamic therapy in oncology.', *The oncologist*, 11(9), pp. 1034–44. doi: 10.1634/theoncologist.11-9-1034.

Trono, J. *et al.* (2009) 'Cellular Uptake of Gold Nanoparticles into Normal and Cancer Cells', pp. 202–205. doi: 10.1007/978-3-642-03887-7_56.

Tseng, K. H. *et al.* (2009) 'Preparation of gold ethanol colloid by the arc discharge method', *Journal of Alloys and Compounds*, 472(1–2), pp. 446–450. doi: 10.1016/j.jallcom.2008.04.084.

Tsoli, M. *et al.* (2005) 'Cellular uptake and toxicity of Au55 clusters', *Small*, 1(8–9), pp. 841–844. doi: 10.1002/smll.200500104.

Tsoukou, E., Bourke, P. and Boehm, D. (2018) 'Understanding the differences between antimicrobial and cytotoxic properties of plasma activated liquids', *Plasma Medicine*, 8(3), pp. 299–320. doi: 10.1615/PLASMAMED.2018028261.

Uhrbom, L. *et al.* (2002) 'Ink4a-Arf loss cooperates with KRas activation in astrocytes and neural progenitors to generate glioblastomas of various morphologies depending on activated Akt', *Cancer Research*, 62(19), pp. 5551–5558.

Vannucci, L. *et al.* (2014) 'Effects of N-acetyl-glucosamine-coated glycodendrimers as biological modulators in the B16F10 melanoma model in vivo (International Journal of

Oncology (2003) 23, (285-296))’, *International Journal of Oncology*, 44(4), p. 1410. doi: 10.3892/ijo.2014.2288.

Vega, S. *et al.* (2004) ‘Snail blocks the cell cycle and confers resistance to cell death’, *Genes and Development*, 18(10), pp. 1131–1143. doi: 10.1101/gad.294104.

Venkatesan, A. M. *et al.* (2010) ‘Novel imidazolopyrimidines as dual PI3-Kinase/mTOR inhibitors’, *Bioorganic and Medicinal Chemistry Letters*, 20(2), pp. 653–656. doi: 10.1016/j.bmcl.2009.11.057.

Verma, A. *et al.* (2008) ‘Surface-structure-regulated cell-membrane penetration by monolayer-protected nanoparticles’, *Nature Materials*, 7(7), pp. 588–595. doi: 10.1038/nmat2202.

Villiers, C. L. *et al.* (2010) ‘Analysis of the toxicity of gold nano particles on the immune system: Effect on dendritic cell functions’, *Journal of Nanoparticle Research*, 12(1), pp. 55–60. doi: 10.1007/s11051-009-9692-0.

Vinogradov, S. V., Bronich, T. K. and Kabanov, A. V. (2002) ‘Nanosized cationic hydrogels for drug delivery: Preparation, properties and interactions with cells’, *Advanced Drug Delivery Reviews*, 54(1), pp. 135–147. doi: 10.1016/S0169-409X(01)00245-9.

Wade Harper, J. *et al.* (1993) ‘The p21 Cdk-interacting protein Cip1 is a potent inhibitor of G1 cyclin-dependent kinases’, *Cell*, 75(4), pp. 805–816. doi: 10.1016/0092-8674(93)90499-G.

Walk, R. M. *et al.* (2013) ‘Cold atmospheric plasma for the ablative treatment of neuroblastoma’, *Journal of Pediatric Surgery*, 48(1), pp. 67–73. doi: 10.1016/j.jpedsurg.2012.10.020.

Wang, C. F. *et al.* (2015) ‘Dual-drug delivery by porous silicon nanoparticles for improved cellular uptake, sustained release, and combination therapy’, *Acta*

Biomaterialia. Elsevier, 16(1), pp. 206–214. doi: 10.1016/j.actbio.2015.01.021.

Wang, H. *et al.* (2014) 'Magnetic/NIR-thermally responsive hybrid nanogels for optical temperature sensing, tumor cell imaging and triggered drug release', *Nanoscale*, 6(21), pp. 13001–13011. doi: 10.1039/c4nr03748k.

Wang, L. H., Rothberg, K. G. and Anderson, R. G. W. (1993) 'Mis-assembly of clathrin lattices on endosomes reveals a regulatory switch for coated pit formation', *Journal of Cell Biology*, 123(5), pp. 1107–1117. doi: 10.1083/jcb.123.5.1107.

Watanabe, K. *et al.* (1996) 'Overexpression of the EGF Receptor and p53 Mutations are Mutually Exclusive in the Evolution of Primary and Secondary Glioblastomas', *Brain Pathology*, 6(3), pp. 217–223. doi: 10.1111/j.1750-3639.1996.tb00848.x.

Watarai, S. *et al.* (2014) 'Application of pH-sensitive fusogenic polymer-modified liposomes for development of mucosal vaccines', *Veterinary Immunology and Immunopathology*, 158(1–2), pp. 62–72. doi: 10.1016/j.vetimm.2013.05.005.

Weltmann, K.-D. *et al.* (2008) 'Antimicrobial treatment of heat sensitive products by miniaturized atmospheric pressure plasma jets (APPJs)', *Journal of Physics D: Applied Physics*, 41(19), p. 194008. doi: 10.1088/0022-3727/41/19/194008.

Welz, C. *et al.* (2015) 'Cold atmospheric plasma: A promising complementary therapy for squamous head and neck cancer', *PLoS ONE*, 10(11), pp. 1–15. doi: 10.1371/journal.pone.0141827.

Whitesides, G. M. (2003) 'The "right" size in nanobiotechnology', *Nature Biotechnology*, 21(10), pp. 1161–1165. doi: 10.1038/nbt872.

von Woedtke, T. *et al.* (2013) 'Plasmas for medicine', *Physics Reports*. Elsevier B.V., 530(4), pp. 291–320. doi: 10.1016/j.physrep.2013.05.005.

Wu, P. H. *et al.* (2016) 'Gold Nanoparticles With RGD Peptide in Radiation Therapy Suppress the Invasion Activity of Breast Cancer Cells', *International Journal of*

Radiation Oncology*Biology*Physics, 96(2), p. E574. doi: 10.1016/j.ijrobp.2016.06.2065.

Wu, Z. *et al.* (2011) 'Dielectric barrier discharge non-thermal micro-plasma for the excitation and emission spectrometric detection of ammonia.', *The Analyst*, 136(12), pp. 2552–7. doi: 10.1039/c0an00938e.

Xia, B. *et al.* (2013) 'Engineered stealth porous silicon nanoparticles via surface encapsulation of bovine serum albumin for prolonging blood circulation in vivo', *ACS Applied Materials and Interfaces*. American Chemical Society, 5(22), pp. 11718–11724. doi: 10.1021/am403380e.

Xu, D. *et al.* (2016) 'The effects of cold atmospheric plasma on cell adhesion, differentiation, migration, apoptosis and drug sensitivity of multiple myeloma', *Biochemical and Biophysical Research Communications*. Elsevier Ltd, 473(4), pp. 1125–1132. doi: 10.1016/j.bbrc.2016.04.027.

Xu, H. *et al.* (2016) 'Nanoparticles in sonodynamic therapy: State of the art review', *RSC Advances*. Royal Society of Chemistry, 6(56), pp. 50697–50705. doi: 10.1039/c6ra06862f.

Xu, W. *et al.* (2015) 'Smart Porous Silicon Nanoparticles with Polymeric Coatings for Sequential Combination Therapy', *Molecular Pharmaceutics*. American Chemical Society, 12(11), pp. 4038–4047. doi: 10.1021/acs.molpharmaceut.5b00473.

Yan, D. *et al.* (2015) 'Principles of using Cold Atmospheric Plasma Stimulated Media for Cancer Treatment.', *Scientific reports*. Nature Publishing Group, 5(November), p. 18339. doi: 10.1038/srep18339.

Yan, D. *et al.* (2016) 'Stabilizing the cold plasma-stimulated medium by regulating medium's composition', *Scientific Reports*, 6. doi: 10.1038/srep26016.

Yan, X. *et al.* (2012) 'Plasma-induced death of HepG2 cancer cells: Intracellular effects

of reactive species', *Plasma Processes and Polymers*, 9(1), pp. 59–66. doi: 10.1002/ppap.201100031.

Yang, J. *et al.* (2014) 'Mesoporous Silica-Coated Plasmonic Nanostructures for Surface-Enhanced Raman Scattering Detection and Photothermal Therapy', *Advanced Healthcare Materials*, 3(10), pp. 1620–1628. doi: 10.1002/adhm.201400053.

Yang, W. *et al.* (2009) 'Targeting cancer cells with biotin-dendrimer conjugates', *European Journal of Medicinal Chemistry*. Elsevier Masson, 44(2), pp. 862–868. doi: 10.1016/j.ejmech.2008.04.021.

Young, R. M. *et al.* (2015) 'Current trends in the surgical management and treatment of adult glioblastoma', *Annals of Translational Medicine*, 3(9), p. 121. doi: 10.3978/j.issn.2305-5839.2015.05.10.

Yu, H. *et al.* (2018) 'Paclitaxel-Loaded Core-Shell Magnetic Nanoparticles and Cold Atmospheric Plasma Inhibit Non-Small Cell Lung Cancer Growth', *ACS Applied Materials and Interfaces*. doi: 10.1021/acsami.8b16487.

Yu, T., Wang, Z. and Mason, T. J. (2004) 'A review of research into the uses of low level ultrasound in cancer therapy', *Ultrasonics Sonochemistry*, 11(2), pp. 95–103. doi: 10.1016/S1350-4177(03)00157-3.

Yuba, E. *et al.* (2010) 'pH-Sensitive fusogenic polymer-modified liposomes as a carrier of antigenic proteins for activation of cellular immunity', *Biomaterials*. Elsevier, 31(5), pp. 943–951. doi: 10.1016/j.biomaterials.2009.10.006.

Zaimy, M. A. *et al.* (2017) 'New methods in the diagnosis of cancer and gene therapy of cancer based on nanoparticles', *Cancer Gene Therapy*. Nature Publishing Group, 24(6), pp. 233–243. doi: 10.1038/cgt.2017.16.

Zalipsky, S. *et al.* (1996) 'Long-circulating, polyethylene glycol-grafted immunoliposomes', in *Journal of Controlled Release*, pp. 153–161. doi: 10.1016/0168-

3659(95)00149-2.

Zelzer, M. *et al.* (2012) 'The role of albumin and fibronectin in the adhesion of fibroblasts to plasma polymer surfaces', *Plasma Processes and Polymers*, 9(2), pp. 149–156. doi: 10.1002/ppap.201100054.

Zhang, H. *et al.* (2015) 'Effects and Mechanism of Atmospheric-Pressure Dielectric Barrier Discharge Cold Plasma on Lactate Dehydrogenase (LDH) Enzyme.', *Scientific reports*, 5(May), p. 10031. doi: 10.1038/srep10031.

Zhang, J. *et al.* (2011) 'Temozolomide: Mechanisms of Action, Repair and Resistance', *Current Molecular Pharmacology*, 5(1), pp. 102–114. doi: 10.2174/1874467211205010102.

Zhao, D. *et al.* (1998) 'Triblock copolymer syntheses of mesoporous silica with periodic 50 to 300 angstrom pores', *Science*. American Association for the Advancement of Science, 279(5350), pp. 548–552. doi: 10.1126/science.279.5350.548.

Zhou, B. P. *et al.* (2001) 'Cytoplasmic localization of p21 CIP1/WAF1 by Akt-induced phosphorylation in HER-2/neu-overexpressing cells', *Nature Cell Biology*, 3(3), pp. 245–252. doi: 10.1038/35060032.

Zhou, Z. *et al.* (2016) 'Reactive oxygen species generating systems meeting challenges of photodynamic cancer therapy', *Chemical Society Reviews*. Royal Society of Chemistry, 45(23), pp. 6597–6626. doi: 10.1039/c6cs00271d.

Zhu, W. *et al.* (2016) 'Synergistic Effect of Cold Atmospheric Plasma and Drug Loaded Core-shell Nanoparticles on Inhibiting Breast Cancer Cell Growth', *Scientific Reports*. Nature Publishing Group, 6(October 2015), p. 21974. doi: 10.1038/srep21974.

Ziuzina, D. *et al.* (2013) 'Atmospheric cold plasma inactivation of Escherichia coli in liquid media inside a sealed package', *Journal of Applied Microbiology*, 114(3), pp. 778–787. doi: 10.1111/jam.12087.

Zivkovic, M. *et al.* (2007) 'Oxidative burst of neutrophils against melanoma B16-F10', *Cancer Letters*, 246(1–2), pp. 100–108. doi: 10.1016/j.canlet.2006.02.002.

Zu, Y. *et al.* (2014) 'Gold nanoparticles enhanced electroporation for mammalian cell transfection', *Journal of Biomedical Nanotechnology*, 10(6), pp. 982–992. doi: 10.1166/jbn.2014.1797.

Zununi Vahed, S. *et al.* (2017) 'Liposome-based drug co-delivery systems in cancer cells', *Materials Science and Engineering C*. Elsevier, pp. 1327–1341. doi: 10.1016/j.msec.2016.11.073.

7. Appendices

7.1 Appendix I First Pages of Peer-reviewed Publications

Only first pages of the manuscripts are attached.

Online research presented at: https://orcid.org/0000-0001-6533-4974

Combination Strategies for Targeted Delivery of Nanoparticles for Cancer Therapy

Zhonglei He[1], Kangze Liu[1], Hugh J. Byrne[1], Patrick J. Cullen[1,2], Furong Tian[1], James F. Curtin[1]

Dublin Institute of Technology, Dublin, Ireland[1]; UNSW, Sydney, NSW, Australia[2]

1. INTRODUCTION

Cancer treatment can be affected by a combination of physical, chemical, and biological technologies. Due to the considerable variation between types and status of tumors and individual patients, the efficiency of cancer therapy is difficult to guarantee and commonly associated side effects and off-target toxicity can be daunting [1]. However, recent technological advances have led to the development of new nanotechnological approaches for cancer therapies, which promise high-precision ways to beat cancer. Nanotechnology can be combined with chemotherapy to facilitate targeted delivery into cancer tissue with high specificity and efficacy [2]. Nanoplatforms allow more accurate, noninvasive and real-time cancer diagnosis and monitoring during therapy using magnetic resonance imaging, ultrasonography, etc. [3–5] Adjuvant nanotechnological devices are used in cancer interventions such as radiotherapy [6], photodynamic therapy [7], and sonodynamic therapy [8], which are capable of achieving considerably higher precision of treatment and reduced side effects. After decades of developing the understanding of nanotechnology, cancer-related nanotreatments have undergone extensive preclinical and clinicaltrial studies and shown promising results [1]. Bregoli et al. have summarized the current state of the art of nanomedicines undergoing clinical trial and clinically approved nanomedicines for cancer therapies [9].

The traditional definition of a nanotechnological device for cancer treatment is that the essential components of the device or the device itself are artificial and have at least one dimension in the 1–100 nm range [2,10]. It has been suggested that there should be less emphasis on the exact definition of size, which could be extended to a range of 1–1000 nm, and define the approaches to bionanotechnology according to their function and purpose [2]. According to this definition, nanotechnologies used in cancer treatment include drug delivery, therapeutic nanovectors, nano sensitizers, diagnostic agents, and macroscopic devices with essential

191

https://doi.org/10.1016/B978-0-12-814029-1.00008-9 (He *et al.*, 2019)

SCIENTIFIC REP⚙RTS

OPEN

Cold Atmospheric Plasma Induces ATP-Dependent Endocytosis of Nanoparticles and Synergistic U373MG Cancer Cell Death

Zhonglei He[1,2], Kangze Liu[1,2], Eline Manaloto[1,2], Alan Casey[2], George P. Cribaro[4],
Hugh J. Byrne [2], Furong Tian[1,2,3], Carlos Barcia[4], Gillian E. Conway[1,2], Patrick J. Cullen[1,5] &
James F. Curtin [1,2,3]

Gold nanoparticles (AuNP) have potential as both diagnostic and therapeutic vehicles. However, selective targeting and uptake in cancer cells remains challenging. Cold atmospheric plasma (CAP) can be combined with AuNP to achieve synergistic anti-cancer cytotoxicity. To explore synergistic mechanisms, we demonstrate both rate of AuNP uptake and total amount accumulated in U373MG Glioblastoma multiforme (GBM) cells are significantly increased when exposed to 75 kV CAP generated by dielectric barrier discharge. No significant changes in the physical parameters of AuNP were caused by CAP but active transport mechanisms were stimulated in cells. Unlike many other biological effects of CAP, long-lived reactive species were not involved, and plasma-activated liquids did not replicate the effect. Chemical effects induced by direct and indirect exposure to CAP appears the dominant mediator of enhanced uptake. Transient physical alterations of membrane integrity played a minor role. 3D-reconstruction of deconvoluted confocal images confirmed AuNP accumulation in lysosomes and other acidic vesicles, which will be useful for future drug delivery and diagnostic strategies. Toxicity of AuNP significantly increased by 25-fold when combined with CAP. Our data indicate that direct exposure to CAP activates AuNP-dependent cytotoxicity by increasing AuNP endocytosis and trafficking to lysosomes in U373MG cells.

Gold nanoparticles (AuNPs) can be used as diagnostic agents, radiosensitizers and drug delivery vehicles, due to their specific physical and chemical properties, such as strong surface plasmon resonance effect, high stability and low cytotoxicity[1–3]. AuNPs can be readily manufactured in various controllable shapes, sizes and monodispersity. Though non-functionalized AuNPs can show selective cytotoxicity to certain cell lines, especially cancer cells[4], AuNPs are generally considered nontoxic to normal cells[5,6]. Cytotoxicity of AuNPs is size dependent, small AuNPs elicit higher cytotoxicity than larger AuNP. AuNPs of ~20 nm diameter elicit relatively low cytotoxicity in both normal and cancer cells[7] and are optimal for traversing the blood brain barrier to enter the brain[8]. The surface chemistry of AuNPs enables bio-conjugation and bio-modification, for example, conjugation of antibodies to assist in targeting or conjugation of chemotherapeutic or detection agents[1,3]. These properties underpin the emergence of gold nanoparticles as promising therapeutic and diagnostic administration systems to treat neoplasms.

Plasma, a form of ionized gas, is one of the four fundamental states of matter and by far the most common form of matter in the universe. Initially, biomedical applications of plasma concentrated on heat and high temperature, i.e. thermal plasmas, for tissue removal, sterilization, and cauterization[9]. Technological advances have allowed researchers to generate plasmas at ambient temperatures and at approximately 1.0 atmospheric pressure, allowing safer application to biological samples and tissues without risking thermal injury. These are known as

[1]BioPlasma Research Group, School of Food Science and Environmental Health, Dublin Institute of Technology, Dublin, Ireland. [2]Nanolab, FOCAS Research Institute, Dublin Institute of Technology, Dublin, Ireland. [3]Environmental, Sustainability and Health Research Institute, Dublin Institute of Technology, Dublin, Ireland. [4]Institut de Neurociències & Department of Biochemistry and Molecular Biology, School of Medicine, Universitat Autònoma de Barcelona, Barcelona, Spain. [5]Department of Chemical and Environmental Engineering, University of Nottingham, Nottingham, UK. Kangze Liu and Eline Manaloto contributed equally to this work. Correspondence and requests for materials should be addressed to J.F.C. (email: james.curtin@dit.ie)

https://doi.org/10.1038/s41598-018-23262-0 (He *et al.*, 2018)

OPEN

Cold Atmospheric Plasma Stimulates Clathrin-Dependent Endocytosis to Repair Oxidised Membrane and Enhance Uptake of Nanomaterial in Glioblastoma Multiforme Cells

Zhonglei He [1,2,3], Kangze Liu [1,2,3,7], Laurence Scally [1,7], Eline Manaloto [1,2], Sebnem Gunes [1,2], Sing Wei Ng [1,3], Marcus Maher [2], Brijesh Tiwari [4], Hugh J. Byrne [2], Paula Bourke [1,3,5], Furong Tian [1,2,3], Patrick J. Cullen [1,6] & James F. Curtin [1,2,3] ✉

Cold atmospheric plasma (CAP) enhances uptake and accumulation of nanoparticles and promotes synergistic cytotoxicity against cancer cells. However, the mechanisms are not well understood. In this study, we investigate the enhanced uptake of theranostic nanomaterials by CAP. Numerical modelling of the uptake of gold nanoparticle into U373MG Glioblastoma multiforme (GBM) cells predicts that CAP may introduce a new uptake route. We demonstrate that cell membrane repair pathways play the main role in this stimulated new uptake route, following non-toxic doses of dielectric barrier discharge CAP. CAP treatment induces cellular membrane damage, mainly via lipid peroxidation as a result of reactive oxygen species (ROS) generation. Membranes rich in peroxidised lipids are then trafficked into cells via membrane repairing endocytosis. We confirm that the enhanced uptake of nanomaterials is clathrin-dependent using chemical inhibitors and silencing of gene expression. Therefore, CAP-stimulated membrane repair increases endocytosis and accelerates the uptake of gold nanoparticles into U373MG cells after CAP treatment. We demonstrate the utility of CAP to model membrane oxidative damage in cells and characterise a previously unreported mechanism of membrane repair to trigger nanomaterial uptake. This knowledge will underpin the development of new delivery strategies for theranostic nanoparticles into cancer cells.

Cold atmospheric plasma (CAP) is increasingly studied in a growing number of clinical trials for cancer treatment[1,2] and research is ongoing to explore the combination of CAP with other therapies, including nanoparticles, radiotherapy and chemotherapy[3–5].

Gold nanoparticles (AuNPs) are known to be weakly-toxic to human cells and be readily manufactured and designed for targeting delivery of various therapeutic compounds into cells. Citrate-capped cationic AuNPs may adsorb serum proteins onto their surface and thereby stimulate receptor-mediated endocytosis[6]. Without special surface functionalisation, AuNPs enter cells and become trapped in vesicles[6–8] or enter the nucleus, depending on their size/shape[9,10]. Meanwhile, AuNPs with functionalised surface chemistries/ligands can directly penetrate the membrane and enter the cytoplasm[11].

[1]BioPlasma Research Group, School of Food Science and Environmental Health,, Technological University Dublin, Dublin, Ireland. [2]Nanolab, FOCAS Research Institute, Technological University Dublin, Dublin, Ireland. [3]Environmental, Sustainability and Health Research Institutes, Technological University Dublin, Dublin, Ireland. [4]Department of Food Biosciences, Teagasc Food Research Centre, Ashtown, Dublin, Ireland. [5]School of Biological Sciences, IGFS, Queens University Belfast, Belfast, United Kingdom. [6]School of Chemical and Biomolecular Engineering, University of Sydney, Sydney, Australia. [7]These authors contributed equally: Kangze Liu and Laurence Scally. ✉e-mail: james.curtin@tudublin.ie

1

https://doi.org/10.1038/s41598-020-63732-y (He *et al.*, 2020)

201

Article

Investigating the Role of Gold Nanoparticle Shape and Size in Their Toxicities to Fungi

Kangze Liu [1,*] , Zhonglei He [1], Hugh J. Byrne [2] , James F. Curtin [1] and Furong Tian [1,*]

[1]   Environmental Sustainability and Health Institute, School of Food Science and Environmental Health,
       College of Sciences and Health, Dublin Institute of Technology, Cathal Brugha Street, Dublin D08 X622,
       Ireland; zhonglei.he@mydit.ie (Z.H.); james.curtin@dit.ie (J.F.C.)
[2]   FOCAS Research Institute, Dublin Institute of Technology, Camden Row, Dublin D08 X622, Ireland;
       hugh.byrne@dit.ie
*   Correspondence: kangze.liu@dit.ie (K.L.); furong.tian@dit.ie (F.T.); Tel.: +353-1-402-7543 (F.T.)

check for updates

Abstract: Gold nanoparticles (GNPs) are increasingly being used in a wide range of applications, and such they are being released in greater quantities into the environment. Consequently, the environmental effects of GNPs, especially toxicities to living organisms, have drawn great attention. However, their toxicological characteristics still remain unclear. Fungi, as the decomposers of the ecosystem, interact directly with the environment and critically control the overall health of the biosphere. Thus, their sensitivity to GNP toxicity is particularly important. The aim of this study was to evaluate the role of GNP shape and size in their toxicities to fungi, which could help reveal the ecotoxicity of GNPs. *Aspergillus niger*, *Mucor hiemalis*, and *Penicillium chrysogenum* were chosen for toxicity assessment, and spherical and star/flower-shaped GNPs ranging in size from 0.7 nm to large aggregates of 400 nm were synthesised. After exposure to GNPs and their corresponding reaction agents and incubation for 48 h, the survival rates of each kind of fungus were calculated and compared. The results indicated that fungal species was the major determinant of the variation of survival rates, whereby *A. niger* was the most sensitive and *M. himalis* was the least sensitive to GNP exposure. Additionally, larger and non-spherical GNPs had relatively stronger toxicities.

Keywords: gold nanoparticle; fungi; nanoparticle shape; nanoparticle size; nanotoxicology

1. Introduction

In the growing field of nanotechnology, gold nanoparticles (GNPs) have received a lot of attention, particularly with respect to their potential applications in bio-related areas [1–5]. The unique physical and chemical properties of noble metal nanoparticles such as GNPs, with specific electronic structures different from atoms or bulk states, have long been of interest and have been widely exploited in diversiform areas such as electronics, chemistry, optics, and biomedicine [1–5]. One of the most important characteristics of GNPs is the localized surface plasmon resonance (LSPR). The LSPR phenomena of GNPs are manifest when the dimensions of the GNP are smaller than the extent of the plasmon wavefunction delocalization, resulting in strong resonances of the surface electronic states with radiation in the visible region of the spectrum [6,7]. Although silver nanoparticles show stronger LSPR phenomena, with a stronger absorption, GNPs are more commonly used in biologically-related applications because of their reputed biocompatibility [6–8]. Moreover, it is worth mentioning that the potential of GNPs in medical and clinical use has been long investigated [9].

Nevertheless, while silver nanoparticles have been widely used as anti-microbial materials due to their high toxicity [10–12], the toxicity of GNPs has not yet been fully understood and has drawn the attention of researchers. Notably, it has been reported that the toxicity of GNPs on microbes depends

SCIENTIFIC REP🦠RTS

OPEN

A novel, rapid, seedless, *in situ* synthesis method of shape and size controllable gold nanoparticles using phosphates

Kangze Liu [1,2,3], Zhonglei He[1,2,3], James F. Curtin[1,2], Hugh J. Byrne[3] & Furong Tian[1,2]

We hereby report a novel synthesis method of size and shape controllable gold nanoparticles that is rapid, *in situ* and seedless. Unlike most currently employed size and shape controllable synthesis methods, it takes place in a single step under room temperature within ~15 minutes. While mixtures of gold nanospheres around 70 nm and gold nanoplates with width ranging from 100 nm to 1000 nm can be synthesized in about 15 minutes by standard synthesis method using *N*-2-hydroxyethylpiperazine-*N*-2-ethanesulphonic acid (HEPES) to reduce Au(III), gold nanoflowers or mixtures of smaller gold nanospheres and nanoplates can be synthesized with the addition of disodium phosphate (Na_2HPO_4) or monosodium phosphate (NaH_2PO_4), respectively. Increasing the concentration of phosphate added significantly reduces the formation time of gold nanoparticles to seconds. By increasing the molar ratio of Na_2HPO_4: HEPES and NaH_2PO_4: HEPES, the size of gold nanoflowers and gold nanoparticle mixtures can be tuned from ~60 nm down to 1 nm and from ~70 nm to ~2.5 nm, respectively. The systematic structural changes are accompanied by similarly systematic colour changes associated with shifting of the surface plasmon resonance. The proposed mechanism of the synthesis process is also presented.

Gold nanoparticles (GNPs) have received increasing attention as nanotechnology has flourished[1–5]. Their peculiar physical and chemical properties, especially the localized surface plasmon resonance (LSPR)[6,7], has enabled them to be widely applied in diverse fields such as surface enhanced Raman scattering (SERS)[8,9], chemical sensing[10], and biomedicine[11]. The characteristics of the LSPR are dependent on the nanoparticle size, shape, composition, and distance and electric environment between nanoparticles, all of which can strongly influence the resonant frequency, which determines the characteristic colour, observable by the naked eye[12]. The electronic properties and associated colour can be employed for a number of application, and therefore, continued refinement of synthesis methods which can control the size and shape of GNPs is desirable.

Current synthesis methods of GNPs include 'top-down'[13] and 'bottom-up'[14] procedures. Top-down procedures lack control of size, shape and functionalization of the GNPs synthesized, whereas, in contrast, bottom-up procedures can often accomplish these, since they involve either chemical or biological reduction and assemble the particles from molecules[13,14]. The bottom-up procedure can be divided into two kinds: the seed-growth method, which can better control the size and shape of the GNPs, yet requires at least two processes since the nucleation and successive growth processes are separate; and the *in situ* method, which entails only one process[15]. To date, in addition to nanospheres[16], GNPs with different shapes such as nanorods[17,18], nanoplates[19–22], planar nanoparticles[23,24], and branched nanostructures like nanoflowers[25,26] and nanostars[27,28] have been synthesized. Among these shapes, the nanoplates have attracted particular attention due to the high local electric field gradients under illumination caused by their sharp edges, which can be applied in SERS[29], and the nanoflowers, with rough surface and dense tips, are able to enhance SERS to a greater degree, and thus have been considered powerful SERS probes[26,30–32].

[1]Environmental Sustainability and Health Institute, Technological University Dublin, Grangegorman, Dublin, 7, Ireland. [2]School of Food Science and Environmental Health, College of Sciences and Health, Technological University Dublin, Cathal Brugha Street, Dublin, 1, Ireland. [3]FOCAS Research Institute, Technological University Dublin, Kevin Street, Dublin, 8, Ireland. Correspondence and requests for materials should be addressed to K.L. (email: kangze.liu@dit.ie)

https://doi.org/10.1038/s41598-019-43921-0 (Liu *et al.*, 2019)

OPEN

Cold Atmospheric Plasma induces accumulation of lysosomes and caspase-independent cell death in U373MG glioblastoma multiforme cells

Gillian E. Conway[1,2,3,6], Zhonglei He[1,2,3], Ana Lacramioara Hutanu[7], George Paul Cribaro[8], Eline Manaloto[1,2,3], Alan Casey[2,4], Damien Traynor[2], Vladimir Milosavljevic[2,4], Orla Howe[2,3,5], Carlos Barcia[8], James T. Murray[7], Patrick J. Cullen[1,2,3,9] & James F. Curtin[1,2,3]

Room temperature Cold Atmospheric Plasma (CAP) has shown promising efficacy for the treatment of cancer but the exact mechanisms of action remain unclear. Both apoptosis and necrosis have been implicated as the mode of cell death in various cancer cells. We have previously demonstrated a caspase-independent mechanism of cell death in p53-mutated glioblastoma multiforme (GBM) cells exposed to plasma. The purpose of this study was to elucidate the molecular mechanisms involved in caspase-independent cell death induced by plasma treatment. We demonstrate that plasma induces rapid cell death in GBM cells, independent of caspases. Accumulation of vesicles was observed in plasma treated cells that stained positive with acridine orange. Western immunoblotting confirmed that autophagy is not activated following plasma treatment. Acridine orange intensity correlates closely with the lysosomal marker Lyso Tracker™ Deep Red. Further investigation using isosurface visualisation of confocal imaging confirmed that lysosomal accumulation occurs in plasma treated cells. The accumulation of lysosomes was associated with concomitant cell death following plasma treatment. In conclusion, we observed rapid accumulation of acidic vesicles and cell death following CAP treatment in GBM cells. We found no evidence that either apoptosis or autophagy, however, determined that a rapid accumulation of late stage endosomes/lysosomes precedes membrane permeabilisation, mitochondrial membrane depolarisation and caspase independent cell death.

Glioblastoma multiforme (GBM), a grade IV malignant astrocytoma, is highly proliferative, invasive and resistant to most therapies. GBM is generally treated using a combination of physical, chemical and biological treatments. Surgical interventions and radiation therapy in combination with either pharmaceuticals or biopharmaceuticals have been the mainstay of cancer treatment for decades[1–3]. While marginal gains are evident in 1 and 2-year survival rates, five-year prognosis for patients diagnosed with GBM remains almost completely refractory to treatment.

[1]School of Food Science & Environmental Health, Technological University Dublin, Dublin, Ireland. [2]FOCAS Research Institute, Technological University Dublin, Dublin, Ireland. [3]Environmental Sustainability & Health Institute, Technological University Dublin, Dublin, Ireland. [4]School of Physics & Clinical & Optometric Sciences, Technological University Dublin, Dublin, Ireland. [5]School of Biological & Health Sciences, Technological University Dublin, Dublin, Ireland. [6]In-Vitro Toxicology Group, Institute of Life Science, Swansea University Medical School, Swansea University, Singleton Park, Swansea, UK. [7]School of Biochemistry & Immunology, Trinity Biomedical Sciences Institute, Trinity College Dublin, Dublin, Ireland. [8]Institut de Neurociències & Department of Biochemistry and Molecular Biology, School of Medicine, Universitat Autònoma de Barcelona, Barcelona, Spain. [9]School of Chemical and Biomolecular Engineering, University of Sydney, Darlington, Australia. Correspondence and requests for materials should be addressed to G.E.C. (email: gillian.conway@swansea.ac.uk) or J.F.C. (email: james.curtin@tudublin.ie)

https://doi.org/10.1038/s41598-019-49013-3 (Conway *et al.*, 2019)

7.2 Appendix II Additional Publications and Outputs not Peer-reviewed
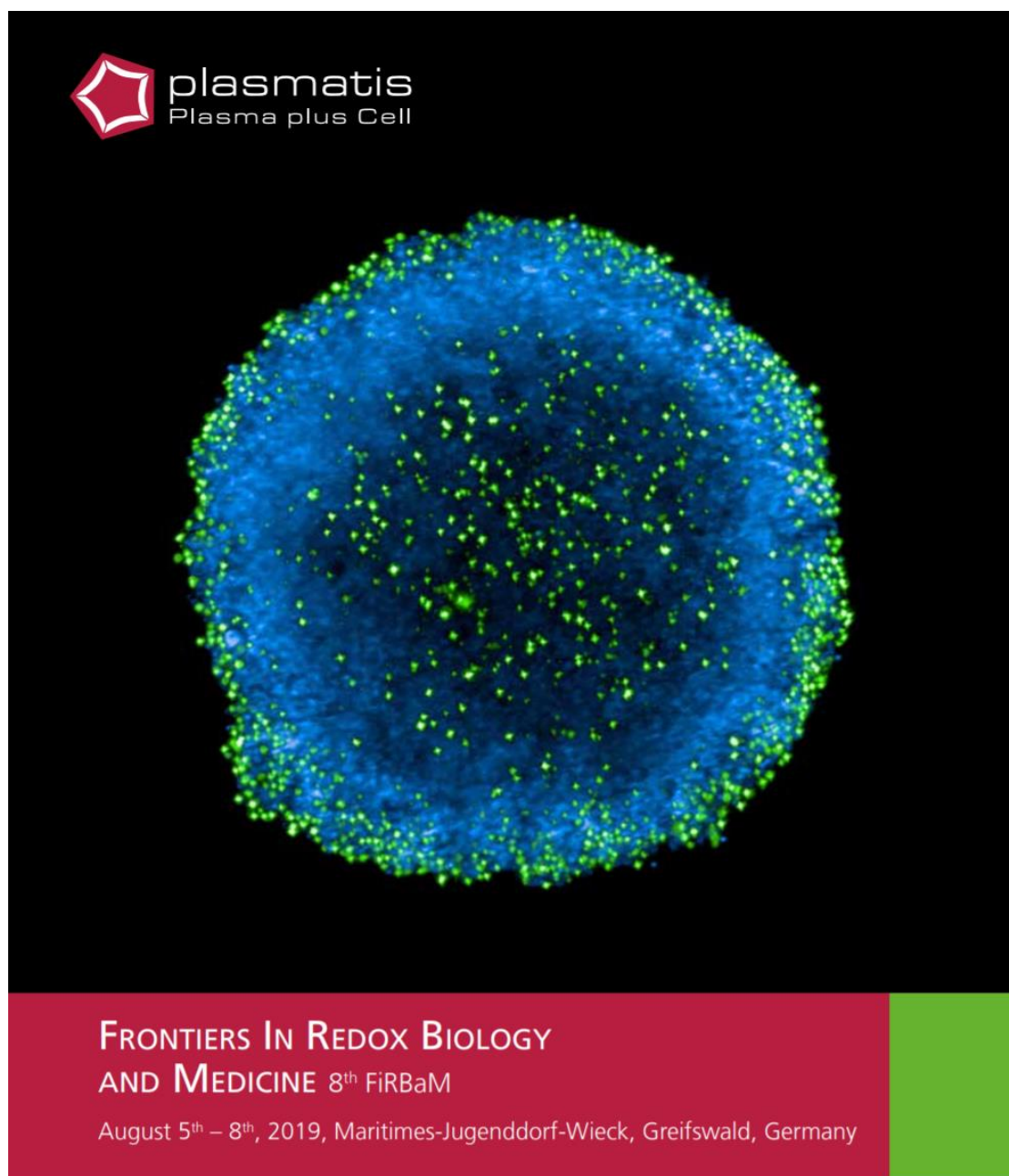
Frontiers in Redox Biology and Medicine 8th Conference, Abstract Book Cover

Investigation of Ca2+-Dependent Endocytic Pathways Induced by Cold Atmospheric Plasma in Glioma Cell Line U373MG

Z. He[1,2], F. Tian[1,2,3], PJ. Cullen[1,4], and J. F. Curtin[1,2,3]

[1]BioPlasma Research Group, School of Food Science and Environmental Health, Technological University Dublin, Ireland;
[2]Nanolab, FOCAS Research Institute, Technological University Dublin, Ireland;
[3]Environmental, Sustainability and Health Research Institutes, Technological University Dublin, Ireland;
[4]School of Chemical and Biomolecular Engineering, The University of Sydney;

Abstract

Gold nanoparticles (AuNP) are known as biocompatible nanomaterial for using as diagnostic and therapeutic vehicles in cancer treatment [1]. Our previous data indicated that direct exposure to cold atmospheric plasma (CAP) activates synergistic cytotoxicity by increasing AuNP uptake and trafficking to lysosomes in U373MG glioblastoma multiforme (GBM) cells [2]. In this research, we further investigated the uptake accelerated by CAP. The reactive oxygen species (ROS) generation during CAP treatment was measured by optical emission spectroscopy (OES). CAP treatment induced lipid peroxidation in cells, which caused membrane damage together with other plasma-induced physical alterations, and therefore, membrane repair system was activated to quickly remove peroxidised lipids form the membrane via endocytosis. Calcium^{2+}-dependent clathrin-media endocytosis was determined to play the main role in the stimulated uptake using a variety of specific inhibitors and silencing of clathrin expression. Disruption of several types of clathrin-independent endocytosis and macropinocytosis, etc. didn't induce significant changes in CAP-accelerated uptake comparing to inhibiting clathrin-mediated endocytosis or depletion of calcium ions. Confocal imaging confirmed AuNPs colocalized in early and late endosomes at early time point of incubation, which supported the hypothesis. Studies explain that the membrane repairing endocytosis stimulated by CAP-caused membrane damage plays key role in the increased uptake of U373MG cells, which can be used to develop new strengthened strategies for cancer treatment and diagnosis.
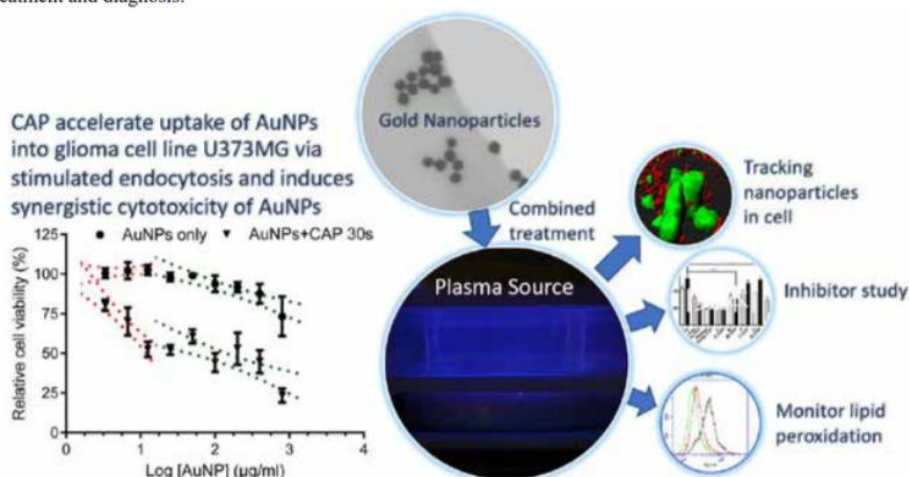
References

[1] He, Zhonglei, et al. "Combination Strategies for Targeted Delivery of Nanoparticles for Cancer Therapy." *Applications of Targeted Nano Drugs and Delivery Systems*. Elsevier. 191-219, 2019.
[2] He, Zhonglei, et al. "Cold atmospheric plasma induces ATP-dependent endocytosis of nanoparticles and synergistic u373mg cancer cell death." *Scientific reports* 8.1: 5298, 2018.

31

Frontiers in Redox Biology and Medicine 8th Conference, Abstract, Oral Presentation.

206

Cold Atmospheric Plasma induces silver nanoparticle uptake, oxidative dissolution and enhanced cytotoxicity in Glioblastoma multiforme cells

Eline Manaloto, (iD) Aoife Gowen, Anna Lesniak, (iD) Zhonglei He, (iD) Alan Casey, (iD) Patrick J Cullen, (iD) James F Curtin

This article is a preprint and has not been certified by peer review [what does this mean?].

Abstract   Full Text   Info/History   Metrics   🗋 Preview PDF

Abstract

Silver nanoparticles (AgNP) emerged as a promising reagent for cancer therapy with oxidative stress implicated in the toxicity. Meanwhile, studies reported cold atmospheric plasma (CAP) generation of reactive oxygen and nitrogen species has selectivity towards cancer cells. Gold nanoparticles display synergistic cytotoxicity when combined with CAP against cancer cells but there is a paucity of information using AgNP, prompting to investigate the combined effects of CAP using dielectric barrier discharge system (voltage of 75 kV, current is 62.5mA, duty cycle of 7.5kVA and input frequency of 50–60Hz) and 10nm PVA–coated AgNP using U373MG Glioblastoma Multiforme cells. Cytotoxicity in U373MG cells was >100–fold greater when treated with both CAP and PVA–AgNP compared with either therapy alone (IC_{50} of 4.30 µg/mL with PVA–AgNP alone compared with 0.07 µg/mL after 25s CAP and 0.01 µg/mL 40s CAP). Combined cytotoxicity was ROS–dependent and was prevented using N–Acetyl Cysteine. A novel darkfield spectral imaging method investigated and quantified AgNP uptake in cells determining significantly enhanced uptake, aggregation and subcellular accumulation following CAP treatment, which was confirmed and quantified using atomic absorption spectroscopy. The results indicate that CAP decreases nanoparticle size, decreases surface charge distribution of AgNP and induces uptake, aggregation and enhanced cytotoxicity *in vitro*.
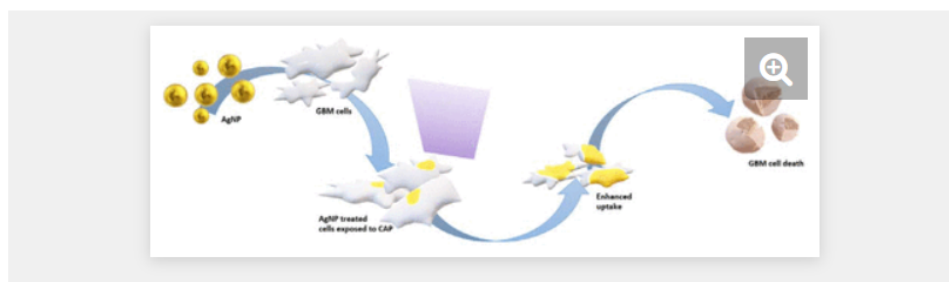
Download figure | Open in new tab

https://doi.org/10.1101/2020.02.28.969758 (Manaloto *et al.*, 2020)

Ursolic acid inhibits cell migration and promotes JNK-dependent lysosomal associated cell death in Glioblastoma multiforme cells

Gillian E. Conway, Deimante Zizyte, Julie Rose Mae Mondala, Zhonglei He, Lorna Lynam, Mathilde Lecourt, Carlos Barcia, Orla Howe, James F Curtin

This article is a preprint and has not been certified by peer review [what does this mean?].

| Abstract	Full Text	Info/History	Metrics		🗋 Preview PDF

Abstract

Ursolic acid (UA) is a bioactive compound which has demonstrated therapeutic efficacy in a variety of cancer cell lines. UA activates various signalling pathways in Glioblastoma multiforme (GBM), however, the relationship between cell death and migration has yet to be elucidated. UA induces a dose dependent cytotoxic response demonstrated by flow cytometry and biochemical cytotoxicity assays. Inhibitor and fluorescent probe studies demonstrated that UA induces a caspase independent, JNK dependent, mechanism of cell death. Migration studies established that UA inhibits GBM cell migration in a time dependent manner that is independent of the JNK signalling pathway. The cytotoxic insult induced by UA resulted in the formation of acidic vesicle organelles (AVOs), speculating activation of autophagy. However, inhibitor and spectrophotometric analysis demonstrated that autophagy was not responsible for the formation of the AVOs and confocal microscopy identified the AVO's as lysosomes. Further investigation using isosurface visualisation of confocal imaging determined co–localisation of lysosomes with the previously identified acidic vesicles, thus providing evidence that lysosomes are likely to be playing a role in UA induced cell death.

Collectively, our data identifies that UA rapidly induces a lysosomal associated mechanism of cell death in addition to UA acting as an inhibitor of GBM cell migration.
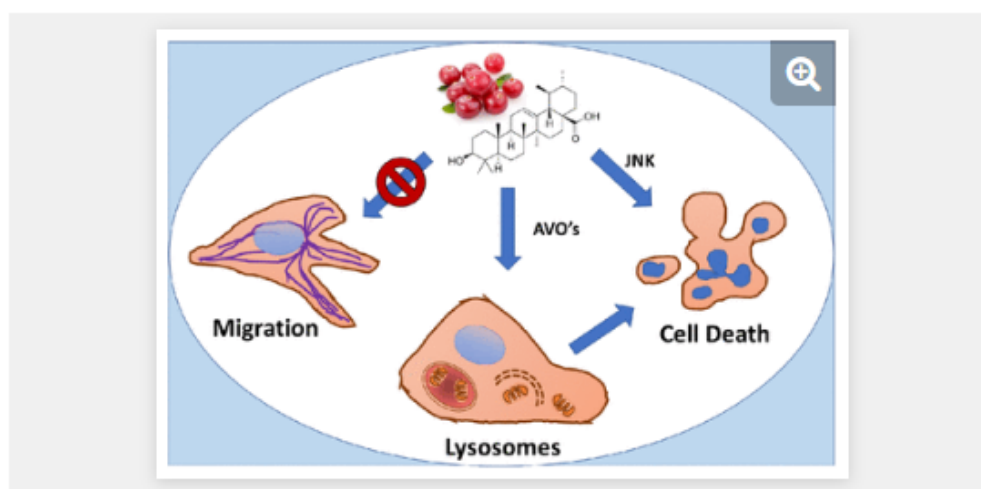
https://doi.org/10.1101/2020.03.11.987578 (Conway *et al.*, no date)

## 7.3 Appendix III Supplementary Information for Chapter 2
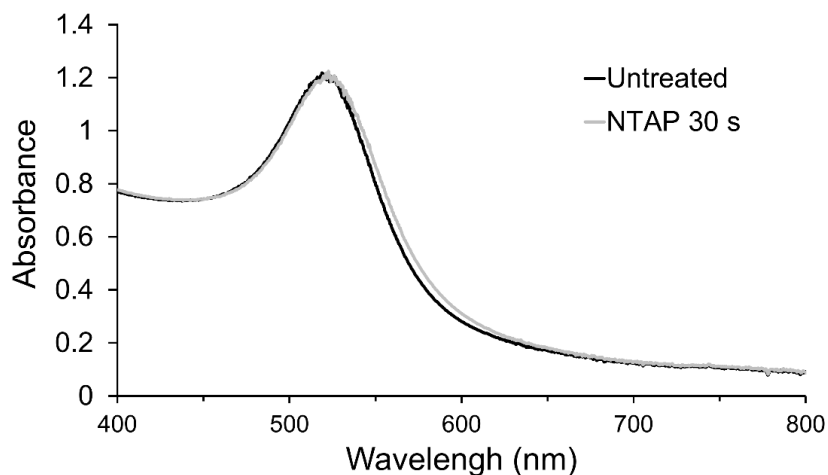
Figure S1. UV-vis absorption spectrum of 100 μg/ml AuNPs dispersed in water. The

AuNPs solutions were treated with CAP at 75 kV for 30 s, or untreated.

Table S1. Raw dataset of the Alamar Blue assay. U373MG cells were treated with

different concentrations of AuNPs (0-800 μg/ml). After incubated for 48 h, cell viability

was analysed using the Alamar Blue assay. The table presented the raw date produced by

the Microplate Reader, Synergy HT (BioTek).

Raw dataset of the Alamar Blue assay										
AuNPs Concentration	Treatment：AuNPs only					Treatment：AuNPs+CAP 30s,75 kV				
800 μg/ml	223	209	289	283	301	113	86	79	81	103
400 μg/ml	292	287	312	321	336	175	122	172	171	183
200 μg/ml	307	325	334	331	320	177	140	219	206	219
100 μg/ml	300	336	337	336	344	164	136	150	184	178
50 μg/ml	33	35	35	35	34	232	210	206	207	238

|										
	5	1	3	2	9					
25 µg/ml	329	346	352	352	346	182	200	198	192	177
12.5 µg/ml	358	356	347	366	374	167	192	210	186	200
6.75 µg/ml	330	356	363	365	379	204	246	277	247	276
3.375 µg/ml	338	348	363	358	360	284	299	269	292	280
0	335	354	352	356	360	242	280	354	292	276
Negative control	13	14	13	14	13					

## 7.4 Appendix IV Supplementary Information for Chapter 3
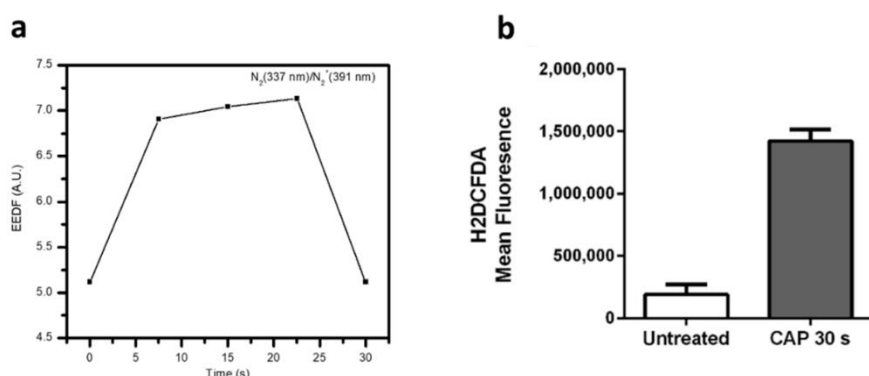
Supplementary Figure S1. *(**a**) Electro energy distribution function (EEDF) of CAP; (**b**) Fluorescence level of intracellular oxidised H₂DCFDA was measured via Flow cytometry, the analysed average of mean FL1-A value.*
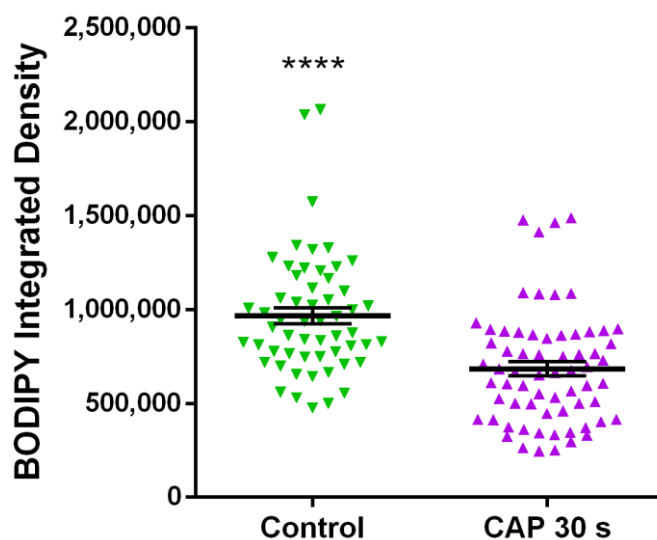
Supplementary Figure S2. *The fluorescent integrated density of non-oxidised BODIPY was quantified using ImageJ. The statistical significance was assessed by one-way ANOVA with Tukey's multiple comparison post-test (*P<0.05, **P<0.01, ***P<0.001, ****p<0.0001), n≥50, see Appendix IV Supplementary Table S1 for original data*
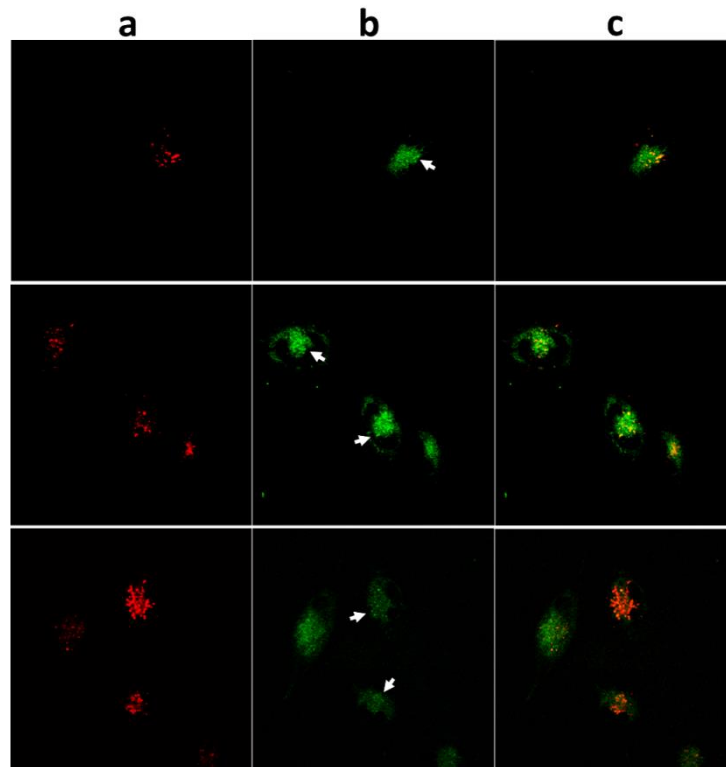
Supplementary Figure S3. *The U373MG cells were loaded with C11-BODIPY (green), then co-stained with and LysoTracker™ Deep Red (red) after CAP treatment (30 s, 75 kV) and observed under confocal microscope, three images are presented in the figure. White arrows point out examples of co-localisation between oxidised C11-BODIPY and lysosomes.*
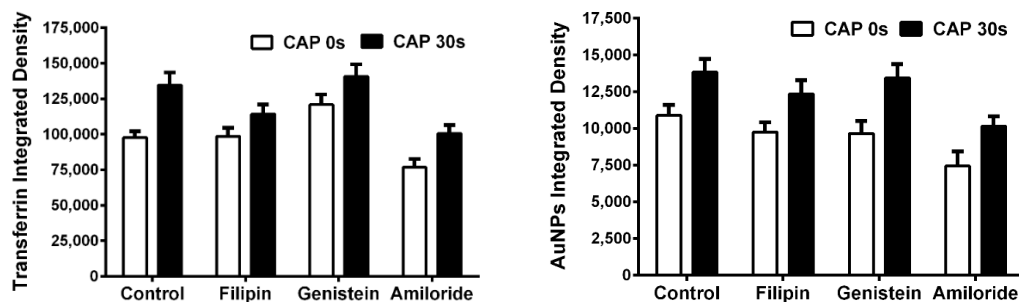
Supplementary Figure S4. *After incubation with various inhibitors as indicated, U373MG cells were treated CAP for 0, 30 s at 75 kV and then loaded with transferrin for 5 min or 100 µg/ml AuNPs for 3 h respectively before observing under confocal microscope, then the fluorescence integrated densities were quantified using ImageJ. The statistical significance was assessed by one-way ANOVA with Tukey's multiple*
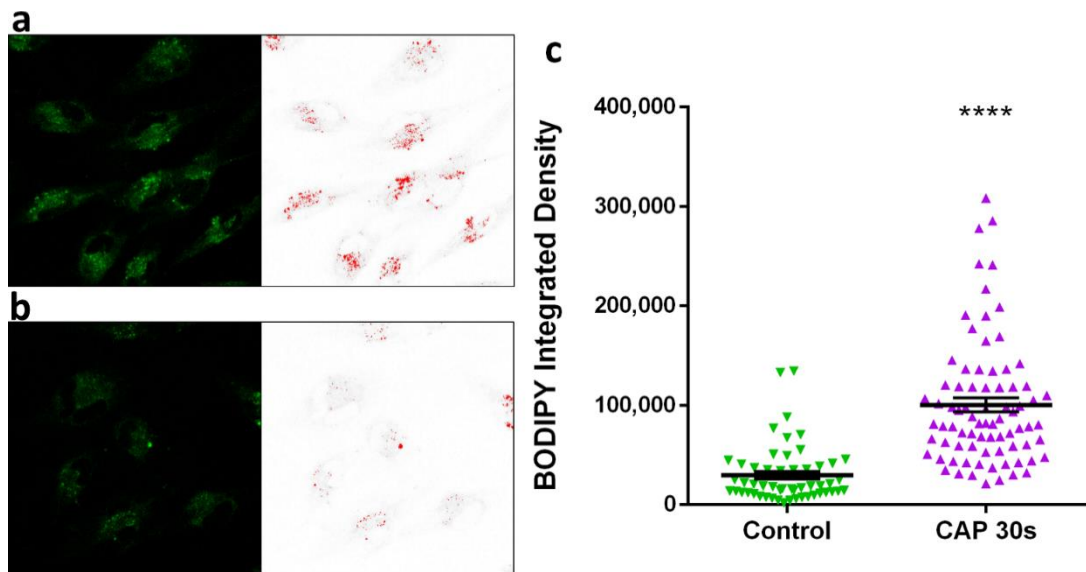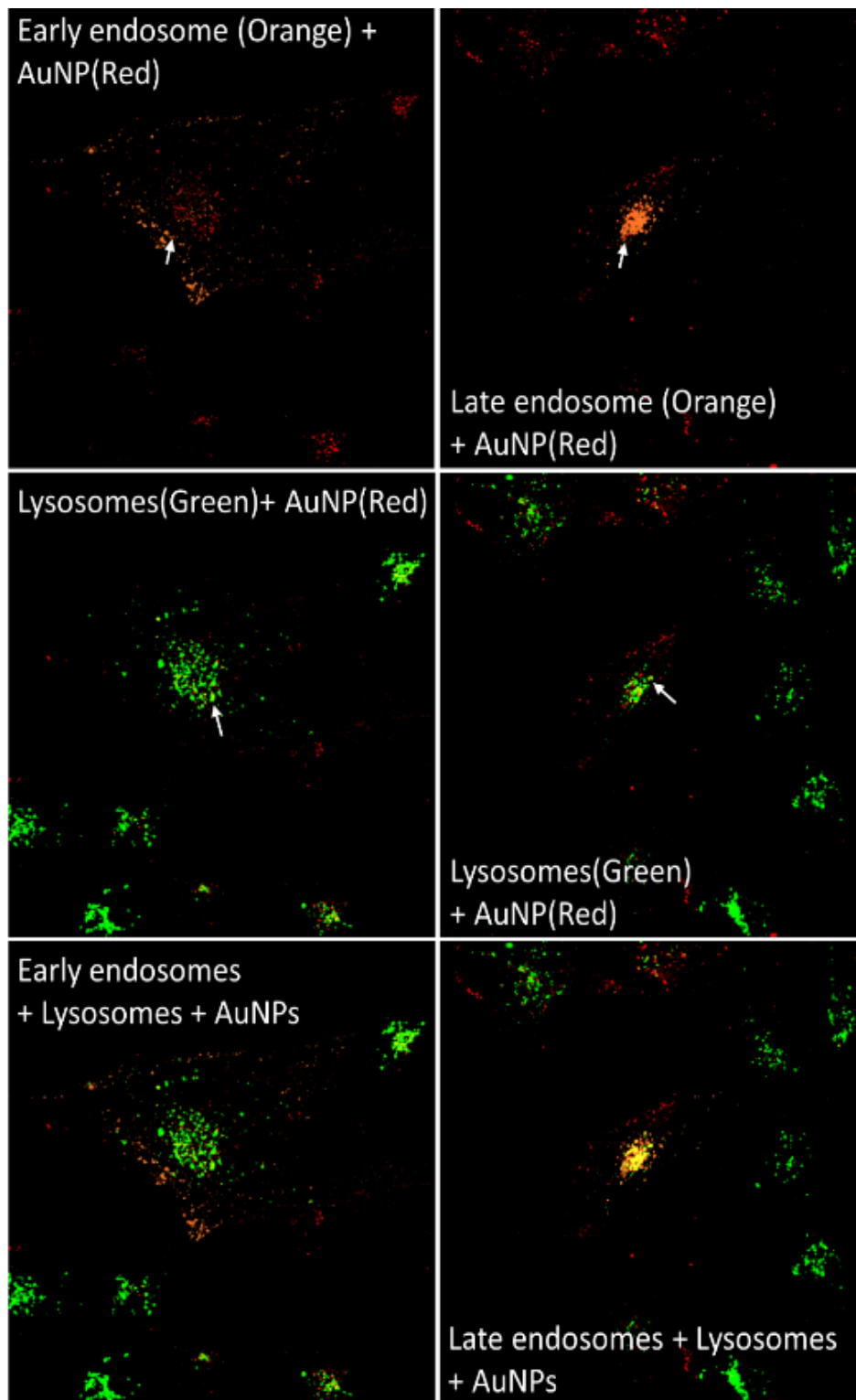
Supplementary Figure S5. *Oxidized C11-BODIPY emission was measured with same threshold to highlight vesicle-like condensed area. (a) Sample of CAP treated cells; (b) Sample of untreated cells; (c) With same threshold, the fluorescence integrated densities were quantified using ImageJ. The statistical significance was assessed by unpaired T-test. (*P<0.05, **P<0.01, ***P<0.001, ****p<0.0001), n≥50.*

Supplementary Discussion:

The intensity of O_3 production may explain why there was no detectable emission of NO, O, NO_x and low intensities of $^{\bullet}OH$ and N_2^+ in Figure 12a, as the free electrons were likely quenched before reaching higher energetic states by the interaction and formation of O_3. Reaction mechanisms (1-4) can further explain how the formation of NO, NO_x, and O was hindered. In these reactions, M is a third body atom or molecule that, in this case, may be N_2^* or O_2.

$$O + O_2 + M^* \rightarrow O_3 + M \tag{1}$$

$$M^* + NO \rightarrow M + N + O \tag{2}$$

$$O + H_2O \rightarrow 2\ ^{\bullet}OH \tag{3}$$

$$2N + M \rightarrow N_2 + M \tag{4}$$

***Supplementary Figure S6. Uptake and subcellular localization of AuNPs observed by
confocal microscopy.*** *After CAP treatment (0, 30 s), U373MG cells were incubated with
100 µg/ml AuNPs for 3 h. Early, late endosomes and lysosomes were stained using
CellLight™ Early/Late Endosomes-RFP (Marked as orange channel in images) and*

LysoTracker™ Green DND-26, respectively. The far-red emission of AuNPs (Red) was

excited using 633 nm laser.

Supplementary Table S1.

Integrated Density of BODIPY			
Control.	**CAP 30s.**	**Control. Oxidized (Figure**	**CAP 30s.**
825441	764257	232430	417629
998949	760580	310618	342874
1060462	665879	327636	495228
859260	1089862	179182	477016
530275	765581	307326	426428
829356	360915	176954	448261
665668	551518	499637	293395
1278050	264406	510195	325466
2038367	596517	356545	273752
936308	760052	292490	464481
1259645	332197	407417	167146
1573896	866259	281113	394278
1019896	499450	227051	302926
963641	296252	181733	221856
862036	846493	189916	454239
812204	881837	248568	374735
1113481	861837	300329	373363
748271	778087	273441	505987
1165023	524382	211968	292939
764072	867958	282522	388750
1232175	508610	317893	597744
1007005	595270	161873	295272
982070	610424	155628	306654
1320705	445595	458594	390399
946150	1463426	399135	890896
1342500	708723	462811	741382
653886	888079	196388	524934
499775	373856	190853	306468
875556	1477152	153302	390161
1037540	653049	163432	651081
906223	1078557	142877	187065
1097569	675892	206789	906811
1207059	402444	37404	312273
718964	1083730	109317	617780
559771	930197	236604	468648
475472	898191	142135	296259
747381	331716	270552	389688
807312	532198	82436	195602
707968	817839	84652	506283
840742	414865	168778	451699
777642	749632	364207	303635
1022745	879071	100734	431292
1228769	1084756	114519	701205
2064986	412708	49002	444981
697882	884861	273032	223330
1220345	566726	58729	423576
775782	667011	169249	569403
1182171	895365	184585	660069
812884	497905	198073	227918
940440	603690	154684	478087
555395	684168	441372	254274

1327438	371186	274210	362961
718786	502118	245082	398478
642920	415450	228162	325251
1050097	1489285	437520	346672
834466	250668	350830	479690
	247114	199513	1122291
	460969	184087	191401
	345379	260743	335414
	325823	234688	346672
	342280		303883
	694899		306629
	607436		1149608
	821919		150280
	1413574		456893
	729336		283002
			269830
			234559
			524097
			372300
			626520
			889340
			691489

Supplementary Table S2.

Integrated Density of Transferrin	
Untreated	**CAP30s**
110807	57027
66999	112562
125539	86679
25907	97764
18663	210017
36431	151799
55003	82789
58136	180386
108838	219322
203364	120825
38237	109507
106023	181812
153065	232475
46973	103867
231021	165690
126260	189547
58261	145942
53516	216243
28616	175271
169818	79758
119425	197285
69592	173238
24623	207385
126382	137586
109035	103140
251395	55164
90739	287846
76501	49045
76803	75313
71061	76832
70167	89317
71700	116572

29972	81825
28606	205643
87132	134411
33269	101051
95125	355132
80060	57270
64769	73021
106737	108349
74147	88346
79054	56330
25151	115220
40603	109490
72073	124859
124198	218535
77852	134532
103302	71167
109488	71050
58064	60830
75705	58081
27911	63689
86282	181942
117192	170011
32705	89790
120661	71784
129909	163049
106761	107358
90118	132343
39569	
164849	
84330	

Supplementary Table S3

Integrated Density of Transferrin					
Untreated	CAP30s	Pitstop	Pitstop+CAP	CPZ	CPZ+CAP
108598	295322	64736	100433	38802	56788
43443	108782	38572	31750	24310	83128
77433	251156	47517	76352	39598	45220
94477	84583	25591	100240	294486	19690
86584	65841	35782	71304	68324	13416
98793	91549	39735	28401	51158	9444
102070	163102	100772	44936	53180	16446
129770	156221	40368	22378	72708	29576
112724	81989	30864	12836	68844	5404
60643	207294	74733	17119	131656	7596
70525	80463	76017	26816	72856	4568
110091	86986	75272	97123	62814	21856
139093	145578	91199	43380	119252	2280
98220	63260	29856	83012	26884	7814
133442	69745	115762	17713	51452	129394
143649	110816	105188	49522	28458	117634
75022	123363	43457	54983	71198	30926
123196	134115	50026	18278	74608	77612
70338	228112	7877	59622	26936	68470
55592	140503	69660	29797	3384	88596
71972	121850	99571	77787	7454	30684
168227	158303	62211	74743	34034	75958
93020	121401	89301	78765	19250	95484
129316	70365	98921	47823	15276	103746

110653	146501	86540	32383	49392	9158
88591	129369	84316	42288	15354	4520
122648	82011	80932	52147	19722	25244
75639	98961	76763	42159	51914	17308
131539	112977	188739	101745	54704	50974
157044	76354	30436	28371	41096	16284
163738	94709	46748	63526	36212	5584
78925	51942	34317	91475	23016	19136
111987	177314	59776	41096	19956	7634
125506	94675	35976	56949	17996	30856
125495	129185	57772	69132	31342	84574
120301	127507	56559	99148	19040	30892
105738	90869	90776	41119	56680	9672
48458	119518	32429	59855	24088	12082
68317	113258	58616	47787	42838	37932
36999	247984	18765	73103	18410	4872
72117	277862	67164	27352	9752	61354
89229	184301	72684	37608	22664	29434
45164	167793	38795	41806	21144	36554
77146	317787	49816	72871	63528	27876
88215	213580	12847	87006	15258	69646
91529	72160	56799	66654	18400	59842
80253	60324	26547	49931	64260	23916
63880	97864	15265	46675	20094	14374
120907	156754	56795	29802	18770	79040
86245	125687	23657	64467	27556	61076
			12833	17776	14866
			28102	69252	85876
			38183	19000	15354
			29502	34386	8102
			37891	8592	38704
			61498	11670	34414
			51505	37184	78286
			35668	8968	16564
			24266	21180	71468
			51119	90982	10220
				22680	19342
				42116	16544
				7278	9582
				6646	77040
				59824	30404
				8114	54566
				19838	48010
					7918
					16944
					6710
					7116
					34934
					7930
					67322
					8512
					5804
					8342
					26376
					33834
					2612
					17928
					20240
					9364
					22084
					53872

							38896
							26456
							15434
							43858
							11738

Integrated Density of Transferrin

MβCD	MβCD+C	Filipin	Filipin	Genistei	Genistein	Amilori	Amiloride
131419	66932	97900	163871	101792	133841	196235	124569
124614	93007	129504	187302	133971	118480	138704	135077
69503	97275	110897	280194	65462	127431	29079	51297
75277	46598	90356	105230	147728	283770	72203	88474
76750	77640	104776	76422	147365	103548	64304	112269
18178	92103	73574	85766	68864	51402	72146	45995
81444	24984	159303	113291	72395	55713	83737	14594
88041	95210	124298	90004	101640	94243	54808	47209
57794	98855	108271	232008	96453	244560	33708	144728
51151	89031	72235	76414	174993	104571	31934	49935
76552	75078	33351	137916	271282	93475	64961	123415
86342	85701	30163	116268	221595	142366	56665	114787
40633	59098	62316	77831	83503	113373	48094	163106
97243	91913	65030	77608	145251	94037	30674	99006
36007	93666	109848	134224	99669	83792	97877	104122
79613	93835	95871	82976	72559	161527	99403	145760
79863	73324	106984	164104	202898	247658	60424	131902
115776	69286	157208	74697	51052	82664	76203	117916
47129	35314	109433	78977	58917	65763	37386	43884
36055	46718	27594	83753	112259	87005	81334	139639
87390	83701	79618	146374	140919	179148	29538	137618
62452	56757	89721	152046	163308	75257	65159	73523
93547	68512	194085	135891	67768	260961	79248	115470
74815	43701	36909	127681	69400	94462	34570	38530
65652	38500	50967	92144	52293	252478	101412	214459
90255	46948	159055	91692	74286	71411	40862	55017
71303	102306	165479	64158	119649	159244	30034	72765

50020	90653	48369	143926	121836	167913	78864	82769
76361	105447	39814	83297	157275	103238	21499	145664
61373	48421	82143	93936	100709	117632	87521	103887
72042	14139	117174	100813	268448	56085	32872	96235
89546	27184	96452	101386	96458	122851	86774	107471
94135	58249	61675	144732	200374	244874	108724	73740
70875	29039	152249	50729	133156	172584	99005	138795
46285	118411	51630	72558	123251	93479	91400	109758
74820	60569	178335	116879	66756	99088	162496	97441
64908	69129	58091	92915	148409	156027	59966	55005
49964	19395	109739	150147	156027	139595	83504	122417
25266	97511	122864	126267	116189	127740	79816	96430
12030	99651	62501	88480	131616	188948	70233	105109
68275	94682	115067	70907	145548	247489	54977	82412
24230	53849	89403	87317	64925	129827	20755	137153
48315	77480	144868	91462	99657	129957	87959	62907
56293	124595	133432	158029	129320	108170	113851	62485
46775	125449	143229		126041	113664	9751	139596
53149	67036	50177		113392	224130	195704	
61754	101836	60733		69885	249655	205460	
18804	127051	147230		81771	112130	71758	
23564	78954	74873		256252	137488	60650	
46598	56597	64963		185763	246213	102646	
		173794		90235	99266	104360	
				87308	88875	72262	
				34485	121148	62646	
				64651	215831	106858	
				116152			
				160153			

Integrated Density of AuNPs					
Untreated	**CAP 30s**	**Pitstop**	**Pitstop+CAP**	**CPZ**	**CPZ+CAP**
5516	22261	6083	3792	7990	8366
3581	12306	4177	6099	1863	1957
27847	10762	1746	2099	1486	8966
15965	3480	3011	1812	1434	6266
2647	10667	4032	1975	5801	1452
3198	4966	4808	6106	4778	3468
6305	8758	3805	2532	7212	2421
5788	20948	7747	1728	5556	2566
3919	8903	7417	3160	5631	3101
17942	10360	1322	3273	4089	4259
4457	17401	2229	2863	2949	2871
18099	50518	4509	4671	4297	3558
5395	21642	5231	5348	2607	3562
10992	9222	2962	2937	5111	7809
16843	11587	2971	4733	2967	7133
7621	14788	2567	3325	8772	4191
17892	13311	6843	5923	5787	3747
21501	20808	1608	7813	5110	8074
2455	12197	10176	2810	3289	5436
8796	8593	6170	2574	2880	3060
11688	10932	1970	9692	7444	2601
3500	15539	3286	2373	9698	3402
13317	20754	8646	4150	3923	3123
4841	8846	2766	8823	5399	2857
2679	4831	1331	4191	2188	5444
17626	16624	5692	1857	5285	6896
1669	10846	4185	3482	4443	3207
8186	16627	5613	4884	4856	4577

9202	19013	6779	10185	3336	3296
9836	18567	5571	4395	7300	3899
8877	12700	3958	2648	2034	3728
10929	10548	3951	1977	2889	2222
8565	6980	2132	4485	5657	3424
7736	12991	2702	5126	3539	6041
2356	15723	1284	4665	3242	3298
2851	29901	2677	5481	7771	8405
23594	7900	5960	2430	3372	4964
14115	24781	4984	4714		4473
5866	12827	7586	3752		1527
25137	11509	4864	4573		3776
11108	31897	9875	1779		4807
9864	4429	5750	2711		2822
16203	5919	6359	4560		4205
11111	7653	6231	3132		3023
9532	14639	4619	1628		10408
8395	13590	1388	6677		
11415	8222	4931	12145		
11279	15100	2072	22026		
11099	26498	3939	5527		
13153	14704	3847	2204		
12553	5136	2878	2964		
13217	17050	5958	3948		
17633	9468	6171	7410		
4742	7312	9188	2197		
11052	4848	3643	1465		
15608	13345	1471	5365		
5281	10442	8934	4764		
15270	17738	7551	1713		
12153	10179	2156	2552		
14067	7909	9601	2816		
13005	12894	15586	1916		
6557	10555	7303	6227		
14369	29626	3134	7636		
28194	9385	3070	16947		
4478	13564	6450	2184		
7769	26029	4504	5572		
15100	18355	1676	2971		
14411	8849		4198		
5912	6822		3081		
9159	10362		8244		
10064	12428		6451		
22400	9474		2825		
15100			733		
3145					
5178					
16426					
27029					
8473					
6730					
4345					
9773					

Integrated Density of AuNPs							
Filipin	**Filipin GAP**	**Genistein**	**Genistein GAP**	**MβCD**	**MβCD GAP**	**Amilori de**	**Amiloride+C**
14925	45932	7861	8525	10364	5563	4919	12384
13177	6400	3124	8659	3826	6803	6343	8314
6253	6224	7004	17234	5294	2748	8187	5489

4841	21801	8737	11437	8912	3850	3139	4808
17947	15017	12423	6792	14276	17048	5059	13403
4950	6373	6463	11330	9686	4090	1863	8839
5319	9478	6621	12569	8051	8453	4450	13091
11753	17365	9855	29753	8871	4153	2650	24387
8816	10640	9297	5810	5919	5268	2781	14911
3601	12295	15754	9558	4132	5229	13092	6714
4623	5898	2416	10012	29822	13267	1360	11432
14331	6364	8974	12247	9759	8702	1107	7042
3477	26822	26687	4487	12254	6550	2166	8005
10509	18101	13251	11413	10175	8515	3635	7039
6237	15876	3005	24979	4763	9959	5746	10338
7240	13389	3677	26444	20656	8809	12468	5008
7500	33586	1610	20449	5935	4552	7872	8225
3569	10446	21888	11668	8371	3501	2171	8509
3443	12871	16131	9829	11152	7595	4149	5992
17505	6565	12798	22269	4376	10268	13666	8063
11009	10467	10002	7997	12687	6862	4572	9861
14142	5683	20026	21671	7365	5081	9826	11328
12541	14049	4944	4504	5930	12182	8787	11552
10120	17180	8411	10937	17596	7779	5460	13135
6846	7140	17666	14563	8740	6003	14653	9408
7556	13706	7391	14822	15900	5778	16330	5093
8475	14675	9217	19264	4593	18306	7051	12713
15018	18780	14439	39774	2451	13608	28750	7968
24729	9029	10800	12115	3554	17698	12822	4766
6180	9180	10289	9980	3791	2271	7980	5260
8662	7303	4240	10558	13315	8238	2636	8735
16450	17269	5030	10707	5436	6113	4535	12229
9587	5057	5329	7643	10356	3952	4568	7559
11228	14892	4067	18347	1700	8427	2574	13070
11317	11273	27835	10790	5436	5052	2969	12427
5662	3751	21257	9966	3554	11620	2219	15870
16028	6097	5817	10412	2462	6685	3242	8116
9972	7096	5579	11849	15179	5245	2159	13472
9829	14357	19417	11330	6384	5810	5537	6946
13112	5305	1497	7456	6338		20414	7951
14690	4870	5149	10368	10377		4421	19438
14599	6517	6111	8107	4391		9412	9825
3840	6081	9586	12417	9562		11953	5042
8961	10141	8745	16088			5431	8533
7528	14356	9156	18577			2471	24524
5024	10728	14895	25898			34529	
10471	4837	10299	16529				
4401	12326	10661	9265				
9953	11511	3269	13413				
	8079	3960	7929				
	20982	6973	9668				
	9719	11519	10979				
	6663	6567					
	16067	3955					
	9929						
	26445						
	13543						
	13793						
	12121						
	13008						
	7982						

Supplementary Table S4.

Integrated Density of AuNPs			
CAP30s Control	**CAP 0s**	**CAP 0s**	**CAP 30s**
540329	172547	71657	81386
317286	431535	52885	26174
366683	78334	50113	83853
118864	227289	98205	62198
389856	182028	58882	113274
260748	95261	213664	176140
255370	67797	32246	90214
143714	155367	84077	155663
254835	143994	18060	167904
241522	409060	130518	52593
173393	91173	82556	22219
437882	98606	20741	19181
301708	372871	42321	16830
283998	42174	50000	36912
529897	192966	22797	11897
132739	43429	32307	67489
325045	171486	111229	22481
256487	155863	165385	45392
225093	218957	243576	12669
459960	332020	115717	14759
242832	163495	32769	59857
102314	178575	134059	29691
274004	43099	91085	36894
319820	116779	96918	46448
144878	33679	42816	24724
313094	281964	92220	41174
215681	474462	163157	12320
426863	78871	107430	42693
169499	25139	78092	54199
449778	157231	44965	26720
207286	25451	46103	68806
600642	105195	99071	50186
191247	124412	169342	18736
175692	128267	80229	16030
167735	312896	36048	55855
195195	129867	76657	106951
195351	127963	117916	17979
131726	352128	22666	39283
328548	257630	66817	17452
212497	116701	53062	34551
453971	134485	35270	10871
318022	113204	33485	43176
335974	203686	37665	6543
135597	81301	39651	20391
226104	258075	18179	9906
136796	117997	56467	43154
168061	189202	26238	33298
530325	354143	16544	6978
310895	179360	42583	10313
156015	249807	10222	7391
118700	104282	19974	18762
122974	189066	53493	56664
133195	84785	27174	8288
267536	141462	21953	72528
200762	345977	148609	24130
299249	77114	73347	13301

94514	47361	62139	18333
293151	43665	54334	20520
176776	9389	4625	17705
	270307	6653	38519
	31190	46708	28687
	257884	50733	15938
	155736	49224	
	345060	17503	
	43585	15541	
	81386	3876	
	23622		
	75993		
	65180		
	568575		
	318601		
	174400		
	52373		
	23718		
	59279		
	38939		
	75419		
	98606		
	24077		
	75776		
	41710		
	22592		
	70125		
	45832		
	98998		
	114681		
	126842		
	72896		
	161663		

7.5 Appendix V Supplementary Information for Chapter 4
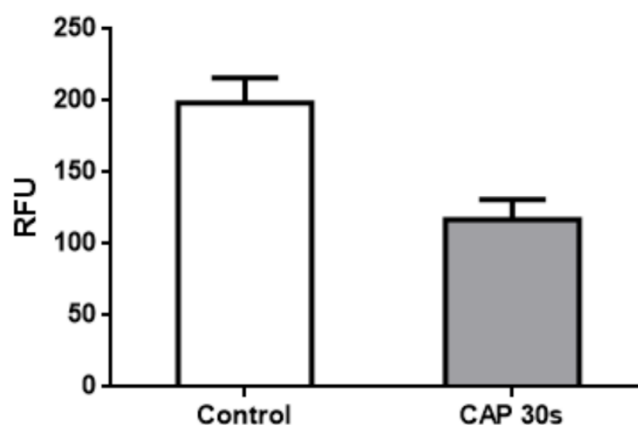
Supplementary Figure S1. The average reading of Alamar Blue assay performed within the plates treated with CAP and Cmpd 6. The control and CAP 30s treated groups presented in this figure were incubated with just culture medium without compounds for 48 h before Alamar Blue assay, demonstrated that this CAP treatment decreased around 50% of cell viability.
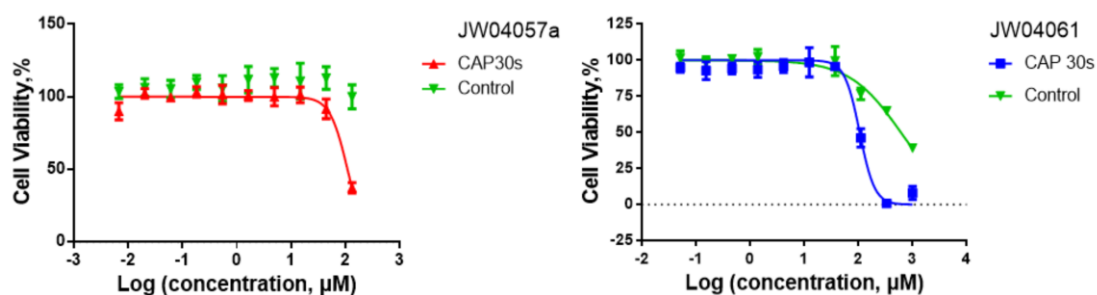
Supplementary Figure S2. The dose response curves of JW-04-061 and JW-04-057a with or without 30 s CAP treatment have been repeated to further confirm the synergistic cytotoxicity.
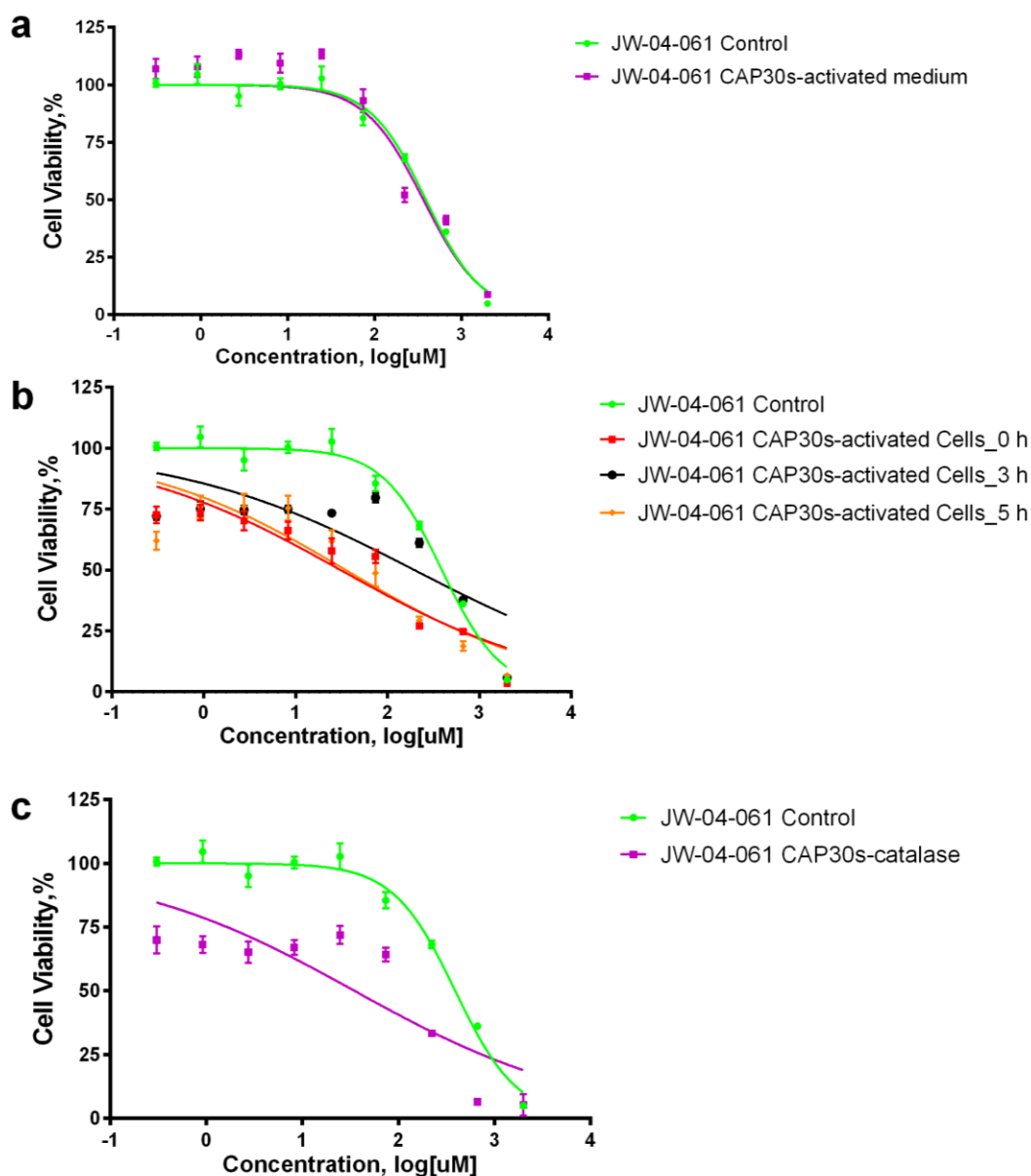
Supplementary Figure S3. Determine the synergistic cytotoxicity between CAP treatment and prodrug JW-04-061.
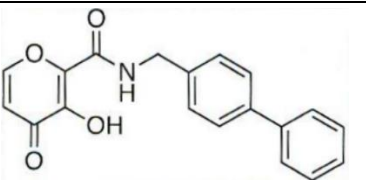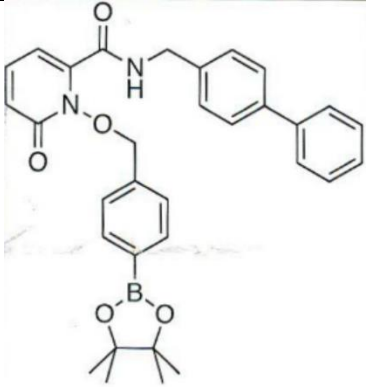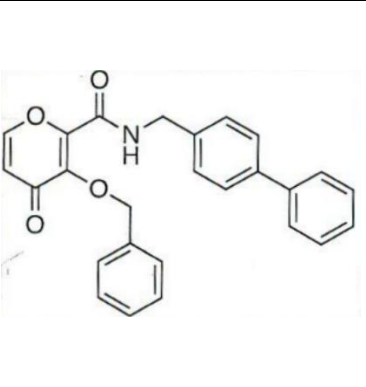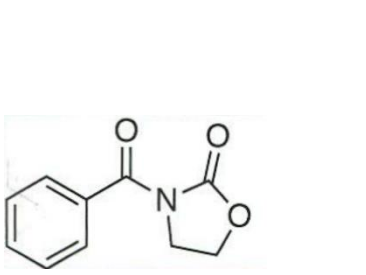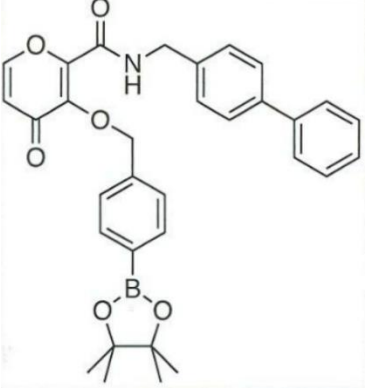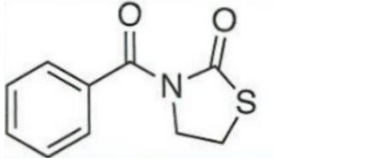
(**a**) The culture medium was treated with CAP for 30 s and storage overnight. The U373MG cells were then incubated with prodrug JW-04-61 in overnight storage CAP-activated medium for 48 hours. (**b**) U373MG cells were treated with CAP and then incubated in the culture medium that has CAP-treated together for 0-5 h, and then incubate with fresh medium containing prodrug JW-04-061. (**c**) The culture medium was

supplemented with 0.1 mg/ml catalase and then added into the 96-well plate during CAP

treatment and incubated with U373MG cells for 48 hours.
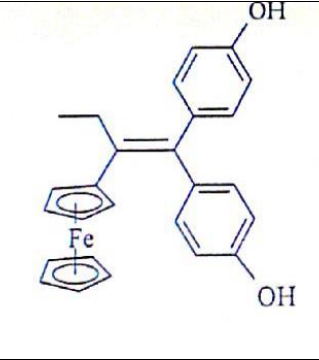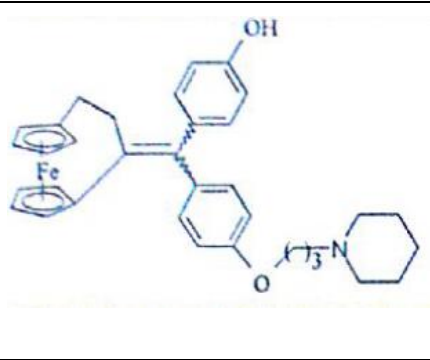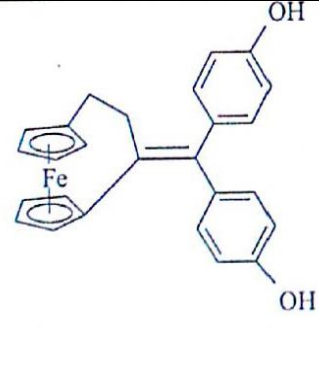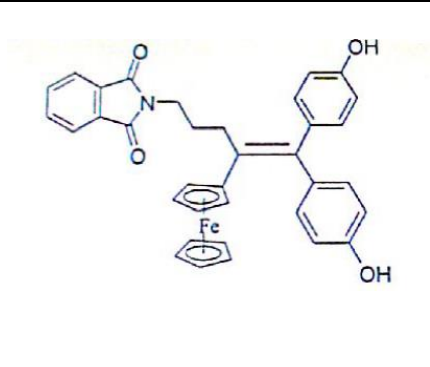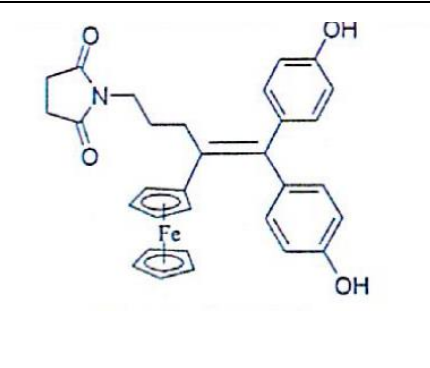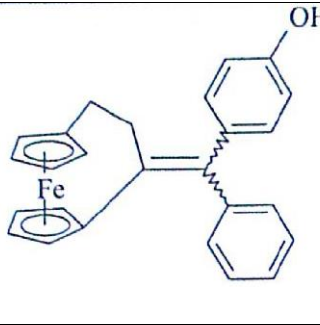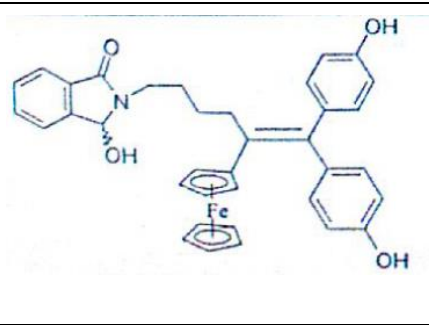
Supplementary Table S1. Structures of compunds provided by Prof. Andriy Mokhir,

Friedrich Alexander University, Germany (Marzenell *et al.*, 2013).

1e		2a	
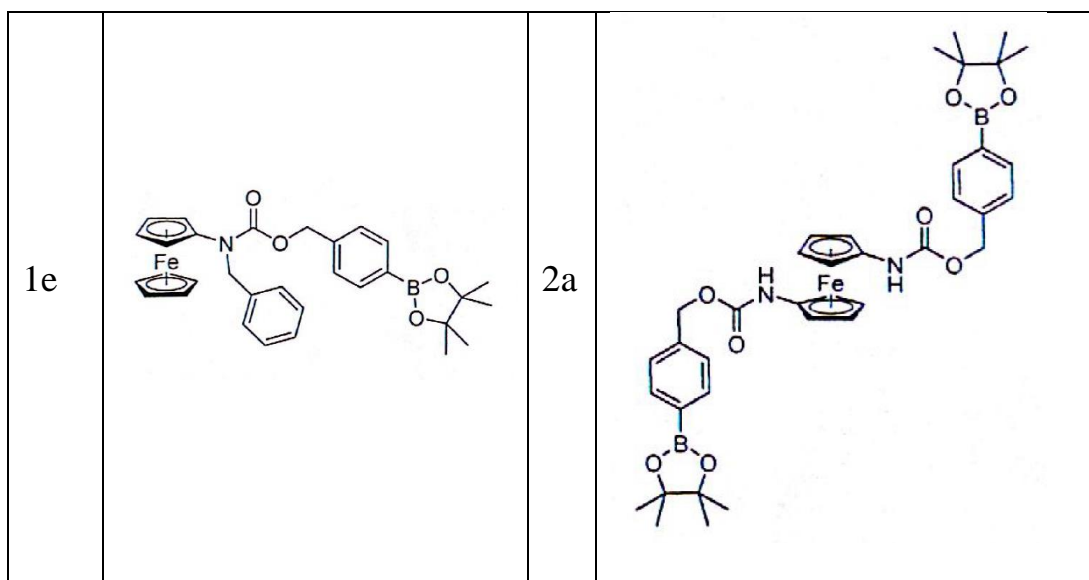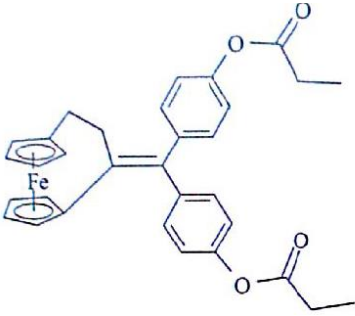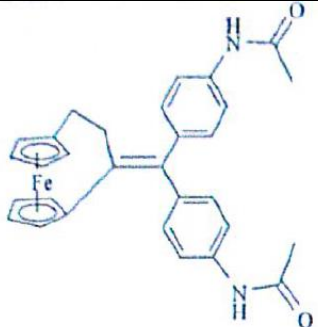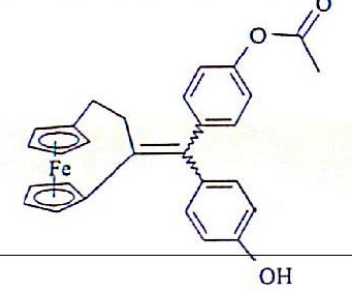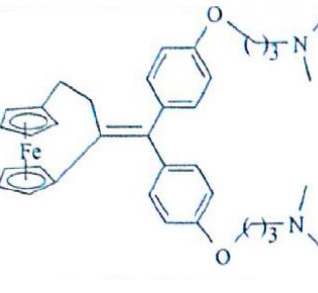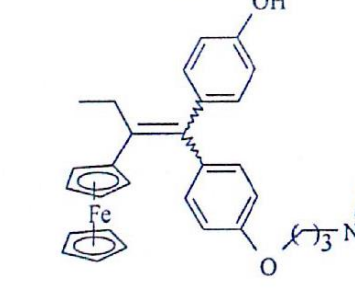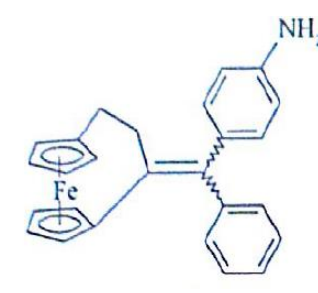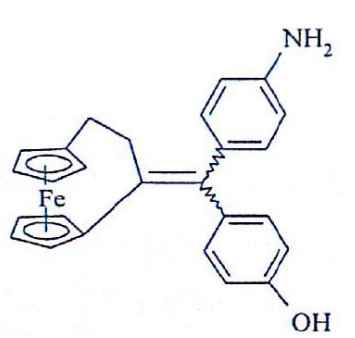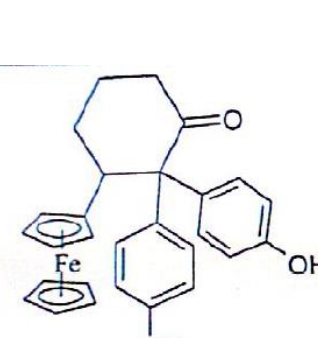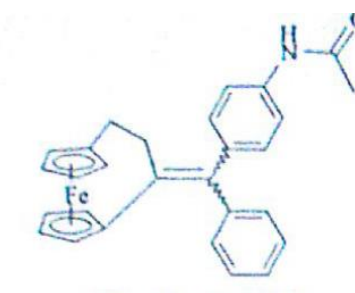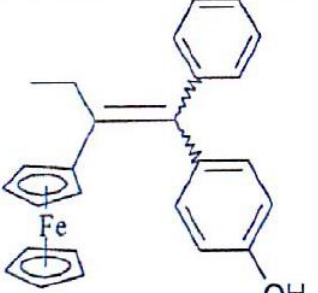
Supplementary Table S2. Structures of compunds provided by Prof. Seth M. Cohen, University of California San Diego, US (Perez *et al.*, 2015).
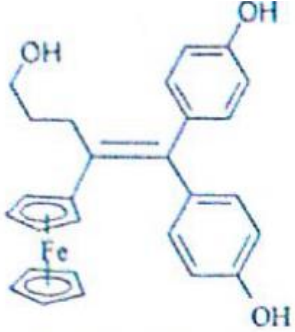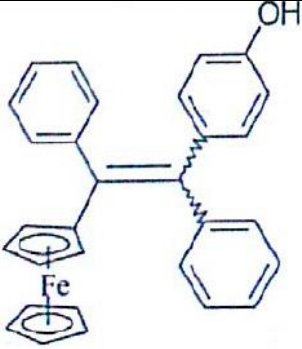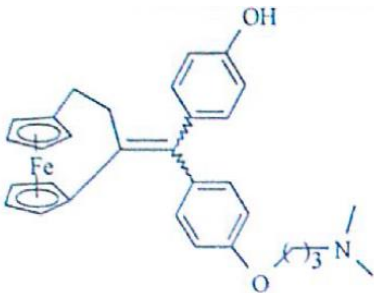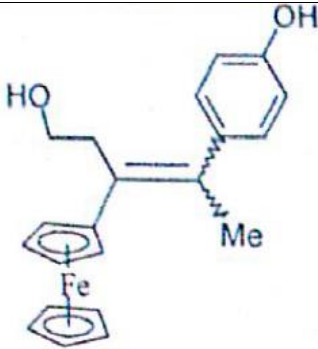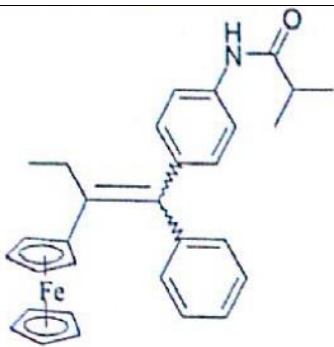
1,2-HOPO-2		PY-2	
1,2-HOPO-2-Boronic		PY-2-Benzyl	
Cmpd1		PY-2-Boronic	
Cmpd2			

Supplementary Table S3. Structures of compunds provided by Prof. Gérard Jaouen, Chimie ParisTech, France (Gormen *et al.*, 2010; Görmen *et al.*, 2010).
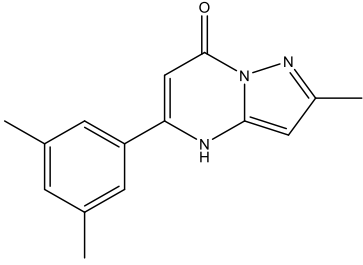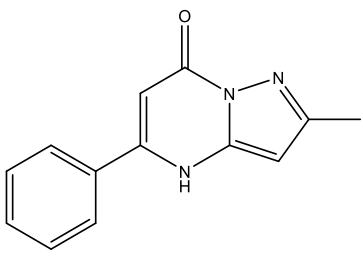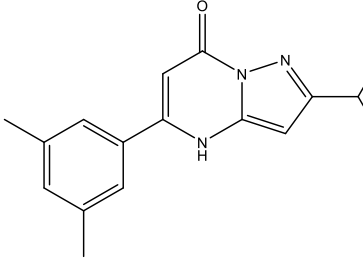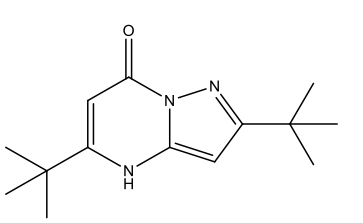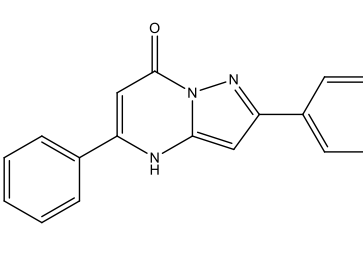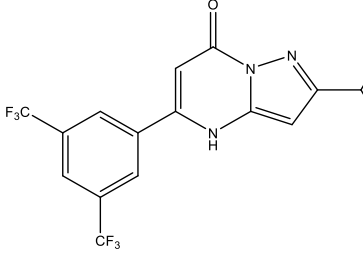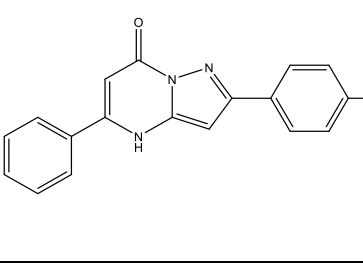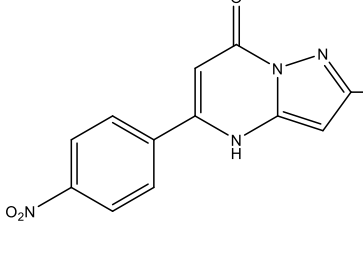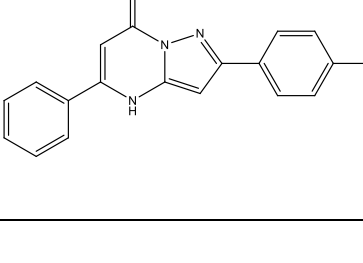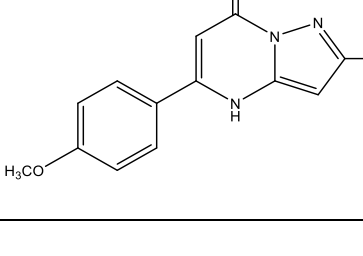
P5		P581	
DP1		P686	
P286		P722	
DP6		P721	
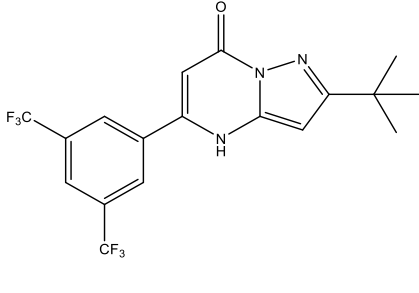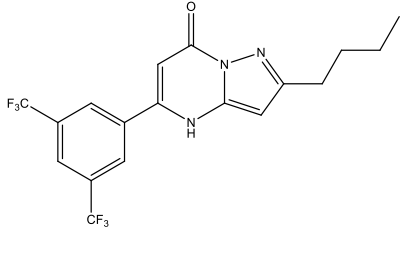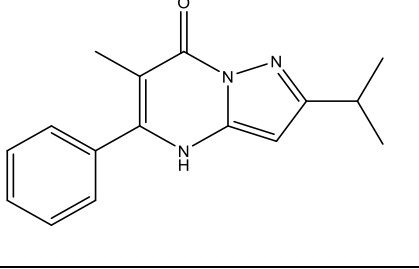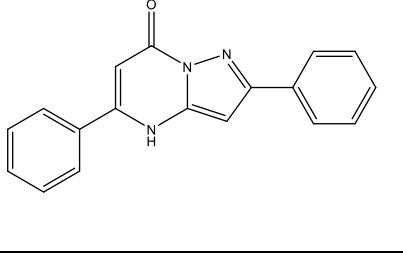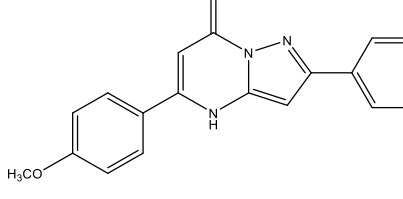
P240		P292	
P284		P283	
P15		P256	
P257		P208	
P258		P85	

231

P53		P388	
CG20		P228	
		P316	

Supplementary Table S4. Structures of compunds provided by Prof. John Stephens, Maynooth University, Ireland (Kelada *et al.*, 2018).

MK2		**JW-04-061**	
MK6		**JW-04-057a**	
MK7		JW-01-072	
MK8		JW-01-009	
MK9		JW-01-037	

Code	Structure	Code	Structure
JW-04-037		JW-01-033	
JW-04-039		JW-04-017	
		JW-04-012	

Supplementary Table S5. List of compounds that have been published.

Code	Publication	Source
P5	1. Metal carbonyl tracers and the ferrocifen family: Two facets of bioorganometallic chemistry	Prof. Gérard Jaouen
DP1	moiety on the expression of a cytotoxic effect on breast cancer cells	Prof. Gérard Jaouen
P286	Synthesis, Cytotoxicity, and COMPARE Analysis of Ferrocene and [3] Ferrocenophane Tetrasubstituted Olefin Derivatives against Human Cancer Cells	Prof. Gérard Jaouen
DP6	Comparative toxicity of [3] ferrocenophane and ferrocene moieties on breast cancer cells	Prof. Gérard Jaouen
P284	Synthesis, Cytotoxicity, and COMPARE Analysis of Ferrocene and [3] Ferrocenophane Tetrasubstituted Olefin Derivatives against Human Cancer Cells	Prof. Gérard Jaouen
P15	A ferrocenyl derivative of hydroxytamoxifen elicits an estrogen receptor-independent mechanism of action in breast cancer cell lines	Prof. Gérard Jaouen
P257	Synthesis, Cytotoxicity, and COMPARE Analysis of Ferrocene and [3] Ferrocenophane Tetrasubstituted Olefin Derivatives against Human Cancer Cells	Prof. Gérard Jaouen

P258	Comparative toxicity of [3] ferrocenophane and ferrocene moieties on breast cancer cells	Prof. Gérard Jaouen
P53	Ferrocifen type anti-cancer drugs	Prof. Gérard Jaouen
CG20	A new series of ferrocifen derivatives, bearing two aminoalkyl chains, with strong antiproliferative effects on breast cancer cells	Prof. Gérard Jaouen
P686	Phthalimido–ferrocidiphenol cyclodextrin complexes: Characterization and anticancer activity	Prof. Gérard Jaouen
P292	Synthesis, Cytotoxicity, and COMPARE Analysis of Ferrocene and [3] Ferrocenophane Tetrasubstituted Olefin Derivatives against Human Cancer Cells	Prof. Gérard Jaouen
P283	A new series of ferrocifen derivatives, bearing two aminoalkyl chains, with strong antiproliferative effects on breast cancer cells	Prof. Gérard Jaouen
P256	Comparative toxicity of [3] ferrocenophane and ferrocene moieties on breast cancer cells	Prof. Gérard Jaouen
P85	Comparative toxicity of [3] ferrocenophane and ferrocene moieties on breast cancer cells	Prof. Gérard Jaouen
P388	THE FERROCIFEN FAMILY AS POTENT AND SELECTIVE ANTITUMOUR COMPOUNDS: MECHANISMS OF ACTION	Prof. Gérard Jaouen
P228	Atypical McMurry Cross-Coupling Reactions Leading to a New Series of Potent Antiproliferative Compounds Bearing the Key [Ferrocenyl-Ene-Phenol] Motif	Prof. Gérard Jaouen
P316	Comparative toxicity of [3] ferrocenophane and ferrocene moieties on breast cancer cells	Prof. Seth M. Cohen
1,2-HOPO-2	Emerging Trends in Metalloprotein Inhibition	Prof. Seth M. Cohen
1,2-HOPO-2-Boronic	Emerging Trends in Metalloprotein Inhibition	Prof. Seth M. Cohen
PY-2	Hydrogen Peroxide Activated Matrix Metalloproteinase Inhibitors: A Prodrug Approach	Prof. Seth M. Cohen
PY-2-Benzyl	Emerging Trends in Metalloprotein Inhibition	Prof. Seth M. Cohen
PY-2-Boronic	Hydrogen Peroxide Activated Matrix Metalloproteinase Inhibitors: A Prodrug Approach	Prof. Seth M. Cohen

Cmpd1	Exploring hydrogen peroxide responsive thiazolidinone-based prodrugs	Prof. Seth M. Cohen
Cmpd2	Exploring hydrogen peroxide responsive thiazolidinone-based prodrugs	Prof. Seth M. Cohen
1e	Aminoferrocene-based prodrugs and their effects on human normal and cancer cells as well as bacterial cells	Prof. Andriy Mokhir
2a	Aminoferrocene-based prodrugs and their effects on human normal and cancer cells as well as bacterial cells	Prof. Andriy Mokhir
MK2	Synthesis of pyrazolopyrimidinones using a "one-pot" approach under microwave irradiation	Prof. John Stephens
MK6	Synthesis of pyrazolopyrimidinones using a "one-pot" approach under microwave irradiation	Prof. John Stephens
MK7	Synthesis of pyrazolopyrimidinones using a "one-pot" approach under microwave irradiation	Prof. John Stephens
MK8	Synthesis of pyrazolopyrimidinones using a "one-pot" approach under microwave irradiation	Prof. John Stephens
MK9	Synthesis of pyrazolopyrimidinones using a "one-pot" approach under microwave irradiation	Prof. John Stephens
JW-04-037	Synthesis of pyrazolopyrimidinones using a "one-pot" approach under microwave irradiation	Prof. John Stephens
JW-04-039	Synthesis of pyrazolopyrimidinones using a "one-pot" approach under microwave irradiation	Prof. John Stephens
JW-04-061	Synthesis of pyrazolopyrimidinones using a "one-pot" approach under microwave irradiation	Prof. John Stephens
JW-04-057a	Synthesis of pyrazolopyrimidinones using a "one-pot" approach under microwave irradiation	Prof. John Stephens

	Synthesis of pyrazolopyrimidinones using a "one-pot" approach under microwave irradiation	Prof. John Stephens
JW-01-072	Synthesis of pyrazolopyrimidinones using a "one-pot" approach under microwave irradiation	Prof. John Stephens
JW-01-009	Synthesis of pyrazolopyrimidinones using a "one-pot" approach under microwave irradiation	Prof. John Stephens
JW-01-037	Synthesis of pyrazolopyrimidinones using a "one-pot" approach under microwave irradiation	Prof. John Stephens
JW-01-033	Synthesis of pyrazolopyrimidinones using a "one-pot" approach under microwave irradiation	Prof. John Stephens
JW-04-017	Synthesis of pyrazolopyrimidinones using a "one-pot" approach under microwave irradiation	Prof. John Stephens
JW-04-012	Synthesis of pyrazolopyrimidinones using a "one-pot" approach under microwave irradiation	Prof. John Stephens

8. List of Publications

He, Z., Liu, K., Manaloto, E. et al. Cold Atmospheric Plasma Induces ATP-Dependent Endocytosis of Nanoparticles and Synergistic U373MG Cancer Cell Death. Sci Rep 8, 5298 (2018). https://doi.org/10.1038/s41598-018-23262-0

He, Z., Liu, K., Byrne, H.J. et al. Combination Strategies for targeted delivery of nanoparticles for cancer therapy. In Applications of targeted nano drugs and delivery systems, pp. 191-219. Elsevier (2019). https://doi.org/10.1016/B978-0-12-814029-1.00008-9

He, Z., Liu, K., Scally, L. *et al.* Cold Atmospheric Plasma Stimulates Clathrin-Dependent Endocytosis to Repair Oxidised Membrane and Enhance Uptake of Nanomaterial in Glioblastoma Multiforme Cells. *Sci Rep* 10, 6985 (2020). https://doi.org/10.1038/s41598-020-63732-y

Liu, K., **He, Z.**, Byrne, H.J. et al. Investigating the role of gold nanoparticle shape and size in their toxicities to fungi. *International journal of environmental research and public health*, *15*(5), p.998 (2018). https://doi.org/10.3390/ijerph15050998

Liu, K., **He, Z.**, Curtin, J.F. *et al.* A novel, rapid, seedless, *in situ* synthesis method of shape and size controllable gold nanoparticles using phosphates. *Sci Rep* **9,** 7421 (2019). https://doi.org/10.1038/s41598-019-43921-0

Conway, G.E., **He, Z.**, Hutanu, A.L. *et al.* Cold Atmospheric Plasma induces accumulation of lysosomes and caspase-independent cell death in U373MG glioblastoma multiforme cells. *Sci Rep* **9,** 12891 (2019). https://doi.org/10.1038/s41598-019-49013-3

Manaloto, E., Gowen, A., Lesniak, A., **He, Z**. et al. Cold Atmospheric Plasma induces silver nanoparticle uptake, oxidative dissolution and enhanced cytotoxicity in Glioblastoma multiforme cells. *BioRxiv (2020)*. https://doi.org/10.1101/2020.02.28.969758

Conway, G.E., Zizyte, D., Mondala, J.R.M., **He, Z**. et al. Ursolic acid inhibits cell

migration and promotes JNK-dependent lysosomal associated cell death in Glioblastoma multiforme cells. *BioRxiv (2020)*. https://doi.org/10.1101/2020.03.11.987578

(**He, Z.** et al. Screening the synergistic cytotoxicity of 47 pro-drugs candidates in combination with low dose cold atmospheric plasma against glioblastoma cells. Work from Chapter 4, manuscript in preparation.)

9. List of Employability Skills and Discipline Specific Skills Training

	Modules	ECTS	Reasons for choosing
Discipline Specific Modules	BIOL 9223: Research Methods and Biostatistics	10	This module introduced knowledge in research methods and especially statistical analysis of data, which benefited my research work.
	BIOL 9220: Advanced Diagnostic Methods and Bioinformatics	10	This module provided many knowledges of biological advanced diagnostic methods, which will be beneficial for my future research carrier.
Employability Skills Modules	MECH 9002: Innovation and Knowledge Management	5	This module provided me great concept about knowledge management and innovation which benefited for my PhD carrier and will be useful for my future work.
	CRDI Techniques & Strategies in Molecular Medicine	5	I'm highly interested in molecular medicine, which wasn't highly related with my current project but can be helpful for research work in near future.
	AFGDP Hot Topics	5	Food science is as important as medicine, and this module inspired me a lot with the variety of the hot topics in food science and healthcare fields.
	GRSO 1012 Research Integrity	5	Research integrity is necessary for every researcher. By taking this module, I understood the integrity better, as a research, and keep it in my mind all the time to not make mistake.